A GFPT1 Deficient Mouse Model of Congenital Myasthenic Syndrome

Yasmin Issop

A thesis submitted for the degree of Doctor of Philosophy

Newcastle University

Faculty of Medical Sciences

Institute of Genetic Medicine

May 2017

Abstract

Congenital myasthenic syndromes (CMS) are inherited disorders characterised by fatigable muscle weakness resulting from impaired transmission at the neuromuscular junction (NMJ). CMS occur due to mutations in genes encoding proteins responsible for maintaining the structure and function of the NMJ.

Glutamine-fructose-6-phosphate transaminase 1 (GFPT1) is the rate-limiting enzyme in the hexosamine biosynthetic pathway which yields precursors required for protein and lipid glycosylation. Mutations in *GFPT1* and genes downstream of this pathway are pathogenic for CMS. One hypothesis is that hypoglycosylation of NMJ proteins results in defective neurotransmission.

The aim of this study is to generate and characterise a GFPT1 deficient mouse model of CMS. One of the challenges we face is the viability of *Gfpt1* knockout mice. Here we generate a novel muscle-specific GFPT1 knockout mouse model using Cre/loxP technology. We demonstrate that a deficiency of GFPT1 in muscle only, is sufficient for causing a CMS phenotype. Our model recapitulates many aspects of the phenotype observed in patients with *GFPT1*-related CMS. Mutant mice display early changes in the morphology of postsynaptic components of the NMJ, which are accompanied by presynaptic alterations. They later develop a myopathic phenotype and formation of tubular aggregates. We further identify proteins in skeletal muscle that are differentially regulated because of GFPT1 deficiency.

Our data demonstrates a critical role for GFPT1 in the development of the NMJ, neurotransmission, and skeletal muscle integrity. The muscle-specific GFPT1 deficient mouse model allows us to investigate the implications of not only *GFPT1* mutations, but may also give us an insight into the pathophysiological consequences of mutations in genes downstream of GFPT1, which also result in hypoglycosylation. This model has the potential to enhance our understanding of current drug therapies, and to drive forward the development of new compounds which can be implemented in the clinic.

Dedication

This thesis is dedicated to patients with
Congenital Myasthenic Syndrome and their families.

Acknowledgments

I would like to thank my supervisors Professor Hanns Lochmüller, Dr Steve Laval and Dr Andreas Roos for their guidance, supervision and support throughout this project. I am grateful for the knowledge, opportunities and experiences I acquired at the John Walton Muscular Dystrophy Research Centre.

I would also like to thank members of our team and the rest of the faculty for their contributions and support. Thanks to my PhD assessors Professor Michael Briggs, Professor Julia Reichelt and Dr Ralf Kist for your suggestions and advice throughout the project. I would also like to thank Steve Smith, Lynne Todd and the rest of FGU staff for their help with the animal work and continuous support, without which this work would not have been possible. Thanks to Professor Clarke Slater for your time, advice and profound knowledge.

I am grateful for the collaboration with Professor Rüdiger Rudolf, Dr Muzamil Khan and their team at the Institute of Toxicology and Genetics, Germany. Thank you for your kindness, generosity and for making me feel welcome. Thanks to Professor Jochaim Weis for his work on electron microscopy, Denisa Hathazi for her work on proteomic profiling, Professor Dominic Wells and Dr Kim Wells from the Royal Veterinary College, London, for providing training with the force measurement experiments.

I would like to thank my friends at the IGM and outside, who have supported me over the years. Emine and Lauren, thank you for always being there.

Finally, to my parents and the rest of my family, thank you for your continuous support and encouragement to strive further.

This work was funded by the Medical Research Council UK and The Barbour Foundation.

Table of Contents

List of Tables

List of Figures

List of Abbreviations

3,4 DAP	3,4-diaminopyridine
ACh	Acetylcholine
AChE	Acetylcholinesterase
AChR	Acetylcholine receptor
AP1	Associated adaptor protein
BAC	Bacterial artificial chromosome
BLAST	Basic Local Alignment Search Tool
BSA	Bovine serum albumin
CDG	Congenital disorders of glycosylation
ChAT	Choline acetyltransferase
CMAP	Compound muscle action potential
CMS	Congenital myasthenic syndrome
CPN	Common peroneal nerve
CSA	Cross-sectional area
DAPI	4,6-diamidino-2-phenylindole
DHPR	Dihydropyridine receptors
Dok-7	Docking-protein 7
Dol-P	Dolichol phosphate
Dol-P-P-GlcNAc	Dolichol pyrophosphate *N*-acetylglucosamine
ECG	Electrocardiogram
EDL	Extensor digitorum longus
EMG	Electromyography
EPP	Endplate potential
ER	Endoplasmic reticulum
ES	Embryonic stem cells
FASP	Filter-aided sample preparation
FLP	Flippase
FNTA	Farnesyltransferase/geranylgeranyltransferase type-1 subunit alpha
GAPDH	Glyceraldehyde 3-phosphate dehydrogenase
GFP	Green fluorescent protein
GFPT1	Glutamine-fructose-6-phosphate transaminase 1

GGT	Geranylgeranyltransferase
GlcNAc	*N*-acetylglucosamine
H&E	Hematoxylin and eosin
HCL	Hydrochloric acid
HSPG	Heparan sulphate proteoglycan
IMPC	International Mouse Phenotyping Consortium
LG	Lateral Gastrocnemius
LRP4	Low-density lipoprotein-related protein receptor 4
MG	Medial Gastrocnemius
MRI	Magnetic Resonance Imaging
MuSK	Muscle specific kinase
$Na_v1.4$	Voltage gated-Na^+ channels
NF	Neurofilament
NMJ	Neuromuscular junction
OGT	O-GlcNAc transferase
ORAI1	Calcium release-activated calcium channel protein 1
PBS	Phosphate buffered saline
PCR	Polymerase chain reaction
PFA	Paraformaldehyde
PL	Plantaris
RT-PCR	Reverse transcription polymerase chain reaction
RyR	Ryanodine receptor
SNARE	Soluble N-ethyleimide-sensitive factor attachment protein receptors
SNAP25	Synaptosomal-associated protein 25
SOL	Soleus
SR	Sarcoplasmic reticulum
STIM1	Stromal interaction molecule 1
Syn	Synaptophysin
TA	Tibialis anterior
UDP-GlcNAc	Uridine diphosphate *N*-acetylglucosamine
VAChT	Vesicular acetylcholine transporter
X-gal	5-bromo-4-chloro-3-indolyl-β-D-galactopyranoside

Chapter 1. Introduction

1.1 Myasthenic syndromes

Myasthenic Syndromes are a group of autoimmune and inherited disorders characterised by muscle weakness and fatigability. Both arise due to impairment of neuromuscular transmission and are categorised in terms of etiological mechanisms and clinical phenotype (Verschuuren *et al.*, 2010; Parr *et al.*, 2014). Congenital Myasthenic Syndromes (CMS) are caused by gene mutations which affect proteins responsible for maintaining the structure and function of the neuromuscular junction (NMJ). CMS differ to the more common myasthenia gravis and Lambert-Eaton myasthenic syndrome, which are autoimmune disorders characterised by the presence of antibodies targeting the acetylcholine receptor (AChR) or the Muscle Specific Kinase (MuSK), and PQ-type voltage-gated calcium channels respectively (Hoch *et al.*, 2001; Jacob *et al*., 2009; Finlayson *et al.*, 2013; Le Panse and Berrih-Aknin, 2013). Whilst there are currently no cures for myasthenic syndromes, symptomatic treatments are widely available. Correct treatment is highly dependent on recognising the type of myasthenic syndrome, molecular pathology, and identification of the gene mutated in inherited myasthenic syndromes (Basiri *et al.*, 2013). Myasthenia gravis and CMS can be distinguished according to phenotypic presentation, onset and progression of disease and response to immunosuppressive therapy (Abicht *et al.*, 2012). More recently, the discovery of gene mutations that give rise to CMS, alongside functional studies to determine whether these mutations are indeed pathogenic have facilitated the differential diagnosis of CMS subtypes and selection of effective drugs for treatment.

1.2 Congenital myasthenic syndromes

CMS are a heterogeneous group of rare inherited disorders of neurotransmission. The prevalence of genetically confirmed CMS is approximately 9.2 cases per million children under 18 years old in the UK (Parr *et al.*, 2014). CMS are usually characterised by fatigable muscle weakness in skeletal muscle affecting the ocular, bulbar and limb muscles, whilst cardiac and smooth muscle remain unaffected. The severity and progression of CMS is highly variable amongst patients, ranging from mild weakness to more disabling symptoms. If left untreated CMS can potentially cause life threatening respiratory insufficiency (Senderek *et al.*, 2011). The different types of CMS are

classified based on the site of the underlying defect, which primarily involves the presynaptic compartment, synaptic cleft or the postsynaptic basal lamina of the NMJ. They are further subdivided according to the pathophysiological involvement of specific proteins that impair the formation, maintenance and function of the NMJ. The genes implicated in CMS encode membrane receptors, enzymes, ion channels and neurally secreted proteins at the NMJ (Huze *et al.*, 2009). More recently, mutations in genes encoding ubiquitously expressed enzymes involved in glycosylation have also been implicated in CMS (Senderek *et al.*, 2011; Belaya *et al.*, 2012; Selcen *et al.*, 2013; Belaya *et al.*, 2015). Table 1.1 provides a summary of the known genes encoding proteins implicated in CMS (Abicht *et al.*, 2016; O'Connor *et al.*, 2016; Souza *et al.*, 2016).

Type of CMS/protein impaired	Genes	% of CMS attributed to pathogenic variants in this gene	Molecular Pathology	Treatment
POSTSYNAPTIC				
AChR deficiency	*CHRNE* *CHRNA* *CHRNB* *CHRND*	<1% *CHRNA*, <1% *CHRNB*, <1% *CHRND*, 50% *CHRNE*	Low expression of AChR in the postsynaptic membrane	Pyridostigmine, 3,4 DAP
AChR-Slow channel syndrome	*CHRNA** *CHRNE** *CHRNB** *CHRND**		Prolonged channel opening in response to ACh	Fluoxetine, quinidine
AChR-Fast channel syndrome	*CHRNA* *CHRNE* *CHRND*		Shortened channel opening in response to ACh	Pyridostigmine, 3,4 DAP
Escobar Syndrome	*CHRNG*	<1%	Low expression of fetal AChR gamma subunit	___
Rapsyn deficiency	*RAPSN*	15%-20%	Impaired AChR clustering	Pyridostigmine, 3,4 DAP
Dok-7 synaptopathy	*DOK7*	10%-15%	Synaptopathy; small and simplified presynaptic and postsynaptic structures	Ephedrine, salbutamol, 3,4 DAP
MuSK	*MUSK*	<1%	Impaired AChR clustering	Pyridostigmine, 3,4 DAP
LRP4	*LRP4*	<1%	Impaired AChR clustering	Pyridostigmine, 3,4 DAP (no/negative effect on patients)
$Na_v1.4$ (voltage-gated sodium channel)	S*CN4A*	<1%	Altered postsynaptic voltage-gated sodium function	AChE inhibitors
Plectin	*PLEC*	<1%	Reduced plectin (cytoskeletal linking protein at the postsynaptic junctional folds)	Pyridostigmine, 3,4 DAP

Type of CMS/Protein impaired	Genes	% of CMS attributed to pathogenic variant in this gene	Molecular Pathology	Treatment
SYNAPTIC				
Laminin beta-2	*LAMB2*	<1%	Reduced β2-laminin, required for the alignment of nerve and muscle at the NMJ	Ephedrine
Acetylcholinesterase deficiency	*COLQ*	10%-15%	Failure to anchor AChE in the synaptic cleft	Ephedrine
PRESYNAPTIC				
Choline acetyltransferase deficiency	*CHAT*	4%-5%	Failure of ACh synthesis	Pyridostigmine, 3,4 DAP
Agrin	*AGRN*	<1%	Impaired AChR clustering	Pyridostigmine, 3,4 DAP
MYO9A	*MYO9A*	<1%	Impairment of neuronal morphology and function	Pyridostigmine
High-affinity choline transporter	*SLC5A7*	<1%	Impairs reuptake of choline from the synaptic cleft	AChE inhibitors, Salbutamol
Vesicular acetylcholine transporter	*SLC18A3*	<1%	Impairs uptake of ACh into presynaptic vesicles	Pyridostigmine
SLC25A1	*SLC25A1*	<1%	Abnormal mitochondrial citrate carrier function.	Pyridostigmine, 3,4 DAP
SNAP25	*SNAP25**	<1%	Compromised quantal release at endplates	3,4 DAP
Synaptobrevin-1	*SYB1 (*also known as *VAMP1)*	<1%	Reduction in EPP amplitude	Pyridostigmine
Synaptotagmin-2	*SYT2**	<1%	Calcium sensors - Disruption of synaptic vesicle exocytosis	3,4 DAP

Type of CMS/Protein impaired	Genes	% of CMS attributed to pathogenic variant in this gene	Molecular Pathology	Treatment
PROTEINS AT MULTIPLE SITES				
Glycosylation deficiency	*DPAGT1* *GFPT1* *ALG2* *ALG14* *GMPPB*	<1% 2% <1% <1% <1%	Abnormal glycosylation of synaptic components	Pyridostigmine, Pyridostigmine & Salbutamol (GMPPB)
PREPL	*PREPL*	<1%	Reduced ACh content within vesicles	Pyridostigmine
COL13A1	*COL13A1*	<1%	Abnormal formation and maintenance of the NMJ	3,4 DAP

Table 1.1. Congenital myasthenic syndromes. 3,4 DAP, 3,4-diaminopyridine; ACh, acetylcholine; AChE, acetylcholinesterase; AChR, acetylcholine receptor. Slow channel syndromes, *SNAP25* and *SYT2* mutations are acquired via autosomal dominant inheritance, *; All other syndromes are autosomal recessive. NB: Agrin is expressed neurally but acts postsynaptically.

1.3 The neuromuscular junction

In order to identify the pathological mechanisms underlying CMS, it is important to understand how the NMJ functions in healthy individuals. The two main processes associated with normal NMJ function involves proteins and signalling events responsible for (i) neurotransmission; (ii) formation and maintenance of the NMJ. Here we describe the functional significance of the proteins that are implicated in CMS.

1.3.1 *The acetylcholine receptor system and neurotransmission*

The neuromuscular junction is highly specialised to enable synaptic transmission through the activation of AChRs on the postsynaptic membrane. When an action potential reaches the presynaptic nerve terminal, voltage gated Ca^{2+} channels are opened causing an increase in intracellular Ca^{2+} levels. This is detected by the Ca^{2+} sensor, synaptotagmin-2 which subsequently results in trafficking of neurotransmitter filled vesicles to the presynaptic membrane. Vesicle fusion to the membrane is facilitated by soluble N-ethylmaleimide-sensitive factor attachment protein receptors (SNARE) proteins, including synaptobrevin-1 attached to synaptic vesicles, and synaptosomal-associated protein 25 (SNAP25) which are anchored in the presynaptic membrane (Mohrmann *et al.*, 2013; Sudhof, 2013; Shen *et al.*, 2014; Salpietro *et al.*, 2017; Shen *et al.*, 2017). Once fused, acetylcholine (ACh) is released from motor neurons into the synaptic cleft where it binds to postsynaptic AChRs. The AChR ion channel opens, allowing a flow of cations through the central pore which depolarises the muscle membrane and generates an endplate potential (EPP). If the EPP reaches threshold, voltage gated- Na^{+} channels ($Na_v1.4$) along the membrane open to produce an action potential resulting in Ca^{2+} release from the sarcoplasmic reticulum (SR) into the cytosol which ultimately induces muscle contraction (Ferraro *et al.*, 2012).

After dissociation from the AChR, ACh molecules are hydrolysed by acetylcholinesterase (AChE) which comprises a collagenic-tail (COLQ). Choline is transported back into the nerve terminal by a high-affinity choline uptake transporter. ACh is resynthesized from choline and acetyl coenzyme A by choline acetyltransferase (ChAT), and is packaged into synaptic vesicles via the vesicular acetylcholine transporter (VAChT), (Figure 1.1).

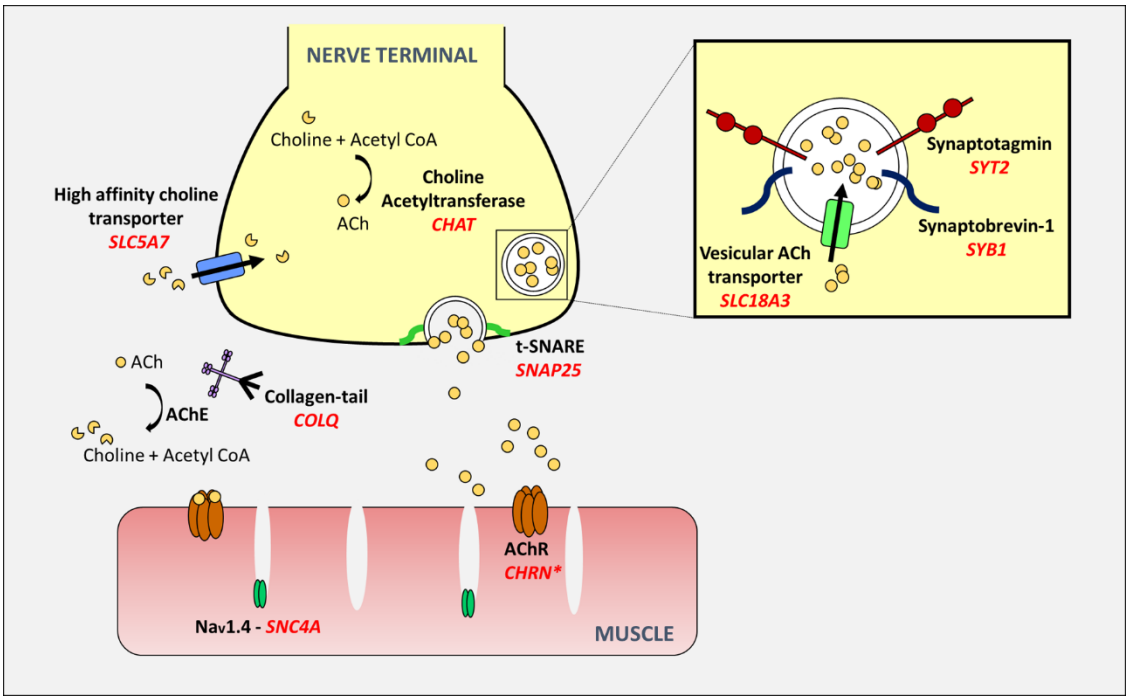

Figure 1.1 Schematic of the acetylcholine receptor system and neurotransmission. Key proteins directly involved in neurotransmission are shown. ACh synthesis is catalysed by ChAT. ACh are packaged into synaptic vesicles via VAChT. Neurotransmitter filled vesicles are transported to the presynaptic membrane and released into the synaptic cleft by SNARE proteins (synaptotagmin-2, synaptobrevin-1 and SNAP25). ACh binds to AChRs to depolarise the muscle membrane. Subsequently $Na_v1.4$ channels along the membrane open to produce an action potential. AChE hydrolyses ACh, and the resulting choline molecules are transported back into the presynaptic terminal for recycling via the high affinity choline transporter. Genes encoding proteins implicated in CMS are shown (red). CHRN* represents genes encoding all the AChR subunits (CHRNA, CHRNB, CHRND, CHRNE).

1.3.2 *Proteins involved in the development and maintenance of the NMJ*

Presynaptic and postsynaptic differentiation of the NMJ involves various proteins that participate in a series of signalling cascades. MuSK is a key molecule located on the postsynaptic muscle membrane. It is an important organiser that acts as a scaffold protein and plays a central role in co-ordinating the formation of the NMJ through its binding partners (Zong and Jin, 2013). Activation of MuSK mediates postsynaptic differentiation and aggregation of AChR on the postsynaptic membrane (Okada *et al.*, 2006; Chevessier *et al.*, 2008). One mechanism by which MuSK is activated is through the binding of neurally secreted agrin to low-density lipoprotein-related protein receptor 4 (LRP4) (Maselli *et al.*, 2010; Choi *et al*., 2013). Formation of the agrin-LRP4-MuSK complex stimulates tyrosine phosphorylation of MuSK. This complex is essential for mediating the downstream signalling cascade required for AChR clustering (Zong and Jin, 2013). Once phosphorylated, MuSK recruits docking-protein 7 (Dok-7), a cytoplasmic adaptor protein selectively expressed in muscle. Dok-7 further stimulates MuSK kinase activity through phosphorylation (Maselli *et al.*, 2010). Together, this stimulates rapsyn which is also a scaffolding protein at the NMJ. Activation of rapsyn results in the reorganisation of the cytoskeleton and anchoring of AChR on the muscle membrane (Ohkawara *et al.*, 2014), (Figure 1.2).

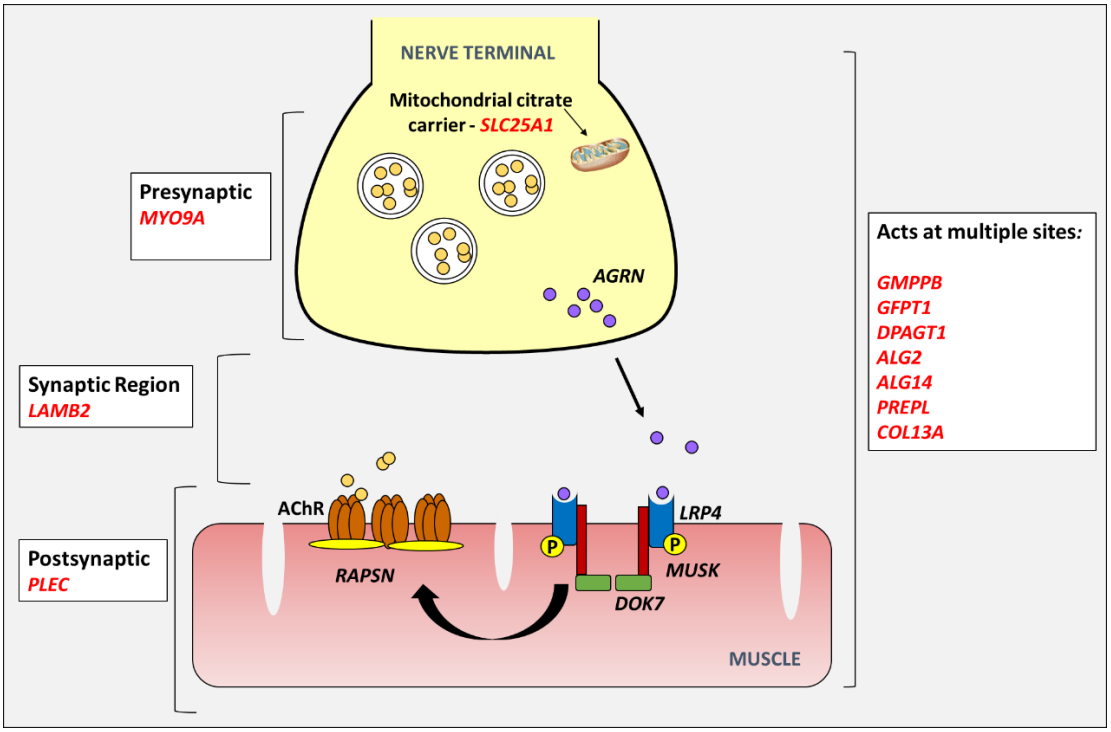

Figure 1.2 Key molecules involved in the development and maintenance of the NMJ. AChRs are recruited and anchored to the muscle membrane through a series of presynaptic and postsynaptic protein interactions involving agrin, LRP4, MuSK, Dok-7 and rapsyn. Genes encoding proteins directly involved in AChR clustering are shown (black). Additional genes encoding proteins that are implicated in CMS are shown (red).

1.4. The safety margin of neurotransmission is compromised in CMS

Neurotransmission is a highly reliable process whereby an excess of neurotransmitters is released into the synaptic cleft, which is more than the amount required to initiate an action potential. Even during prolonged high-frequency activation of muscles, transmission does not fail due to the substantial number of neurotransmitters available. This has given rise to the idea of a 'safety margin' at the NMJ. The safety margin of the NMJ is described as the factors that maintain the efficacy of chemical synapses. In CMS, the safety margin of neurotransmission is compromised by one or more mechanisms. Factors affecting the ability to propagate an action potential are grouped into the following categories: (i) compromised number of ACh molecules available per synaptic vesicle which arises due to impaired synthesis, hydrolysis and packaging of ACh into vesicles, and the reuptake of choline; (ii) impaired quantal release of ACh due to impairment in trafficking, vesicle docking and fusion to the membrane; (iii) factors affecting the efficacy of quanta released such as the rate of ACh hydrolysis in the synaptic space, AChR affinity for ACh, and the density, kinetic properties and localization of AChRs and $Na_v1.4$ ion channels. These factors ultimately compromise the amplitude of the EPP and formation of an action potential (Wood and Slater, 2001; Engel and Sine, 2005; Slater, 2008; Engel, 2012).

The safety margin may also be compromised by structural changes in presynaptic or postsynaptic components of the NMJ. The number of neurotransmitters released is relative to the size of the motor nerve terminal, therefore abnormally smaller nerve terminals may impair quantal release. Postsynaptic junctional folds harbour a high density of Na^+ channels in the troughs of the folds and increase the series resistance of the postsynaptic membrane, which are both important for membrane depolarisation. Another possibility is an increased chance of acetylcholine escaping the synaptic cleft before it reaches the postsynaptic membrane. Simplification of the folds may therefore be a major contributor to impaired neurotransmission (Wood and Slater, 2001).

1.4.1 *Pathology of the acetylcholine receptor system*

The most common type of CMS arises due to defects in the nictonic AChR itself, which accounts for approximately 60% of all CMS cases (Hantai *et al.*, 2013). The adult AChR is a pentameric structure composed of alpha (α), beta (β), delta (δ), and epsilon

(ε) subunits in a 2:1:1:1 ratio. The fetal form of AChR contains a gamma (γ) subunit in place of the ε subunit. This structure permits binding of two ACh molecules to the AChR ion channel. The correct configuration of AChR is important for neurotransmission. Mutations in individual subunits can result in reduced expression of the AChR or impair the kinetic properties of the channel, giving rise to fast and slow channel CMS. Dominantly inherited slow channel syndromes occur because of prolonged opening of the AChR ion channel. This is in contrast to the recessively inherited fast channel syndromes, which occur due to premature closure of the AChR channel (Webster *et al.*, 2013). Each AChR subunit is also subject to post-translational modifications including glycosylation. Defective glycosylation of AChR subunits impair the assembly, structure, and function of AChRs on the postsynaptic membrane (Ramanathan and Hall, 1999). Mutations in the *CHRNG* gene encoding the fetal γ subunit of the ACh gives rise to the fetal myasthenic disease, Escobar syndrome. This disease is believed to affect neuromuscular organogenesis, with no pathogenicity later in life since γ expression is restricted to early development (Hoffmann *et al.*, 2006).

CMS also arise due to defects in the processes involved in the synthesis and hydrolysis of ACh. Mutations in *SLC5A7* encoding the high affinity choline transporter impairs reuptake of choline into the presynaptic nerve terminal (Bauche *et al.*, 2016), and mutations in *SLC18A3* encoding the vesicular ACh transporter impairs uptake of ACh into synaptic vesicle (O'Grady *et al*., 2016; Aran *et al.*, 2017). The synthesis of ACh is impaired as a result of *CHAT* mutations (Brandon *et al.*, 2003; Dilena *et al.*, 2014), and mutations in *COLQ*, (the gene encoding the collagenic-tail subunit that binds AChE) resulting in endplate AChE deficiency (Sigoillot *et al*., 2016). Consequently, hydrolysis of ACh is disrupted (Guven *et al.*, 2012; Wargon *et al.*, 2012).

More recently, genes encoding proteins required for mediating exocytosis have been identified as pathogenic in CMS. Mutations in *SYT2*, the gene encoding synaptotagmin-2, impairs trafficking of neurotransmitter filled vesicles to the presynaptic membrane (Herrmann *et al*., 2014; Whittaker *et al.*, 2015). Docking and fusion of vesicles to the presynaptic membrane is compromised by mutations in *SNAP25* (Mohrmann *et al.*, 2013*)* and *SBY1* (Shen *et al.*, 2017) that express defective SNAP25 and synaptobrevin-1 proteins respectively. Defects in any of the processes described that lead to compromised quantal release and a reduction of EPP amplitude, ultimately leads to impaired neurotransmission.

Defective $Na_v1.4$ channels on the muscle membrane directly affects the ability to propagate an action potential which demonstrates that the safety margin for neuromuscular transmission can be compromised despite have a normal EPP (Tsujino *et al.*, 2003).

1.4.2 *Impaired development and maintenance of the NMJ*

Efficient neurotransmission can only occur upon the correct assembly and maintenance of the NMJ which is dependent on several signalling molecules and sequential communication between the presynaptic motor neuron and the postsynaptic muscle membrane (Witzemann *et al.*, 2013; Zong and Jin, 2013). Neurotransmission is compromised in the absence of fully functional proteins encoded by *AGRN*, *MUSK*, *LRP4*, *DOK7*, and *RAPSN* (Gautam *et al.*, 1996; Ioos *et al.*, 2004; Okada *et al.*, 2006; Chevessier *et al.*, 2008; Huze *et al.*, 2009;). Ultimately, defective proteins involved in this signalling complex affect the clustering properties of AChR on the postsynaptic membrane.

1.4.3 *Mutations in CMS-causing genes with indirect functions*

Several proteins have been identified as causative genes in CMS other than those having a direct effect on the development and maintenance of the NMJ and neurotransmission. Some of these proteins are known to affect NMJ morphology, which subsequently affects neurotransmission. Other proteins are required to yield precursors, or undergo protein interactions upstream or downstream of NMJ formation and synaptic transmission.

Mutations in genes encoding plectin, laminin beta-2, COL13A, and MYO9A induce morphological changes to the NMJ. A deficiency in plectin results in a lack of cytoskeletal support of the junctional folds at the NMJ. Simplified junctional folds affect the density of $Na_v1.4$ channels concentrated in troughs between the folds, thus increasing the threshold for the generation of an action potential (Selcen *et al.*, 2011). Laminin beta-2 deficiency also induces simplification of synaptic folds as well as hypoplastic nerve terminals. Together these morphological changes impair EPP quantal content and efficacy (Maselli *et al.*, 2009).

A deficiency in COL13A results in impaired maturation and maintenance of the synaptic structure, whereby AChR clustering and co-localisation of the nerve terminal and postsynaptic AChR is compromised, and overshooting of the presynaptic nerve terminal is observed (Logan *et al.*, 2015). Mutations in *MYO9A* lead to impairment of neuronal morphology and function through the regulation of Rho activity in neurons (O'Connor *et al.*, 2016). Mutations in *SLC25A1* results in abnormal mitochondrial citrate carrier function, and abnormal nerve outgrowth and synapse formation is observed (Chaouch *et al.*, 2014). Defects in the geometry of both presynaptic and postsynaptic structures reduces the surface contact at the NMJ which ultimately impairs neurotransmission.

The safety factor of neurotransmission is also compromised by mutations in *PREPL*. PREPL is an essential activator of the clathrin associated adaptor protein 1 (AP1). AP1 facilitates packaging of ACh molecules into synaptic vesicles. Impaired PREPL function results in decreased vesicular content of ACh (Régal *et al.*, 2014; Engel *et al.*, 2015).

1.4.4 *The role of glycosylation defects in CMS*

Whilst mutations in proteins active at the NMJ are known to be pathogenic in CMS, recent genetic analysis has also led to the implication of genes involved in the glycosylation of these proteins. Protein glycosylation is important for protein folding, secretion, solubility, stability and ability to bind to other proteins (Ramanathan and Hall, 1999; Martin, 2003). To date, 5 CMS-causing glycosylation genes have been discovered, *GFPT1* (Senderek *et al.*, 2011), *DPAGT1* (Belaya *et al.*, 2012), *ALG2* and *ALG14* (Cossins *et al.*, 2013), and *GMPPB* (Belaya *et al.*, 2015). *GFPT1* encodes an enzyme that catalyses the rate-limiting step of the hexosamine pathway (Figure 1.5). *DPAGT1*, *ALG2* and *ALG14* encode the early components of the N-linked glycosylation pathway (Bretthauer, 2009; Basiri *et al.*, 2013; Cossins *et al.*, 2013). *GMMPB* catalyses the synthesis of GDP-mannose which is a precursor for N- and O-linked glycosylation (Belaya *et al.*, 2015).

All 5 glycosylation genes identified are ubiquitous and potentially modify hundreds of proteins in other biological process in addition to NMJ proteins. *DPAGT1* (Wu *et al.*, 2003; Carrera *et al.*, 2012; Wurde *et al.*, 2012), *ALG2* (Thiel *et al.*, 2003) and *GMPPB*

(Carss *et al.,* 2013) have previously been associated with congenital disorders of glycosylation (CDG). CDG encompass an array of phenotypically diverse disorders affecting multiple systems including the central nervous system, muscle function, transport of molecules, the immune and endocrine systems, and coagulation (Leroy, 2006; Scott *et al.,* 2014). It is therefore surprising why mutations in CMS-causing genes predominantly affect the NMJ with little or no involvement of multiple organ systems.

1.5 Glycosylation

Glycosylation is a post-translational modification which occurs in numerous biosynthetic pathways and is essential for obtaining functional lipids and proteins (Parkinson *et al.*, 2013; Freeze *et al.*, 2014). The attachment of glycans (sugar residues) to a protein through enzymatic glycosylation is essential to produce functional proteins (Parkinson *et al.*, 2013; Zoltowska *et al.,* 2013). Two major protein glycosylation pathways are the N- and O-glycosylation pathways (Spiro, 2002).

1.5.1 *N- and O- linked glycosylation pathways*

N-glycosylation is the most prevalent type of post-translational modification where glycans attach onto an amide nitrogen on an asparagine residue of the protein being modified. The *N*-acetylglucosamine (GlcNAc) glycan linkage is the most common type of N-glycosylation (Parkinson *et al.,* 2013). O-linked carbohydrate attachments to proteins involve a linkage between a monosaccharide and amino acids serine or threonine. There are many different classes of O-linked glycosylation that differ based on the monosaccharide involved in the linkage. Examples of O-linked glycans include O-GalNAc, O-fucose, O-glucose, O-mannose and O-GlcNAc. In this study we are interested in the O-GlcNAc modification whereby proteins are modified by the attachment of GlcNAc in an O-glycosidic linkage to serine or threonine residues (Figure 1.3).

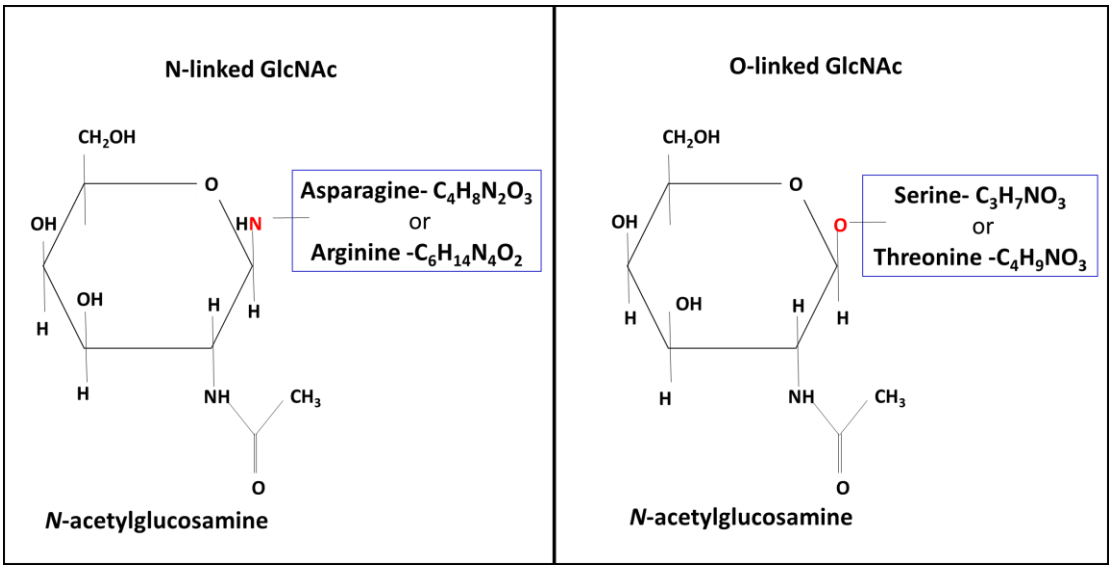

Figure 1.3. Examples of protein-glycan linkages in N- and O-linked glycosylation. The difference between the two types of glycosylation is where the oligosaccharide is attached to the protein. In N-linked glycosylation the glycan is attached through a nitrogen atom (*N*H) at the asparagine or arginine residues on the protein. In O-linked glycosylation the glycan is attached through an oxygen on a hydroxyl group (*O*H) to a serine or threonine residue. This image was adapted from (Lodish *et al*., 2000).

The biosynthesis of N-linked glycans occurs via 3 major steps. The first step is the synthesis of a dolichol-linked precursor oligosaccharide. This process occurs whereby dolichol phosphate (Dol-P) located on the cytoplasmic face of the endoplasmic reticulum (ER) membrane receives GlcNAc-1-P from the nucleotide sugar donor Uridine diphosphate *N*-acetylglucosamine (UDP-GlcNAc) to generate dolichol pyrophosphate *N*-acetylglucosamine (Dol-P-P-GlcNAc). This reaction is catalysed by Dolichyl-Phosphate N-Acetylglucosaminephosphotransferase 1 enzyme encoded by *DPAGT1*.

The second step involves the addition of glucose and mannose sugar molecules in a step-wise manner. The addition of each sugar is catalysed by specific glycotransferases. *ALG2* and *ALG14* encode glycotransferase enzymes required for extension of the glycan.

During assembly, the oligosaccharide is transported to the luminal side of the ER where further sugar residues are added. Once formation of the oligosaccharide is completed, the glycan is transferred from the dolichol to a nascent protein. The final step is remodelling of the protein bound N-glycan in the ER and Golgi through the addition and removal of sugar residues to produce different glycoforms (Figure 1.4), (Stanley *et al*., 2009; Aebi, 2013).

O-linked glycosylation is a more diverse and complex process which involves the attachment of a single monosaccharide to a hydroxyl group on serine or threonine residues on the newly synthesised protein. The O-GlcNAc modification is a highly dynamic process that takes place within the nuclear and cytoplasmic compartments of a cell. This reaction utilises the UDP-GlcNAc precursor and is catalysed by O-GlcNAc transferase (OGT) (Hanover *et al.*, 2010). The GlcNAc is generally not extended by sugar residues to form more complex structures. Instead, it is attached and removed several times at the same or different O-linked sites on a polypeptide, mimicking phosphorylation of proteins rather than the extension of sugars observed in the typical protein glycosylation system (Yang *et al.*, 2007). This process is commonly referred to as O-GlcNAcylation (Hart and Akimoto, 2009).

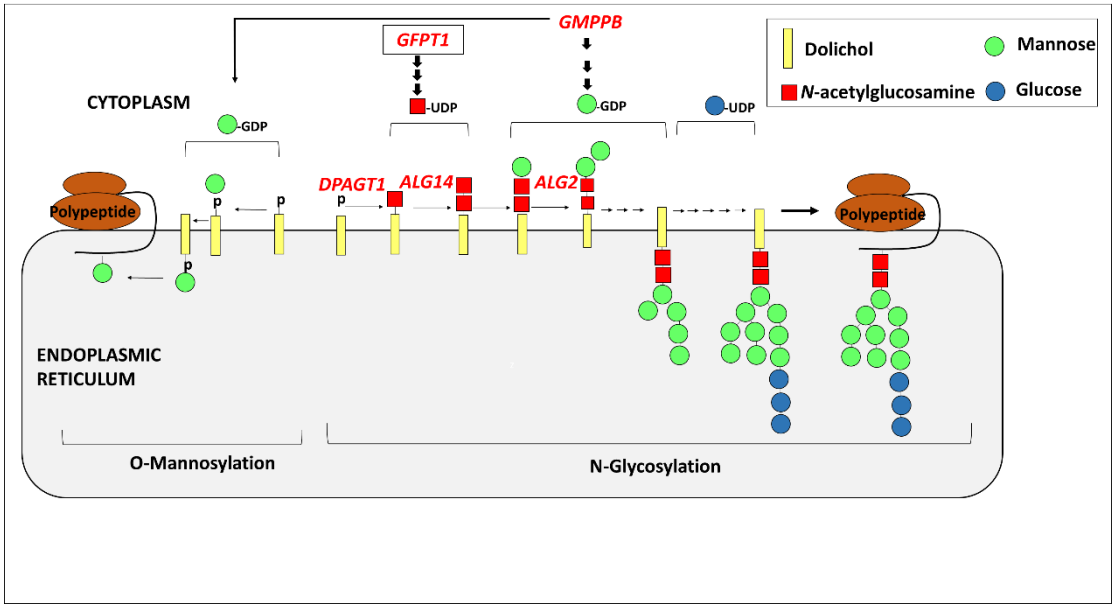

Figure 1.4. Schematic showing the N-glycosylation and O-mannosylation pathways. N-glycosylation begins with the addition of UDP-GlcNAc to a dolichol anchor. Subsequent steps involve the addition of sugar residues in the cytoplasm and ER. Once assembled, the oligosaccharide is transferred to an N-linked site on a nascent protein. O-mannosylation involves the transfer of a mannose sugar to an O-linked site on a nascent protein. All 5 glycosylation enzymes associated with CMS are shown (red). This image was adapted from (Belaya *et al.*, 2015).

1.5.2 *Essential precursors for N- linked glycosylation, O-GlcNAcylation, and O-mannosylation*

The first step of the N-linked glycosylation and O-GlcNAcylation pathways require UDP-GlcNAc which acts as a nucleotide sugar donor. This activated precursor is produced by a series of enzymatic reactions in the hexosamine biosynthesis pathway (Freeze *et al.*, 2014). The GFPT1 enzyme catalyses the first rate-limiting step of these reactions which ultimately yields UDP-GlcNAc (Figure 1.5).

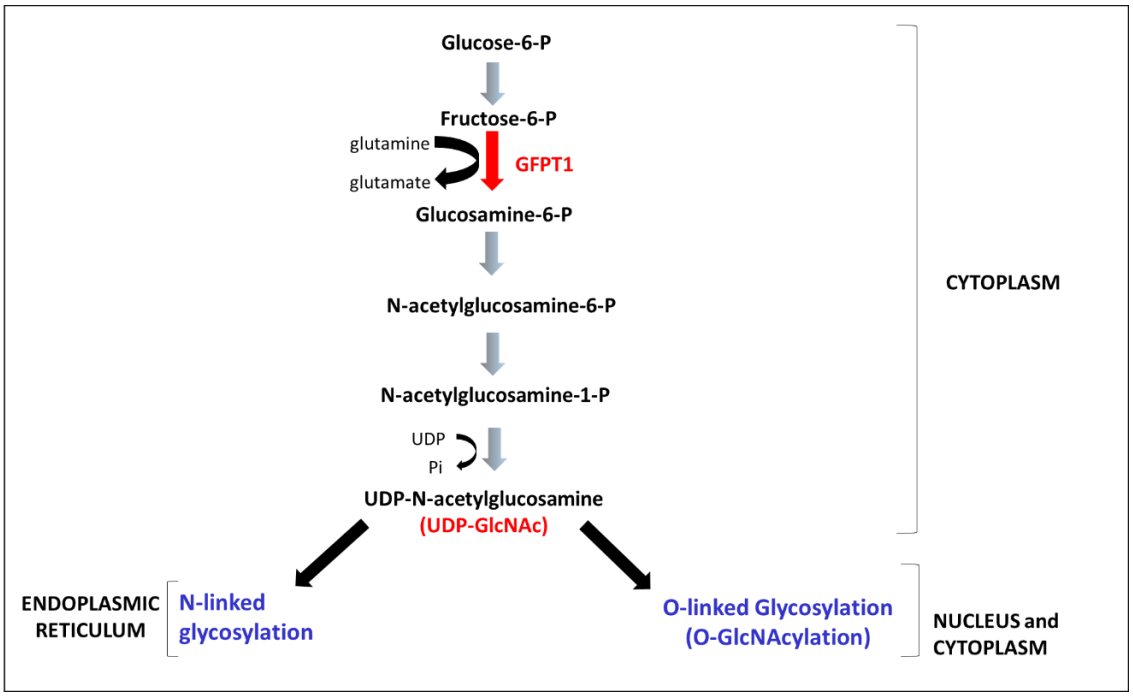

Figure 1.5. The hexosamine biosynthetic pathway. GFPT1 catalyses the conversion of fructose-6-phosphate and glutamine to glucosamine-6-phosphate and glutamate. Subsequent steps yield UDP-GlcNAc, an important precursor required for N- and O-linked glycosylation of proteins. This figure was adapted from (Zoltowska *et al.*, 2013).

Subsequent steps involving the extension of glycans in the N-glycosylation pathway require GDP-mannose precursor molecules. GDP-mannose is also the substrate of cytosolic mannosyltransferases required for the first step in O-mannosylation of proteins (Figure 1.4) (Carss *et al.*, 2013; Belaya *et al.*, 2015; Rodriguez Cruz *et al.*, 2016). GMPPB catalyses the synthesis of GDP-mannose from GTP and mannose-1-phosphate. Mutations in *GMPPB* have also been implicated in CMS (Belaya *et al.*, 2015).

1.5.3 *NMJ proteins that undergo glycosylation*

Several presynaptic, synaptic and postsynaptic NMJ proteins are known to harbour N-linked glycosylation sites (Table 1.2). These proteins use UDP-GlcNAc as the initial precursor for N-linked glycosylation. Importantly, some proteins mentioned here also undergo O-linked glycosylation, but are processed in pathways which require sugar nucleotide donors other than GlcNAc. Mutations in these proteins have previously been implicated in CMS (Herbst *et al.*, 2009; Senderek *et al.*, 2011; Zoltowska *et al.*, 2013).

Protein	Gene
PRESYNAPTIC	
Agrin	*AGRN*
High-affinity choline transporter	*SLC5A7*
Vesicular acetylcholine transporter	*SLC18A3*
Synaptotagmin-2	*SYT2*
SYNAPTIC	
Collagen-like tail of AChE	*COLQ*
Laminin beta-2	*LAMB2*
POSTSYNAPTIC	
MuSK	*MUSK*
LRP4	*LRP4*
$Na_v1.4$ - voltage-gated sodium channel	*SCN4A*
AChR (α, β, δ, ε, fetal γ) subunits	*CHRN**
MULTIPLE SITES	
Dolichyl-Phosphate N-Acetylglucosaminephosphotransferase 1	*DPAGT1*

Table 1.2. NMJ proteins with known N-linked glycosylation sites. Mutations in these proteins have previously been implicated in CMS, (* represents any AChR subunit).

1.6 Mutations in *GFPT1* cause CMS

1.6.1 *Biology of the* GFPT1 *protein*

The *GFPT1* gene is located on chromosome 2p13.3 and comprises 19 exons, plus an additional alternative exon 8a. Splicing of *GFPT1* gives rise to two variants, the ubiquitous GFPT1 isoform and GFPT1-L. The latter is a long muscle-specific isoform expressed predominantly in skeletal muscle and the heart. This isoform contains a 54-bp (18 amino acid) insertion (exon 8a) in the coding sequence of GFPT1, at the position 229 in human GFPT1. Missense mutations in *GFPT1* have been found outside of the muscle-specific exon, yet impaired function seems to be restricted to the muscle, and in particular the NMJ (Zoltowska *et al.*, 2013). Since protein glycosylation is an essential process for cell survival, it is believed that mutations in *GFPT1* may generate hypomorphic alleles. A total of 31 GFPT1 pathogenic variants have been identified which comprise missense, frameshifts, nonsense and one variant in the 3'-UTR (Figure 1.6). No individual with CMS that harbour 2 null variants have been identified (Abicht *et al*., 2016). These variants lead to reduced expression of the GFPT1 protein. Only one patient has been identified who harbours a nonsense mutation in the ubiquitous GFPT1 isoform and a second mutation that disrupts the muscle-specific exon, leading to a complete loss of glycoprotein expression in muscle (Senderek *et al*., 2011; Selcen *et al*., 2013).

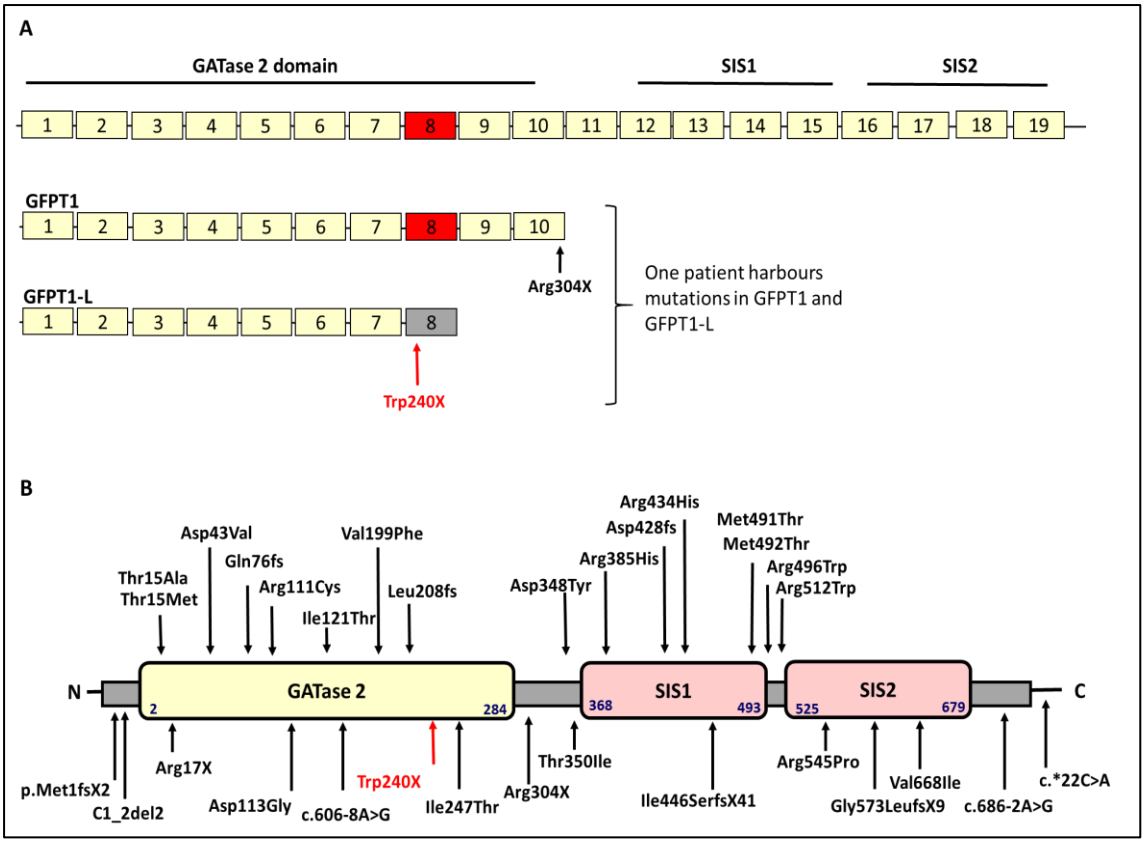

Figure 1.6. Schematic representation of the GFPT1 exon and protein structure. (A) GFPT1 exon structure with 3 domains. The muscle-specific exon is shown in red. Predicted peptides of mutant transcripts from a patient with a nonsense mutation in the ubiquitous GFPT1 isoform, and a nonsense mutation in the muscle-specific GFPT1 isoform are shown. (B) The localization of the missense and truncation mutations identified in *GFPT1*-CMS patients are shown. A single mutation was identified in the muscle specific exon (red). GATase_2, glutamine amidotransferase type 2 domain; SIS1, sugar isomerase domain-1, SIS-2, sugar isomerase domain-2. This image was adapted from (Zoltowska *et al.*, 2013).

1.6.2 *Clinical presentation of patients with mutations in GFPT1*

Patients with mutations in *GFPT1* usually display a limb-girdle pattern of weakness that may present as early as infancy through to adulthood. The limb-girdle phenotype is characterised by weakness of the proximal limb muscles including the shoulders and pelvis. The weakness is slowly progressive, but the rate of progression varies between patients. These patients also demonstrate sparing of the ocular, facial and bulbar muscles (Guergueltcheva *et al*., 2012; Huh *et al*., 2012; Selcen *et al*., 2013).

Studies have shown that some patients display a decremental response to electromyography (EMG) (Selcen *et al*., 2013; Maselli *et al*., 2014) and repetitive nerve stimulation (Guergueltcheva *et al*., 2012; Huh *et al*., 2012). Patients display endplates with a simplification of the postsynaptic membrane with fewer poorly developed junctional folds and the presence of tubular aggregates of the SR in muscle biopsies (Huh *et al*., 2012; Selcen *et al*., 2013; Maselli *et al*., 2014). These individuals demonstrate an improvement in symptoms in response to cholinesterase inhibitors and 3,4-diaminopyridine (3,4-DAP) (Nicole *et al.*, 2014). More recently magnetic resonance imaging (MRI) studies have detected fatty infiltration of muscles in *GFPT1*-CMS patients, indicative of progressive muscle damage (Finlayson *et al.*, 2016).

Until now there has only been one report of a mutation which disrupts the GFPT1-L isoform resulting in the absence of glycosylated proteins. A muscle biopsy from this patient demonstrates a vacuolar autophagic myopathy with abnormal variation of myofibre size, sparse regenerating and necrotic muscle fibres and densely packed membranous tubular aggregates (Selcen *et al*., 2013). A molecular link between the presence of tubular aggregates and NMJ remains to be established.

Notably, patients with *GFPT1*-related CMS share many phenotypic and morphological characteristics to patients with mutations in other glycosylation enzymes implicated in CMS. Patients with mutations in *DPAGT1* also demonstrate a limb-girdle pattern of weakness, tubular aggregates in muscle biopsies and a prominent fatty infiltration of muscles revealed by MRI imaging (Belaya *et al.*, 2012; Basiri *et al.*, 2013; Carss *et al.*, 2013; Belaya *et al.*, 2015; Finlayson *et al.*, 2016).

1.7 Diagnosis and treatment of CMS

1.7.1 *Diagnosis of CMS*

Indications for CMS at initial presentation are based on a clinical examination and family history of fatigable weakness consistent with the patterns of autosomal dominant or recessive inheritance. Electrophysiological testing using a decremental EMG response of the compound muscle action potential (CMAP) is also a good indicator of CMS. Differential diagnosis is based on the absence of AChRs and anti-MuSK auto-antibodies in serum, and failure to respond to immunosuppressive therapy as a test to rule out myasthenia gravis. Furthermore, lack of major pathology in skeletal muscle biopsies can help distinguish CMS from other neuromuscular diseases (Abicht *et al.*, 2012).

Pharmacological intervention greatly depends on our understanding of the mechanisms underlying the different subtypes of CMS. Some drugs used to treat one subtype of CMS may worsen symptoms in a patient suffering from another subtype (Engel, 2007; Lorenzoni *et al.*, 2012; Engel *et al*., 2015). The use of functional studies to enhance our understanding of the molecular mechanisms underlying a CMS subtype may prove useful when choosing a personalised treatment regime (Schara and Lochmüller, 2008; Barisic *et al.*, 2011).

Clinical manifestations amongst individuals harbouring the same genetic defect vary in terms of onset and course of disease which often hinders correct diagnosis. This is overcome by *in vitro* electrophysiological studies of the patient endplate and molecular genetic studies. A definitive genetic diagnosis is important for choosing treatment regimes, prognosis and genetic counselling (Engel, 2012).

1.7.2 *Treatment of CMS*

Common drugs used to alleviate CMS symptoms include AChE inhibitors, 3,4-DAP, fluoxetine, quinidine sulphate, salbutamol and ephedrine (Schara and Lochmüller, 2008).

Pyridostigmine is an AChE inhibitor that has demonstrated positive effects in several different forms of CMS. AChE inhibitors prevent the hydrolysis of ACh in the synaptic cleft, prolonging ACh activity. Patients who suffer from CMS as a result of AChE deficiency should not be given AChE inhibitors as it may worsen muscle weakness and have harmful effects (Schara and Lochmüller, 2008). 3,4-DAP is a potassium channel blocker which acts on the presynaptic nerve terminal resulting in an increase in the quantal release of ACh into the she synaptic cleft. Again, it may be detrimental to administer 3,4-DAP to individuals with fast-channel CMS emphasising the importance of understanding the pathophysiology at the NMJ (Abicht *et al.*, 2012). Both pyridostigmine and 3,4-DAP reduce myasthenic weakness by facilitating neurotransmission.

Slow-channel CMS are often treated with quinidine sulphate and fluoxetine. Both drugs are AChR channel blockers which reduces the amount of time that the AChR pore remains open and may be harmful in the other forms of CMS (Engel, 2007).

Orally administered salbutamol, a β2-adrenergic receptor agonist demonstrates improved muscle function in patients harbouring mutations in *DOK-7* (Burke *et al.*, 2013). Ephedrine has also shown to exert positive effects in various forms of CMS. *In vitro* studies demonstrate its ability to increase quantal ACh release and reduce AChR opening time. However, this mechanism is yet to be seen in humans (Schara and Lochmüller, 2008). CMS drugs are frequently used in combinations to achieve optimal relief from symptoms.

1.8 Functional models used to study CMS

To date several experimental assays have been developed to help broaden our understanding of the molecular mechanisms responsible for the formation and maintenance of the NMJ. Whole exome sequencing has accelerated the rate at which new disease-causing genes are being discovered (Lyon and Wang, 2012). As more and more gene mutations are identified, we need to be able to investigate and understand the functions of NMJ proteins in order to choose the best possible treatment options for patients with CMS. Methods currently being used include observing structural and functional abnormalities in patient muscle biopsies and analysing changes in the level of protein expression (Belaya *et al.*, 2012; Zoltowska *et al.*, 2013). Functional assays

which have been developed include recombination expression studies, the use of siRNAs to knockdown gene function in cell culture and zebrafish, and *in vitro* electrophysiological tests to measure AChR activity (Senderek *et al.*, 2011; Cossins *et al.*, 2013; Zoltowska *et al.*, 2013). Several *in vivo* mouse models have also been developed which have contributed to our understanding of major synaptic regulators at the NMJ which are implicated in CMS. These include models for studying the role MuSK (Chevessier *et al.*, 2008; Messéant *et al.*, 2015), AGRN (Bogdanik and Burgess, 2011), DOK-7 (Okada *et al.*, 2006), ChAT (Brandon *et al.*, 2003), ColQ (Sigoillot *et al.*, 2016) and the AChR epsilon subunit at the NMJ (Chevessier *et al.*, 2012; Webster *et al.*, 2013). As of yet, there are no mouse models for the 5 glycosylation genes found to be pathogenic in CMS.

1.8.1 *Functional studies that have contributed to understanding the role of* GFPT1 *at the NMJ*

Several experiments were conducted in attempt to deduce the molecular pathogenesis of GFPT1 in neurotransmission. There are several lines of evidence which suggest that GFPT1 has a direct effect on the number of AChR clusters expressed on the muscle membrane. The use of siRNA to silence *GFPT1* and a chemical inhibitor to reduce the levels of GFPT1 in cell culture, have both demonstrated a reduction in AChR expression, consistent with AChR expression pattern in patient muscle biopsies (Zoltowska *et al.*, 2013). Furthermore, treatment with tunicamycin, an N-glycosylation inhibitor was also found to reduce the levels of AChR expression *in vitro* (Merlie *et al*., 1982; Belaya *et al*., 2012). Further investigation has shown that silencing *GFPT1* results in a reduction in AChR α, δ, and ε subunits (Zoltowska *et al.*, 2013). This observation is consistent with the idea that glycosylation is an essential process for the correct assembly and export of the AChR pentamer from the ER. The CMS phenotype was examined in zebrafish embryos using morpholino-mediated knockdown of *gfpt1*. Embryos show a delayed onset of NMJ maturation alongside aberrant motility and swimming behaviour (Senderek *et al*., 2011). Together these data reinforce the importance of GFPT1 in normal formation of the NMJ.

There is currently no knockout mouse model for studying the role of GFPT1 in muscle and NMJ structure and function. A *Gfpt1* knockout mouse model will provide an invaluable tool for studying numerous pathological changes occurring because of glycosylation defects.

1.9 The use of mouse models for studying CMS

Mouse models serve as better tools for studying CMS related gene mutations than *in vitro* and zebrafish models due to the disparity between the latter and the patients. Morphological abnormalities in zebrafish can only be studied in the developmental phenotype as morpholino knockdowns that are currently available are only effective for 4-5 days. This model therefore does not allow for long-term progression studies.

There are many advantages of using mouse models over other model organisms. There is ~99% genetic homology between mice and humans (Waterston *et al.*, 2002; Vandamme, 2014), whereas zebrafish display ~70% genetic homology to humans (Kerstin *et al*., 2013). Furthermore, the structural components and functional properties encompassing mouse muscle closely resembles that of human muscle. Knockout mice provide valuable information about the function of a gene and the pathways it is involved in. The development of transgenic mice has been greatly facilitated by advancements in technology that have made genetically modified mice widely available.

In addition to the parameters measured *in vitro*, mouse models allow phenotype analysis and observation of general muscle pathology, examination of whole NMJ and testing for fatigue, which can be correlated to phenotypes seen in CMS patients. More importantly, they enable the assessment and development of therapeutic compounds.

1.10 Strategies for generating knockout mouse models

Advancements in mouse mutagenesis has made the mouse model a valuable tool for studying gene function. Numerous techniques have been developed to create knockin and knockout mouse models of human disease. Here we describe the gene targeting strategies used to modify *Gfpt1* in the mouse genome for this study.

1.10.1 *Gene targeting strategies*

In a germline knockout strain, the target gene is inactivated in all cells throughout development (Figure 1.7A). Often knockout mice homozygous for the null allele may result in embryonic or postnatal lethality due to unpredicted activity of that gene and whether it is essential for the viability of the mice. One method to overcome this problem is using a conditional knockout strategy which allows inactivation of the gene in specific cell types. In conditional knockout strains, the gene of interest is modified in the germline, but is only inactivated following intervention (Figure 1.7 B). A third strategy often used in an inducible-Cre transgenic mouse model. This model allows for spatial and temporal regulation of Cre-mediated recombination which can be activated by *in vivo* administration of tamoxifen (Figure 1.7C), (Friedel *et al*., 2011).

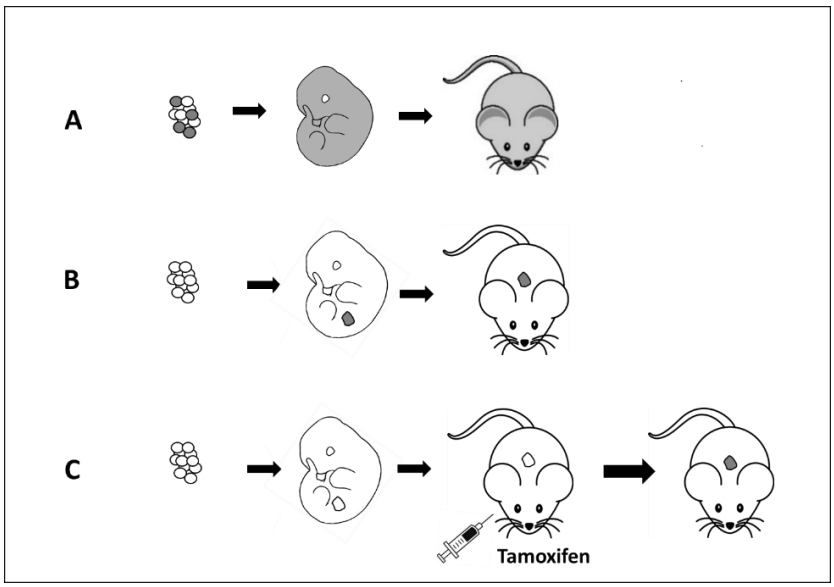

Figure 1.7. Gene targeting strategies. (A) Germline inactivation of a gene results in inactivation of all cells. (B) Conditional mutants demonstrate knockout of a gene in targeted tissues only. (C) Selected cells are inactivated following administration of tamoxifen. Inactivation of genes are shown in grey. This image was adapted from (Friedel *et al*., 2011).

1.10.2 *Site specific recombination using Cre/loxP technology*

One method of gene targeting is site-specific recombination widely used to carry out deletions, translocations and inversions at specific sites in DNA. This method relies on site-specific recombinases, Cre recombinase derived from bacteriophage P1 and flippase (FLP) recombinase derived from yeast which recombine DNA between identical *loxP* and *FRT* sites respectively. The 34 base pair recombinase target site sequence consists of an asymmetric 8bp sequenced flanked by 13bp palindromic sequences. The orientation of the *loxP* and *FRT* sites is important for determining the type of recombination (Nagy *et al*., 2000; Skarnes *et al*., 2011). The forthcoming chapters will further describe the Cre/loxP techniques used to generate a knockout mouse model in this study.

1.11 Statement of aims

Chapter 3

To generate a GFPT1 deficient mouse model using Cre/loxP technology. The efficiency and specificity of Cre activity will be assessed to verify GFPT1 deficiency.

Chapter 4

To observe the viability of homozygous and heterozygous *Gfpt1*^{tm1a} and *Gfpt1*^{tm1b} mice. Viable mouse models will be investigated to see whether they display phenotypical abnormalities. The *Gfpt1*^{tm1b} allele will be used to track GFPT1 expression in mouse muscle using the *lacZ*-reporter.

Chapter 5

To further characterise the muscle-specific *Gfpt1* knockout mouse model. The morphology of the synapse will be studied paying attention to the clustering properties of AChRs. This will be tested using immunohistochemical labelling of NMJs. Ultra-structural analyses will be used to identify any abnormalities at the NMJ and in muscle. Functional tests will be used to assess muscle strength. Any failure of efficient assembly and maintenance of the structures at the synapse will be investigated. Proteomic studies will enhance our understanding of the pathophysiological changes in muscle because of GFPT1 deficiency.

Chapter 2. Material and methods

2.1 Standard molecular biology techniques

2.1.1 *DNA extractions*

Ear clips and tail tips were digested in 0.5 mg/ml Proteinase K in DNA digestion buffer (Table 2.1) and incubated at 55˚C overnight. The next day 700 µl of phenol/chloroform/isoamyl alcohol was added and mixed vigorously. Samples were centrifuged at 14,000 rpm for 5 minutes. The supernatant was mixed with 100% ethanol and incubated at -80˚C for 2 hours. Samples were centrifuged at 14,000 rpm for 20 minutes at 4˚C. Supernatants were discarded and pre-cooled 75% ethanol was added to each sample. Samples were centrifuged at 8,000 rpm for 5 minutes at 4˚C. Supernatants were discarded and pellets were suspended in TE buffer.

DNA was extracted from muscle and heart tissues using a DNeasy Blood and Tissue kit (Qiagen). 25 mg of tissue was minced and transferred to a microcentrifuge tube. Samples were processed according to the manufacturer's instructions.

2.1.2 *RNA extractions*

Tissues were homogenised with 1ml Trizol and incubated for 5 minutes at room temperature. Samples were then centrifuged at 12,000 *g* for 10 minutes at 4°C. The supernatant was mixed with 200 µl chloroform and samples were incubated for 3 minutes at room temperature. Next, samples were centrifuged at 12,000 *g* for 15 minutes at 4°C. The resulting upper aqueous phase was transferred to a fresh microcentrifuge tube and mixed with 500 µl of isopropanol. The samples were incubated for 10 minutes at room temperature and centrifuged at 12,000 *g* for 15 minutes at 4°C. The supernatant was discarded. The remaining RNA pellet was washed with 500 µl 70% ethanol in DEPC-treated H_2O and centrifuged at 12,000 *g* for 5 minutes at 4 °C. The supernatant was discarded and the pellet was air dried. The pellet was resuspended in 30 µl DEPC-treated H_2O.

2.1.3 *Reverse transcription cDNA synthesis*

Reverse transcription was performed using a High Capacity cDNA Reverse Transcription Kit (Applied Biosystems) according to the manufacturer's guidelines. The reverse transcription master mix was prepared in a 10 µl reaction mixture listed below.

Component	Volume/Reaction
10X RT Buffer	2.0 µl
25X dNTP mix (100 mM)	0.8 µl
10X RT Random Primers	2.0 µl
MultiScribe™ Reverse Transcriptase	1.0 µl
Nuclease-free H_2O	4.2 µl
Total per reaction	**10 µl**

10 µl of RNA was mixed with 10 µl of the reverse transcription master mix and the samples were placed in a thermocycler.

The thermocycler was set to the following program:

Step 1: 10 minutes at 25°C

Step 2: 120 minutes at 37°C

Step 3: 5 minutes at 85°C

Step 4: ∞ at 4°C

2.1.4 *DNA and RNA measurement*

DNA and RNA concentrations were determined using a NanoDrop spectrophotometer (Thermo Scientific, NanoDrop 2000).

2.1.5 *Genotyping and RT-PCR*

Genotyping was performed by polymerase chain reaction (PCR) using genomic DNA isolated from ear punches and muscle tissue from adult mice, and tail tips from embryos and neonatal mice. RNA isolated from ear punches from adult mice was used for reverse transcription polymerase chain reaction (RT-PCR).

2.1.6 *Polymerase chain reaction*

PCR amplification was conducted using a thermal cycler (SensoQuest, Labcycler 48). Primers used are listed in Table 2.2, 2.3 and 2.4. The PCR reaction was prepared in a 25 µl reaction mixture as listed below.

Component	**Volume (25 µl)**
dNTP mix	1 µl
10x PCR Buffer	2.5 µl
PCR Enhancer	2 µl
Forward primer (10 µM)	1 µl
Reverse primer (10 µM)	1 µl
Template DNA (50 ng/µl)	1 µl
Moltaq DNA polymerase	1 µl
ddH2O	15.5 µl
Total	**25 µl**

PCR reactions were run using the following program:

1. Initial denaturation: 94 °C for 5 minutes
2. Denaturation: 94 °C for 30 seconds
3. Annealing: 60 °C for 30 seconds
4. Extension: 72 °C for 30 seconds
5. Last extension: 72 °C for 5 minutes

39 cycles for steps 2-4. Hold at 4 °C

2.1.7 *Agarose gel electrophoresis*

0.8-2% agarose gels were prepared containing 1 x Tris-Acetate-EDTA (Table 2.1) and SafeView nucleic acid stain (NBS Biologicals). 5 µl of samples were mixed with 6x Blue/Orange loading dye (Promega) and loaded onto gels. Gels were run at 80V for 1 hour. DNA was visualised under UV light using GelDoc-it 310 Imaging System (UVP). The size of the DNA fragments were measured relative to a 100 bp DNA ladder (Promega).

2.1.8 *DNA purification by gel extraction*

For the isolation and purification of a single DNA band, the desired product was visualised and excised under a UV transilluminator. The band was extracted and purified from the agarose gel using QIAquick Gel Extraction Kit (Qiagen) according to manufacturer's instructions.

2.1.9 *DNA sequencing and alignments*

Sequencing was carried out by sequencing service MWG Biotech in Ebersberg, Germany. 15 µl of purified plasmid DNA at a concentration of 100 ng/µl was sent with 15 µl of the appropriate primer at 5 pmol/µl. Sequence alignments were carried out using the online Basic Local Alignment Search Tool (BLAST).

2.2 Immunofluorescence and histology

2.2.1 *Sample preparation*

Mice were euthanized via cervical dislocation. Tissues were dissected and mounted onto labelled cork disks. Tissues were covered in O.C.T compound and frozen by immersion in isopentane cooled on dry ice. Samples were stored at -80˚C until sectioning.

2.2.2 *Cryosectioning tissues*

10 µm serial sections of frozen tissues were cut with a cryostat (Microm HM 560, Zeiss) and mounted on Superfrost Plus Slides (VWR). Slides were wrapped in cling film and stored at -80 °C.

2.2.3 *Immunofluorescence labelling of tissue sections*

Slides were thawed at room temperature and sections were circled with an ImmEdge Hydrophobic Barrier PAP Pen (Vector Laboratories). Sections were fixed in 4% PFA (Paraformaldehyde, Sigma) in 1x PBS (Phosphate Buffered Saline, Gibco) for 5 minutes and permeabilised with 0.1% Triton X-100 (Sigma) in 1x PBS for 15 minutes. Sections were subsequently blocked with 4% BSA (Bovine Serum Albumin, Sigma) in 1x PBS for 1 hour at room temperature. Sections were incubated with 50 µl primary antibody diluted in blocking medium (Table 2.1) at 4 °C overnight. The next day sections were incubated with a secondary antibody diluted in blocking medium for 1 hour at room temperature. Sections were washed several times with 1x PBS between incubation periods. Sections were mounted in Vectashield mounting medium with 4,6-diamidino-2-phenylindole (DAPI) (Vector Laboratories).

2.2.4 *Whole-mount staining of adult muscle*

Whole muscles were dissected and fixed in 1% PFA in 0.1 M phosphate buffer for 30 minutes. They were then incubated with α-bungarotoxin, Alexa Fluor 594 conjugate (Life Technologies) in Liley's solution (Table 2.1) for 1 hr, and washed thoroughly. Muscle fibres were teased into small bundles during washes. Muscles were permeabilised in ethanol followed by methanol (10 minutes at -20˚C each), followed by incubation in 0.1% Triton-X-100 in PBS for 15 minutes at room temperature. Tissues were washed thoroughly in PBS. Muscles were incubated with anti-neurofilament (1:200) and anti-synaptophysin (1:100) antibodies in PBS containing 3% BSA and 0.1 M lysine (Sigma-Aldrich). The next day, muscles were washed thoroughly in PBS and incubated in goat anti-rabbit 488 (1:500) and goat anti-mouse 488 (1:500) secondary antibodies for 3 hours at room temperature. Bundles were washed in PBS

overnight. The next day they were mounted on slides with Vectashield mounting medium with DAPI (Vector Laboratories).

2.2.5 *In vivo* visualization and measurement of AChR turnover rate

Mice were administered an intramuscular injection of α-bungarotoxin 488 (green) in the tibialis anterior (TA) muscle. This was repeated using α-bungarotoxin 647 (red) 10 days later to label the old and new receptor pool respectively. Following the second administration, superficial TA muscles were examined immediately. Briefly, 3D stacks at 512 × 512 pixel resolution were taken of α-bungarotoxin 488 signals ("old receptors") and of α-bungarotoxin 647 signals ("new receptors") using a 63x objective and confocal *in vivo* imaging. The 3D stacks were automatically segmented using a custom-made algorithm, and pixel signal intensity values for each channel were extracted. The fraction of pixels per NMJ was calculated.

2.2.6 *Hematoxylin and eosin staining*

Frozen tissue sections were air-dried for 30 minutes and stained with Hematoxylin Harris (VWR) for 10 minutes. Slides were washed in running tap water for 1 minute, dipped in 1% HCl (Hydrochloric Acid, Fluka; diluted in 70% ethanol) for 5 seconds, and rinsed in tap water for 30 seconds. Slides were immersed in eosin for 30 seconds and rinsed in running tap water for 30 seconds. Slides were dipped in an ascending alcohol series of 70%, 90% and 100% ethanol for 5 seconds each and placed in Histoclear (National Diagnostics) twice for 2 minutes each. The slides were then mounted with DPX Mounting Medium (LAMB).

2.2.7 *β-galactosidase staining of whole mouse embryos*

Pregnant mice were sacrificed via cervical dislocation. The embryo sack was removed and immediately placed in cold PBS on ice. Embryos were separated from their extraembryonic membranes, washed twice with cold PBS and placed in fixing solution (Table 2.1) for 15 minutes at 4°C. Embryos were washed 3 times in wash buffer (Table 2.1) at room temperature. Embryos were gently shaking during fixation and wash steps.

5-bromo-4-chloro-3-indolyl-β-D-galactopyranoside (X-gal) staining solution (Table 2.1) was prepared fresh, placed on ice for 10 minutes and the precipitate was spun down for 5 minutes. Embryos were incubated with X-gal staining solution between 4 hours to overnight at 37°C in the dark. Embryos were washed twice with wash buffer and fixed in 1% PFA overnight. The next day embryos were stored in fresh 1% PFA until imaging.

2.2.8 *β-galactosidase staining of adult mouse tissues*

Frozen tissue sections (10 µm) were air dried for 30 minutes and fixed in 1.5% gluteraldehyde in PBS pH 7.4 for 1 minute and washed briefly in pure H_2O 3 times followed by PBS once. Sections were incubated overnight with X-gal staining solution (Table 2.1) at 37°C in a humidified chamber. Following the overnight incubation, sections were washed three times for 5 minutes each with PBS. Samples were mounted with DPX mounting medium.

2.3 Electron microscopy

2.3.1 *Transmission electron microscopy*

Fresh tissue samples of intercostal muscles were fixed in 3.9 % buffered glutaraldehyde, osmicated in 1 % phosphate-buffered osmiumtetroxyde, dehydrated and embedded in epoxy resin. 1 µm semithin sections were stained with toluidine blue. Ultrathin sections (100 nm) of at least one transverse and one longitudinal block per animal were contrasted by uranyl acetate and lead citrate as previously described (Weis *et al.*, 1995). Electron microscopy images were recorded using a CM10 transmission electron microscopy (Philips, Amsterdam, The Netherlands).

2.4 Protein extraction and western blotting

2.4.1 *Preparation of lysates*

Whole tissues were homogenised in 400 µl lysis buffer (Table 2.1) using a tissue raptor (Qiagen). The lysate was transferred to an eppendorf tube and spun at 700 *g* and 4 °C for 10 minutes. The supernatant was transferred into a clean eppendorf tube and spun down at 10,000 *g* for 30 minutes. The supernatant containing the cytosol fraction was collected. The resulting pellet containing membrane protein was lysed in 50 µl lysis buffer.

2.4.2 *Protein quantification*

Protein concentration was measured using the Qubit Fluorometer (Invitrogen by Life Sciences) according to the manufacturer's recommendations.

2.4.3 *SDS-PAGE and western blotting*

25 µg of protein in a final volume of 20 µl was placed in an eppendorf tube. 7.5 µl NuPAGE LDS Sample Buffer 4x (Life Technologies) and 3 µl NuPAGE Reducing Agent 10x (Life Technologies) were added to the sample and denatured on a heat block at 95 °C for 5 minutes. 10 µl Chameleon Duo Ladder (Licor) and the total volume of samples (30 µl) were loaded on Novex NuPAGE 4-12% Bis-Tris Gels (Life Technologies), and the tank (Life Technologies, Novex Mini-Cell) was filled with MOPS running buffer. The gel was run at 200 V for 45 minutes. Proteins were transferred onto a PVDF membranes (Licor) in a transfer tank (Mini Trans-Blot Electrophoresis Transfer Cell, BIO-RAD). The chamber was filled with chilled 1x transfer buffer (Table 2.1) and surrounded by ice at 350 mA for 1.5 hours. Following transfer, the membrane was soaked in methanol for 1 minute then rinsed in ultra-pure water. The membrane was blocked in 1x TBS (Table 2.1) followed by an incubation in TBS blocking buffer (Licor) on a shaker for 1 hour. The membrane was incubated with primary antibodies diluted in TBS blocking buffer overnight. The next day primary antibodies were drained off and the membrane was rinsed three times in 1x TBS-T (Table 2.1) for 5 minutes each. The membrane was incubated with secondary antibodies diluted in TBS blocking buffer containing 0.2% tween and 0.01% SDS, at room

temperature on a shaker for 1 hour in the dark. Membranes were washed with TBS-T 3 times for 5 minutes each, followed by a rinse in TBS. Protein bands were detected with an Odyssey Family Imaging System (Licor Biosicences).

A list of primary antibodies and dilutions used for these experiments are shown in Table 2.5.

2.5 Proteomic profiling experiments

2.5.1 *Cell lysis, sample preparation and trypsin digestion*

Approximately 5 mg of muscle tissue was lysed in 500 µl lysis buffer (Table 2.1) using a manual glass grinder, and samples were centrifuged for 5 minutes at 4°C and 5000 *g*. Protein concentration of the supernatant was determined using a BCA assay (Thermo Fisher Scientific, Dreieich, Germany) (according to the manufacturer's protocol). Cysteines were reduced by addition of 10 mM dithiothreitol (Roche Diagnostics) and subsequent incubation at 56°C for 30 minutes. Free thiol groups were alkylated with 30 mM iodoacetamide (Sigma Aldrich) at room temperature in the dark for 30 minutes.

Sample preparation were performed using filter-aided sample preparation (FASP) (Wisniewski *et al.*, 2009) with some minor changes. Briefly, 100 µg of protein lysate was diluted 10-fold with freshly prepared buffer composed of 8 M urea (Sigma Adrich) and 100 mM Tris-HCl (pH 8.5) (Kollipara and Zahedi, 2013) and placed on a Microcon centrifugal device (30 kDa cut off). The filter was centrifuged at 13,500 *g* at room temperature for 15 minutes (all the following centrifugation steps were performed under the same conditions). Three washing steps were carried out with 100 µl of 8 M urea/ 100 mM Tris-HCl (pH 8.5). For buffer exchange, the device was washed three times with 100 µl of 50 mM NH_4HCO_3 (pH 7.8). 100 µl of digestion buffer (Table 2.1) was added to the concentrated proteins and the samples were incubated at 37°C for 14 hours. Resulting tryptic peptides were recovered by centrifugation with 50 µl NH_4HCO_3 (50 mM) followed by 50 µl of ultra-pure water. Finally, acidification of the peptides was achieved by addition of 10% trifluoroacetic acid (Biosolve, Valkenswaard, The Netherlands(v/v)). The digests were quality controlled as described previously (Burkhart *et al.*, 2012).

2.5.2 *LC-MS/MS analysis*

Samples were measured using an Ultimate 3000 nano RSLC system coupled to an Orbitrap Fusion Lumos mass spectrometer (both Thermo Scientific) and analyzed in a randomized order to minimize systematic errors. Briefly, peptides were pre-concentrated on a 100 µm x 2 cm C18 trapping column for 10 minutes using 0.1 % trifluoroacetic acid (v/v) at a flow rate of 20 µl/min followed by separation on a 75 µm x 50 cm C18 main column (both Pepmap, Thermo Scientific) with a 120 minutes LC gradient ranging from 3-35 % of 84 % acetonitrile (Biosolve, Valkenswaard, Netherlands), 0.1 % formic acid (Biosolve, Valkenswaard, Netherlands (v/v) at a flow rate of 230 nl/min. MS survey scans were acquired in the Orbitrap from 300 to 1500 m/z at a resolution of 120000 using the polysiloxane ion at *m/z* 445.12003 as lock mass (Olsen *et al.*, 2005), an automatic gain control target value of $2.0x10^5$ and maximum injection times of 50 ms. Top speed most intense signals were selected for fragmentation by HCD with a collision energy of 30 % and MS/MS spectra were acquired in the Orbitrap using a target value of $2.0x10^3$ ions, a maximum injection time of 300 ms and a dynamic exclusion of 15 s.

2.6 Microscopy and image analysis

2.6.1 *Microscopy*

Whole-mount immunofluorescent samples were visualised using a Nikon A1R laser inverted scanning confocal microscope. Z-stack images were acquired and processed using NIS-elements AR 4.20.02 software. Images of histological sections were captured using a Zeiss Axioplan brightfield imaging microscope and AxioVision software. Embryos were imaged using a Zeiss stereomicroscope and AxioVision software.

2.6.2 *Image analysis*

Image analysis software ImageJ was used for the following: (i) quantification of AChR cluster area, (ii) quantification of muscle fibre cross-sectional area, (iii) to measure the relative expression levels of proteins in immunoblots using the gel analysis tool.

2.7 Statistical analysis

Statistical analyses were performed with IBM SPSS Statistics 22.0 software. Data were analysed using a two-sample *t*-test. An independent sample Mann–Whitney *U* test was performed to compare myofibre size variation. Proteomic data were analysed using analysis of variance (ANOVA) (Progenesis Stats). $p<0.05$ was considered statistically significant.

2.8 Transgenic mouse models

2.8.1 *Animal care and husbandry*

Mice used for this study were bred in the animal facility at the Functional Genomics Unit, Newcastle University, Institute of Genetic Medicine (Table 2.6). Breeders were housed as pairs of one male and one female, or trios of one male and two females. Offspring were housed together in groups of 2-6. All procedures were approved by the Home Office and were carried out under Animals Scientific Procedures Act of 1986 under project licence PPL70/8538, and personal licence PIL I1D9CFB05. AChR turnover experiments were approved by German authorities and were conducted according to national law (TierSchG7).

2.9 *In vivo* experiments

2.9.1 *Four limb inverted screen test*

Animals were suspended from an inverted wire grid and their latency to release the grid was recorded. Mice were allowed to hold on for a fixed maximum time of 600 seconds. Mice that released their grasp before reaching 600 seconds were allowed to rest for a period of 5 minutes and were given two more tries. The maximum hang time was used for further analysis. Data was collected from mice as early as 6 weeks old. Animals were tested once a week over a period of 6 months. This procedure was carried out in accordance with TREAT-NMD protocols (Carlson, 2011).

2.9.2 *Ex vivo isometric tension analysis*

3 month old mice were sacrificed via cervical dislocation and a strip of diaphragm muscle from the central tendon to the ribs was excised immediately and assembled in a tissue organ bath (Aurora Scientific) filled with oxygenated Krebs- Ringer solution (Table 2.1) at pH 7.4, maintained at 22°C. One end of the diaphragm was attached to a 300C dual-mode servomotor transducer (Aurora scientific) and the central tendon secured to a rigid post using 4-0 surgical thread. Diaphragm muscles were stimulated by supramaximal 0.2 ms square wave pulses delivered via platinum electrodes positioned on either side of the muscle. Data acquisition and control of the servomotor was conducted using a LabView based DMC program (Dynamic muscle control and Data Acquisition; Aurora Scientific, Version 3.2). We established a force-frequency relationship and assessed the muscles resistance to fatigue. The fatigue protocol involved 100 isometric contractions at a frequency of 150 Hz. This procedure was carried out in accordance with TREAT-NMD protocols (Barton, 2008).

2.9.3 *In situ force measurement*

Mice were anaesthetized with an intraperitoneal injection of Hypnorm®/Hypnovel®/water (1:1:2) at a dosage of 6 µl/g. Anaesthesia was maintained by mask inhalation of isoflurane vaporized at concentrations of up to 4% during surgical procedures and at 0.8-1.3% throughout the rest of the procedure. The distal tendon of the TA muscle was exposed and freed from surrounding fascia and the tendon tied with 4-0 surgical braided silk. The sciatic nerve was exposed and all branches were severed except for the common peroneal nerve (CPN) that innervates the TA. A piece of silk thread was secured on the sciatic nerve and the nerve was transected proximal to this ligature. The mouse was placed on a heated stage (Aurora scientific) to maintain body temperature at 37˚C. The TA tendon was attached to the lever arm of a 300C dual-mode servomotor transducer (Aurora scientific). Contractions of the TA muscle were stimulated via supramaximal square-wave pulses of 0.02 ms (701B Stimulator; Aurora Scientific) to the distal part of the CPN via bipolar platinum electrodes. Data acquisition and control of the servomotor was conducted using a LabView based DMC program (Dynamic muscle control and Data Acquisition; Aurora Scientific, Version 3.2). We established the force-frequency relationship and assessed the susceptibility of the TA

muscle to fatigue. At the end of the experiment muscles were excised and weighed. This procedure was carried out in accordance with TREAT-NMD protocols (Lynch, 2009).

Reagent	Application	Recipe	Supplier
Blocking buffer	Immunofluorescence	2.5 % BSA and 5 % goat serum in 0.5 % Triton X-100/PBS)	BSA (NBS Biologicals), goat serum (Thermo Scientific), Triton X-100 (Sigma)
Digestion Buffer	DNA extraction	50 mM Tris, 20 mM NaCl, 1 mM EDTA, 1% SDS. pH 8.	All chemicals from Sigma-Aldrich
Digestion Buffer	Proteomic profiling experiments	Trypsin (Promega) (1:25 w/w, protease to substrate), 0.2 M GuHCl and 2 mM $CaCl_2$ in 50 mM NH_4HCO_3 (pH 7.8)	Sequencing grade modified trypsin (Promega, Madison, WI USA), Benzonase®, $CaCl_2$ (Merck, Darmstadt). All other components from sigma.
Fixing Solution	*β*-galactosidase Staining Mouse Embryos	0.1 M phosphate buffer, 2% PFA 5 mM EGTA pH 8, 0.2% glutaraldehyde, 2 mM $MgCl_2$	All chemicals from Sigma-Aldrich
Kreb's-Ringer's Solution	*Ex vivo* isometric tension analysis	154 mM NaCl, 5 Mm KCl, 2 mM CaCl2, 1 mM MgCl2, 11 mM Glucose, 5 mM HEPES	All chemicals from Sigma-Aldrich
Liley's Solution	Immunofluorescence	12 mM $NaHCO_3$, 4 mM KCl, 1 mM KH_2PO_4, 138.8 mM NaCl, 1 mM $MgCl_2$, 2 mM $CaCl_2$, 11 mM Glucose	All chemicals from Sigma-Aldrich
Lysis Buffer	Proteomic profiling experiments	50 mM Tris-HCl (pH 7.8), 150 mM NaCl, 1 % SDS, and cOmplete Mini, EDTA-free protease inhibitor	Tris-HCL (Applichem Biochemica, Darmstadt, Germany), NaCl (Merck, Darmstadt), Sodium dodecyl sulfate (Carl Roth, Karlsruhe, Germany), EDTA-free protease inhibitor (Complete Mini) (Roche Diagnostics)
Lysis Buffer	Western Blots	RIPA Buffer, 1 tablet cOmplete ULTRA Tablets, Mini, EDTA-free protease inhibitor	RIPA buffer (Thermo Scientific), protease inhibitor (Roche)

Reagent	Application	Recipe	Supplier
TBS (10 X) and TBS-T	Western Blot	24 g Tris-HCl, 5.6 g Tris base, 88 g NaCl, Dissolve in 900 mL distilled water. For TBST- add 0.1% Tween-20.	All chemicals from Sigma-Aldrich
Transfer Buffer	Western Blot	25 mM Tris, 190 mM glycine, 20% methanol. pH 8.3	All chemicals from Sigma-Aldrich
Tris-Acetate-EDTA	Agarose gel, gel electrophoresis	40 mM Tris, 20 mM acetic acid, and 1mM EDTA	All chemicals from Sigma-Aldrich
Wash Buffer	*β*-galactosidase Staining of Whole Mouse Embryos	0.1 M phosphate buffer, 0.01 % Na-deoxycholate, 0.02% Igepal CA-630, 2 mM $MgCl_2$	All chemicals from Sigma-Aldrich
X-gal staining solution	*β*-galactosidase Staining of Whole Mouse Embryos	10 mM Potassium Ferricyanide, 10 mM Potassium Ferrocyanide, 1 mg/ml X-Gal (made up in wash buffer)	All chemicals from Sigma-Aldrich
X-gal staining solution	*β*-galactosidase Staining of adult mouse tissues	5 mM Potassium Ferricyanide, 5 mM Potassium Ferrocyanide, 1 mM $MgCl_2$ and 2mg/ml of X-gal	All chemicals from Sigma-Aldrich

Table 2.1. Reagents and buffers used in this project

Primer name	Primer Sequence (5'-3')
5arm-WTF	CAT GCG TGA ACC TGT GTA CA
SV40-FRT-F	CGC GTC GAG AAG TTC CTA TT
Crit-WTR	GTC AGA GTT TGC TCA CAT CA
5mut-R1	GCT TCA AGG ATA AGG CTT CAA G
3arm-WTR	GGG TTT CGT AAT TGG AAG AG
FlpE-F1	GGA CCG GCA ATT CTT CAA GCA
FlpE-R1	CCA CGG CAG AAG CAC GCT TAT
Transgene Forward	TAA GTC TGA ACC CGG TCT GC
Cre R	GTG AAA CAG CAT TGC TGT CAC TT

Table 2.2. Primers used for genotyping

Genotype	Forward Primer	Reverse Primer	Band Size
Wild type	5arm-WTF	Crit-WTR	~310bp
All targeted alleles	5arm-WTF	5mut-R1	~170bp
***Gfpt1*^{tm1a}**	SV40-FRT-F	3arm-WTR	~910bp
***Gfpt1*^{tm1b}**	SV40-FRT-F	3arm-WTR	~140bp
***Gfpt1*^{tm1c}**	5arm-WTF	Crit-WTR	~500bp
***Gfpt1*^{tm1d}**	5arm-WTF	3arm-WTR	~290bp
Cre	Transgene Forward	Cre R	~450bp
Flp	FlpE-F1	FlpE-R1	~230bp

Table 2.3. Combinations of primers used for genotyping. *Forward primers*: 5arm-WTF (F1), SV40-FRT-F (SV40F)**,** Transgene Forward (CreF), FlpE-F1 (FlpE-F1). *Reverse primers*: Crit-WTR (R1), 5mut-R1 (mutR1), 3arm-WTR (R2), Cre R (CreR), FlpE1-R1 (FLpE1-R1).

Primer name	Primer Sequence (5'-3')
Exon6F	TGA AAC AGA CAC AGA AAC CAT TGC C
NeoF	GAA TGG GCT GAC CGC TTC C
NeoR	GCT CGC GCC AGC CGA ACT G
Exon7R	GGC GCC TTT GCT CTT GTG
Exon8R	CGG AGT GAA CAT AAG CTT TC
Exon8aR	CAT GGT GGG GAT CAC AGG CAG
Exon7/8R	CAG TTG GCA CAA GGC GAG GTA
Exon8/8aR	GTA CAG AAC AGCT AGG ACT C
Exon8/9R	GTA CAG AAC AGG CAA AGA CAA G

Table 2.4. Primers used for RT-PCR

Antibody	Description	Application in this study	Supplier
Anti-Neurofilament heavy polypeptide	Mouse monoclonal	IHC (1:200)	Abcam
Anti-Synaptophysin	Rabbit polyclonal	IHC (1:100)	Fisher Scientific
Anti-GFPT1	Rabbit polyclonal	WB (1:500)	Proteintech
Anti-GAPDH	Mouse monoclonal	WB (1:1000)	Abcam
Anti-Glypican 1	Rabbit polyclonal	WB (1:1000)	Abcam
Anti-MuSK	Rabbit polyclonal	WB (1:1000)	Abcam
Anti-alpha Actinin	Mouse monoclonal	WB (1:250)	Sigma
Alexa Fluor® 594	α-Bungarotoxin conjugate	IHC (1:500)	Life Technologies
Alexa Fluor® 488	Goat anti-Mouse	IHC (1:500)	Life Technologies
Alexa Fluor® 488	Goat anti-Rabbit	IHC (1:500)	Life Technologies
IRDye® 800CW	Donkey anti-Mouse IgG	WB (1:15000)	Licor
IRDye® 680CW	Goat anti-Rabbit IgG	WB (1:15000)	Licor
Alexa Fluor® 647	α-Bungarotoxin conjugate	AChR Turnover (25 pmol)	Life Technologies
Alexa Fluor® 488	α-Bungarotoxin conjugate	AChR Turnover (25 pmol)	Life Technologies

Table 2.5. Antibodies used in this study

Strain name	Origin
Wild type *C57BL/6*	MRC Mammalian Genetics Unit, Harwell
C57BL/6NTac-*Gfpt1*$^{tm1a(EUCOMM)Wtsi}$/H	MRC Mammalian Genetics Unit, Harwell
C57BL/6NTac-*Gfpt1*$^{tm1b(EUCOMM)Wtsi}$/H	MRC Mammalian Genetics Unit, Harwell
C57BL/6NTac-*Gfpt1*$^{tm1c(EUCOMM)Wtsi}$/H	MRC Mammalian Genetics Unit, Harwell
C57BL/6NTac-*Gfpt1*$^{tm1d(EUCOMM)Wtsi}$/H	Functional Genomics Unit
B6.FVB(129S4)-Tg*(Ckmm-cre)*5Khn/J	The Jackson Laboratory
B6;SJL-Tg(ACT*Flpe*)9205Dym/J	FGU- *originally from The Jackson Laboratory*
B6;129S4-Gt*(ROSA)26Sor*^{tm1Sor}/J	FGU- *originally from The Jackson Laboratory*

Table 2.6. Mice used in this study

Chapter 3: Generation of transgenic mice

3.1 Introduction

Over the years the use of rodents to model human disease has become increasingly popular. Rodents serve as powerful tools for studying disease progression, understanding the roles of specific genes in biological pathways, and preclinical screening and safety testing of new compounds. The advantages of using mice over other model organisms are numerous. Genomic studies have established that the house mouse (*Mus musculus*) exhibits a remarkable 99% genetic homology to humans (Waterston *et al.*, 2002; Vandamme, 2014). Moreover, due to their small size, short gestation period and ease of maintenance in the laboratory, mice have become increasingly desirable models to use for scientific research.

Advancements in technology which enable genetic manipulation of the mouse genome and the availability of a substantial number of knockin and knockout strains has rapidly enhanced our understanding of the pathology behind human diseases and the development of therapies (Vandamme, 2014). Deciding whether a germline or conditional knockout mouse is a more appropriate model for studying gene function depends on the viability of transgenic mice and the parameters that you wish to investigate. The Cre/loxP strategy utilises gene-trap mutagenesis which facilitates modification of the knockout first allele in crosses to transgenic *Flp* and *Cre* mice to generate null or conditional tissue-specific alleles (Skarnes *et al.*, 2011; Heffner *et al.*, 2012). As of yet, there is currently no *Gfpt1* knockout mouse model. A GFPT1 deficient mouse model will provide an invaluable tool in which to study numerous pathological changes occurring as a result of glycosylation defects. In this study we breed mice that will generate a complete *Gfpt1* knockout mouse model. Offspring that inherit the *lacZ* reporter gene will allow us to track GFPT1 expression during development and in the adult mouse. One of the challenges we face is the viability of the *Gfpt1* knockout mouse. Therefore, we also generate a conditional knockout mouse model which will overcome the problem of embryonic or early postnatal lethality in mice that harbour both copies of the null allele.

A full understanding of Cre mediated excision of one or more exons relies on a well-characterised *Cre*-line. Several reports have shown unspecific activity of a number of Cre-driver lines displaying gene excision beyond the desired cell type or time point, due

to poorly characterised expression of the promoter (Heffner *et al.*, 2012). Premature Cre expression may result in a false positive phenotype or perhaps even embryonic lethality. There are also reports of inconsistent Cre activity depending on whether the *Cre* transgene is inherited maternally or paternally (Hayashi *et al.*, 2003; Gallardo *et al.*, 2007). When using this experimental strategy, it is important to monitor Cre activity to ensure we achieve the desired spatio-temporal excision of our gene of interest. A number of transgenic Cre-reporter mouse lines have been developed to track Cre expression. In this study we use the [B6;129S4-Gt(ROSA)26Sortm1Sor/J] (ROSA26R-*lacZ*) mouse line which allows us to evaluate expression of the *Ckm-Cre* transgene using *β*-galactosidase activity in the developing mouse embryo and adult tissues.

3.1.1 *Aims*

- To generate a GFPT1 knockout mouse model as part of the IMPC international effort at the MRC mammalian Genetics Unit, Harwell. Mice carrying one copy of the *Gfpt1*^{tm1a} and *Gfpt1*^{tm1b} allele obtained from the International Knockout Mouse Consortium will be bred and maintained at the Functional Genomics Unit, Newcastle University.

- To generate a homozygous *Gfpt1*^{tm1c} line through conversion of the *Gfpt1*^{tm1a} allele using Flp recombinase.

- To generate the conditional muscle-specific GFPT1 knockout mouse using a muscle-specific Cre line.

- To demonstrate the efficiency and specificity of Cre activity using genomic PCR, western blotting and *β*-galactosidase activity in the ROSA26R reporter mouse.

3.2 Generation of transgenic mice

The European Conditional Mouse Mutagenesis (EUCOMM) program uses promoterless and promotor-driven targeting cassettes to generate the 'knockout-first allele' in C57BL/6N embryonic stem (ES) cells. The design of conditional alleles is facilitated by a computational tool used to identify oligonucleotide sequences suitable for recombineering. These sequences are used to replace the coding sequence of GFPT1 with a *lacZ* reporter and promoter-driven selection cassette using bacterial artificial chromosome (BAC) recombineering. Successful targeted events were identified using a novel high-throughput allele-counting assay. The final targeting constructs were used for ES cell electroporation. Homologous recombinants were screened using long-range PCR and sequencing. Positive clones were implanted into the host mouse blastocyst and implanted into the mouse (Friedel *et al*., 2011; Skarnes et al., 2011).

3.2.1 *Gene targeting via homologous recombination*

A gene-trap cassette containing a *neomycin* and *lacZ*-reporter gene flanked by *FRT* sites has been inserted in the intronic region of mouse *Gfpt1* between exons 6 and exon 7. The critical exon (exon 7) is flanked by *loxP* sites producing the initial targeted allele *Gfpt1*^{tm1a}. The marker allele *Gfpt1*^{tm1b}, expected to be a null, and the conditional allele *Gfpt1*^{tm1c}, expected to be wildtype, can be generated upon exposure to Cre or Flp recombinases respectively. The *Gfpt1*^{tm1b} allele reports the activity of the promoter and can be used to track the expression pattern of GFPT1 during development and across tissues using lacZ staining. Upon Cre mediated recombination, the *Gfpt1*^{tm1c} allele can be converted to the *Gfpt1*^{tm1d} knockout allele (Figure 3.1).

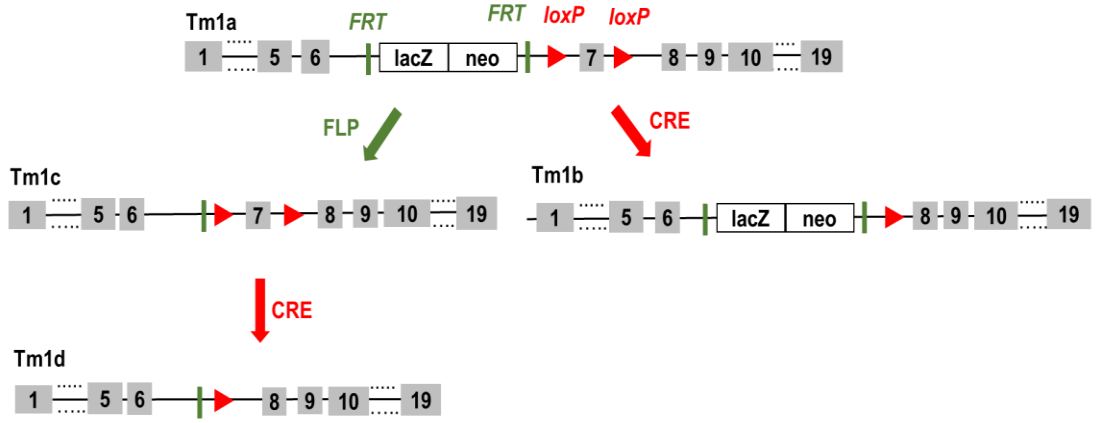

Figure 3.1. Schematic diagram of the targeting strategy. The knockout-first allele *Gfpt1*^{tm1a} contains a *lacZ-neomycin* trapping cassette. Cre deletes the loxP flanked exon of the *Gfpt1*^{tm1a} allele to generate the *lacZ*-tagged marker allele, *Gfpt1*^{tm1b}. The conditional allele *Gfpt1*^{tm1c} is generated by removal of the gene-trap cassette by Flp recombinase which restores the allele to wild type except for insertion of *loxP* sites. Cre deletes the *Gfpt1*^{tm1c} floxed exon to generate a frameshift mutation, *Gfpt1*^{tm1d}.

3.2.2 *Generation of Gfpt1*^{tm1a}*, Gfpt1*^{tm1b} *and Gfpt1*^{tm1c} *alleles*

Mice heterozygous for the *Gfpt1*^{tm1a} *and Gfpt1*^{tm1b} alleles were obtained from the International Knockout Mouse Consortium, Harwell. These mice were generated using the EUCOMM strategy to develop the 'knockout-first' conditional allele as previously described. Mouse lines were maintained via heterozygote crosses. To generate the *Gfpt1*^{tm1c} allele, *Gfpt1*$^{+/tm1a}$ mice were bred with mice carrying the *Flp* transgene. The *lacZ-neomycin* cassette was excised upon FlpE recombinase activity to generate *Gfpt1*$^{+/tm1c}$ offspring which carry the *Flp* gene. *Gfpt1*$^{+/tm1c}$ mice were crossed with wild type mice. *Gfpt1*$^{+/tm1c}$ offspring negative for *Flp* were selected and crossed to generate *Gfpt1*$^{tm1c/tm1c}$ mice (Figure 3.2).

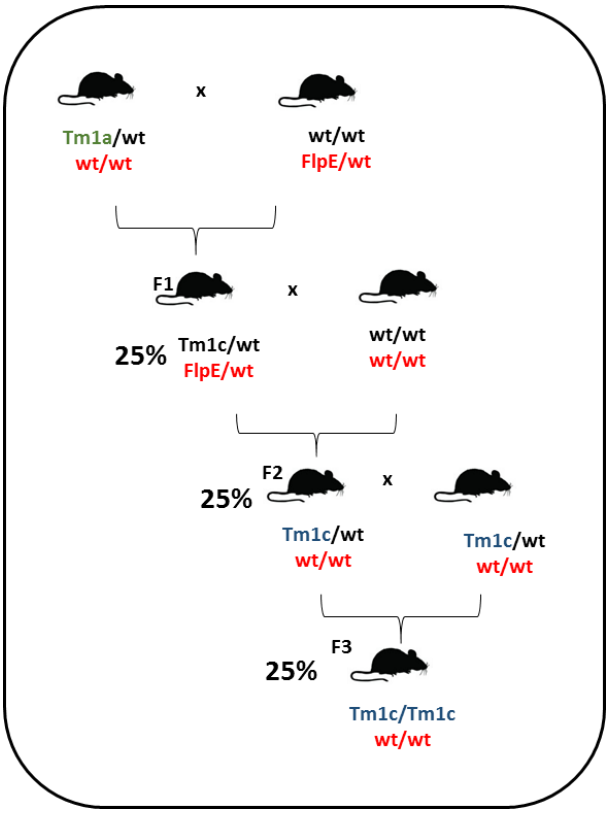

Figure 3.2. Generation of *Gfpt1*$^{tm1c/tm1c}$ mice. *Gfpt1*$^{+/tm1a}$ mice were crossed with mice hemizygous for FlpE recombinase resulting in the conversion of the *Gfpt1*^{tm1a} allele to the *Gfpt1*^{tm1c} allele in 25% of progeny (F1). *Gfpt1*$^{+/tm1c}$ mice carrying the *FlpE* transgene were crossed with wild type mice. *Gfpt1*$^{+/tm1c}$ offspring (F2) free of the *FlpE* transgene (25%) were selected and crossed to generate *Gfpt1*$^{tm1c/tm1c}$ mice. 25% of offspring were *Gfpt1*^{tm1c} homozygous. These mice were obtained after 3 generations of breeding.

3.2.3 *Generation of the GFPT1 muscle-specific knockout mouse*

To generate a conditional *Gfpt1* knockout allele, homozygous *Gfpt1*$^{tm1c/tm1c}$ mice were bred with mice harbouring the muscle creatine kinase, *Ckm-Cre* transgene [B6.FVB(129S4)-Tg(Ckmm-cre)5Khn/J] obtained from Jackson Laboratories. These mice express Cre recombinase under the control of the *Ckm* promoter. Cre mediated recombination results in the deletion of *Gfpt1* in skeletal and cardiac muscle after 2 generations of breeding. Offspring are referred to as muscle-specific *Gfpt1*$^{tm1d/tm1d}$ (Figure 3.3).

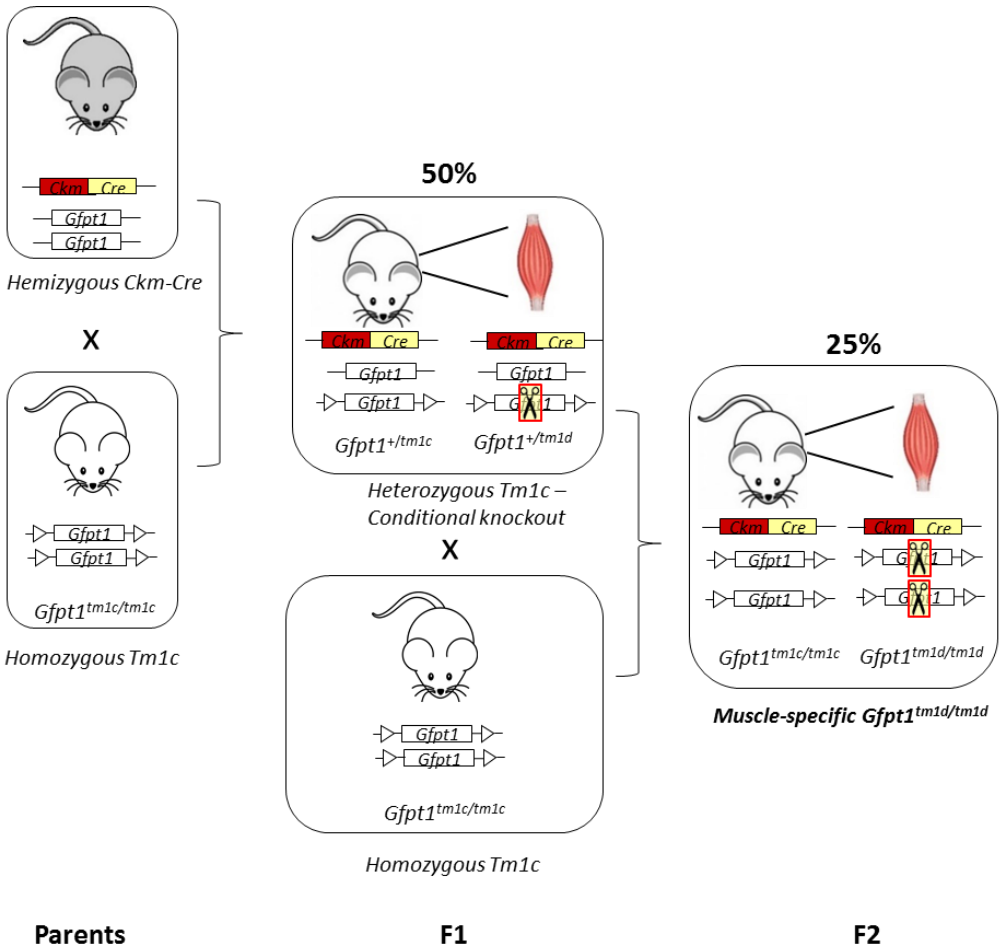

Figure 3.3. Breeding strategy for generating the muscle-specific *Gfpt1* knockout mouse. The homozygous *tm1c* allele, *Gfpt1*$^{tm1c/tm1c}$ is bred with a hemizygous *Ckm-Cre* mouse. 50% of offspring are heterozygous for the *tm1c* allele, *Gfpt1*$^{+/tm1c}$ and express Cre recombinase activity in striated muscle only (F1). These mice are crossed with homozygous *Gfpt1*$^{tm1c/tm1c}$ mice. 25% of offspring are homozygous for the *tm1c* allele, *Gfpt1*$^{tm1c/tm1c}$ and express Cre recombinase activity in striated muscle only to generate the muscle-specific *Gfpt1*$^{tm1d/tm1d}$ mouse (F2).

3.2.4 *Genotyping and sequencing transgenic lines*

Insertion of the gene-trap cassette, deletion of the critical exon, conversion to the conditional allele and the presence of the *Cre* transgene was validated by PCR. Primers were designed to produce a fragment of ~310 bp in the *Gfpt1* wild type allele. Primers positioned on the 5' homology arm and the first *FRT* site produce bands of ~170 bp in

all targeted alleles (*Gfpt1*^{tm1a}, *Gfpt1*^{tm1b,} and *Gfpt1*^{tm1c}). The *Gfpt1*^{tm1a} allele also produces a band of ~910 bp band when amplified with primers flanking the floxed critical exon. Upon Cre-mediated recombination the same primers generate a smaller product of ~140bp following excision of the critical exon to produce the *Gfpt1*^{tm1b} allele. Flp mediated recombination of the *Gfpt1*^{tm1a} allele removes the gene-trap cassette to produce the *Gfpt1*^{tm1c} conditional allele producing a band of ~500bp. Upon Cre mediated recombination the conditional allele is converted to the *Gfpt1*^{tm1d} allele by removal of the critical exon in muscle only. DNA extracted from ear clip biopsies from these mice are homozygous for the *Gfpt1*^{tm1c} conditional allele in the presence of Cre (*Gfpt1*$^{tm1c/tm1c}$ *Cre)*. Primers were designed within the *Cre* gene to produce a band of ~450bp (Figure 3.4A, B). All alleles were verified via DNA sequencing.

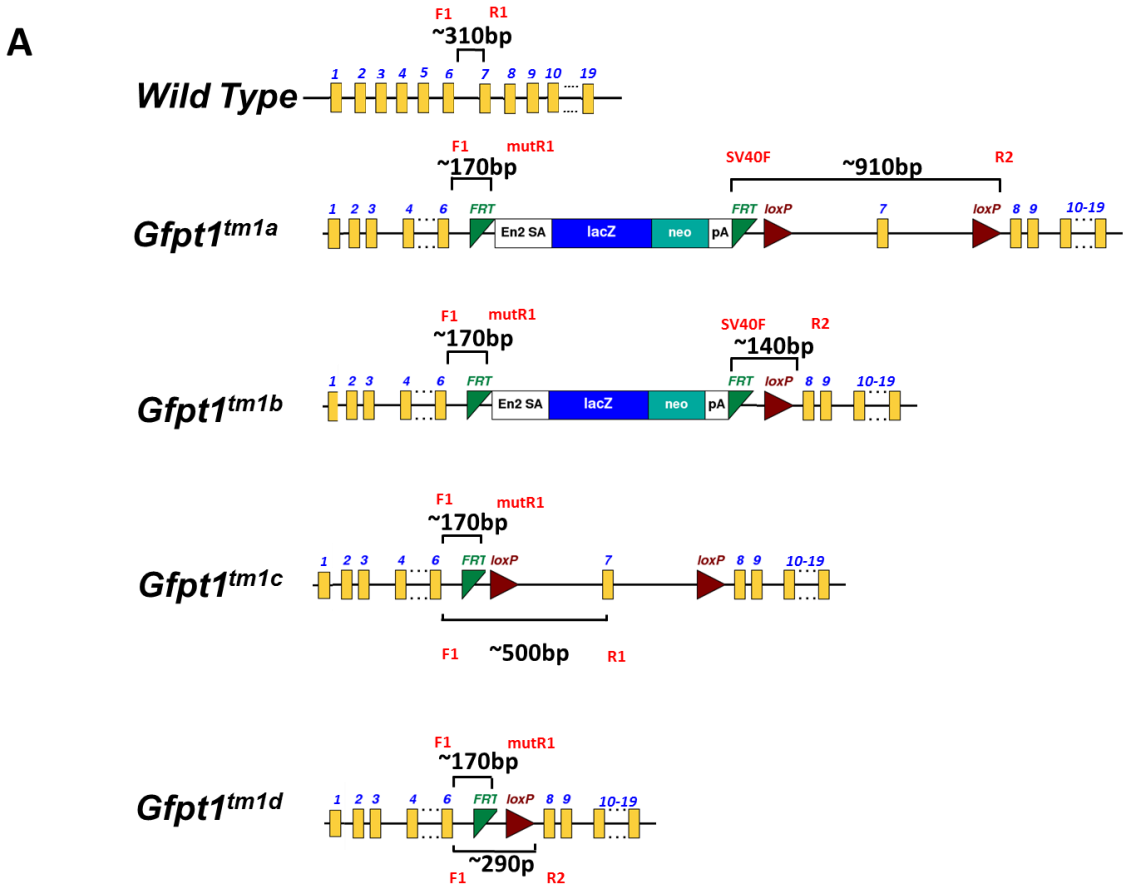

B

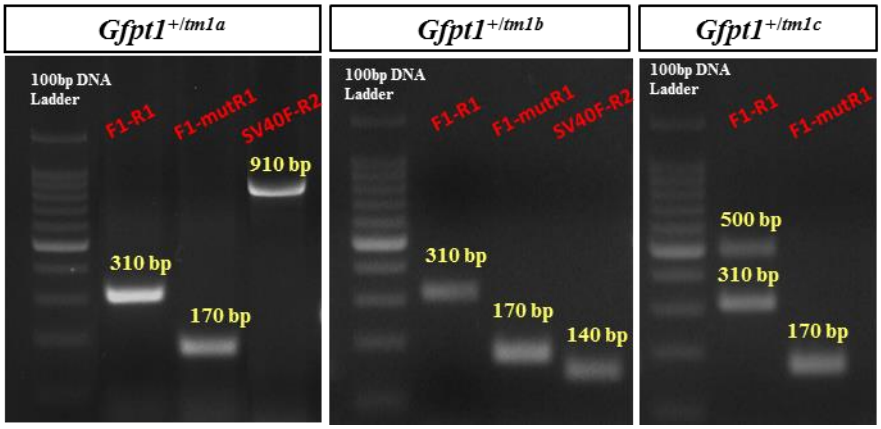

Figure 3.4. Analysis of targeting events in the *Gfpt1* gene. (A) Schematic representation of the targeting vector. Exons are shown in numbered rectangles and the positions of the inserted *FRT* and *loxP* sites are shown. The positions of primers used for genotyping and the length of the amplified PCR products in wild type, *Gfpt1*^{tm1a}, *Gfpt1*^{tm1b}, *Gfpt1*^{tm1c} and *Gfpt1*^{tm1d} are indicated. (B) PCR on genomic DNA extracted from ear clips showing amplified fragments of ~310bp for the *Gfpt1* wild type allele, ~170 bp fragment for all targeted alleles, ~910bp for the *Gfpt1*^{tm1a} allele, ~140 bp for the *Gfpt1*^{tm1b} allele and ~500 bp for the *Gfpt1*^{tm1c} allele. All bands are measured against a 100 bp DNA ladder. Each gel represents PCR products derived from heterozygous mice (*Gfpt1*$^{+/tm1a}$, *Gfpt1*$^{+/tm1b}$ and *Gfpt1*$^{+/tm1c}$). *Forward primers*: 5arm-WTF (F1), SV40-FRT-F (SV40F). *Reverse primers*: Crit-WTR (R1), 5mut-R1 (mutR1), 3arm-WTR (R2).

3.3 Efficiency and specificity of Cre recombinase activity

The efficiency and specificity of Cre-mediated activity was verified using genomic PCR, immunoblotting, and the ROSA26R-*lacZ* reporter line which demonstrates Cre expression.

3.3.1 *Tissue specific genotyping*

Cre-mediated gene alteration in muscle of *Gfpt1* mutant mice was confirmed by genomic PCR. Primers were designed to detect the deletion of exon 7. PCR on genomic DNA extracted from muscle tissues and non-muscle tissues from *Gfpt1*$^{tm1c/tm1c}$ mice produce fragments of ~500 bp. DNA amplified from muscle specific *Gfpt1*$^{tm1d/tm1d}$ mice produce fragments of ~500 bp in non-muscle tissues and a band of ~290 bp in skeletal and cardiac muscle in the presence of *Cre* (~450 bp). All targeted alleles produce fragments of ~170 bp. Tissues analysed include ear clips, brain, kidney, heart and skeletal muscle (Figure 3.5).

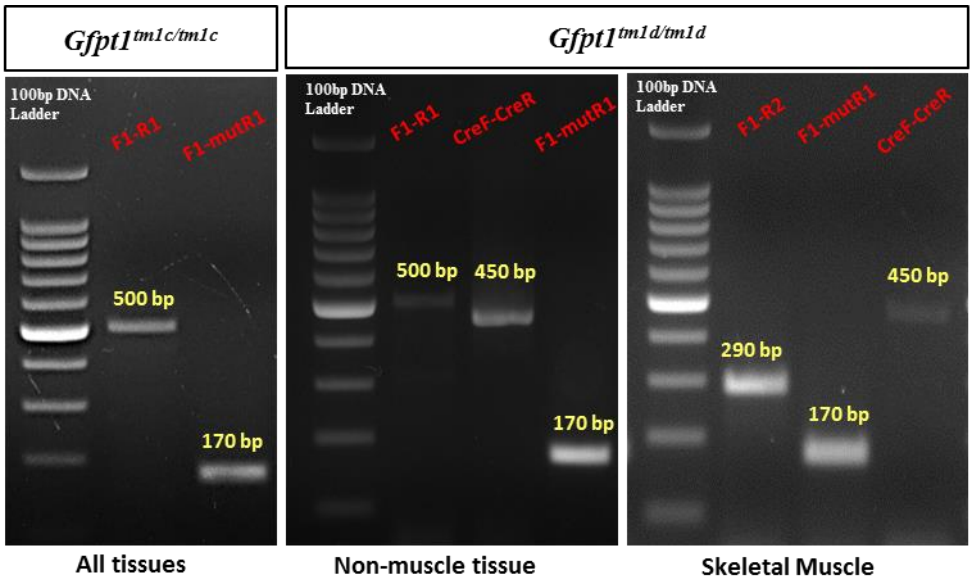

Figure 3.5. Muscle-specific allele conversion in *Gfpt1*^{tm1d} mice. Representative images verifying the conversion of *Gfpt1*^{tm1c} allele to the *Gfpt1*^{tm1d} allele in skeletal and cardiac muscle of *Gfpt1* mutant mice carrying the *Cre* transgene under the control of the *Ckm* promoter. Cre-mediated recombination does not take place in non-muscle tissues. *Forward primers*: 5arm-WTF (F1), Transgene Forward (CreF). *Reverse primers*: Crit-WTR (R1), 5mut-R1 (mutR1), 3arm-WTR (R2), Cre R (CreR).

3.3.2 *Immunoblot analysis of* GFPT1 *expression in control and Gfpt1$^{tm1d/tm1d}$ mice*

We performed immunoblotting analyses on lysates from control and *Gfpt1$^{tm1d/tm1d}$* mouse tissues. Here *Gfpt1$^{tm1c/tm1c}$* littermates were used as controls. Expression of GFPT1 in tissues was examined by western blotting using a polyclonal antibody against GFPT1. GFPT1 (~79 kDa) is expressed in muscle and non-muscle components in control mice. Results confirmed the absence of GFPT1 in skeletal and cardiac muscle from *Gfpt1$^{tm1d/tm1d}$* mice but not in brain or kidney. Glyceraldehyde 3-phosphate dehydrogenase (GAPDH) (~38 kDa) was used as a loading control (Figure 3.6).

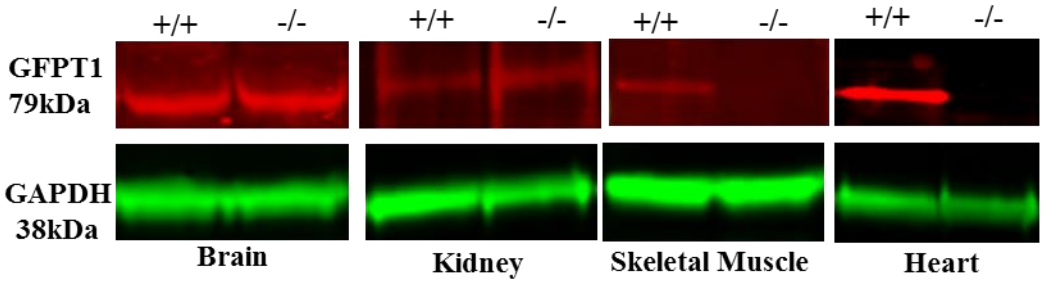

Figure 3.6. Western blot analysis of GFPT1 expression in muscle and non-muscle tissues from control and *Gfpt1$^{tm1d/tm1d}$* mice. GFPT1 protein (~79kDa) is detected in muscle and non-muscle tissues in control mice. GFPT1 is not detected in skeletal muscle from *Gfpt1$^{tm1d/tm1d}$* mice. GAPDH (~38kDa) was used as a loading control. All bands were measured against an 8-260 kDa Chameleon Duo Pre-stained protein ladder.

3.3.3 *ROSA26R-lacZ as a Cre reporter mouse line*

To understand the spatial and temporal expression of Cre recombinase we use the *lacZ* reporter mouse line ROSA26R-*lacZ* which demonstrates the activity of the *Ckm* promoter. ROSA26R mice have a *loxP* flanked transcriptional termination element, or a 'stop' sequence inserted downstream of a transcription start site at the ubiquitously expressed *ROSA26* locus, between the promoter and transgene *lacZ* sequence. When intact this cassette inhibits transcription of the *lacZ* reporter transgene. Tissues expressing Cre recombinase undergo Cre-mediated recombination resulting in excision of the 'stop' sequence allowing expression of *β*-galactosidase encoded by the *lacZ* transgene (Figure 3.7A).

Hemizygous *Ckm-Cre* mice were crossed with homozygous ROSA26R mice. Male and female mice were mated accordingly to generate offspring with either maternal or paternal *Cre* inheritance. Offspring were used to investigate whether Cre expression varied based on parental inheritance (Figure 3.7B).

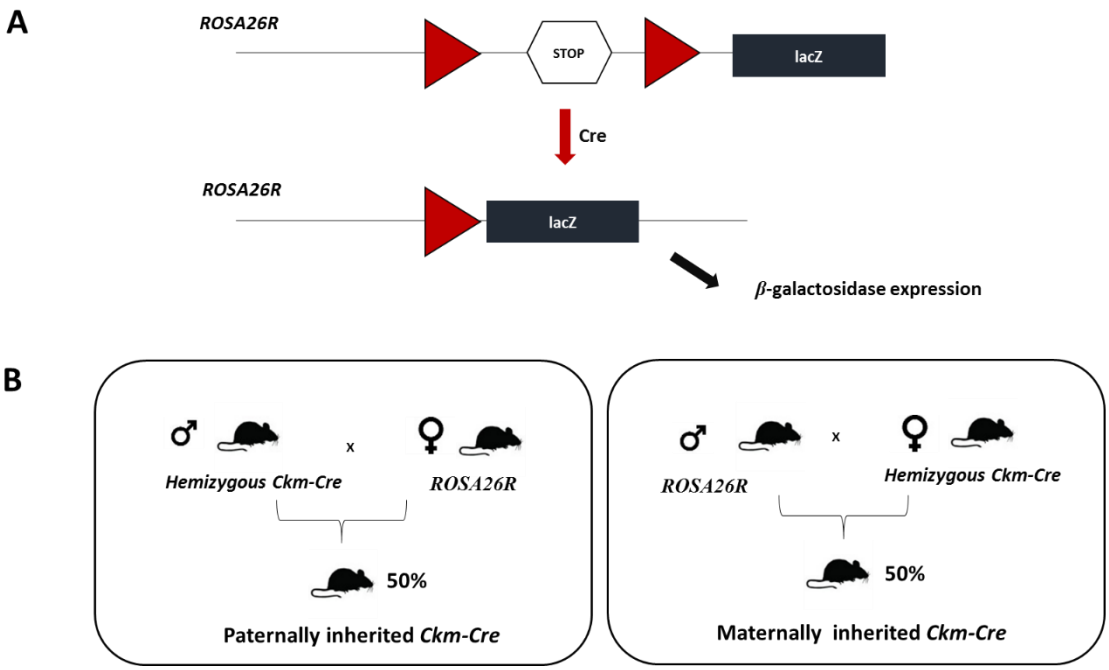

Figure 3.7. Mechanism of the ROSA26R-*lacZ* reporter line and generation of ROSA26R-Cre mice. (A) Schematic demonstrating Cre-mediated recombination events in the ROSA26R-*lacZ* reporter mouse. When intact the 'stop' cassette prevents the expression of *β*-galactosidase from the downstream *lacZ* coding sequence. Upon exposure to Cre recombinase, the stop cassette is excised by recombination of *loxP* sites, allowing the expression of *β*-galactosidase. (B) Schematic showing mice mated in order to generate offspring that acquire the *Cre* transgene via maternal or paternal inheritance. 50% of progeny will inherit the *Cre* transgene.

3.3.4 *Ckm-Cre activity in the developing mouse embryo*

ROSA26R-Cre mice carry the *lacZ*-reporter gene which expresses *β*-galactosidase. To analyse Cre expression pattern in the mouse, we detected the enzymatic activity of *β*-galactosidase using X-gal. Cells which express Cre recombinase are stained blue. We analysed *Ckm*-Cre expression in the developing mouse embryo. Whole ROSA26R-Cre embryos were isolated at E10.5, E11.5, E12.5 and E13.5, and were subsequently treated with X-gal. The expression of *β*-galactosidase activity is evident from E11.5 in muscles of the head and neck. As the embryo develops we see expression in the somites (E12.5) and a rapid accumulation in other skeletal muscles by E13.5. *β*-galactosidase expression appears to be restricted to muscle only (Figure 3.8). No differences were seen in embryos that inherited the *Cre* transgene via maternal or paternal inheritance, or amongst littermates.

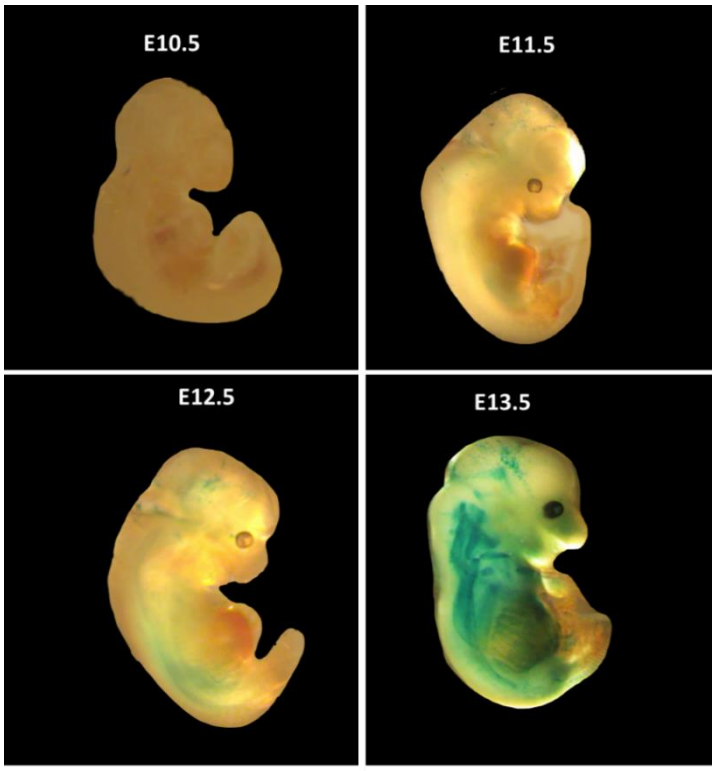

Figure 3.8 Expression of *β*-galactosidase in ROSA26R-Cre embryos. Representative whole-mount images of embryos at various embryonic stages demonstrating the temporal and spatial specificity of Cre activity. Expression of the *lacZ* reporter transgene is restricted to skeletal and cardiac muscle only.

3.3.5 *Ckm-Cre reporter activity in the adult mouse tissues*

To determine the expression pattern of the *lacZ* transgene in the adult mouse, transverse sections of muscle and non-muscle tissues from adult mice were sectioned and stained with X-gal. *β*-galactosidase activity is present in skeletal and cardiac muscle only. Gastrocnemius, TA, extensor digitorum longus (EDL), soleus, intercostal, extraocular and diaphragm muscles display *β*-galactosidase activity when treated with X-gal forming a blue precipitate. *β*-galactosidase activity was absent in non-muscle treated tissues including the brain, kidney and non-muscle components of the eye. There were no observed differences in the pattern of *β*-galactosidase activity between tissues obtained from mice that acquired the *Cre* transgene via maternal and paternal inheritance.

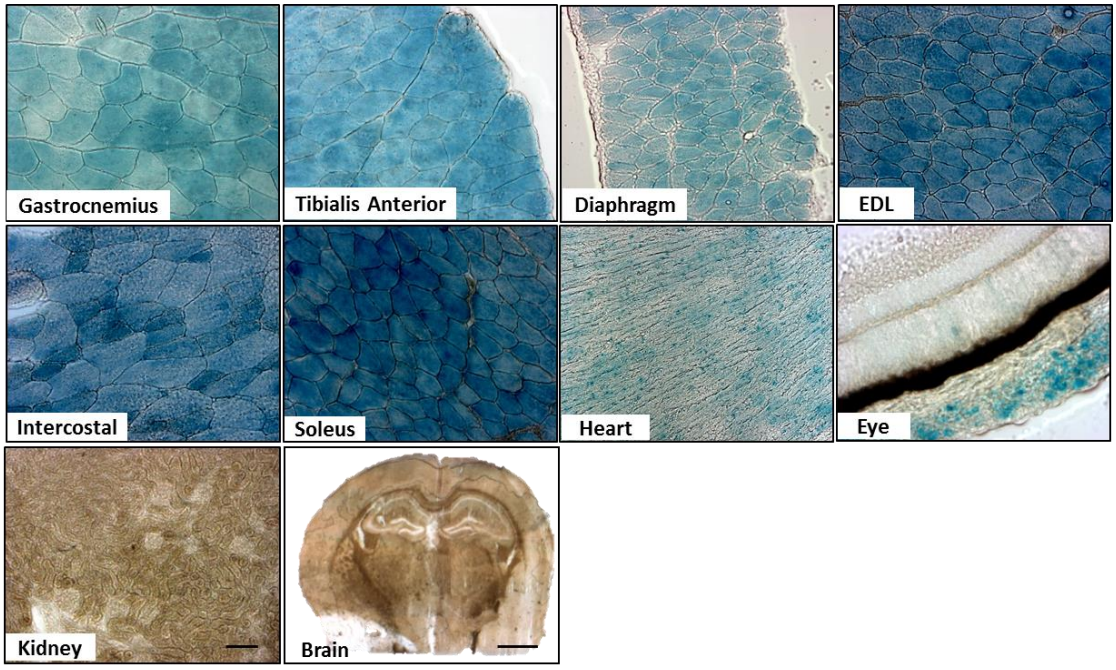

Figure 3.9. Expression of *β*-galactosidase in ROSA26R-Cre adult mouse tissues. There is abundant expression of *β*-glactosidase in skeletal (gastrocnemius, TA, EDL, soleus, intercostals, diaphragm and extraocular) and cardiac muscles. *β*-galactosidase activity is absent in non-muscle tissues (brain, kidney and eye). Scale bar = 400µm (brain), 20µm (all other tissues).

3.4 Discussion

Our ability to understand the molecular mechanisms underlying disease states has rapidly progressed due to advancements in genomic manipulation, making the mouse model one of the most desirable research tools used for studying human disease (Perlman, 2016). Mouse models are particularly useful for the investigation of rare diseases as low patient numbers and phenotype heterogeneity greatly impede the establishment of clinical trials. The generation of CMS mouse models have enabled phenotype analysis which can be correlated to features seen in patients (Chevessier *et al.*, 2008; Bogdanik and Burgess, 2011; Chevessier *et al.*, 2012; Messéant *et al.*, 2015).

Here we report the generation of a GFPT1 deficient mouse model which will allow us to explore the pathological molecular involvement of GFPT1 which contributes to the phenotype observed in patients with CMS. We also describe the generation of mouse variants which will enhance our understanding of GFPT1 expression and allow us to investigate the spatio-temporal activity of Cre recombinase. Together these data verify that any phenotypes we observe in our mouse model will be purely as a consequence of GFPT1 deficiency.

The gene-trap strategy used in our study relies on identification of the 5'-most critical exon that will lead to a frameshift mutation when deleted, is common to all transcript variants, and disrupts at least 50% of the protein-coding sequence of the gene of interest (Skarnes *et al.*, 2011). Since alternative splicing of the *GFPT1* muscle-specific exon occurs downstream of exon 7, positioning of the gene-trap cassette ensures disruption of both isoforms. Due to the ubiquitous nature of GFPT1 (Dehaven *et al.*, 2001; Yang *et al.*, 2007), it is highly probable that homozygous *Gfpt1* knockout mice are embryonic lethal. For this reason, we have also generated a conditional model whereby GFPT1 is knocked out in skeletal and cardiac muscle only. Several studies have reported metabolic and behavioural phenotypes in mouse strains expressing Cre recombinase (Loonstra *et al.*, 2001; Forni *et al.*, 2006; Naiche and Papaioannou, 2007). It is therefore important to generate a pure model free from Flp and Cre recombinases, or use appropriate controls which rule out the possibility of false positive phenotypes. In our conversion of the $Gfpt1^{tm1a}$ allele to the $Gfpt1^{tm1c}$ allele, we ensure that progeny used for subsequent breeding steps are free from FlpE recombinase. Since our conditional $Gfpt1^{tm1d/tm1d}$ mice maintain the expression of Cre recombinase, we will also use the Cre line for some initial characterisation to ensure that the presence of Cre is not a

confounding variable which contributes to the observed phenotype. High levels of Cre expression can also lead to Cre toxicity affecting cell physiology and possibly the viability of animals. Thus, when setting up matings we ensure that offspring only inherit one copy of the *Cre* transgene, making it is less likely that the mice will acquire a Cre phenotype.

Optimising gene targeting relies largely on the choice of the Cre recombinase expressing mouse line, which needs to target the gene of interest in the correct tissues at the right time. Therefore, when choosing a Cre recombinase it is important to keep in mind the aims of the study. In this project we want to understand the role of GFPT1 in the formation and maintenance of the NMJ. Formation of the NMJ begins with pre-patterning of AChRs from embryonic day 12.5, and by embryonic day 18.5 AChR clusters have differentiated and are well innervated (Lin *et al.*, 2001; Wu *et al.*, 2010). The expression of muscle creatine kinase has been reported in skeletal and cardiac muscle of the mouse embryo 13 days post coitum, which rapidly increases by embryonic day 15 (Lyons *et al.*, 1991; Bruning *et al.*, 1998). Using a *Ckm-Cre* mouse line is ideal for generating a mouse model which will allow us to achieve our aims as the expression of *Ckm-Cre* and hence depletion of GFPT1 temporally correlates with events taking place during the formation of the NMJ. Consequently, the phenotype we observe is a reflection of pathophysiology of the formation as well as the maintenance of the NMJ.

Reproducible excision is vital for the analysis of experimental data. Numerous studies have reported mosaic or inconsistent Cre activity in other Cre lines (Heffner *et al.*, 2012). Discrepancies arise depending on whether the *Cre* transgene is maternally or paternally inherited due to persistence of the Cre protein in the female germline (Hayashi *et al.*, 2003; Gallardo *et al.*, 2007; Heffner *et al.*, 2012), inconsistent Cre recombination between littermates and unreported Cre activity in certain tissues due to poorly characterised promoters (Heffner *et al.*, 2012). Therefore, in order to interpret our data informatively, we need to be certain of time/tissue-specific Cre activity. Several Cre-reporter lines have been developed which express fluorescent proteins such as green fluorescent protein (GFP) and other fluorescent colour variants, EYFP and ECFP (Srinivas *et al.*, 2001). Additional Cre reporter lines include luciferase reporters (Ishikawa and Herschman, 2011) and the ROSA26R-*lacZ* reporter (Soriano, 1999). Extensive characterisation of the different Cre-reporter lines have demonstrated the

ROSA26R-*lacZ* reporter line appears to be amongst the most desirable due to their reliability and minimal level of background signal, allowing easy identification of reporter expression (Heffner *et al.*, 2012). We examined offspring produced from hemizygous *Ckm-Cre* and ROSA26R matings and tracked Cre activity by tracing *β*-galactosidase expression. Cre activity seems to be present in the head mesenchyme in the mouse embryo at E11.5, consistent with reports which first detect Ckm mRNA in the head and neck region, followed by remaining skeletal muscles in the developing mouse embryo (Lyons *et al.*, 1991). Here we also show that Cre activity is restricted to skeletal and cardiac tissue only in the adult mouse.

Collectively, our immunoblot analyses, tissue-specific genotyping and analysis of Cre expression data verify that GFPT1 is knocked out in the desired tissues in our model. We confirm the generation of a robust GFPT1 deficient mouse model which will subsequently be characterised to enhance our understanding of the pathological changes occurring as a result of hypoglycosylation.

Chapter 4: Characterisation of the *Gfpt1*^{tm1a} and *Gfpt1*^{tm1b} allele

4.1 Introduction

Full understanding of the pathophysiological consequences of a knockout mouse model is dependent on knowing where and when the gene of interest is expressed. Only then can we make informative genotype-phenotype correlations in transgenic mice. The *Gfpt1*^{tm1b}*lacZ* reporter allele provides a means of detecting where GFPT1 is normally expressed in the mouse. One advantage of using this line is that *β*-galactosidase expression can easily be detected in the developing mouse embryo and in adult tissues using simple well established protocols. This overcomes having to design and troubleshoot a protocol specific to the gene of interest. There is currently no GFPT1 antibody that demonstrates the localisation of GFPT1 in mouse tissues. Furthermore, the specificity of antibodies in general is often poor and requires optimisation. Since a single copy of the *lacZ* transgene expresses sufficient levels of *β*-galactosidase (Coleman *et al.*, 2015), we are able to use the *Gfpt1*$^{+/tm1b}$ line to track GFPT1 expression.

Occasionally heterozygous knockout mice display a sufficient reduction in the amount of protein expressed to produce a phenotype. In some cases, these mice can be used to further investigate gene function. Based on the positioning of insertion of the *lacZ-neomycin* trapping cassette, the *Gfpt1*^{tm1a} allele is predicted to produce either a hypormorphic or null allele, and the *Gfpt1*^{tm1b} allele a null allele. Should homozygous mice be viable, or heterozygous mice demonstrate an adequate reduction in the amount of GFPT1 expression to produce a muscle phenotype, these mice could serve as potential models to investigate GFPT1 deficiency.

The most prominent feature examined in existing mouse models of CMS is the morphology of the neuromuscular junction. The neuromuscular junction in adult mouse muscle has a highly specialised ending. AChR display a ’pretzel’-like structure which are innervated by presynaptic motor axons. Endplate pathologies commonly seen in mouse models of CMS include smaller and fragmented AChRs, reduced intensity of AChR staining, and reduced expression of AChRs. Motor nerves often project beyond their target, lose their ability to innervate AChR, and sprouting is often observed in nerve terminals (Brandon *et al.*, 2003; Chevessier *et al.*, 2008; Bogdanik and Burgess,

2011; Chevessier *et al.*, 2012; Barik *et al.*, 2014; Messéant *et al.*, 2015). A developmental delay in maturation of the NMJ is also observed in both MuSK and agrin associated mouse models of CMS (Chevessier *et al.*, 2008; Kim and Burden, 2008; Bogdanik and Burgess, 2011).

In this study, we wish to investigate the pathophysiology of the NMJ as a consequence of GFPT1 deficiency. Furthermore, due to the ubiquitous nature of GFPT1, it is highly probable that we will observe pathological changes in muscle which we will examine using standard histological techniques.

4.1.1 *Aims*

- To breed and observe the viability of *Gfpt1*$^{+/tm1a}$, *Gfpt1*$^{+/tm1b}$, *Gfpt1*$^{tm1a/tm1a}$ and *Gfpt1*$^{tm1b/tm1b}$ mice.

- To validate mutant transcripts from the *Gfpt1*^{tm1a} and *Gfpt1*^{tm1b} allele using RT-PCR.

- To study the morphology of the synapse and perform histological analyses on muscle from viable mouse models.

- To study the relative expression levels of GFPT1 in mouse tissues using immunoblot analyses.

- To track GFPT1 expression in mouse tissues using the *lacZ*-reporter in the *Gfpt1*^{tm1b} allele.

4.2 Viability of mice harbouring the *Gfpt1*^{tm1a} and *Gfpt1*^{tm1b} allele

4.2.1 *Frequency of heterozygous and homozygous Gfpt1*^{tm1a} *and Gfpt1*^{tm1b} *mice*

Offspring generated from heterozygote crosses do not follow the expected Mendelian pattern of inheritance with an expected genotypic ratio of 1:2:1; (*Gfpt1*$^{+/+}$:*Gfpt1*$^{+/tm1a}$: *Gfpt1*$^{tm1a/tm1a}$); (*Gfpt1*$^{+/+}$:*Gfpt1*$^{+/tm1b}$: *Gfpt1*$^{tm1b/tm1b}$) . Only wild type (27%) and *Gfpt1*$^{+/tm1a}$ (73%) mice were obtained from heterozygote *Gfpt1*^{tm1a} crosses (Figure 4.1A). No *Gfpt1*$^{tm1a/tm1a}$ mice were observed. Similarly, only wild type (39%) and *Gfpt1*$^{+/tm1b}$ (61%) mice were obtained from heterozygote *Gfpt1*^{tm1b} crosses. No *Gfpt1*$^{tm1b/tm1b}$ mice were born (Figure 4.1B).

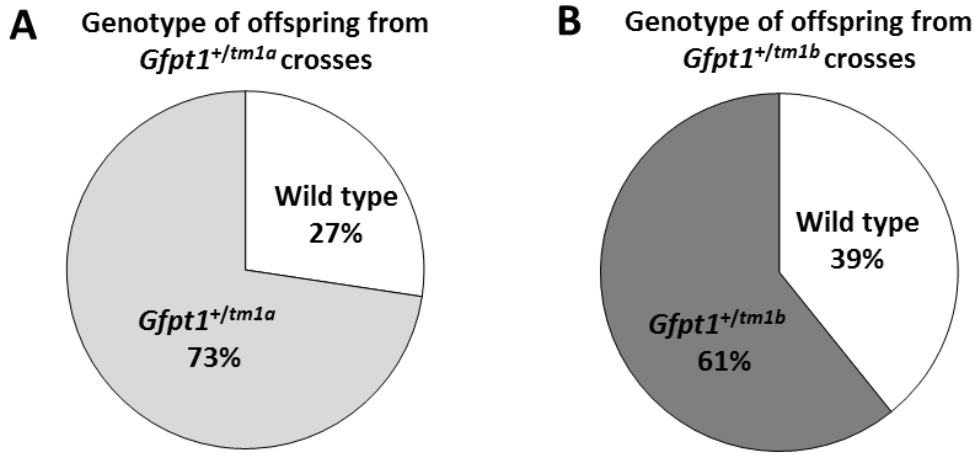

Figure 4.1 The percentage of offspring representing each genotype. (A) *Gfpt1*$^{+/tm1a}$ crosses generated wild type and *Gfpt1*$^{+/tm1a}$ offspring only. *Gfpt1*$^{tm1a/tm1a}$ mice were never observed (n=132). (B) *Gfpt1*$^{+/tm1b}$ crosses generated wild type and *Gfpt1*$^{+/tm1b}$ offspring only. *Gfpt1*$^{tm1b/tm1b}$ mice were never observed (n= 153).

4.2.2 *Frequency of heterozygous and homozygous Gfpt1^{tm1a} and Gfpt1^{tm1b} embryos*

Since no homozygous offspring were observed, we analysed the genotype of embryos generated from heterozygote crosses. The age of embryos taken ranged from E11.5 to E15.5. No *Gfpt1$^{tm1a/tm1a}$* or *Gfpt1$^{tm1b/tm1b}$* embryos were observed (Figure 4.2).

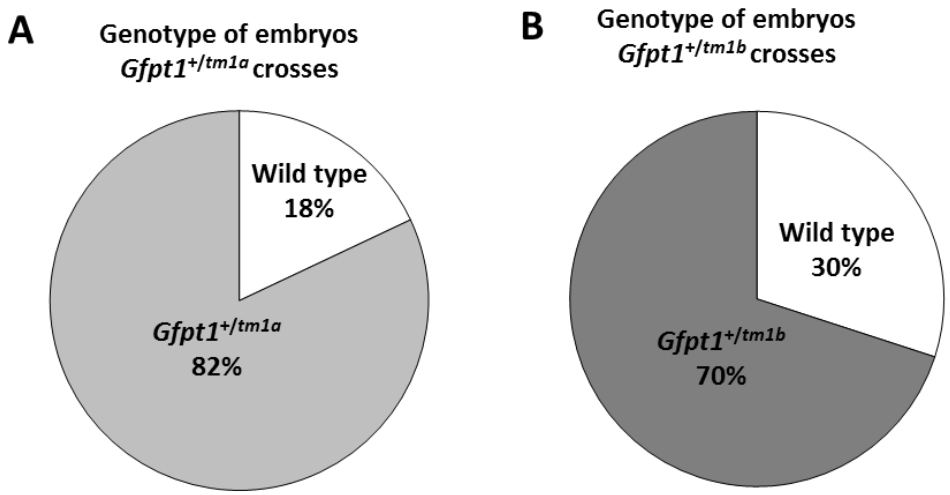

Figure 4.2. The percentage of embryos representing each genotype between E11.5-E15.5. (A) *Gfpt1^{tm1a}* crosses generated wild type and *Gfpt1$^{+/tm1a}$* embryos only. *Gfpt1$^{tm1a/tm1a}$* embryos were never observed (n=28). (B) *Gfpt1^{tm1b}* crosses generated wild type and *Gfpt1$^{+/tm1b}$* embryos only. *Gfpt1$^{tm1b/tm1b}$* embryos were never observed (n= 33).

4.3 Validation of mutant transcripts by RT-PCR

We used RT-PCR to identify transcripts generated from wild type, *Gfpt1*^{tm1a} and *Gfpt1*^{tm1b} alleles. RNA extracted from heterozygous *Gfpt1*$^{+/tm1a}$ and *Gfpt1*$^{+/tm1b}$ mice was transcribed to cDNA. A forward primer was designed in exon 6 and reverse primers in exons 7, 8, 8a. For further confirmation, we designed reverse primers in 7/8, 8/8a, and 8/9. Fragments from the wild type allele produces expected bands of 130 bp, 217 bp, 293 bp, 179 bp, 260 bp and 262 bp (Figure 4.3A, Table 4.1). The *Gfpt1*^{tm1a} allele is predicted to produce either a hypormorphic or null allele, and the *Gfpt1*^{tm1b} is expected to produce a null allele. To detect *Gfpt1*^{tm1a} and *Gfpt1*^{tm1b} transcripts, reactions were run using a forward primer designed in the gene trapping neomycin cassette, and reverse primers in the neomycin cassette and exons 7, 8, 8a, 7/8, 8/8a, and 8/9. We observe a control band of 220 bp corresponding to an amplicon within the neomycin cassette from *Gfpt1*^{tm1a} and *Gfpt1*^{tm1b} transcripts. No transcripts were detected downstream of the neomycin cassette (Table 4.1, Figure 4.3B).

Allele	Forward Primer	Reverse Primer	Expected Amplicon	Observed Amplicon
Wild type	Exon6F	Exon7R	130 bp	✓
		Exon8R	217 bp	✓
		Exon8aR	293 bp	✓
		Exon7/8R	179 bp	✓
		Exon8/8aR	260 bp	✓
		Exon8/9R	262 bp	✓
Gfpt1^{tm1a}	NeoF	NeoR	220bp	✓
		Exon7R	None/211 bp	×
		Exon8R	None/298 bp	×
		Exon8aR	None/374 bp	×
		Exon7/8R	None/260 bp	×
		Exon8/8aR	None/341 bp	×
		Exon8/9R	None/343 bp	×
Gfpt1^{tm1b}	NeoF	NeoR	220bp	✓
		Exon7R	No bands	×
		Exon8R	No bands	×
		Exon8aR	No bands	×
		Exon7/8R	No bands	×
		Exon8/8aR	No bands	×
		Exon8/9R	No bands	×

Table 4.1. PCR reactions used to detect transcripts from wild type, *Gfpt1*^{tm1a} and *Gfpt1*^{tm1b} alleles. A list of primers used with the expected and observed band size for each reaction are shown.

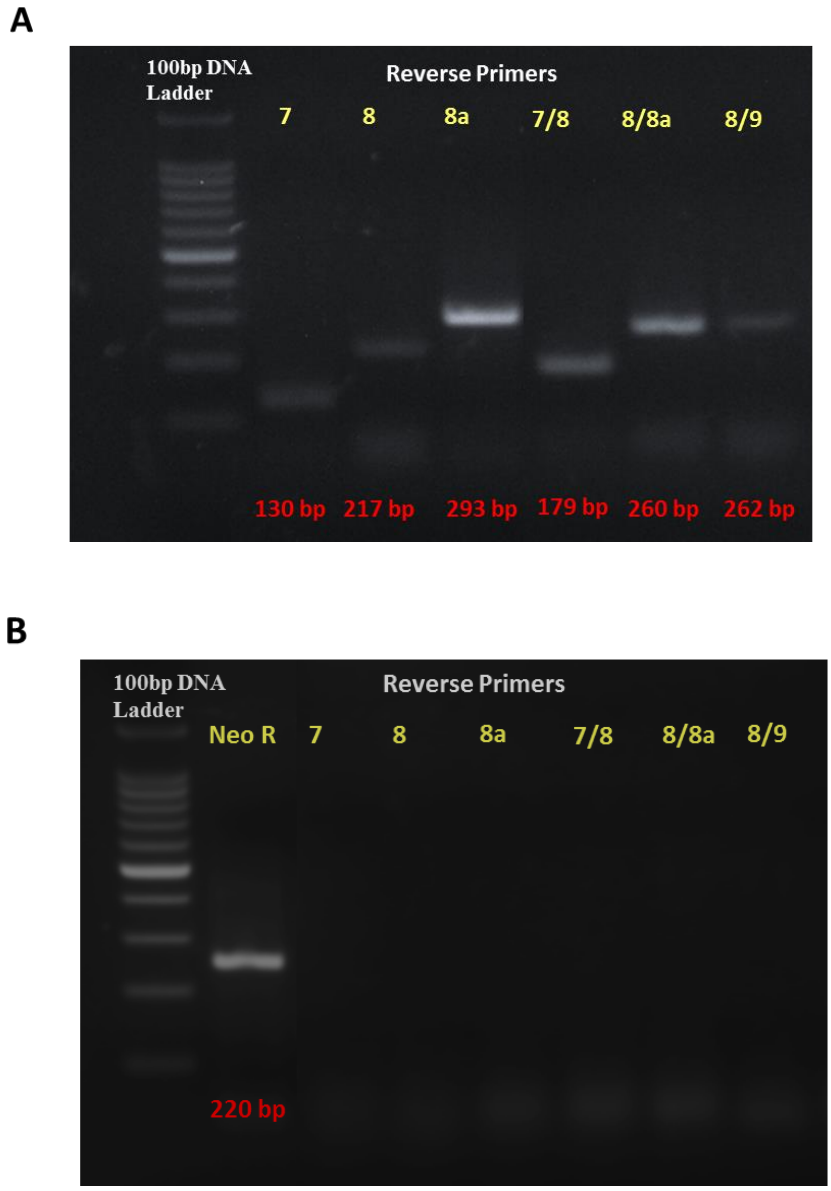

Figure 4.3. Representative RT-PCR showing transcripts from *Gfpt1*$^{+/tm1a}$ and *Gfpt1*$^{+/tm1b}$ mice. (A) We observe bands with expected sizes corresponding to transcripts from the wild type allele. (B) Example of PCR products from the *Gfpt1*^{tm1a} and *Gfpt1*^{tm1b} allele. We observe a 220 bp band for the control reaction (NeoF and NeoR), but no bands were detected in all other reactions. All bands are measured against a 100 bp DNA ladder.

4.4 Histological analysis of skeletal muscle in *Gfpt1*$^{+/tm1b}$ mice

4.4.1 *Hematoxylin and eosin staining of skeletal mouse muscle*

Histological analysis of skeletal muscle was achieved by staining with hematoxylin and eosin (H&E). TA, gastrocnemius, diaphragm, intercostal, soleus and EDL muscles were dissected from 3 month old wild type and *Gfpt1*$^{+/tm1b}$ mice. 10 µm thick transverse sections were prepared and the muscles were stained with H&E. There appears to be no histological difference between wild type and *Gfpt1*$^{+/tm1b}$ mice. Myofibres maintain their characteristic polygonal shape with peripheral nuclei. The sarcolemma and sarcoplasm remain intact and muscle tissues show a homogenous fibre size distribution (Figure 4.4).

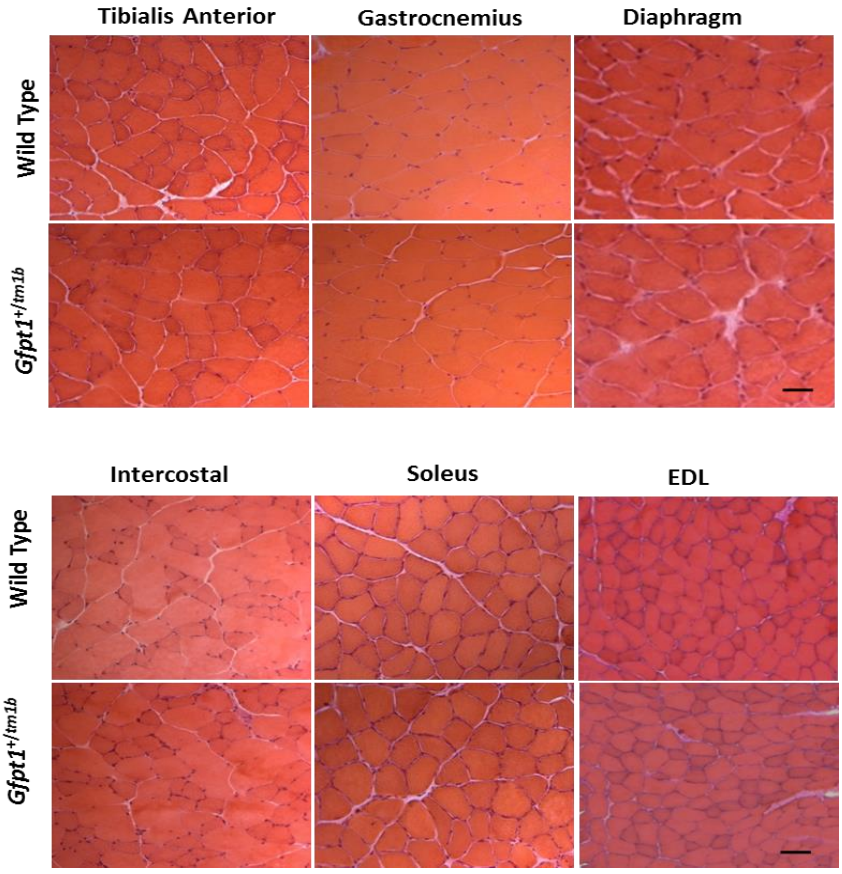

Figure 4.4 Histological analysis of skeletal muscle in wild type and *Gfpt1*$^{+/tm1b}$ mice. Brightfield images of H&E stained TA, gastrocnemius, diaphragm, intercostal, soleus, and EDL muscles from wild type and *Gfpt1*$^{+/tm1b}$ mice. Eosin labels the sarcoplasm (pink). Hematoxylin labels the nuclei (blue). No histological difference was observed in *Gfpt1*$^{+/tm1b}$ muscle tissue compared to controls. Scale bar = 10µm for diaphragm, and 20 µm for all remaining tissues.

4.4.2 *Quantification of myofibre area*

The cross-sectional area of individual myofibres were measured using ImageJ software (Figure 4.5A). There were no significant differences in myofibre size in all muscles examined compared to their corresponding controls (Figure 4.5B).

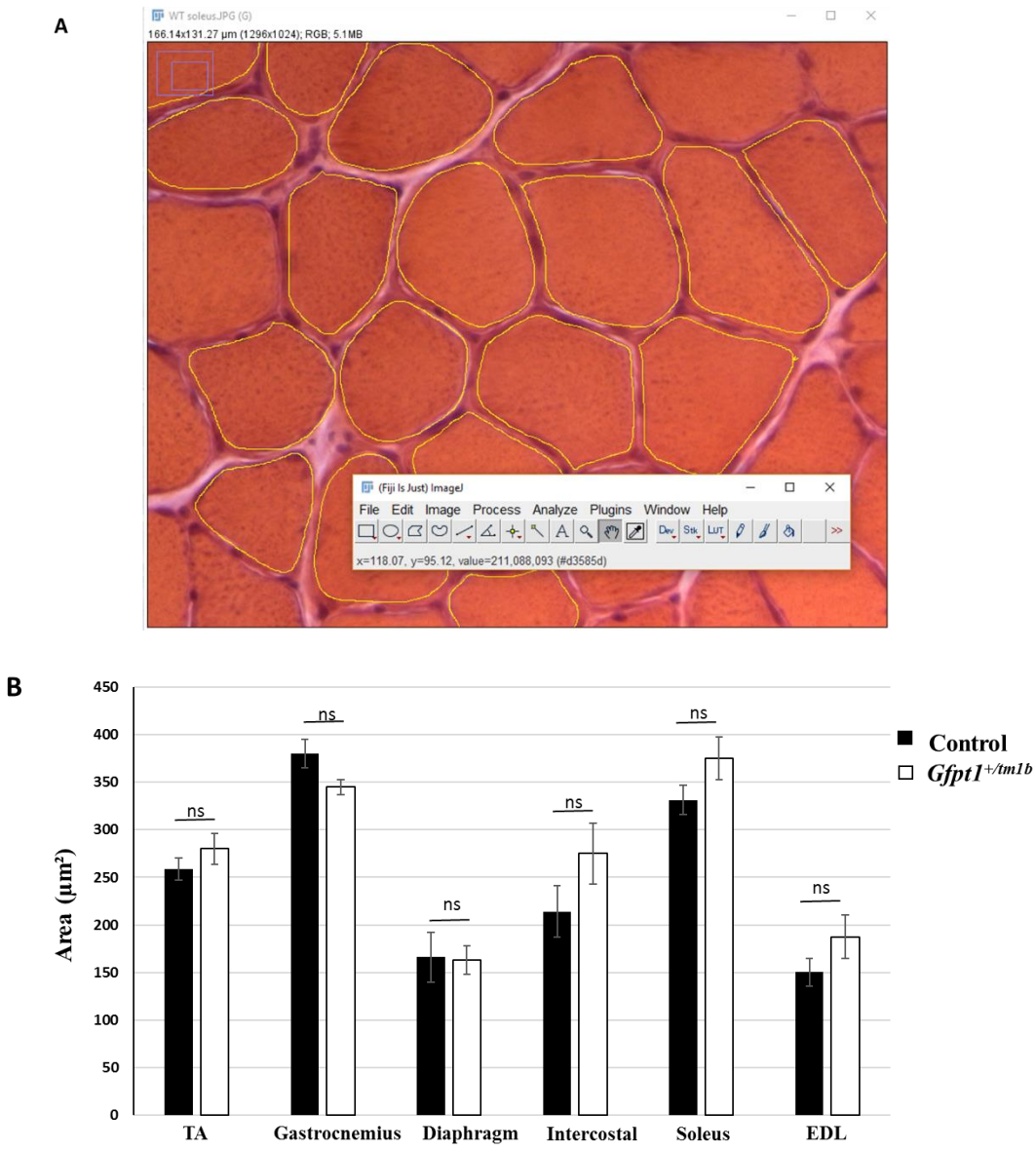

Figure 4.5. Quantitative analysis of the area of individual myofibres in skeletal muscle. (A) Screenshot image demonstrating how myofibre area was calculated using ImageJ software. (B) Muscles analysed include TA, gastrocnemius, diaphragm, intercostal, soleus, and EDL muscles from wild type and *Gfpt1*$^{+/tm1b}$ mice. No significant differences in the area of individual myofibres was observed. Data represent mean ± SEM. (n=4 mice per genotype) p>0.05, ns, not significant.

4.5 Analysis of the NMJ in *Gfpt1*$^{+/tm1b}$ mice

4.5.1 *Immunofluorescence staining of AChRs*

In order to establish whether transgenic mice display an NMJ phenotype, we analysed AChRs in TA, diaphragm, intercostal, and EDL muscles from 3 month old control and *Gfpt1*$^{+/tm1b}$ mice. Whole-mount muscles were stained with α-bungarotoxin to label AChRs. AChRs maintain their characteristic 'pretzel'-like structure and appear normal in size in all muscles analysed (Figure 4.6).

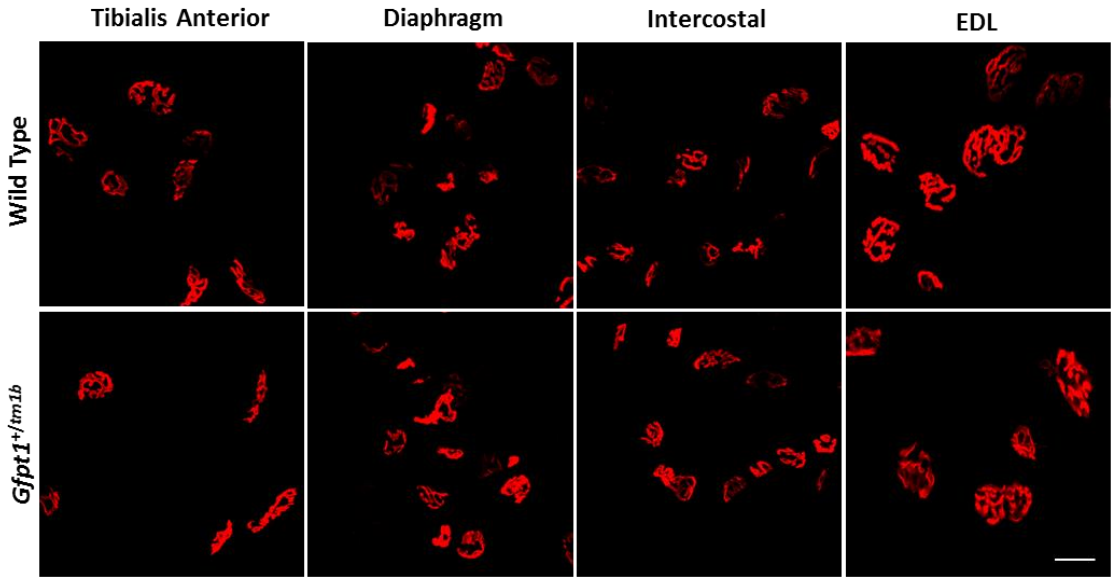

Figure 4.6. Immunofluorescence analysis of AChRs in skeletal mouse muscle from wild type and *Gfpt1*$^{+/tm1b}$ mice. Confocal Z-stack projections of whole-mount TA, diaphragm, intercostal and EDL muscles were labelled with Alexa fluor 594 α-bungarotoxin (red) to label AChRs. Scale bar = 20µm.

4.5.2 *Quantification of AChR cluster area*

For quantification of AChR cluster area, single-projected images derived from overlaying image stacks were quantified using ImageJ analysis software (Figure 4.7A). No significant differences in the area of individual AChR clusters was observed between wild type and *Gfpt1*$^{+/tm1b}$ mice (Figure 4.7B).

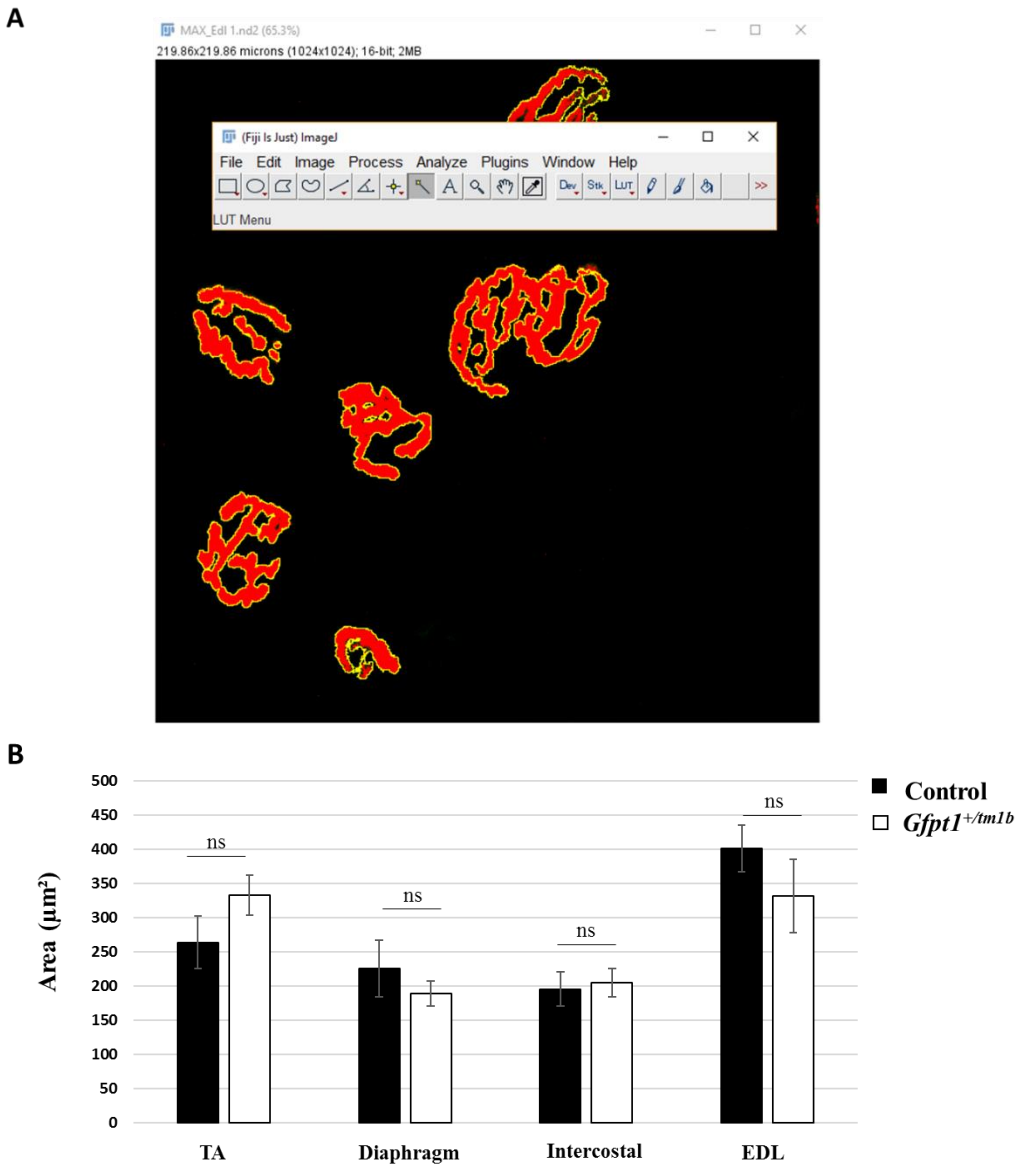

Figure 4.7 Quantitative analysis demonstrating AChR cluster area. (A) Screenshot image demonstrating how the area of individual AChR clusters was calculated using ImageJ software. (B) No differences in the size of AChR was observed between wild type and *Gfpt1*$^{+/tm1b}$ mice. (n=4 mice per genotype). Data are mean ± SEM. (n=6) p>0.05, ns, not significant.

4.5.3 *Immunofluorescence staining of presynaptic and postsynaptic components of the NMJ*

To study presynaptic and postsynaptic co-localisation and morphology, whole-mount muscles were stained with α-bungarotoxin to label AChRs and antibodies against neurofilament and synaptophysin to label axonal branches and nerve terminals, respectively. Neurofilament is a key component of the neuronal cytoskeleton and synaptophysin is a major synaptic vesicle protein p38. In control mice, axonal branches project normally and innervate the well-defined 'Pretzel'-like AChR. *Gfpt1*$^{+/tm1b}$ show normal morphology of the NMJ which resemble endplates seen in wild type mice. AChRs maintain their characteristic 'Pretzel'-shape and axons project normally forming synaptic contacts with AChRs (Figure 4.8).

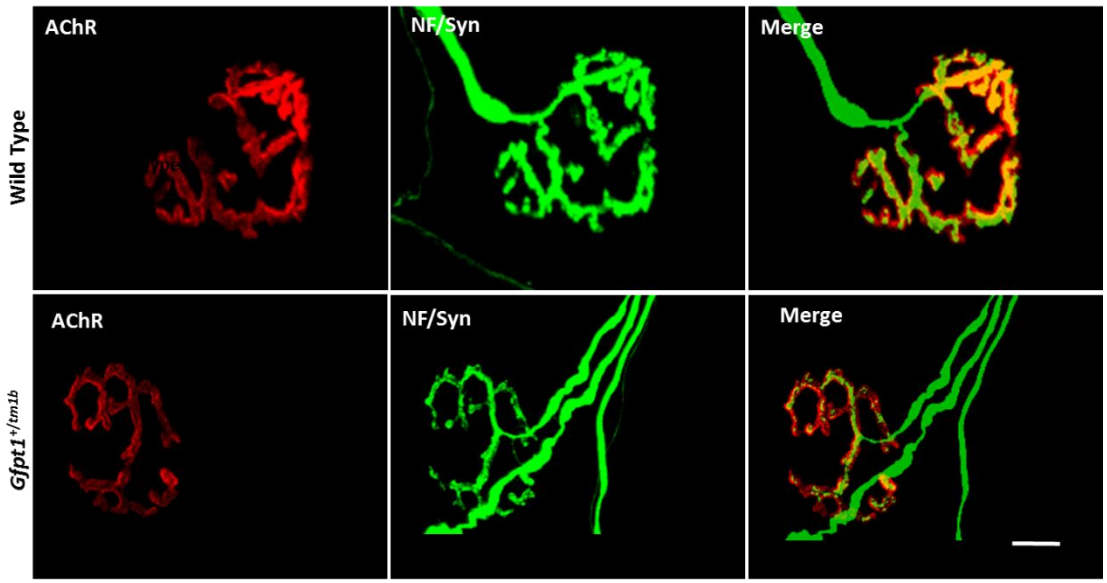

Figure 4.8. Immunofluorescence analysis of endplates in skeletal mouse muscle from wild type and *Gfpt1*$^{+/tm1b}$ mice. Confocal Z-stack projections of whole-mount TA muscles labelled with Alexa fluor 594 α-bungarotoxin (red), anti-neurofilament (green) and anti-synaptophysin (green). Neurofilament (NF), Synaptophysin (Syn). Scale bar = 10µm.

4.6 Summary of phenotypes observed in *Gfpt1*$^{+/tm1b}$ mice

The International Mouse Phenotyping Consortium (IMPC) is a collaborative team of research centres and funding organisations whose goal is to discover a functional insight for every gene by generating and systematically characterising knockout mouse strains. Each mutant line available is characterised according to a broad criterion which covers all the major adult organ systems and human disease. The phenotype data collected for the *Gfpt1*$^{+/tm1b}$ mouse line demonstrates that the *Gfpt1*^{tm1b} allele results in haploinsufficiency which is evident in some organ systems. We have collected and summarised the phenotype data from *Gfpt1*$^{+/tm1b}$ mice (Table 4.2) (Brown and Moore, 2012).

System	Outcome	Statistical Significance
Spleen	Decreased weight	**p<0.001**
Tibia length	Reduction in length	
Eye morphology	Persistence of hyaloid vascular system	
Intraperitoneal glucose tolerance test	Increased mean blood glucose concentration	
Body Composition (DEXA lean/fat)	Reduced bone area (BMC/BMD)	**p<0.01**
	Reduced bone mineral content (excluding skull)	
X-ray	Abnormal shape of vertebrae	
Organ Weight	Increase weight of kidney	
Clinical Blood Chemistry	Increased levels of potassium	
Hematology	Increased red blood cell count	
Body Composition (DEXA lean/fat)	Reduced lean mass	**p<0.05**
Clinical Blood Chemistry	Increased HDL-cholesterol	
	Increased total cholesterol	
	Variable Iron	
	Variable alkaline phosphatase	
	Variable total bilirubin	
Contact Righting	Impaired righting reflex	
Electrocardiogram (ECG)	Variable ST	
	Variable PR	
	Variable QRS	
Haematology	Variable white blood cell count	
	Variable platelet count	
	Increased haemoglobin	
	Decreased mean cell volume	
Intraperitoneal glucose tolerance test	Increased mean blood glucose concentration (fasting)	
X-ray	Abnormal pelvis shape	
Muscle	Grip strength	**Not significant, p>0.05**
	Myofibre area	
	Neuromuscular junction – AChR cluster area	

Table 4.2. A summary of clinical findings observed in *Gfpt1*$^{+/tm1b}$ mice. Data collected from the IMPC and in-house (bold) demonstrates some phenotypical differences between wild type and *Gfpt1*$^{+/tm1b}$ mice.

4.7 Analysis of GFPT1 expression

4.7.1 *Western blot analysis of* GFPT1 *expression*

Expression of GFPT1 in tissues from wild type mice was examined by western blotting using a polyclonal antibody against GFPT1. GFPT1 (~79 kDa) is expressed in the heart, TA, gastrocnemius, diaphragm, intercostal, soleus, brain and kidney. Glyceraldehyde 3-phosphate dehydrogenase (GAPDH) (~38 kDa) was used as a loading control (Figure 4.9).

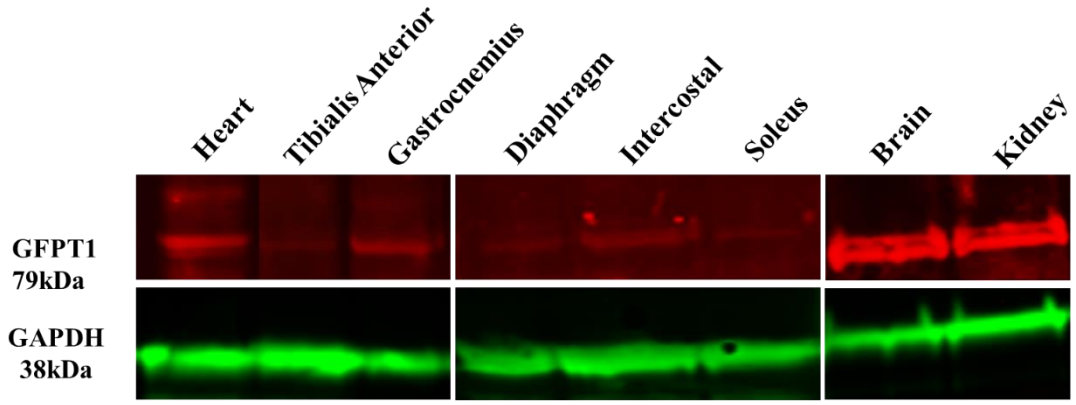

Figure 4.9. Western blot analysis of GFPT1 expression in muscle and non-muscle tissues from wild type mice. GFPT1 protein (~79kDa) is detected in the gastrocnemius, TA, diaphragm, intercostal, EDL, soleus, heart, brain and kidney. GAPDH (~38kDa) was used as a loading control. All bands were measured against an 8-260 kDa Chameleon Duo Ladder protein ladder.

4.7.2 *Densitometry analysis showing the relative expression of* GFPT1 *in mouse tissues*

The relative expression levels between tissues was analysed using the gel analysis tool on ImageJ software. All blots were converted to greyscale images and bands were analysed by producing profile plots representing the relative density of each band (Figure 4.10A). The area of the peaks in the profile plots correspond to the intensity of the bands. The software subtracts the background and represents each peak as a percentage of the total intensity. The density of GFPT1 bands were normalised, followed by that of GAPDH loading control bands. The relative density of GFPT1 was then divided by the relative density of the corresponding loading control. The levels of GFPT1 expression varies between different tissues. The greatest amount of GFPT1 appears to be expressed in the brain, followed by the kidney, heart and skeletal muscles. The level of GFPT1 expression varies between different skeletal muscles (Figure 4.10B).

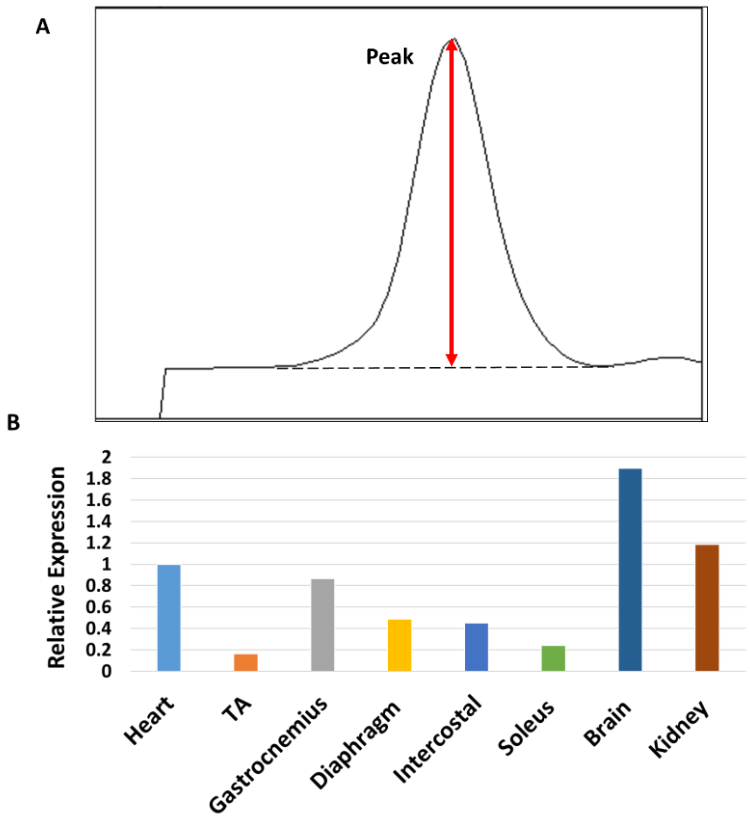

Figure 4.10. Quantitative analysis showing the relative expression levels of GFPT1 in mouse tissues. (A) Modified screenshot image of a profile plot demonstrating how band intensity was quantified using ImageJ gel analysis. (B) Graph demonstrating GFPT1 expression levels normalised to their corresponding GAPDH loading controls. Data corresponds to immunoblot bands seen in Figure 4.9.

4.7.3 GFPT1 expression detected by *β*-galactosidase activity in mice

Gfpt1$^{+/tm1b}$ mice carry the *lacZ*-reporter gene which expresses *β*-galactosidase under the control of the *Gfpt1* promoter. To analyse the pattern of GFPT1 expression we detected the enzymatic activity of *β*-galactosidase using X-gal in mouse embryos and adult tissues.

β-galactosidase activity in the mouse embryo

We mated *Gfpt1*$^{+/tm1b}$ mice which generated wild type and *Gfpt1*$^{+/tm1b}$ embryos. Embryos aged E11.5, E12.5 and E13.5 were isolated and stained with X-gal. We observe ubiquitous expression of *β*-galactosidase in *Gfpt1*$^{+/tm1b}$ embryos but not in control littermates. Tail tips were taken from the embryos which was used for genotype verification.

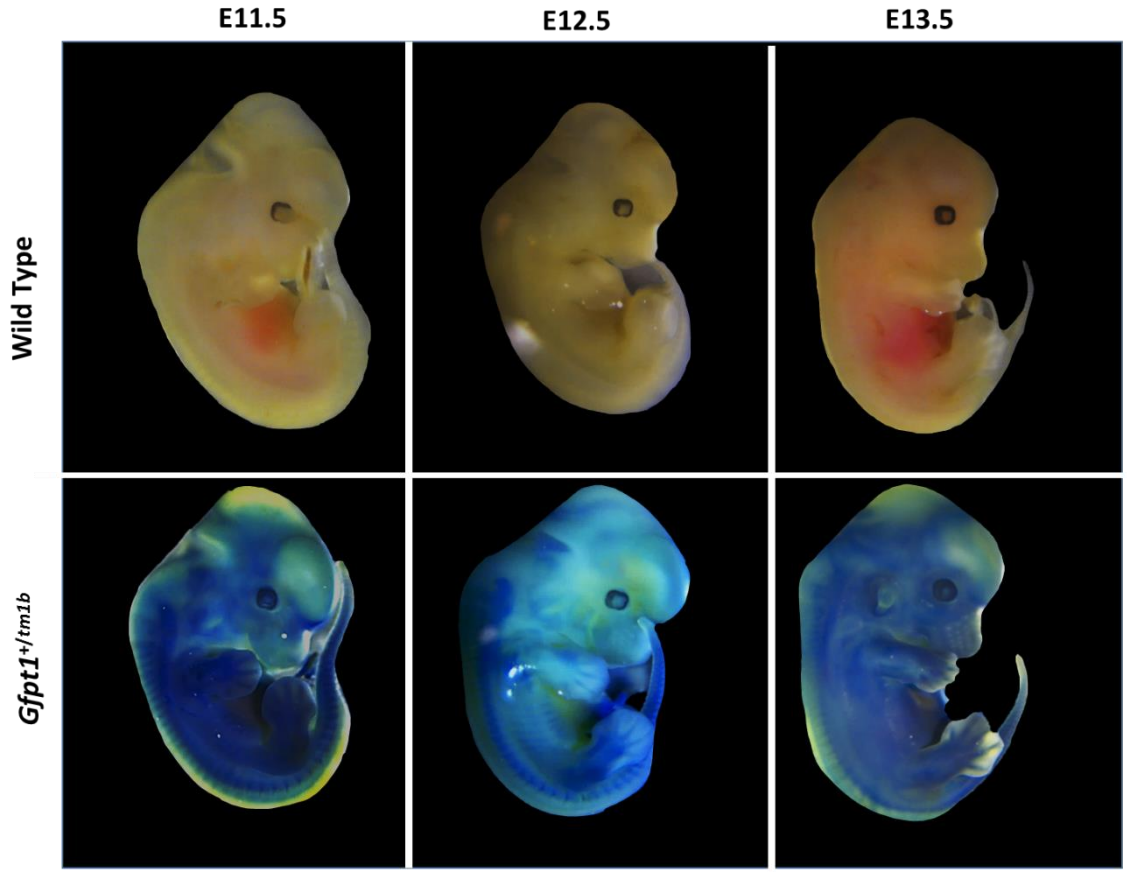

Figure 4.11. *Gfpt1 lacZ* transgene expression in mouse embryos. E11.5, E12.5 and E13.5 wild type and *Gfpt1*$^{+/tm1b}$ embryos were stained with X-gal. *β*-galactosidase activity (blue) was detected throughout the entire *Gfpt1*$^{+/tm1b}$ embryo at all time points. *β*-galactosidase activity is not observed in wild type embryos.

β-galactosidase activity in adult mouse tissues

We analysed the pattern of GFPT1 expression in the adult mouse by tracking the enzymatic activity of *β*-galactosidase in the gastrocnemius, TA, diaphragm, EDL, intercostal, soleus, and heart muscles. We also analysed non-muscle tissues including the eye, kidney and brain. Transverse sections of adult mouse tissues were sectioned and stained with X-gal. We observed *β*-galactosidase activity in all skeletal muscles and the heart. GFPT1 is also expressed in extraocular muscles, eyes, kidneys and the brain.

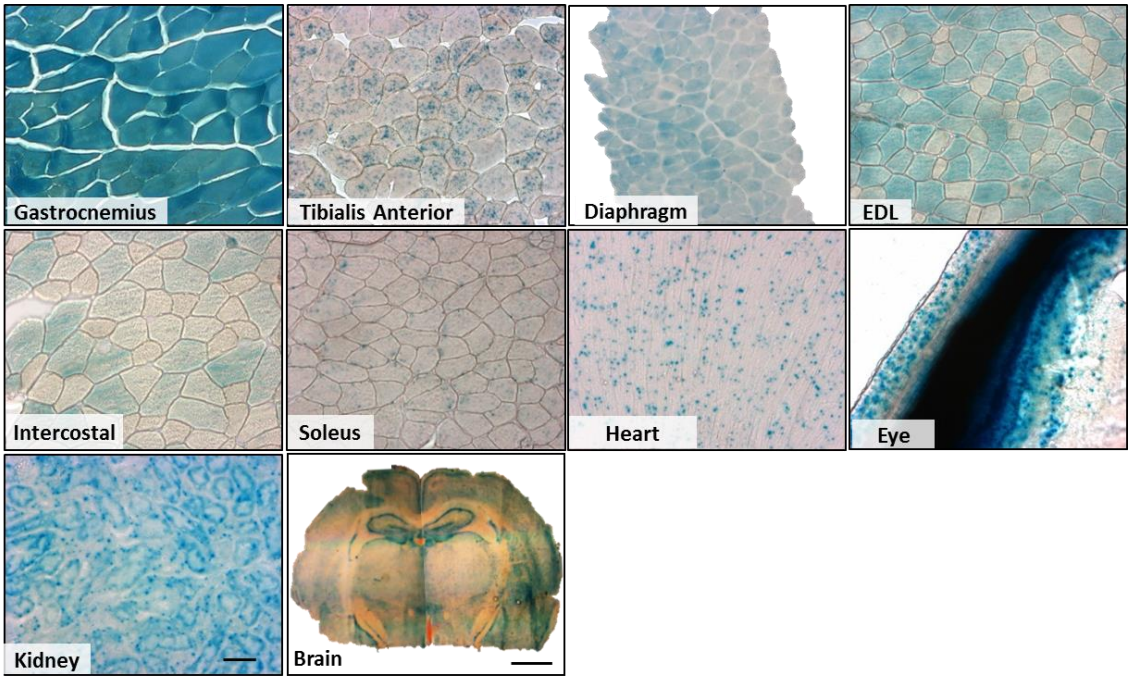

Figure 4.12. *Gfpt1 lacZ* transgene expression in adult mouse tissues.
β-galactosidase activity was detected with X-Gal as a substrate on sections of tissues from 3 month old *Gfpt1*$^{+/tm1b}$ mice. *β*-galactosidase activity (blue) is present in all tissues analysed. Scale bar = 400µm in the brain; 20µm in all remaining tissues.

4.7.4 *Summary of* GFPT1 *expression in Gfpt1$^{+/tm1b}$ mice*

The IMPC also work on understanding the pattern of protein expression of mouse lines which harbour the *lacZ*-reporter gene that expresses *β*-galactosidase. The GFPT1 expression data collected for the *Gfpt1$^{+/tm1b}$* mouse line demonstrates ubiquitous expression of GFPT1 in numerous organ systems (Table 4.3) (Dehaven *et al.*, 2001; Petryszak *et al.*, 2016).

Systems/structures	Adult tissues
Cardiovascular	**Heart**, aorta
Musculoskeletal	**Gastrocnemius**, **TA**, **diaphragm**, **EDL**, **soleus**, **intercostal**, bone, cartilage
Nervous	**Cerebral cortex**, **hippocampus, striatum**, olfactory lobe, hypothalamus, cerebellum, brainstem, spinal cord, peripheral nervous system
Reproductive	Ovary, oviduct, uterus, prostate, lower urinary tract, testis, prostate
Sensory	**Eye - including extraocular muscles**
Integumentary	Skin, mammary glands
Endocrine	Adrenal gland, thyroid gland, parathyroid gland, pituitary gland
Renal/urinary	Lower urinary tract, **kidney - renal medulla**, **renal cortex**
Respiratory	Trachea, lungs, cartilage
Digestive/ alimentary system	Large intestine, liver, gall bladder, small intestine, stomach, esophagus
Lymphatic	Lymph node, spleen
Immune	Thymus, payers patch

Table 4.3. A summary of GFPT1 expression in adult mouse tissues. Data summarised represents observations of *β*-galactosidase activity in numerous organ systems. Data collected from the IMPC and those generated in-house (bold) are shown.

4.8 Discussion

The frequency of mice born does not reflect the Mendelian frequencies for the expected genotypes. Homozygous *Gfpt1*$^{tm1a/tm1a}$ and *Gfpt1*$^{tm1b/tm1b}$ mice were never obtained from heterozygote crosses, but *Gfpt1*$^{+/tm1a}$ and *Gfpt1*$^{+/tm1b}$ are viable. Genotype analysis of embryos revealed no GFPT1 deficient homozygous mice were observed as early as embryonic day 11.5. This information is supported by data from the IMPC, which states that no viable homozygous embryos were observed at E12, but when screening E9.5 *Gfpt1*^{tm1b} embryos few were viable (Brown and Moore, 2012). For the purpose of our study, we need to examine the morphology of the NMJ. AChR cluster formation and innervation occurs between E12-E18.5 in the mouse embryo (Lin *et al.*, 2001; Wu *et al.*, 2010). Therefore, viable embryos younger than E12 are inadequate for our study as they do not permit investigation of the NMJ.

We do not detect transcripts from the *Gfpt1*^{tm1a} and *Gfpt1*^{tm1b} alleles, suggesting that insertion of the *lacZ* gene-trap cassette in the *Gfpt1* gene completely disrupts its function generating a null allele. Since both alleles are essentially nulls, we selected one model (*Gfpt1*$^{+/tm1b}$) to analyse whether these mice present with haploinsufficiency. *Gfpt1*$^{+/tm1b}$ display normal morphology of both the presynaptic and postsynaptic components at the NMJ in all muscles analysed. Moreover, histological analysis of different muscles revealed no signs of a muscle pathology. Analysis of myasthenia conducted using a grip strength assay carried out as part of the IMPC revealed no significant changes in *Gfpt1*$^{+/tm1b}$ mice when compared to age-matched controls. Together these data suggest that haploinsufficiency does not impair muscle function in *Gfpt1*$^{+/tm1b}$ mice. These findings reflect the asymptomatic status of human carriers with loss of function GFPT1 mutations. The IMPC report significant variations in a number of non-muscle related phenotypes in *Gfpt1*$^{+/tm1b}$ mice. Although many of these findings are not representative of the human *GFPT1*-CMS phenotype, previous reports have established that GFPT1 is implicated in glucose metabolism and insulin resistance in humans (Elbein *et al.*, 2004) and mice (Hebert *et al.*, 1996; Cooksey *et al.*, 1999). More recently, studies have demonstrated that upregulation of SIL-1, which is commonly found in surviving neurons of Alzheimer's patients, leads to an increase in GFPT1 expression (Labisch *et al.*, 2017).

Immunoblot analyses of control tissue shows ubiquitous expression of GFPT1 in both muscle and non-muscle tissues consistent with findings from previous studies (Dehaven *et al.*, 2001; Niimi *et al.*, 2001). Furthermore, there appears to be differences in the relative expression levels between individual muscle and non-muscle tissues. Increasing the number of replicates in immunoblot experiments will confirm these preliminary findings. β-galactosidase activity used to analyse GFPT1 expression further demonstrates widespread GFPT1 expression in tissues from numerous organ systems. This data emphasises the importance of GFPT1 for normal development and function, and is indicative as to why homozygous knockout mice are not viable.

In summary, these data suggest that GFPT1 is essential for mouse embryogenesis and is responsible for proper functioning of numerous organ systems. Although haploinsufficiency is apparent in the *Gfpt1*$^{+/tm1b}$ model, the phenotypes observed are not specific to muscle or the NMJ. This model is therefore not particularly useful for investigating pathomechanisms in CMS, but has proven useful for tracking GFPT1 expression.

Chapter 5: Characterisation of the muscle-specific GFPT1 deficient mouse model

5.1 Introduction

The overall aim of this project is to generate a mouse model that recapitulates the phenotypes seen in patients with CMS as a result of GFPT1 deficiency. Most of these patients harbour mutations in the ubiquitous GFPT1 isoform, resulting in reduced, but not complete loss of GFPT1 expression (Guergueltcheva *et al.*, 2012; Huh *et al.*, 2012). The only exception is seen in a single patient with a nonsense mutation in the muscle-specific exon, which is predicted to result in complete loss of GFPT1-L, but conserves the ubiquitous isoform (Selcen *et al.*, 2013). Since homozygous *Gfpt1* knockout mice are embryonic lethal, we generated the *Gfpt1* muscle-specific knockout mouse model which disrupts both isoforms in muscle only. All remaining tissues continue to express the ubiquitous GFPT1 isoform.

To evaluate the validity of the GFPT1 deficient mouse model, we must investigate whether this model exhibits phenotypes observed in human *GFPT1*-CMS. The general pathological changes observed in human CMS include morphological alterations at the endplate, and histopathological changes in muscle including the presence of tubular aggregates due to a deficiency in glycosylation enzymes. Initially, these features will be analysed in the *Gfpt1*$^{tm1d/tm1d}$ model.

Patients with CMS present with fatigable muscle weakness. A series of tests have been devised to assess muscle function in mouse models. Tests that do not enhance disease progression allows evaluation of the natural course of disease and the efficacy of potential treatments on muscle function. The four-limb inverted screen test is a functional tool which measures the ability of mice to oppose their gravitational force through sustained limb tension. This test has proven useful for demonstrating fatigable muscle weakness in mice with neuromuscular disorders (Bogdanik and Burgess, 2011; Webster *et al.*, 2013; Messéant *et al.*, 2015). *In situ* isometric force measurements provide a means of assessing muscle fatigue through neural stimulation under physiological conditions. *In vitro* isometric force measurements allow critical evaluation of muscle contractile function. These tests are commonly used to assess myopathic and dystrophic phenotypes in mice (Chiu *et al.*, 2009; Sharp *et al.*, 2011;

Tamayo *et al.*, 2016) and can be used to identify changes in muscle strength and fatigue in GFPT1 deficient mice.

Ultimately, our goal is to discover the pathological mechanisms which can be therapeutically targeted with the aim of relieving CMS symptoms. This requires a thorough understanding of the molecular mechanisms underlying glycosylation deficient CMS. One method of enhancing our knowledge of disease causing mechanisms, and subsequently how the body responds to these changes, is through investigation of differentially regulated proteins. Proteome profiling is a powerful tool which can be used for the unbiased investigation of pathophysiological processes in neuromuscular disorders (Roos *et al.*, 2016). Identification of regulated proteins as a consequence of abnormal glycosylation will prove useful in deducing the molecular pathways implicated in the CMS phenotype observed.

In this chapter *Gfpt1*$^{tm1c/tm1c}$ mice are used as controls and muscle-specific GFPT1 knockout mice are referred to as *Gfpt1*$^{tm1d/tm1d}$. We also show preliminary characterisation of the Cre line using *Ckm-Cre* mice.

5.1.1 *Aims*

The overall aim of this chapter is to characterise the muscle-specific *Gfpt1* knockout mouse model, *Gfpt1*$^{tm1d/tm1d}$. This entails the following:

- To study the morphology of presynaptic and postsynaptic components of the NMJ.
- To investigate histopathological changes in mouse muscle.
- To use functional tests to assess muscle strength and fatigue in mutant mice.
- To analyse contractile properties of the diaphragm muscle using an *in vitro* test apparatus.
- Global proteomic analysis of regulated proteins as a result of GFPT1 deficiency.
- Immunoblot analysis of protein targets downstream of GFPT1.

5.2 Frequency and gross phenotype of *Gfpt1*$^{tm1d/tm1d}$ mice

5.2.1 *Frequency of Gfpt1*$^{tm1d/tm1d}$ *mice*

Gfpt1$^{tm1c/tm1c}$ mice were mated with *Gfpt1*$^{+/tm1c}$ *Ckm-Cre* mice to generate *Gfpt1*$^{tm1c/tm1c}$ *Ckm-Cre* (*Gfpt1*$^{tm1d/tm1d}$) mice. According to our breeding strategy, offspring generated do not follow the expected Mendelian pattern of inheritance with an expected genotypic ratio of 1:1:1:1 (*Gfpt1*$^{tm1c/tm1c}$: *Gfpt1*$^{+/tm1c}$: *Gfpt1*$^{+/tm1c}$ *Ckm-Cre: Gfpt1*$^{tm1c/tm1c}$ *Ckm-Cre*). Instead *Gfpt1*$^{+/tm1c}$ (5%), *Gfpt1*$^{+/tm1c}$ *Ckm-Cre* (50%), *Gfpt1*$^{tm1c/tm1c}$ (41%), and *Gfpt1*$^{tm1c/tm1c}$ *Ckm-Cre* (4%) of mice were obtained from crosses using this breeding strategy (Figure 5.1). We observe a very low frequency of *Gfpt1*$^{tm1d/tm1d}$ mice.

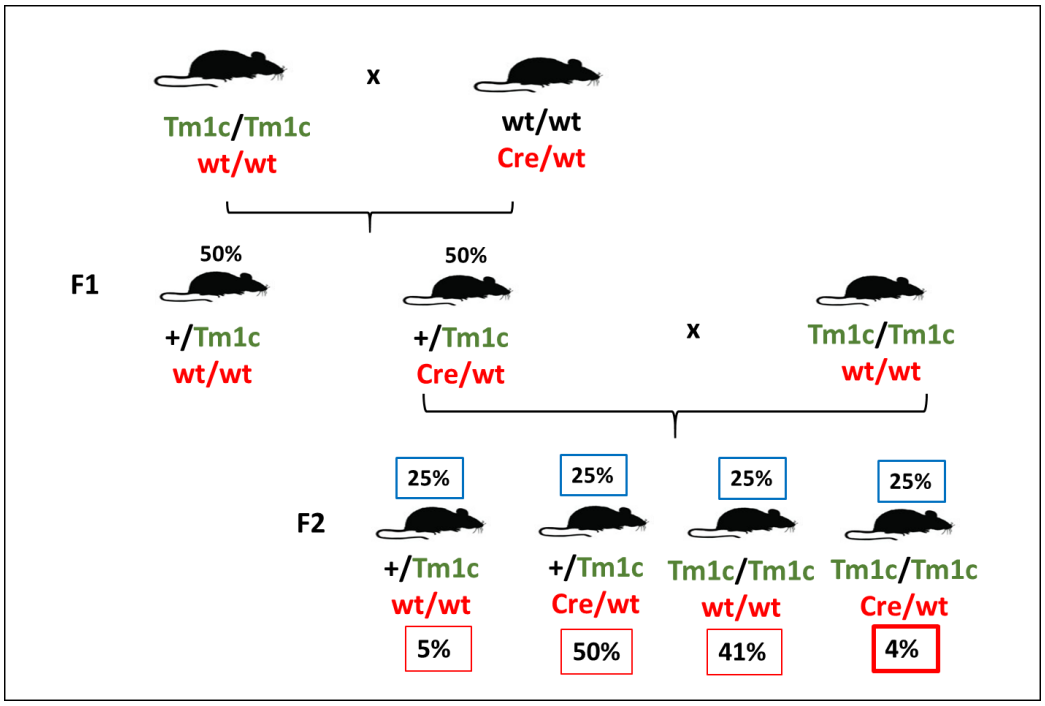

Figure 5.1. The percentage of offspring representing each genotype. 50% of offspring from *Gfpt1*$^{tm1c/tm1c}$ and *Ckm-Cre* crosses carry the *Cre* allele (F1). We acquire offpring from all the expected genotypes; *Gfpt1*$^{+/tm1c}$, *Gfpt1*$^{+/tm1c}$ *Ckm-Cre*, *Gfpt1*$^{tm1c/tm1c}$ and *Gfpt1*$^{tm1c/tm1c}$ *Ckm-Cre*. The frequency of mice expected (blue boxes) and obtained (red boxes) for each genotype are shown (F2).

5.2.2 *Gross phenotype and growth of Gfpt1$^{tm1d/tm1d}$ mice*

Gfpt1$^{tm1d/tm1d}$ mice do not exhibit gross phenotypical defects when compared to age-matched control mice. Control, *Ckm-Cre* controls and *Gfpt1$^{tm1d/tm1d}$* were weighed weekly from 6 weeks old to 6 months old. The general trend shows that *Gfpt1$^{tm1d/tm1d}$* mice are slightly smaller when compared to control mice over the course of development. However, no significant difference was observed in the growth curve between control and *Gfpt1$^{tm1d/tm1d}$* mice (Figure 5.2). We further demonstrate there is no change in body weight between control mice (Cre negative) and mice carrying the *Cre* transgene (Figure 5.2).

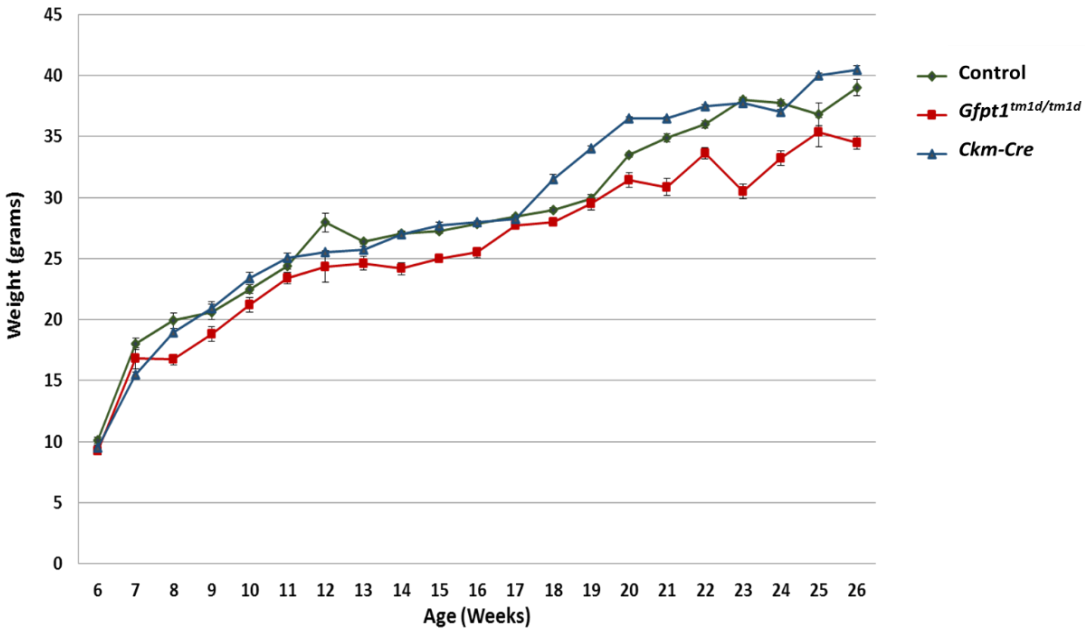

Figure 5.2. Growth curve of control, *Ckm-Cre* and *Gfpt1$^{tm1d/tm1d}$* mice. Growth curves demonstrating changes in body weight over a 6 month period. Data = mean ± SEM. p>0.05. Not significant. Control and *Gfpt1$^{tm1d/tm1d}$* mice (n=8), *Cre* (n=6).

5.3 Morphology of the neuromuscular junction

5.3.1 *Immunofluorescence of the NMJ*

We analysed the presynaptic and postsynaptic structure of NMJ in TA, intercostal, soleus, lumbrical and EDL muscles from 3 month old mice. Whole-mount muscles were stained with α-bungarotoxin to label AChRs, and with antibodies against neurofilament and synaptophysin to label axonal branches and nerve terminals, respectively. In control mice, axonal branches project normally and innervate the well-defined 'Pretzel'-like AChR. Observation of presynaptic components showed that *Gfpt1*$^{tm1d/tm1d}$ mice exhibit some morphological differences including the appearance of discontinuous and rather disorganised axonal projections. Nevertheless, axons project to endplates and form synaptic contacts with existing AChR. We do not observe overshooting, retractions or axonal sprouting. Analysis of postsynaptic structures revealed that AChR in *Gfpt1*$^{tm1d/tm1d}$ mice do not maintain the characteristic 'Pretzel'-shape that we see in control mice. Instead they appear smaller and fragmented in all muscles analysed in comparison to control mice (Figure 5.3).

Figure 5.3

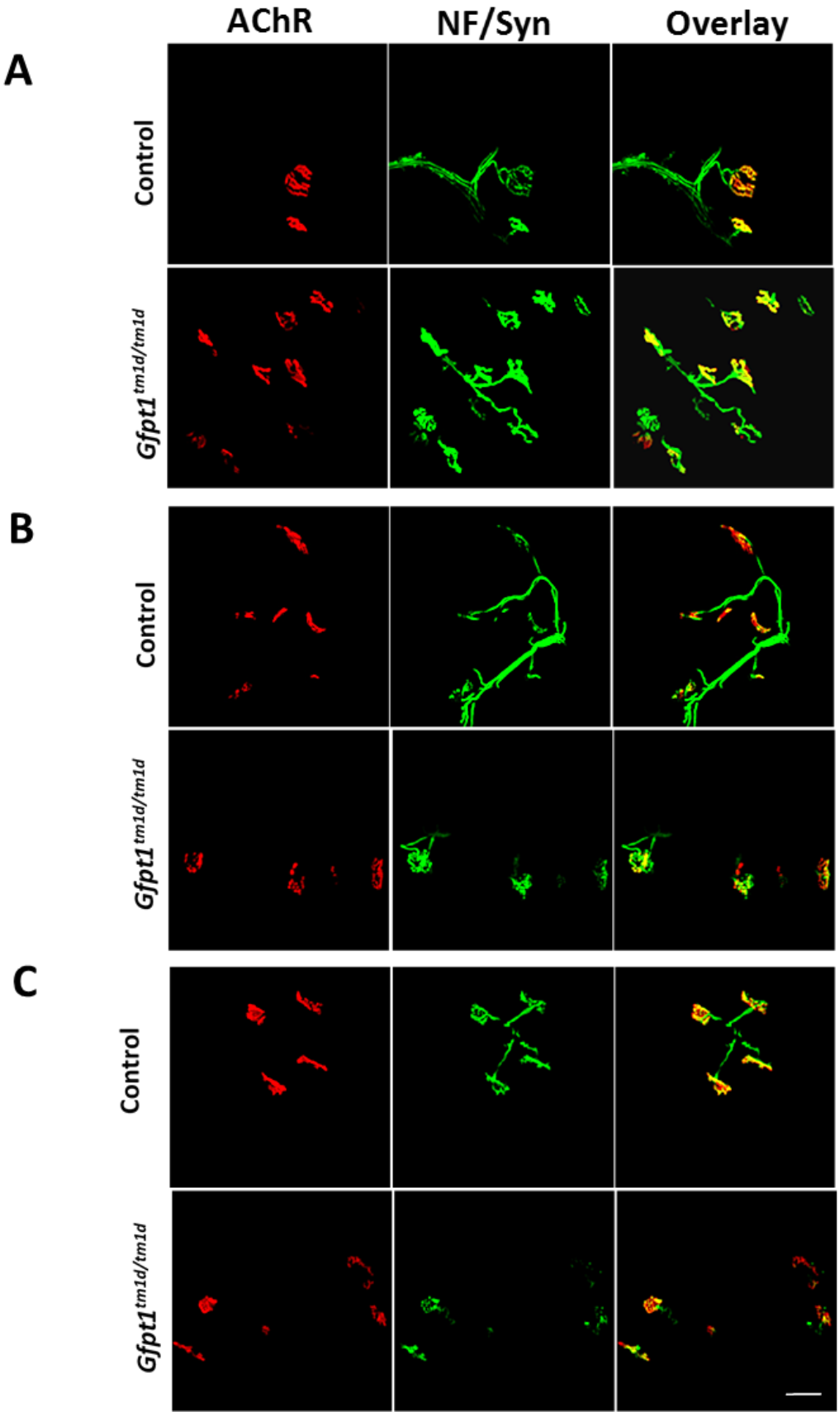
AChR
NF/Syn
Overlay
A
Control
Gfpt1tm1d/tm1d
B
Control
Gfpt1tm1d/tm1d
C
Control
Gfpt1tm1d/tm1d

Figure 5.3 continued

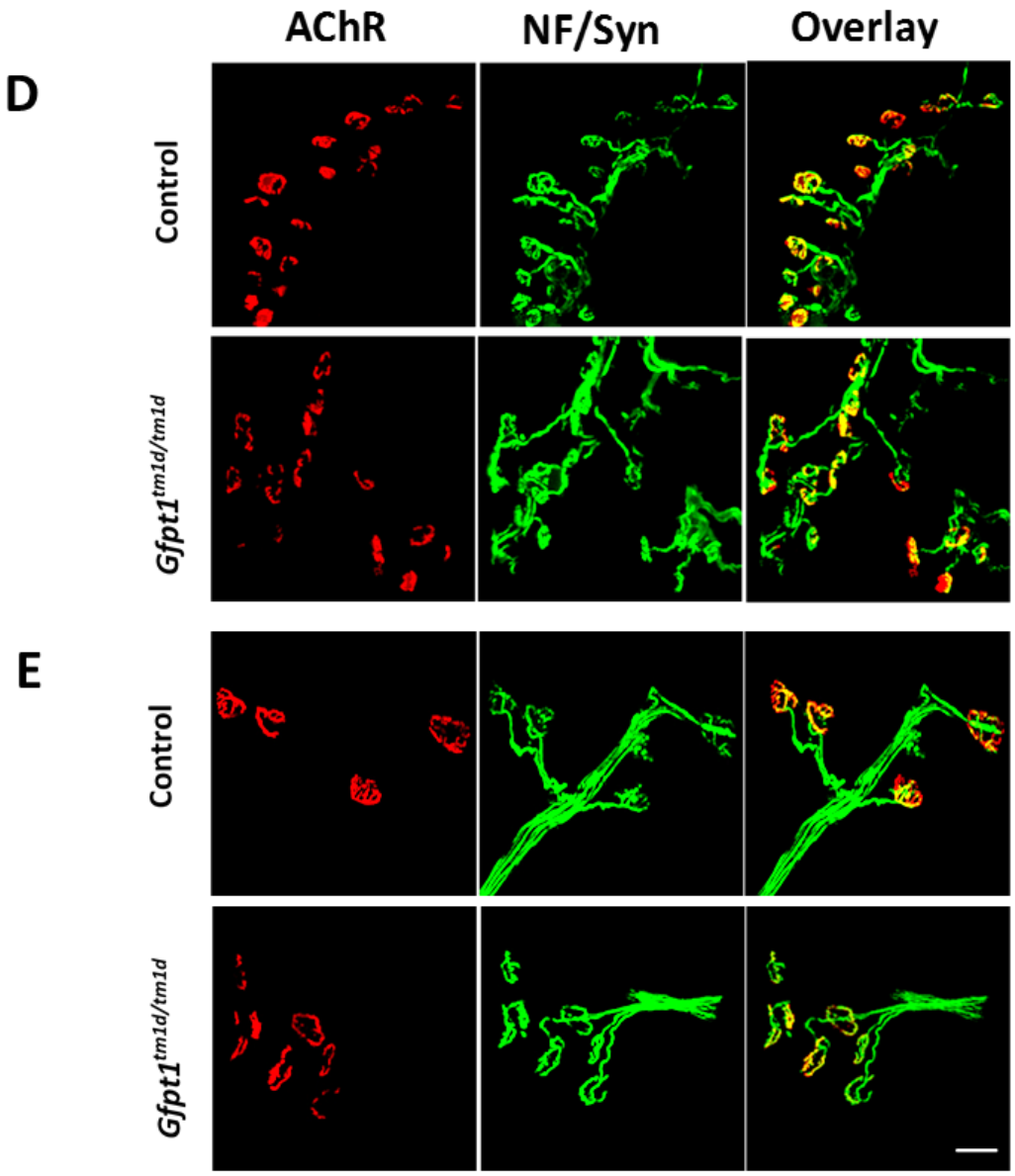

Figure 5.3. Aberrant NMJ in 3 month old *Gfpt1*$^{tm1d/tm1d}$ mice. Confocal Z-stack projections of whole-mount TA (A), intercostal (B), soleus (C), lumbrical (D) and EDL (E) muscles were labelled with anti-neurofilament (green), anti-synaptophysin (green) and Alexa fluor 594 α-bungarotoxin (red). Neurofilament (NF), Synaptophysin (Syn). Scale bar = 20μm.

5.3.2 *Co-localisation of presynaptic and postsynaptic components of the NMJ*

To further analyse remodelling of endplates in *Gfpt1*$^{tm1d/tm1d}$ mice, whole-mount TA, intercostal, soleus, lumbrical and EDL muscles from 3 month old mice were stained with α-bungarotoxin to label AChR and with antibodies against synaptophysin to visualise nerve terminals. In control mice, we see a precise spatial overlap of nerve terminals and their respective AChR. Synaptophysin labelling in *Gfpt1*$^{tm1d/tm1d}$ mice revealed fragmented nerve terminals which appear to align and form synaptic contacts with the existing AChR fragments. The overlap of nerve terminals and their respective AChR appear normal, as seen in control mice. These findings are consistent across all muscles analysed (Figure 5.4).

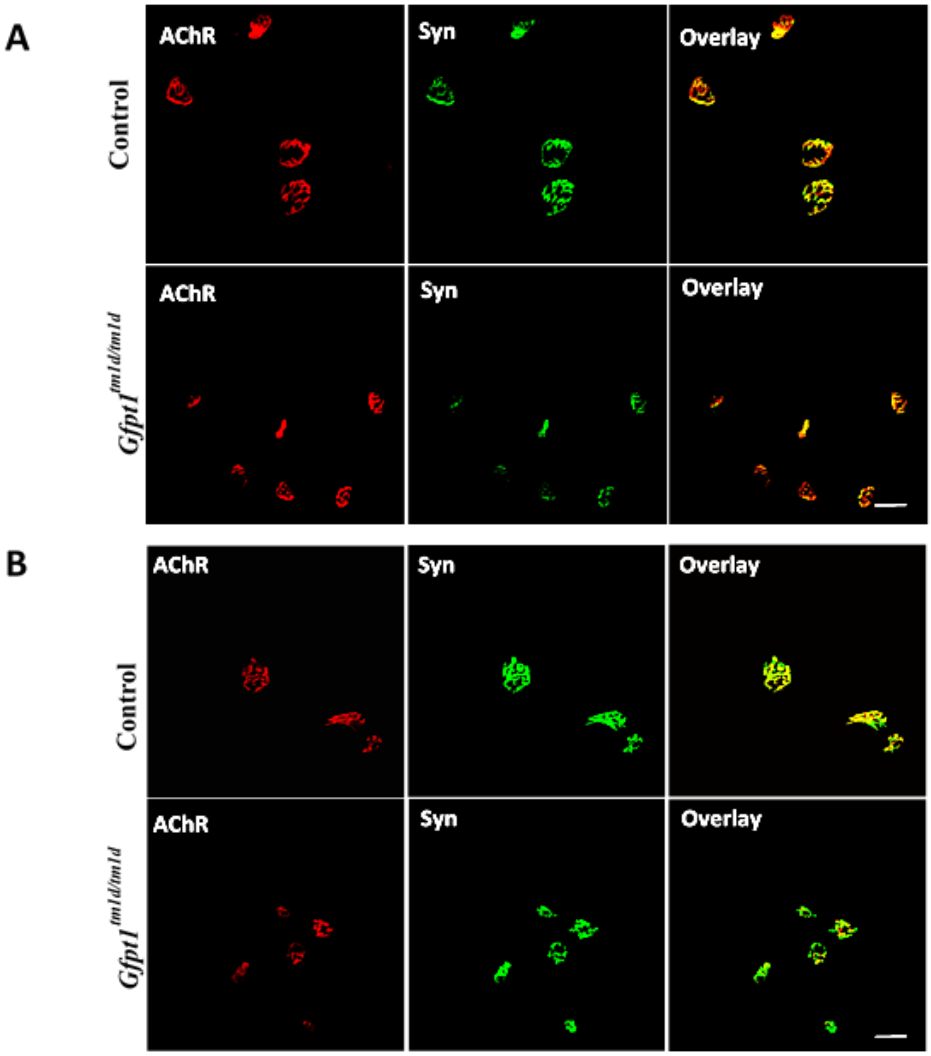

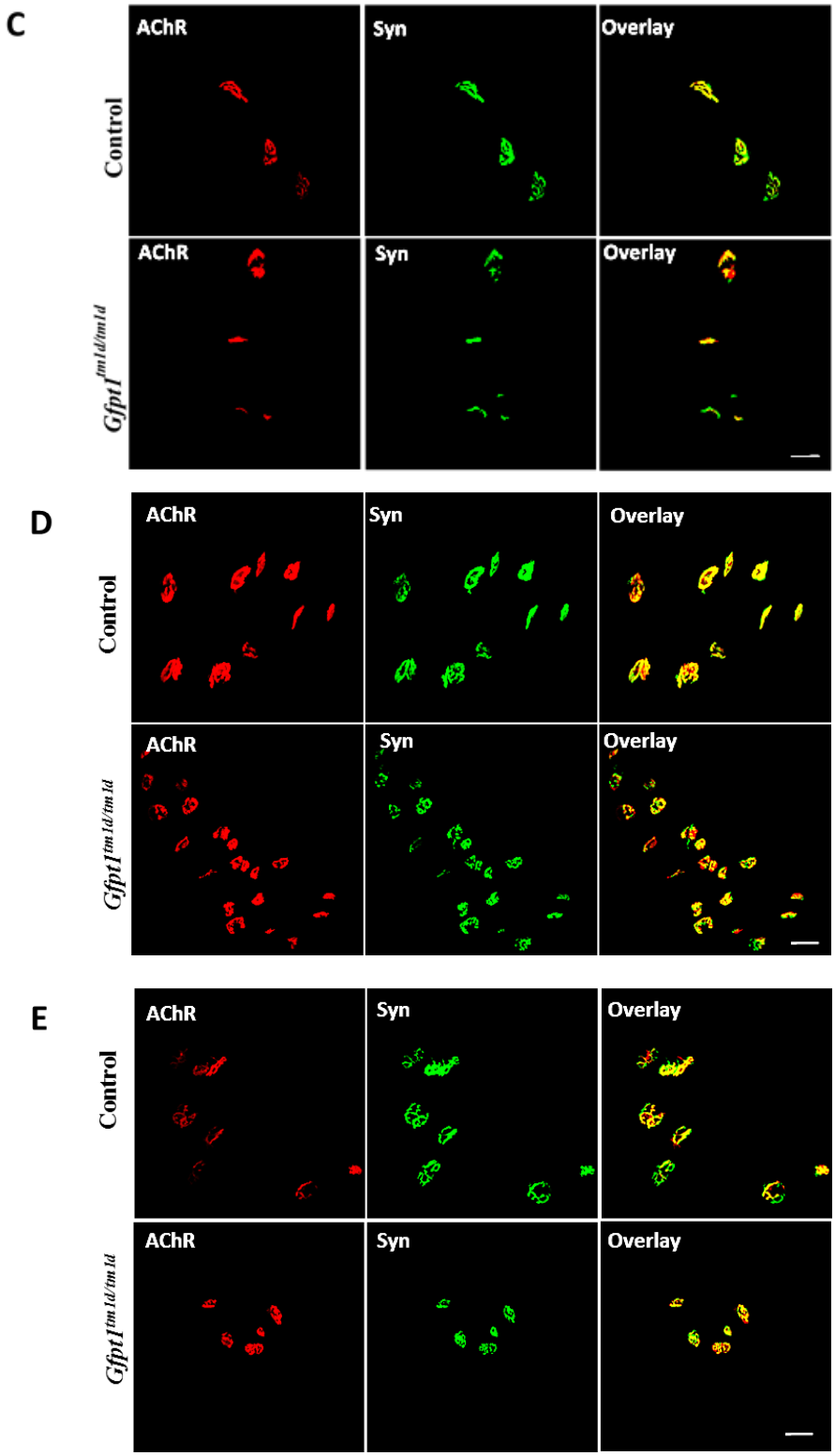

Figure 5.4. Co-localisation of nerve terminals and AChR. Confocal Z-stack projections of whole-mount muscles labelled with Alexa fluor 594 α-bungarotoxin (red) and anti-synaptophysin (green) demonstrate the degree of nerve terminal and AChR overlap from TA (A), intercostal (B), soleus (C), lumbrical (D) and EDL (E) muscles. Synaptophysin (Syn). Scale bar = 20μm (A-E).

5.3.3 *Quantitative analysis demonstrating the changes in AChR structure and the area of synaptic contacts between presynaptic and postsynaptic components*

To study presynaptic and postsynaptic changes at the NMJ, TA, intercostal, EDL, lumbrical and soleus muscles from 3 month old control and *Gfpt1*$^{tm1d/tm1d}$ mice were used to analyse the area, degree of fragmentation, and expression of AChR clusters. We further analysed the overlap area between presynaptic and postsynaptic components using AChR and nerve terminal stained muscles.

Single-projected images derived from overlaying image stacks were quantified using ImageJ analysis software as previously described. Quantitative analysis revealed a reduction in the size of AChRs which were greatest in the lumbrical muscles, followed by the TA, EDL, soleus and intercostals muscles (Figure 5.5A), (Percentage decrease in AChR cluster area lumbrical: 62.8% TA: 45%, EDL: 33%, soleus: 28%, intercostals: 27%.). The degree of fragmentation was measured by a mean fold increase in the no. of fragments per AChR cluster, (TA: 2.2 fold, EDL: 1.9 fold, intercostals: 1.8 fold, soleus: 1.3 fold and lumbrical: 0.3). Statistical analysis revealed the greatest degree of fragmentation was observed in the soleus, followed by the EDL, intercostal, TA and lumbrical muscles (Figure 5.5B). The number of AChR clusters expressed per field view remained unchanged in all muscles analysed (Figure 5.5C). Analysis of the overlap area between presynaptic and postsynaptic components revealed no significant difference in NMJ from control and *Gfpt1*$^{tm1d/tm1d}$ mice (Figure 5.5D).

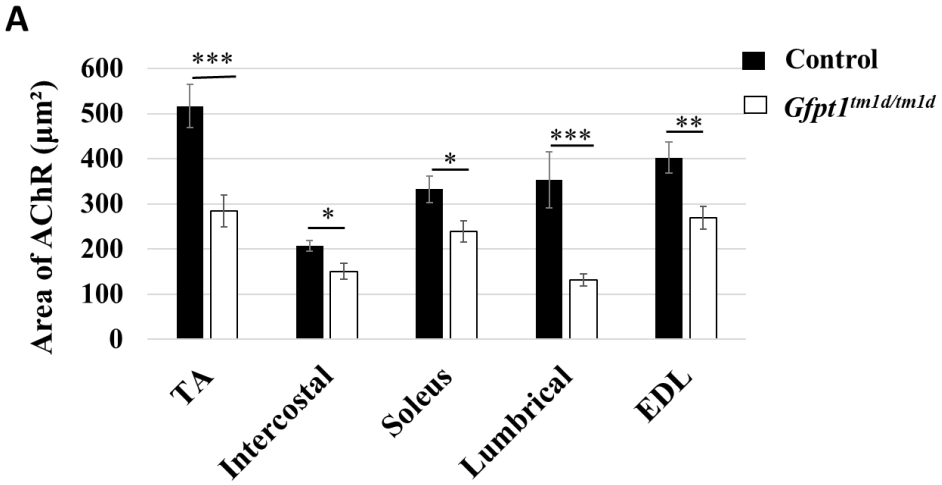

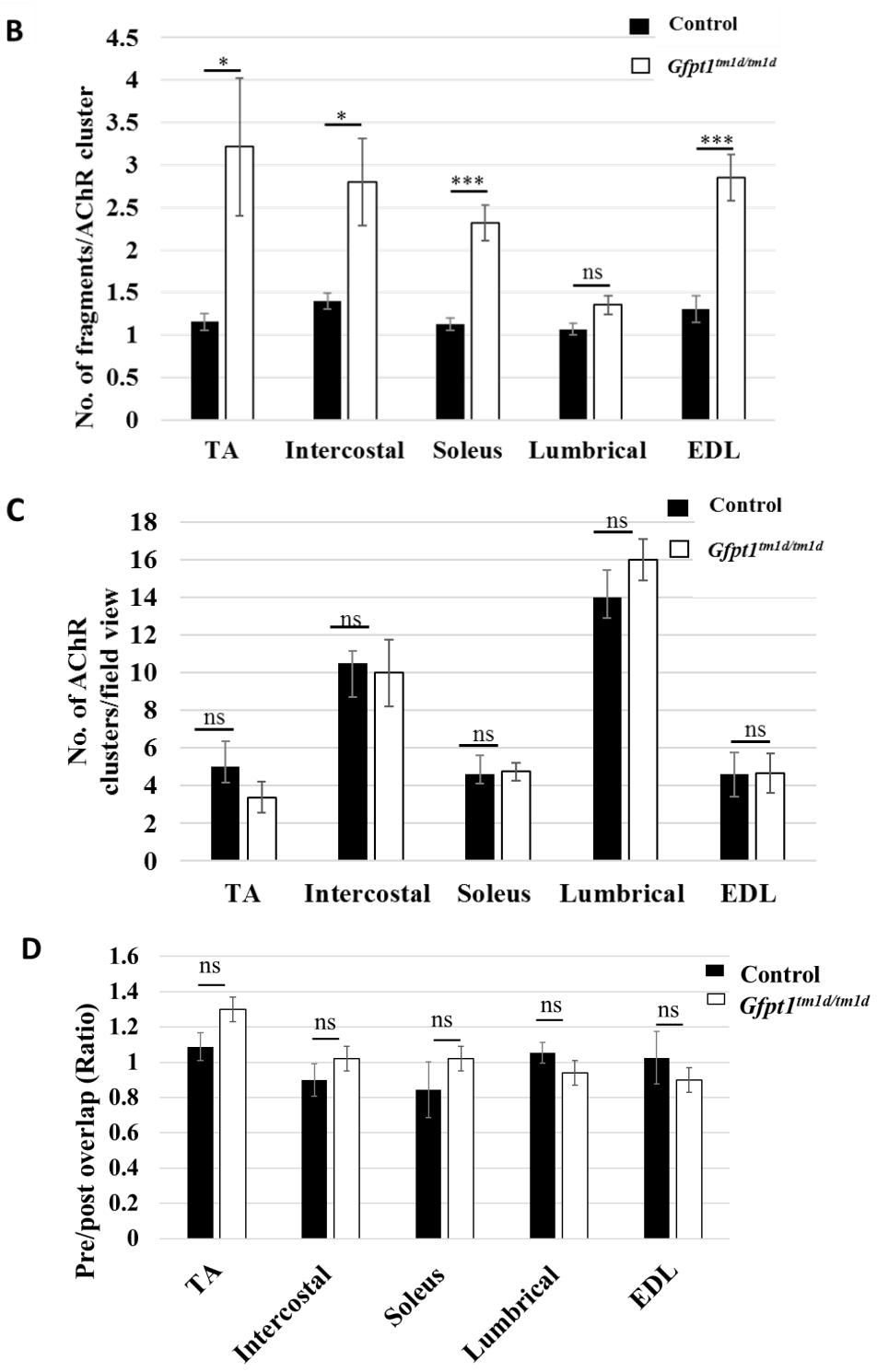

Figure 5.5. Quantification of AChR cluster area, fragmentation, expression and overlap area of presynaptic and postsynaptic elements. Quantitative analysis demonstrating area of AChR clusters (A), fragmentation of AChR clusters (B), the number of AChR clusters expressed per field view (C), and the presynaptic and postsynaptic overlap in control and *Gfpt1*$^{tm1d/tm1d}$ mice (n = 6-8 animals per genotype). Data are mean ± SEM. *p<0.05, **p<0.01 ***p<0.001. ns, Not significant.

5.4 Electron microscopy

To gain an enhanced understanding of the phenotype observed in *Gfpt1*$^{tm1d/tm1d}$ mice, we examined endplates and muscle at the ultrastructural level using electron microscopy in intercostal muscles from 3 month old control and mutant mice.

5.4.1 *Examination of NMJ ultrastructures*

Endplates in control mice exhibit uniform postsynaptic junctional folds at the NMJ. We also observe subcellular specialisations such mitochondria and synaptic vesicles in the presynaptic nerve terminal (Figure 5.6A). In contrast, analysis of endplates from *Gfpt1*$^{tm1d/tm1d}$ mice revealed fewer, simplified or highly disorganised junctional folds. Presynaptic terminals appear smaller, but maintain their subcellular specialisations (Figures 5.6B and 5.6C). Further examination of presynaptic elements show that control mice display regular concentric myelin sheaths (Figure 5.6D). Differences observed in *Gfpt1*$^{tm1d/tm1d}$ mice include occasional highly irregular convoluted myelin sheaths surrounding axons (Figures 5.6E and 5.6F).

Examination of the sarcoplasm revealed an abundant accumulation of tubular aggregates beneath the sarcolemma in mutant mice (Figure 5.6G). We also see the presence of subsarcolemmal vesicular structures that may correspond to caveolae (Figure 5.6H). Tubular aggregates were absent in control mouse muscle. These data indicate both presynaptic and postsynaptic alterations in *Gfpt1*$^{tm1d/tm1d}$ mice.

Figure 5.6

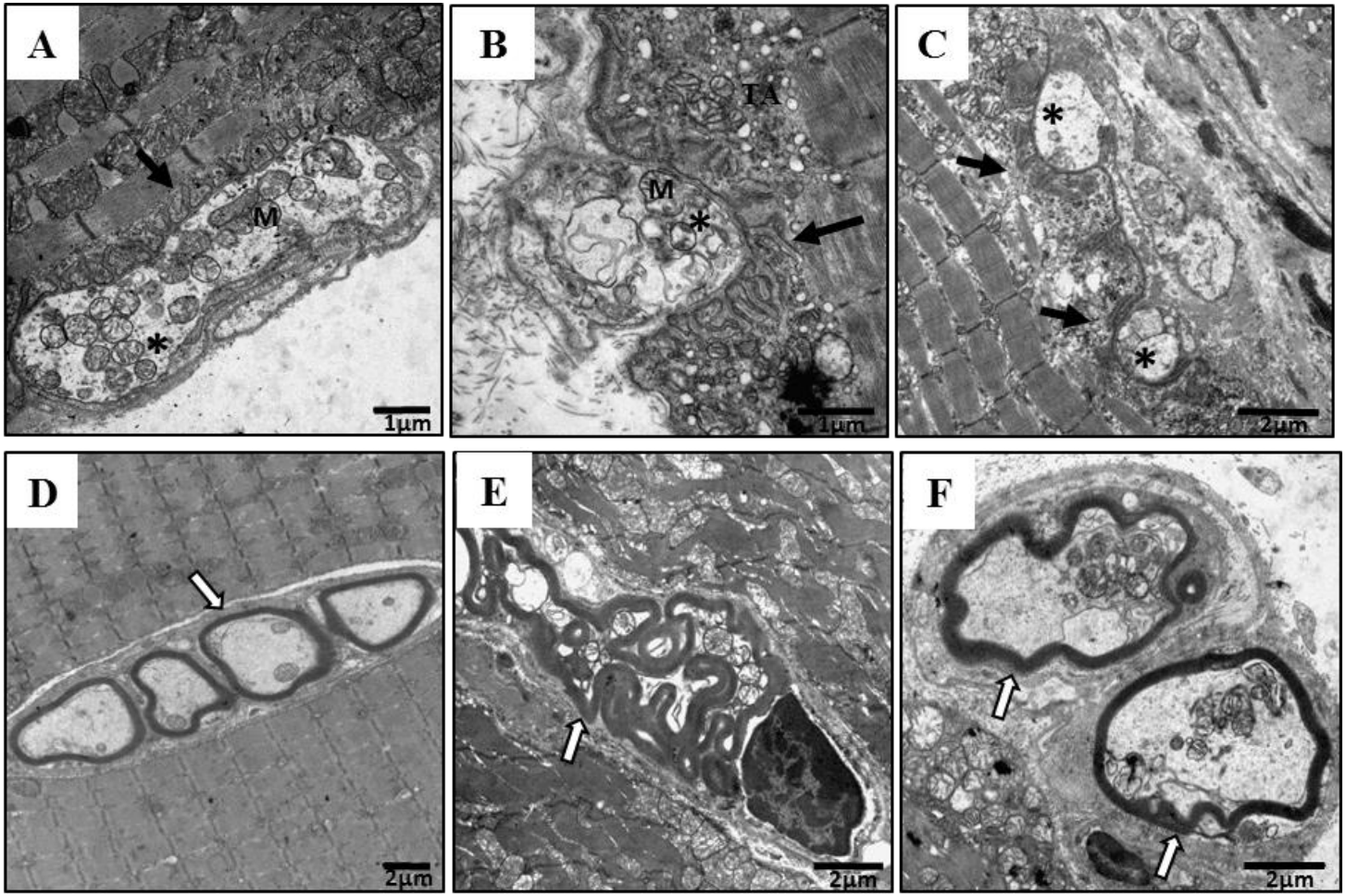

Figure 5.6 continued

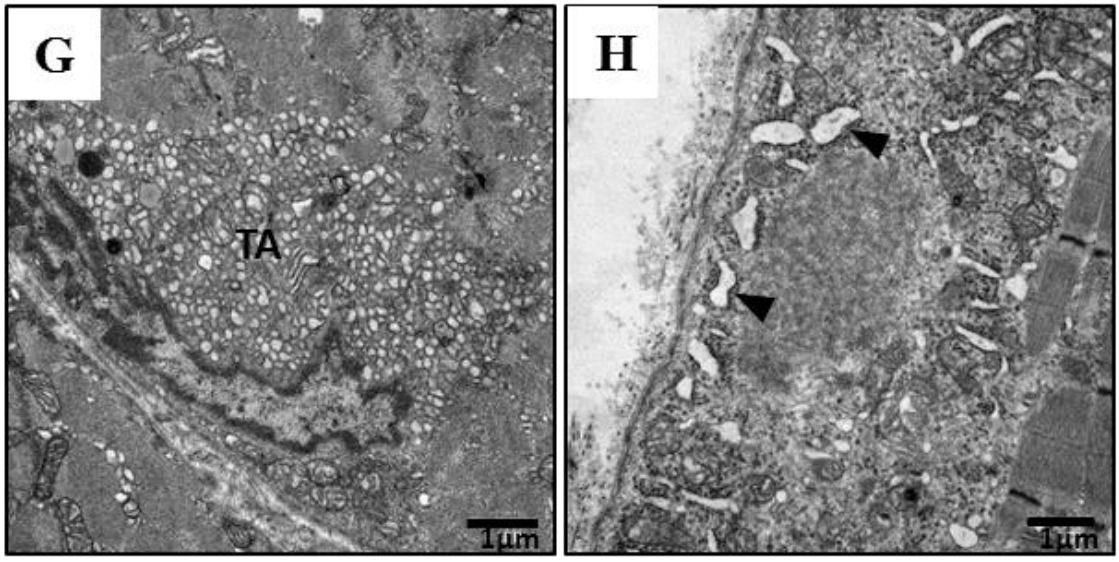

Figure 5.6. Altered morphology at the ultrastructural level in *Gfpt1*$^{tm1d/tm1d}$ mouse muscle. Representative electron micrographs from 3 month old control and *Gfpt1*$^{tm1d/tm1d}$ intercostal muscles. Examples of NMJs from control (A), and *Gfpt1*$^{tm1d/tm1d}$ (B, C) mice. Examples of control (D), and *Gfpt1*$^{tm1d/tm1d}$ (E, F) myelin sheaths. Accumulation of tubular aggregates (G) and subsarcolemmal vesicular structures (H) in *Gfpt1*$^{tm1d/tm1d}$ mouse muscle. Synaptic vesicles (*), junctional folds (black arrow), mitochondria (M), myelin sheaths (white arrows), rounded tubular aggregates (TA), subsarcolemmal vesicular structures (black arrow head). Scale bar = 1µm (A,B,G,H); 2µm (C,D,E,F).

5.4.2 *Quantification of presynaptic and postsynaptic changes in Gfpt1$^{tm1d/tm1d}$ mouse muscle*

Presynaptic and postsynaptic changes *in Gfpt1$^{tm1d/tm1d}$* mouse muscle were quantified by analysing the number of postsynaptic junctional folds per nerve terminal, the diameter of myelin sheaths, and sarcomere length by measuring the distance between z-lines.

The number of junctional folds were counted manually, and the diameter of myelin sheaths and the distance between z-lines were measured using ImageJ software. Mutant mice display fewer junctional folds (34% decrease) on the postsynaptic membrane (Figure 5.7A). Analysis of myelin sheaths showed a reduction in diameter (32% decrease) (Figure 5.7B). Analysis of the sarcoplasm revealed smaller sarcomeres shown by a decrease in the distance between z-lines (11%) (Figure 5.7C). All data were analysed relative to data from control mice.

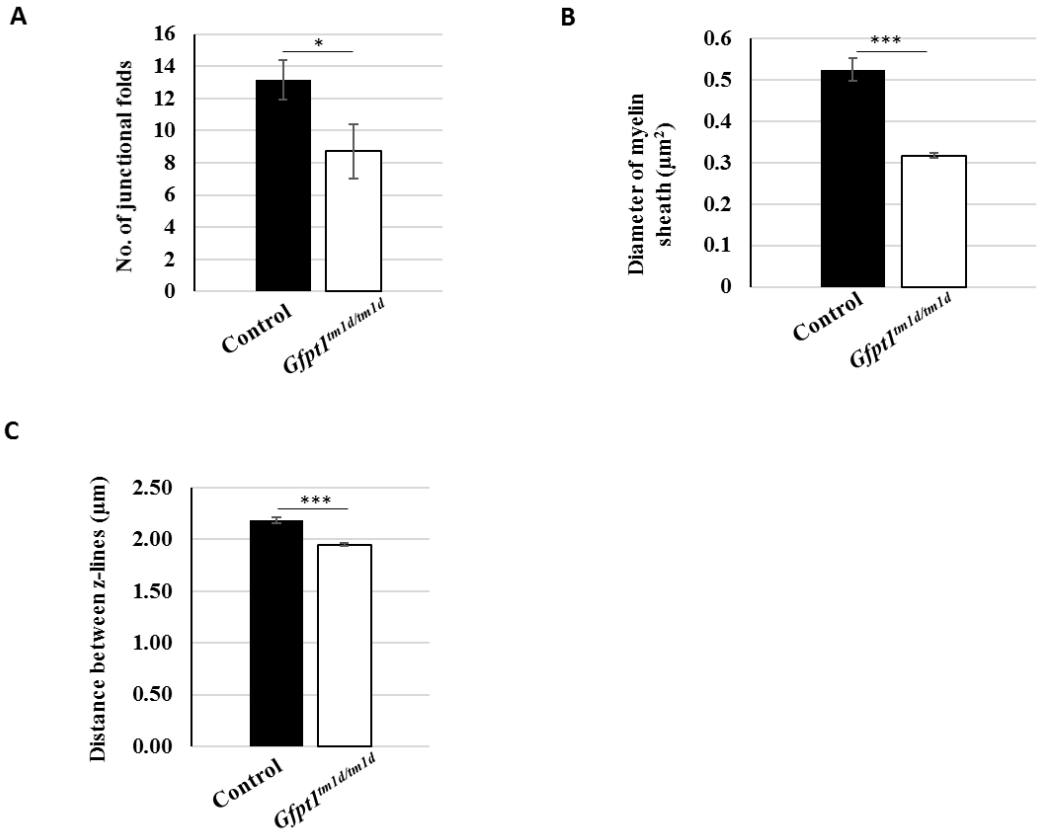

Figure 5.7. Quantification analyses demonstrating presynaptic and postsynaptic alterations in *Gfpt1$^{tm1d/tm1d}$* mouse muscle. Quantitative analysis demonstrating the number of junctional folds (A), myelin sheath diameter (B), and distance between z-lines (C), in control and *Gfpt1$^{tm1d/tm1d}$* mouse muscle. (n=4 animals per genotype). Data are mean ± SEM. *p<0.05, ***p<0.001.

5.5 Histological analysis of skeletal muscle in *Gfpt1*$^{tm1d/tm1d}$ mice

5.5.1 *Histological analysis of skeletal muscle using hematoxylin and eosin staining*

TA, intercostal, soleus, EDL and diaphragm muscles were dissected from 3 month old control and *Gfpt1*$^{tm1d/tm1d}$ mice. 10 µm thick transverse sections were prepared and the muscles were stained with hematoxylin and eosin.

Whilst control mice maintain their characteristic polygonal shape and peripherally located nuclei, we observe numerous myopathic changes in *Gfpt1*$^{tm1d/tm1d}$ mouse muscle (Figure 5.8). Muscles from *Gfpt1*$^{tm1d/tm1d}$ mice exhibit occasional rounded myofibres, and a few fibres with internal nuclei indicative of regenerating fibres. There also appears to be a greater variability in myofibre size due to the presence of atrophic and hypertrophic myofibres, which occasionally exhibit splitting. We observe necrotic fibres in the TA, EDL and diaphragm muscles, and the presence of tubular aggregates which are stained as dark aggregates or appear like slits within the myofibre. Tubular aggregates are found in some myofibres in all muscles examined. Analysis of the EDL and diaphragm muscle demonstrates the replacement of myofibres with fibro-adipose tissue. This finding is more prevalent in the diaphragm muscle.

Figure 5.8

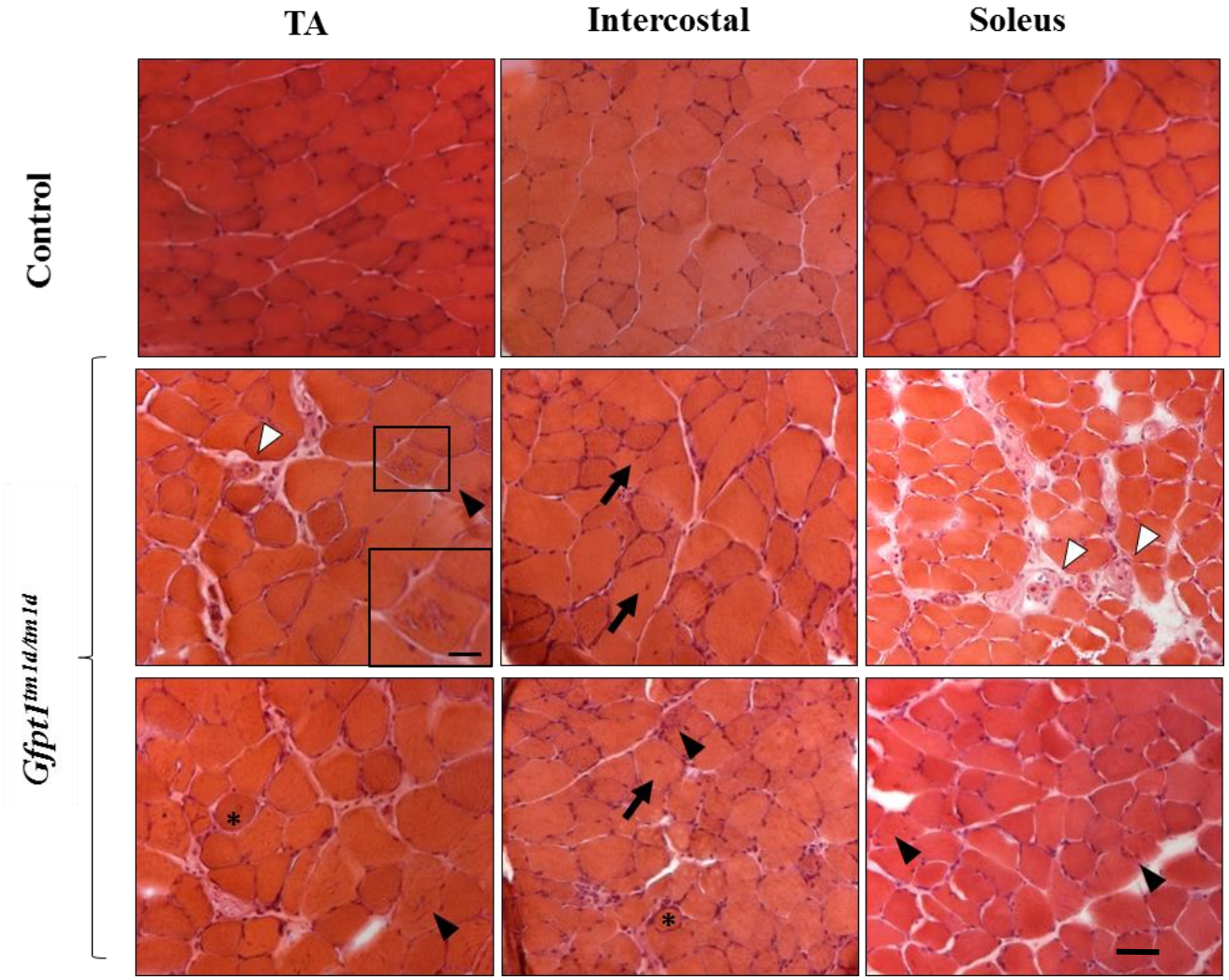

Figure 5.8 continued

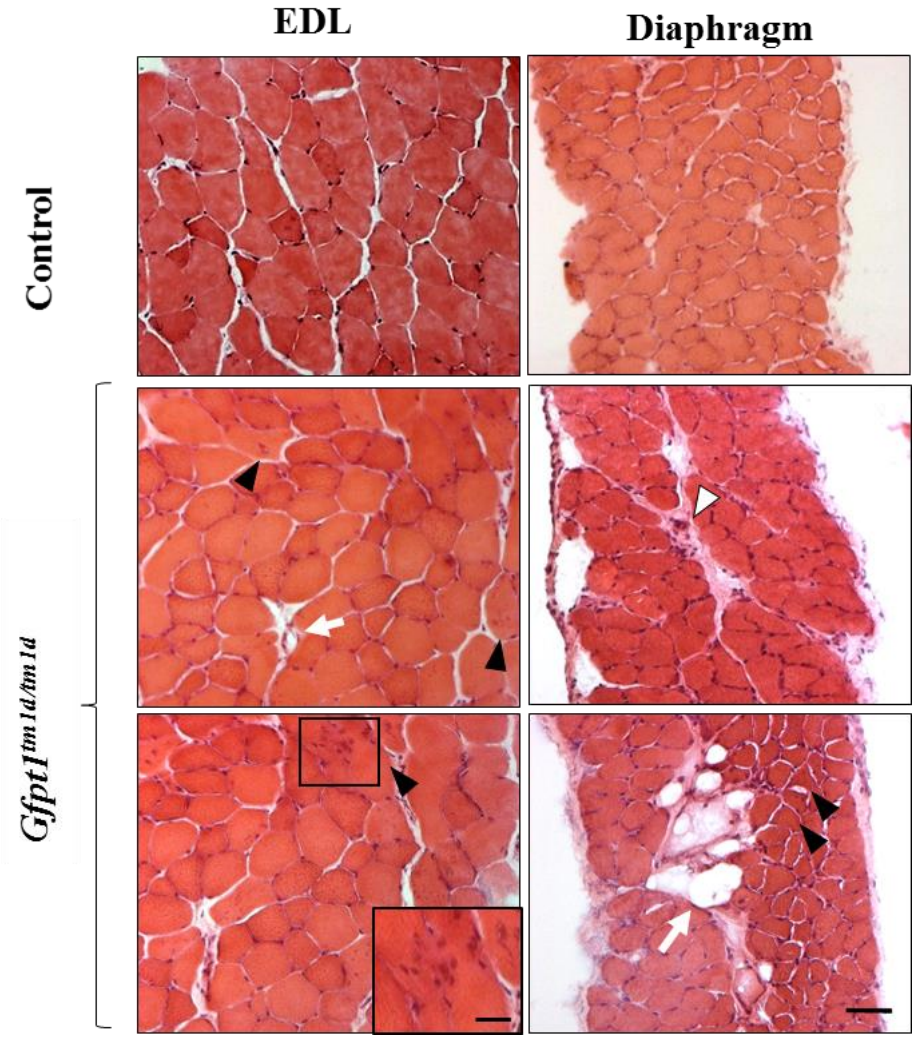

Figure 5.8. Myopathic changes in muscle from *Gfpt1*$^{tm1d/tm1d}$ mice. Brightfield images of TA, intercostal, soleus, EDL and diaphragm muscles stained with hematoxylin and eosin from 3 month old control and *Gfpt1*$^{tm1d/tm1d}$ mice. Legend: Black star indicates rounded myofibres, black arrow points to centrally-located nuclei in myofibres, black arrow head points to tubular aggregates, white arrow head points to necrotic fibres, white arrow points to adipose tissues. Hypertrophic and atrophic myofibres are also present. Scale bar = 20μm for main figures and 10μm for insets.

5.5.2 *Quantification of myofibre variation*

The cross-sectional area of individual myofibres from control and *Gfpt1*$^{tm1d/tm1d}$ mice were measured using ImageJ software as described previously. Quantitative analysis of myofibre area showed higher variability in *Gfpt1*$^{tm1d/tm1d}$ mouse muscle when compared to control mouse muscle. Variations in fibre size between control and *Gfpt1*$^{tm1d/tm1d}$ mouse muscle are greatest in the EDL (61%), followed by the soleus (56%), intercostal (29%) and TA (26%) muscles as shown by the percentage difference of the interquartile range. Median cross-sectional area measurements are indicative of the proportion of fibres that tend to be either smaller or larger when comparing control and mutant muscles. The intercostal (28.91%) and soleus (25.84%) muscles exhibit a shift towards smaller fibres, the EDL exhibits a shift towards larger fibres (17.72%), whilst the TA fibres remain unchanged in *Gfpt1*$^{tm1d/tm1d}$ mice (Figure 5.9).

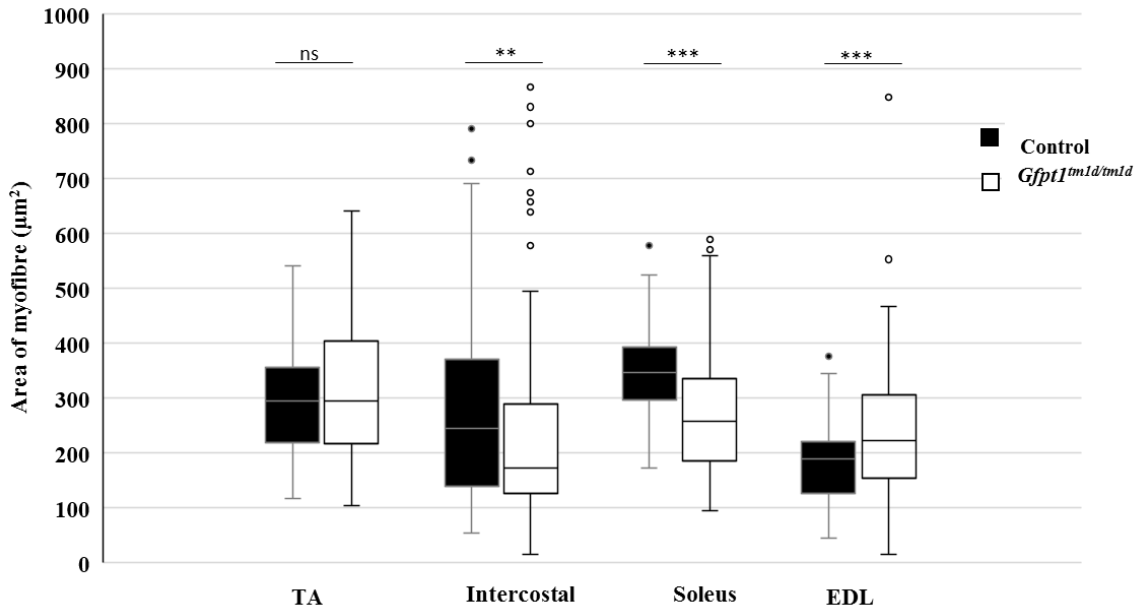

Figure 5.9. Quantitative analyses demonstrating the distribution of myofibre size according to cross-sectional area. The cross-sectional area of individual myofibres from control and *Gfpt1*$^{tm1d/tm1d}$ mice were measured (n=4 animals per genotype). Data are median, 25th percentile, 75th percentile, minimum and maximum values (including outliers). **p<0.01,***p<0.001. ns, Not significant.

5.6 Evaluation of myasthenia in transgenic mice

5.6.1 *The four limb inverted screen test*

Fatigable muscle weakness was measured using an inverted screen test. Mice were suspended from a wire grid and the length of time it took for the mice to release their grasp of all four limbs was recorded. Data was collected from mice from 6 weeks of age. The mice were set a maximum time of 10 minutes. Control mice up to the age of 18 weeks old demonstrate the ability to hold on for the maximum threshold of 10 minutes. There was a small reduction in the latency to fall in older mice which is accounted for by an increase in body weight. *Gfpt1*$^{tm1d/tm1d}$ mice demonstrate poor motor performance detected as early as 6 weeks old up until 6 months old as shown by a reduction in the latency to fall from the grid compared to controls (Latency decrease: 8 weeks old, 62%; 12 weeks old, 69%; 16 weeks old, 66%; 20 weeks old, 64%; 24 weeks old, 63%; Figure 5.10). The deficit in motor performance is not progressive over time. We further demonstrate there is no difference in the longest hang time between control mice (Cre negative) and mice carrying the *Cre* transgene over the 6 month period.

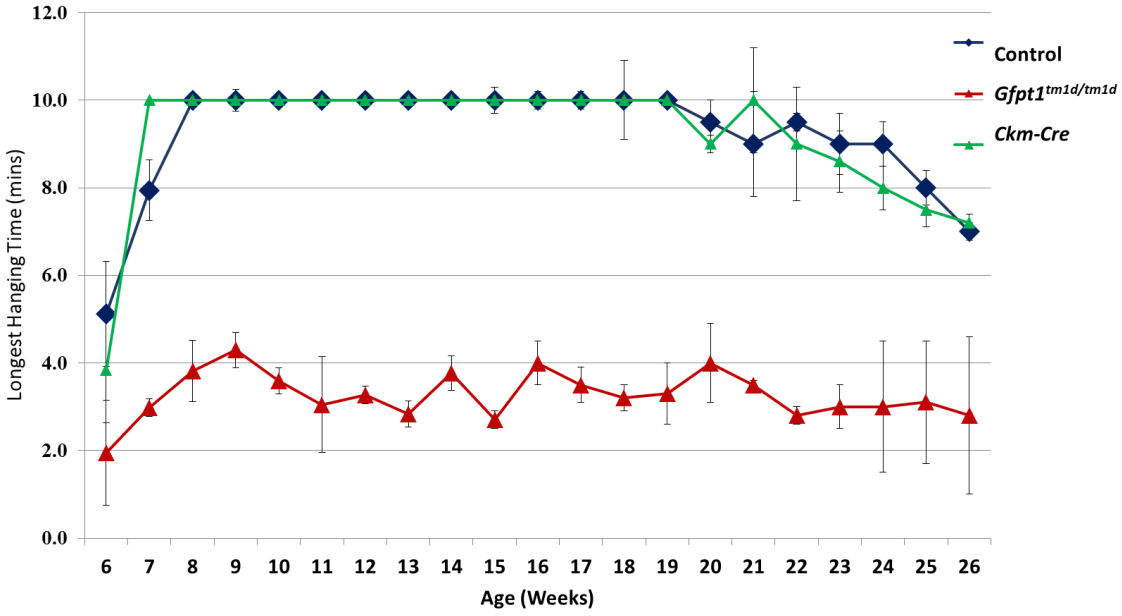

Figure 5.10. A comparison of muscle strength between control, *Ckm-Cre* controls and *Gfpt1*$^{tm1d/tm1d}$ mice. Quantitative analysis of latency to fall from a wire grid at various time points up to the age of 6 months. *Gfpt1*$^{tm1d/tm1d}$ mice perform worse than control mice at all time points ($p<0.01$) (n=8). *Ckm-Cre* control mice do not exhibit any changes compared to controls (n=6). $p>0.05$, not significant. Data are mean $\pm$ SEM.

5.6.2 *Isometric force measurements in situ*

The main procedure for preparing the mouse for measuring force measurements produced by the TA muscle is described in the materials and methods chapter of this thesis. The electrophysiology measurements were made using an *in vivo* protocol that has been previously described (Dellorusso *et al.*, 2001; Sharp *et al.*, 2008; Sharp *et al.*, 2011; TREAT- NMD protocols).

Surgical preparation

The sciatic nerve branches into the sural, tibial and peroneal nerves. The sural and tibial nerves were transected, but the peroneal nerve was left intact. This ensures that only the TA muscle remains innervated, and there is no contraction from any other muscle. The sciatic nerve was also transected proximally. The sciatic nerve was then placed over bipolar platinum electrodes (Figure 5.11).

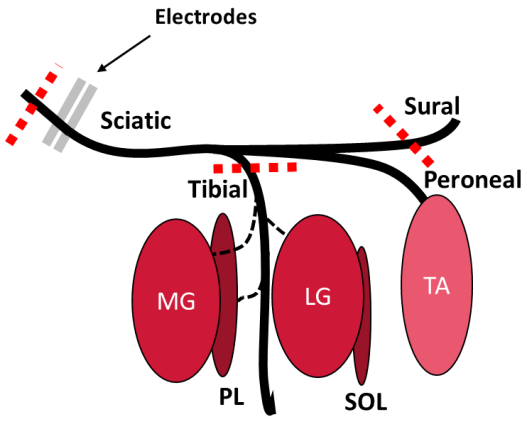

Figure 5.11. Schematic demonstrating surgical preparation required prior to *in situ* force measurements. The tibial and sural nerves were transected. The peroneal nerve that innervates the TA muscle was left intact. Finally, the sciatic nerve was transected proximally, and bipolar platinum electrodes (grey), were place beneath the sciatic nerve. All nerves were transected as indicated (red dotted lines). Medial Gastrocnemius (MG), Lateral Gastrocnemius (LG), Plantaris (PL), Soleus (SOL), Tibialis Anterior (TA). This image was adapted from (Duraku et al., 2012; Lorenz and Jones, 2014).

Isometric force measurements

To confirm the presence of muscle weakness in *Gfpt1*$^{tm1d/tm1d}$ mice, we studied the ability of TA muscles from 3 month old control and *Gfpt1*$^{tm1d/tm1d}$ mice to evoke twitch and tetanic contractions in response to stimulation of the sciatic nerve *in situ*. Muscles were stimulated using a warm up protocol which consisted of 5 stimulations at 50 Hz with a minute rest period between each stimulation. The muscle was subject to a series of single twitches at increasing tensions (Figure 5.12). The muscle's optimum length (L_o) was determined and the resting tension that produced the strongest twitch was used for the remainder of the experiment. The force frequency relationship was determined using a series of stimulations at 10, 30, 40, 50, 80, 100, 120, 150 and 180 Hz, each 1 minute apart. A small drop in force occurs during the contractions elicited at stimulation frequencies of 150 Hz and 180 Hz, which is indicative of fatigue. A stimulation frequency 120 Hz produces a fully fused tetanus with no reduction in force over the stimulation period (Figure 5.13). This is the maximum isometric tetanic force (P_o) which is used for the remaining fatigue experiments.

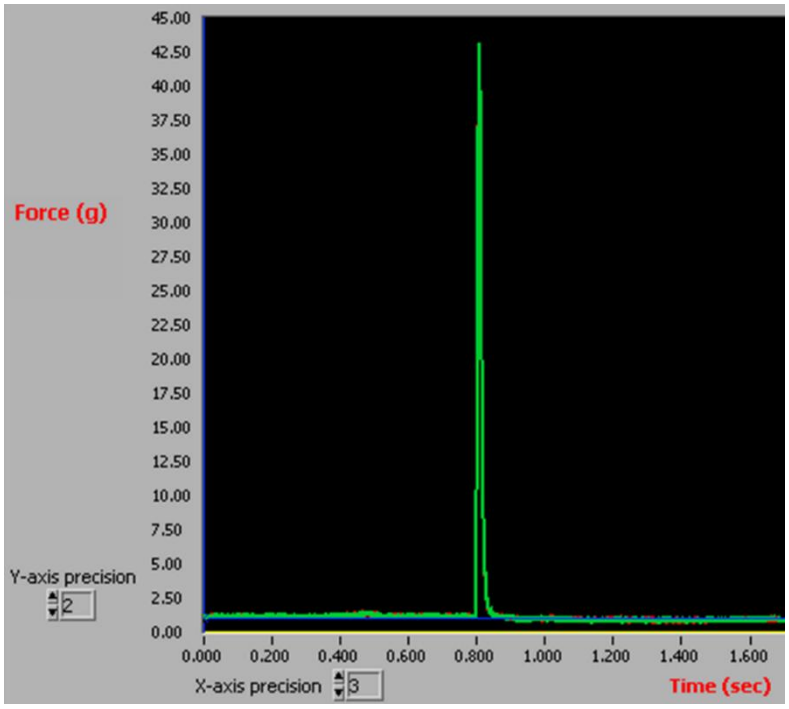

Figure 5.12. Representative trace demonstrating the force produced by a single twitch in the TA muscle. Twitches were produced by stimulation of the common peroneal branch of the sciatic nerve. The resting tension was adjusted until the maximum twitch force was produced. The resulting trace was analysed to obtain the peak twitch force.

.

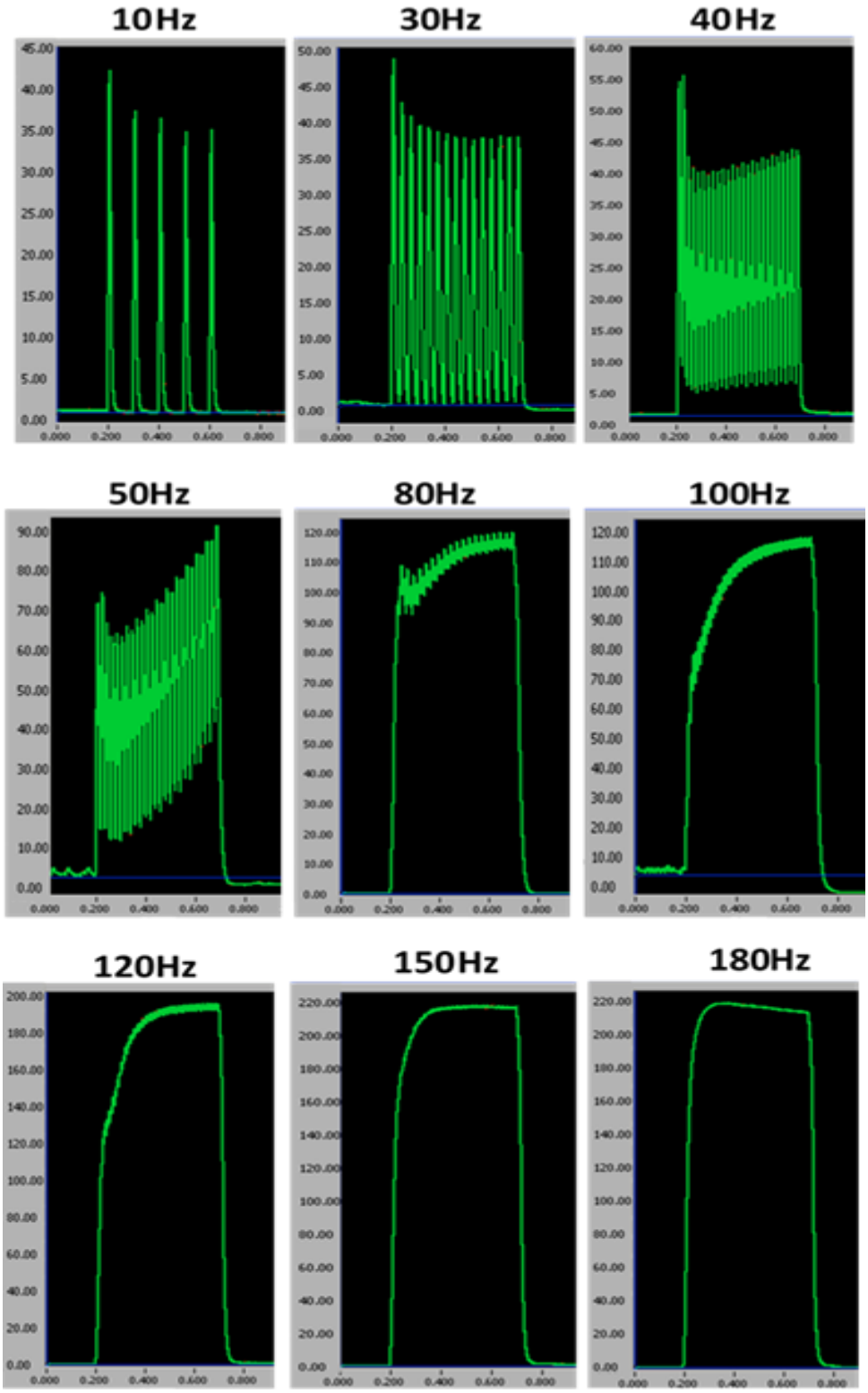

Figure 5.13. Representative traces demonstrating the force produced by tetanic stimulation of the TA muscle. The sciatic nerve was stimulated at increasing frequencies (10, 30, 40, 50, 80, 100, 120, 150 and 180 Hz) with a rest period of 1 minute between each stimulation.

Determining specific force

The force readings at each frequency recorded in grams (absolute force) were converted to specific force (kN/m^2). Specific force is the absolute force normalised to cross-sectional area (CSA) of the of the muscle.

The following formula was used to determine the CSA of the muscle:

CSA = muscle weight (g)/[Optimum TA fibre length (Lf, cm) × 1.06 (g/cm^3]

$1.06g/cm^3$ is the density of mammalian skeletal muscle.
Lf = optimal length (L_o) x 0.6 which represents the fibre length: muscle length ratio for the TA (Brooks and Faulkner, 1988).

The force produced at each stimulation frequency was measured in grams and converted to Newtons (N) by multiplying by 0.00981.

Specific force (N/cm^2) was calculated using the following formula:

Specific force (N/cm^2) = Absolute force (N)/CSA (cm^2)

Specific force was plotted against frequency. Our data demonstrates that there is no significant difference in muscle strength between control and *Gfpt1*$^{tm1d/tm1d}$ mouse following upon tetanic stimulations (Figure 5.14).

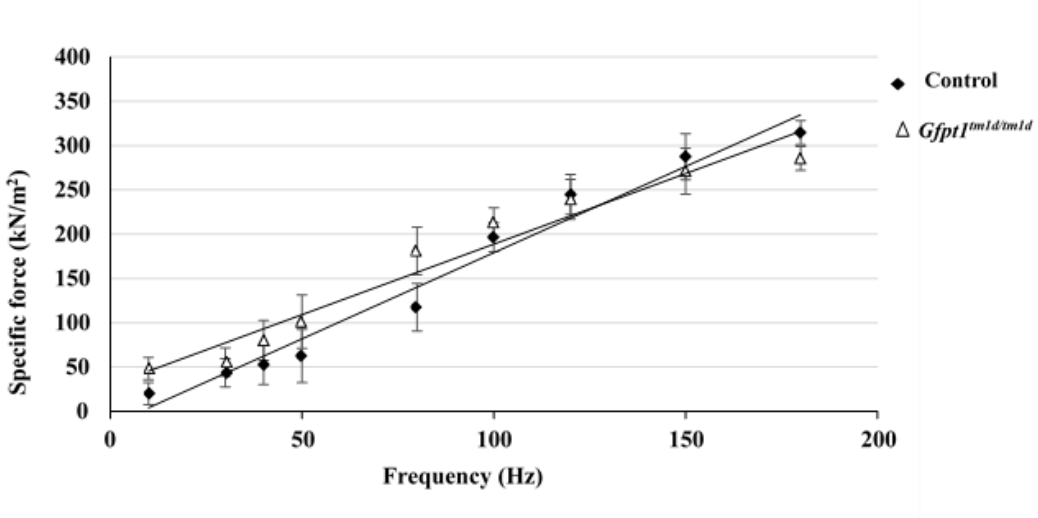

Figure 5.14. Mean specific force produced by the TA muscle following tetanic stimulation of the sciatic nerve at increasing stimulation frequencies in 3 month old control and *Gfpt1*$^{tm1d/tm1d}$ mice. The sciatic nerve was stimulated by a series of isometric contractions with frequencies of 10, 30, 40, 50, 80, 100, 120, 150 and 180 Hz, with a delay of 1 minute between each stimulation. There is no observed difference in the force produced between control and *Gfpt1*$^{tm1d/tm1d}$ mice. (n=5). Data are mean $\pm$ SEM. $p>0.05$. ns, not significant at any frequency.

Testing for fatigue in *Gfpt1*$^{tm1d/tm1d}$ mice

We assessed muscle fatigue following a series of tetanic nerve stimulations at 120 Hz (the frequency that usually resulted in P_o) over 100 stimulations. Muscle fatigue was observed in both control and *Gfpt1*$^{tm1d/tm1d}$ mice. After 100 stimulations control mice demonstrated a 26.1% reduction in force produced compared to baseline, whereas *Gfpt1*$^{tm1d/tm1d}$ mice showed a 64.7% deficit, exhibiting a more pronounced degree of fatigue. A progressive decrease in the force produced in *Gfpt1*$^{tm1d/tm1d}$ mice is evident from 60 stimulations (60, 22.3%; 70, 26.0%; 80, 42.9; 90, 47.7%; 100, 64.7%), whereas a significant reduction in control mice is only evident following 100 stimulations compared to baseline (Figure 5.15A). A comparison of fatigability between control and *Gfpt1*$^{tm1d/tm1d}$ mice showed the latter exhibit a significant and progressive reduction in force produced after 80 (20.77%), 90 (26.37%) and 100 (38.67%) stimulations (Figure 5.15B). Our data demonstrates that although *Gfpt1*$^{tm1d/tm1d}$ mice do not display pronounced changes in TA muscle strength, the muscle is more susceptible to fatigability.

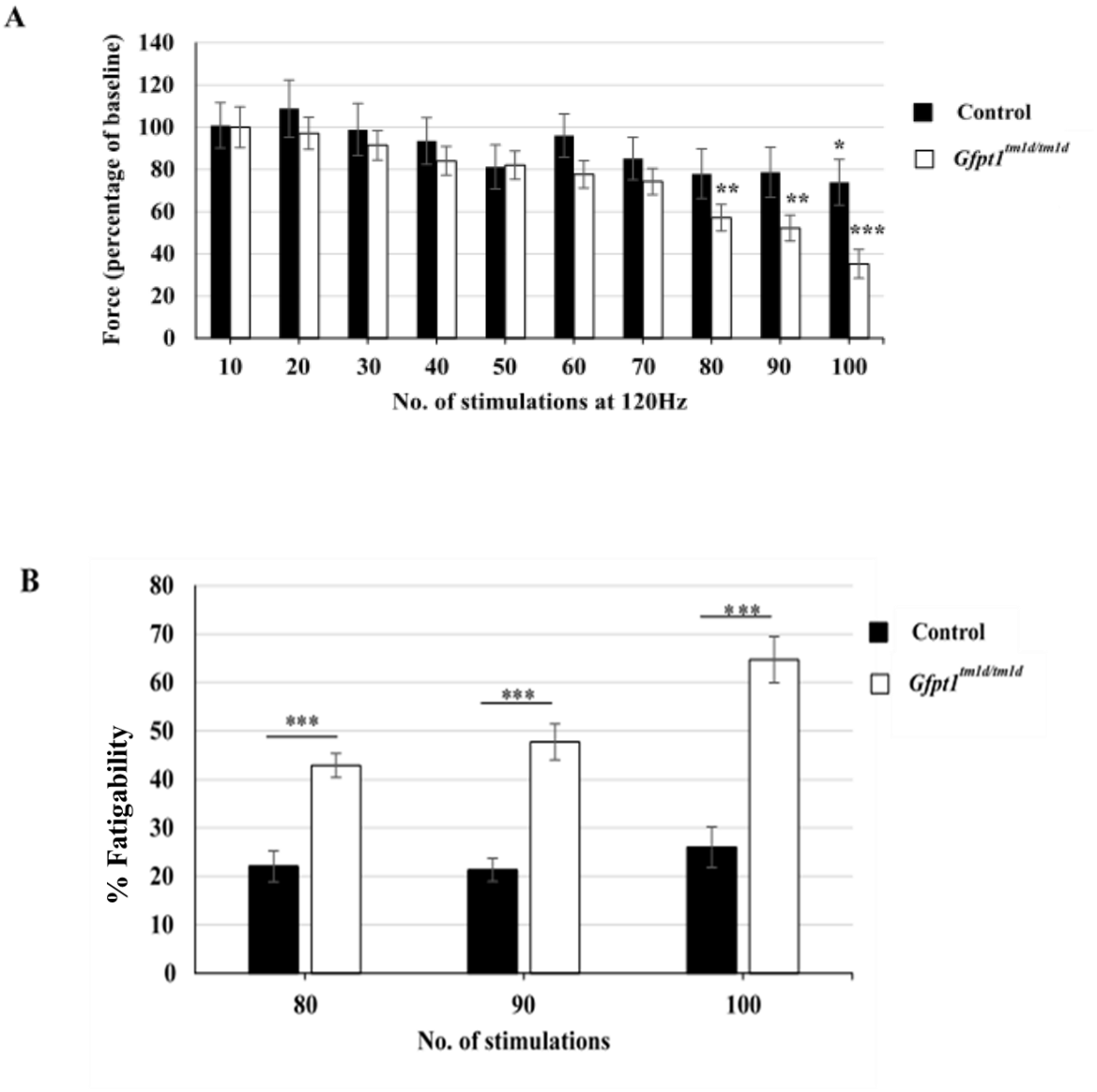

Figure 5.15. Analysis of muscle fatigue. (A) Quantitative analysis of force generated by the TA muscle after every 10 stimulations of the sciatic nerve in 3 month old control and *Gfpt1*$^{tm1d/tm1d}$ mice (n=5). Data are expressed as a percentage of baseline force. (B) Quantification of fatigability of the TA muscle after 80, 90 and 100 stimulations of the sciatic nerve in 3 month old control and *Gfpt1*$^{tm1d/tm1d}$ mice (n=5). Data are expressed as the percentage decrease of baseline force. Data are mean $\pm$ SEM. *p<0.05, **p<0.01, ***p<0.001.

5.6.3 *Isometric force measurements in vitro*

We assessed the contractile properties of the diaphragm muscle from *Gfpt1*$^{tm1d/tm1d}$ mice using an *in vitro* test apparatus which has been previously described in Chapter 2 of this thesis. We examined the ability of muscles to contract following a series of tetanic stimulations. Control and *Gfpt1*$^{tm1d/tm1d}$ muscles maintained tetanic contractions with stimulation frequencies ranging from 30-150 Hz. However, *Gfpt1*$^{tm1d/tm1d}$ muscles develop less force than control ones (Figure 5.16). Quantitative analysis revealed that the isometric tetanic maximal force on muscle strength was significantly reduced compared to controls (150 Hz, 35.3%).

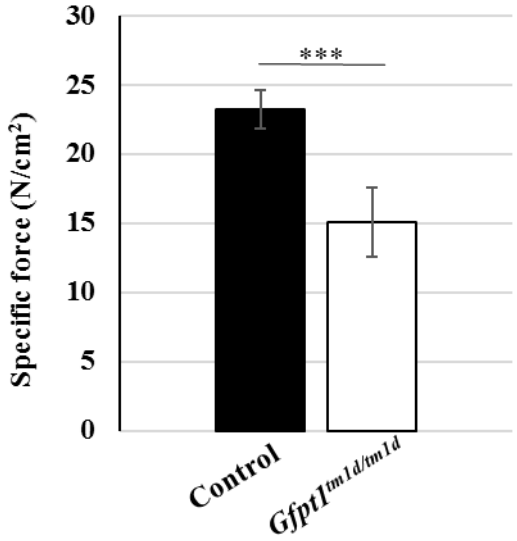

Figure 5.16. Analysis of contractile properties of diaphragm muscle from *Gfpt1*$^{tm1d/tm1d}$ mice. Average isometric tetanic maximal force at 150 Hz on diaphragm muscle from control and *Gfpt1*$^{tm1d/tm1d}$ mice (n = 4). Data are mean ± SEM. ***p<0.001.

Fatigue

We tested for fatigue using a series 100 tetanic nerve stimulations at 150 Hz (the frequency resulting in P_o). We did not observe signs of fatigue in control diaphragms, but we see a progressive reduction in force between 50 and 100 stimulations in *Gfpt1*$^{tm1d/tm1d}$ diaphragms compared to baseline *(*50, 5.6%; 60, 16.8%; 70 19.4%; 80, 20.9%; 90, 23.5%; 100, 29.8%) (Figure 5.17A). We compared the reduction in force produced between control and *Gfpt1*$^{tm1d/tm1d}$ mice expressed as percentage fatigability. *Gfpt1*$^{tm1d/tm1d}$ mice demonstrate a significant and progressive reduction in force from 50-100 stimulations when compared to controls, (50, 5.6%; 60, 16.8%; 70, 19.4%; 80, 20.9%; 90, 23.5%; 100, 29.8%) (Figure 5.17B).

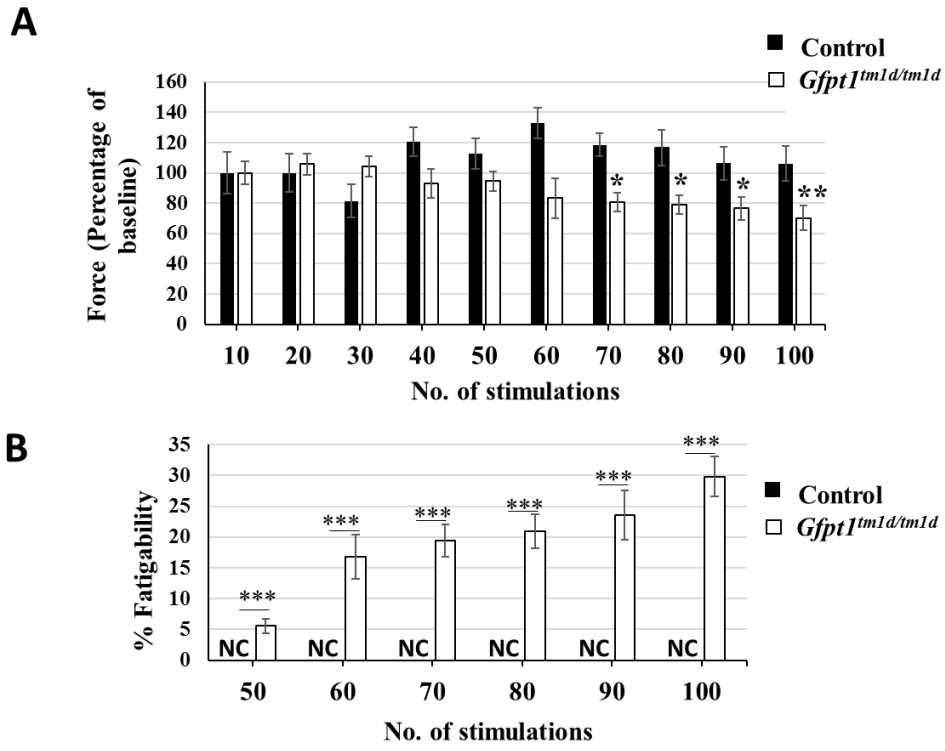

Figure 5.17. Analysis of fatigue in diaphragm muscle from *Gfpt1*$^{tm1d/tm1d}$ mice. (A) Quantitative analysis of force generated by the diaphragm muscle after every 10 stimulations in 3 month old control and *Gfpt1*$^{tm1d/tm1d}$ mice. Data are expressed as a percentage of baseline force. (B) Quantification of fatigability of the diaphragm muscle between 50 and 100 stimulations in 3 month old control and *Gfpt1*$^{tm1d/tm1d}$ mice. Data are expressed as a percentage reduction in force. (n=4). Data are mean ± SEM. NC, no change. *p<0.05, **p<0.01,***p<0.001.

5.7 Evaluation of AChR stability

To establish whether the stability of AChRs is compromised in *Gfpt1*$^{tm1d/tm1d}$ mice, we assessed the turnover rate of AChR in the TA muscle of 3 month old control and mutant mice over a 10 day period. Fluorescence signals of 'old' and 'new' receptors labelled green and red respectively were monitored using confocal microscopy (Figure 5.18A). Quantitative assessment of relative pixel intensities using automated image analysis demonstrates no significant difference between *Gfpt1*$^{tm1d/tm1d}$ and control mice (Figure 5.18B).

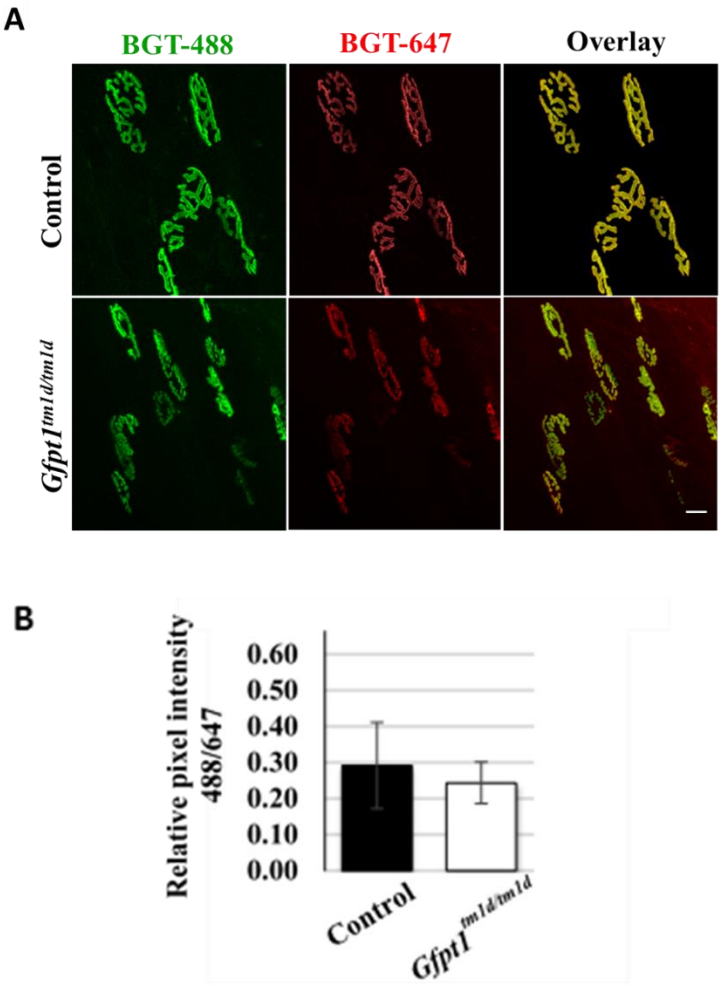

Figure 5.18. AChR turnover in TA muscles from control and *Gfpt1*$^{tm1d/tm1d}$ mice. (A) Confocal Z-stack images of old-receptor signals labelled with BGT-488 (green), new-receptor signals labelled with BGT-647 (red) and overlay. (B) Quantification of relative pixel intensity between control and *Gfpt1*$^{tm1d/tm1d}$ mouse muscle (n=3). Data are mean ± SEM. p>0.05, ns, not significant.

5.8 Proteomic profiling experiments

5.8.1 *Effects of* GFPT1 *deficiency on the intercostal muscle proteome*

Proteomics is a powerful tool for the unbiased investigation of pathophysiological processes in neuromuscular disorders (Roos *et al.*, 2016). We compared the proteome profile of intercostal muscles from 3 month old control and *Gfpt1*$^{tm1d/tm1d}$ mice using quantitative mass spectrometry (label-free shotgun proteomic approach). We found that 2.8 % of the quantified proteins (43 out of 1517) were differentially expressed upon GFPT1 deficiency in intercostal muscles, 39 of these proteins were upregulated (29 identified with two or more unique peptides and 10 with one unique peptide) and 4 downregulated (all identified with one unique peptide). Most of the affected proteins are localized in the ER-Golgi network, plasma membrane, cytoplasm, nucleus and mitochondria. For a list of regulated proteins, their subcellular localization and proposed functions, see Appendix A (Pundir *et al.*, 2017). 5 out of the 39 upregulated proteins, and 1 out of the 4 downregulated proteins harbour N-glycosylation (N-GlcNAc) sites. 1 out of the 4 downregulated proteins harbor O-glycosylation (O-GlcNAc) sites, (Table 5.1). To provide insight into GFPT1 myopathology, the spectrum of affected proteins was analyzed for enriched gene ontology (GO) terms using STRING (Figure 5.19). Regulated proteins found to have connections with each other are shown in the STRING.

Protein	Gene	Abundance	Type and no. of glycosylation sites
Aminopeptidase N	*Anpep*	Upregulated	N- GlcNAc (17)
Complement C4-B	*C4b*	Upregulated	N- GlcNAc (4)
Glypican-1	*Gpc1*	Upregulated	N- GlcNAc (2) O-Xylose (3)
Vesicular integral-membrane protein	*Lman2*	Upregulated	N- GlcNAc (1)
Vitronectin	*Vtn*	Upregulated	N- GlcNAc (3)
UDP-N-acetylglucosamine-peptide N-acetylglucosaminyltransferase	*Ogt*	Upregulated	O- GlcNAc (2)
Uncharacterized family 31 glucosidase KIAA1161	*Kiaa1161*	Downregulated	N- GlcNAc (3)

Table 5.1. Regulated proteins with N- and O-glycosylation sites.

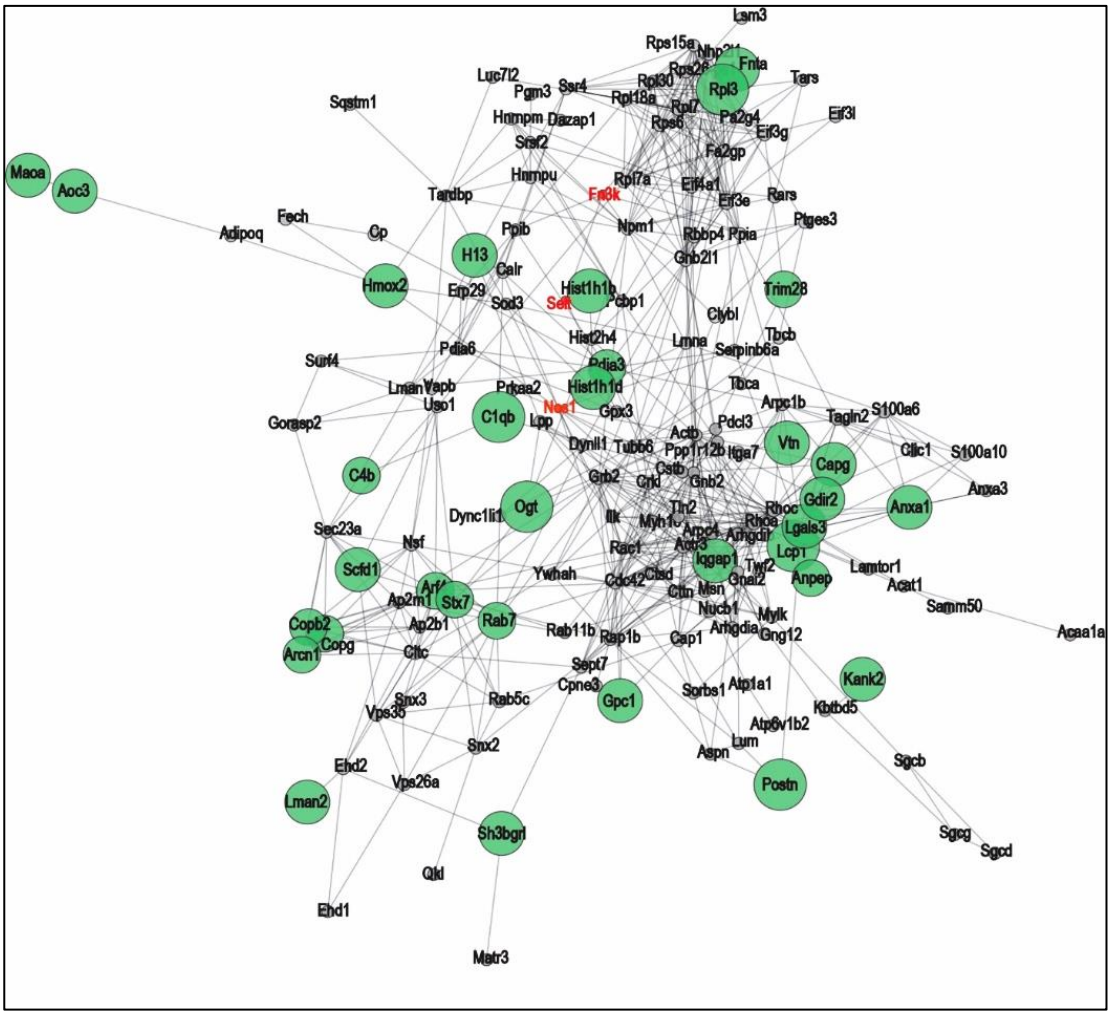

Figure 5.19. Analysis of protein interaction network by STRING. The spectrum of affected proteins was analyzed for enriched gene ontology (GO) terms. Upregulated proteins are shown in green and downregulated proteins are shown in red; $p \leq 0.05$. The relative expression of remaining proteins did not change. All proteins shown demonstrate known and predicted protein-protein interactions.

5.8.2 *Immunoblot analysis showing the relative expression of glypican-1 and MuSK in control and Gfpt1$^{tm1d/tm1d}$ mouse tissues*

Using immunoblot studies, we have verified the proteomic findings for glypican-1, a cell surface proteoglycan that bears heparan sulfate and participates in axon guidance, Schwann cell myelination and is required for proper skeletal muscle differentiation. Moreover, we demonstrated an increased abundance of the MuSK protein, a major regulator required for the formation and maintenance of the NMJ (Figure 5.20A). Muscles used for analysis were derived from 3 month old control and *Gfpt1*$^{tm1d/tm1d}$ intercostal muscles. The relative expression levels between control and mutant intercostal tissues was analysed using the gel analysis tool on ImageJ software. Glypican-1 (Figure 5.20B) and MuSK (5.20C) are considerably more abundant in *Gfpt1*$^{tm1d/tm1d}$ mice when compared to controls.

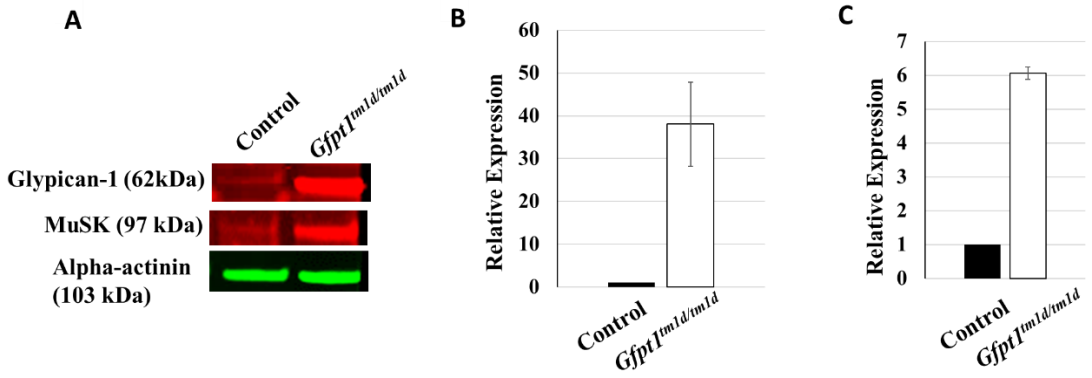

Figure 5.20. Immunoblot analyses showing the relative expression levels of glypican-1 and MuSK in mouse tissues. Glypican-1 (~62 kDa) and MuSK (~97 kDa) proteins are upregulated in *Gfpt1*$^{tm1d/tm1d}$ intercostal muscles (A). Alpha-actinin (~103 kDa) was used as a loading control. All bands were measured against an 8-260 kDa Chameleon Duo Ladder protein ladder. Graph demonstrating the relative expression levels of glypican-1 (B) (n=3), and MuSK (C) (n=2), normalised to their corresponding alpha-actinin loading controls.

5.9 Discussion

The frequency of mice born does not reflect the Mendelian frequencies of the four expected genotypes. Only 4% of offspring harbour the *Gfpt1*$^{tm1d/tm1d}$ genotype, instead of the expected 25%. These findings suggest potential embryonic lethality upon disruption of *Gfpt1*. Why some mutant mice survive and not others will require further investigation. In Chapter 3 we describe the spatial and temporal expression of Cre recombinase using the ROSA26R-*lacZ* reporter line. Although we rule out inconsistent Cre activity in the developing embryo and major adult tissues, there may be some Cre activity which remains undetected. *Ckm-Cre* may be expressed prematurely in embryos or in extraembryonic tissues, which consequently depletes GFPT1 required for survival. Since we observe normal litter sizes, it is possible that the mice are lethal prior to pre-implantation due to premature GFPT1 depletion. Alternatively, it is possible that the embryos that experience Cre activity on the lower end of the spectrum, i.e. lower recombination efficiency, can survive through to adulthood due to small amounts of residual GFPT1 expression. Although we do not address the level of GFPT1 depletion at different stages in the developing embryo, we demonstrate complete knockout of GFPT1 in skeletal and cardiac tissues of the adult mouse using immunoblot analyses, which validates this model for studying the maintenance of the NMJ. Whilst the survival of CMS knockout mouse models often result in embryonic or early postnatal lethality (Dechiara *et al.*, 1996; Gautam *et al.*, 1996; Okada *et al.*, 2006; Weatherbee *et al.*, 2006), *Gfpt1*$^{tm1d/tm1d}$ offspring survive through to adulthood and do not die prematurely. Furthermore, we do not observe any gross phenotypical defects or significant changes in body weight in mutant mice.

In humans GFPT1 expression is ubiquitous. Consequently, the NMJ phenotypes we see in patients may be due to a deficiency of GFPT1 in both presynaptic and postsynaptic structures at the NMJ. The *Gfpt1*$^{tm1d/tm1d}$ mouse model conserves GFPT1 expression in all tissues except muscle. Prior to this study it was unknown whether depletion of GFPT1 in muscle only would be sufficient to produce a CMS-like phenotype.

Examination of NMJs in muscles from *Gfpt1*$^{tm1d/tm1d}$ mice demonstrate changes in endplate architecture, highlighting the importance of muscle derived GFPT1 in NMJ differentiation. Pathology of the AChR is illustrated by fragmentation and reduction in size of AChR clusters in all muscles examined.

Pathological endplates were also evident at the ultrastructural level in NMJs of intercostal muscles which harboured fewer, simplified junctional folds; a common feature seen in GFPT1 patients (Selcen *et al.*, 2013; Maselli *et al.*, 2014), as well as other mouse models of congenital myasthenia (Chevessier *et al.*, 2008; Bogdanik and Burgess, 2011; Messéant *et al.*, 2015). Structural changes in the presynaptic or postsynaptic components of the NMJ may compromise the safety margin of neurotransmission. Junctional folds harbour a high density of Na+ channels in the troughs of the folds as well as increase the series resistance of the postsynaptic membrane. Both factors are important for membrane depolarisation. Simplification of the folds may therefore be a major contributor to impaired neurotransmission. Another possible pathomechanism is an increased chance of acetylcholine escaping the synaptic cleft before it reaches the postsynaptic membrane (Wood and Slater, 2001). This theory is supported by patient use of cholinesterase inhibitors which ameliorate muscle weakness in many subtypes of CMS. A reduction in the number of junctional folds may therefore be accountable for the fatigable muscle weakness we observe in *Gfpt1*$^{tm1d/tm1d}$ mice.

We also observe presynaptic morphological alterations in mutant mice. We see remodelling of motor nerve terminals which form synaptic contacts with the fragmented AChRs. Since our model conserves GFPT1 expression in non-muscle tissues we hypothesise that the presynaptic alterations we observe in *Gfpt1*$^{tm1d/tm1d}$ NMJs are secondary to the pathological changes in the postsynaptic apparatus, via impaired retrograde signalling required for axon guidance during synaptogenesis (Chen and Cheng, 2009; Wu *et al.*, 2010). Previous studies have shown the implication of muscle derived BMP in stimulating presynaptic growth and development (Ball *et al.*, 2010; Berke *et al.*, 2013). Furthermore, the inducible LRP4 muscle-specific knockout mouse model displays both presynaptic and postsynaptic remodelling (Barik *et al.*, 2014), where muscle derived LRP4 has been shown to mediate presynaptic differentiation via a retrograde signalling mechanism (Yumoto *et al.*, 2012). Similarly, a muscle-specific conditional β-catenin knockout mouse strain demonstrates morphological and functional defects in nerve terminals at the NMJ, yet in motor neuron specific β-catenin knockout mice, the morphology and function of the NMJ remains unaffected (Li *et al.*, 2008). These findings indicate the roles of muscle-derived proteins in regulating presynaptic differentiation and function. It is therefore highly plausible that the presynaptic changes

we observe in *Gfpt1*$^{tm1d/tm1d}$ mice, occurs due to defective secreted proteins from the muscle. We speculate that misglycosylation of muscle derived proteins in this mouse model impairs retrograde signalling mechanisms required for neuronal differentiation or maintenance. Interestingly BMP and LRP4 harbour N-glycosylation sites for GlcNAc and β-catenin undergoes O-GlcNAcylation. These proteins could potentially be affected by GFPT1 deficiency. Alternatively, misglycosylated binding partners or activators of retrograde signalling proteins can also disrupt their function. Examples include N-linked Wnt glycoproteins of Wnt/β-catenin pathway and N-glycosylated LRP4 binding partners such as agrin and MuSK (Zhang *et al.*, 2009).

We also observe thinner, irregular myelin sheaths in mutant mice. Perisynaptic Schwann cells that myelinate motor axons at the NMJ are known contributors of synaptogenesis and synaptic transmission (Feng *et al.*, 2005; Cao and Ko, 2007; Wu *et al.*, 2010). Cross-talk between proteins of the postsynaptic membrane, motor nerve and Schwann cells is essential for the integrity and function of the synapse (Wu *et al.*, 2010). Previous studies have shown the role of laminin β2 (Maselli *et al.*, 2009), agrin (Maselli *et al.*, 2012) and COL13A1 (Latvanlehto *et al.*, 2010; Logan *et al.*, 2015) in the correct organisation of Schwann cells. A deficiency in these proteins results in remodelling of Schwann cells often resulting is encasement of the nerve terminal and invasion of the synaptic space, which subsequently impairs surface contact for neurotransmission. The changes we see in myelination in GFPT1 deficient mice may occur because of misglycosylated muscle proteins that directly affect Schwann cell morphology and function. Alternatively, the changes we observe in the motor neuron may subsequently induce changes in Schwann cell myelination. It is challenging to study the precise mechanisms underlying presynaptic alterations due to the complexity of processes underlying NMJ differentiation, together with the ubiquitous nature of the GFPT1 glycosylation pathway which may give rise to thousands of NMJ proteins that are potentially affected.

Examination of muscle biopsies from patients with mutations in GFPT1 revealed variations in myofibre size, an increase in the number of central nuclei, atrophic fibres, fibres that showed splitting and few necrotic and regenerating fibres. Additionally, there is an increase in glycogen staining, rimmed vacuoles and tubular aggregates (Selcen *et al.*, 2013; Brady *et al.*, 2016). Analyses of second biopsies from the same patients

demonstrate that pathological changes are progressive over time. Tubular aggregates further appear to increase in size, but their relative expression remains unchanged (Brady *et al.*, 2016). Histopathological alterations seen in muscle biopsies from patients with mutations in *GFPT1* closely resembles those with mutations in *DPAGT1*.

Examination of *Gfpt1*$^{tm1d/tm1d}$ mouse muscle revealed abnormal variations in myofibre size, few regenerating and necrotic fibres and the presence of tubular aggregates. Our model more closely resembles the myopathic phenotype that we see in a single patient harbouring the c.686-2A>G mutation which disrupts the longer muscle-specific isoform of GFPT1 resulting in the absence of glycosylated protein expression (Selcen *et al.*, 2013). In the diaphragm muscle, we observe a progressive replacement of muscle tissue by fibroadipose tissue, indicative of muscle fibre atrophy, which was not apparent in younger (6 week old) mice. Similar features are also seen in muscle biopsies from *DPAGT1*-CMS patients (Basiri *et al.*, 2013). Recent investigations into myopathic changes in patients has been facilitated by muscle MRI. Findings demonstrate fatty infiltration in muscle which is more pronounced in patients with mutations in genes encoding proteins in the glycosylation pathway (Finlayson *et al.*, 2016). Whilst minor myopathic changes are sometimes seen in some subtypes of CMS, secondary to neurotransmission failure (Selcen *et al.*, 2011; Nicole *et al.*, 2014), myopathic changes are more pronounced in patients with mutations in *GFPT1* and *DPAGT1*. Dystrophic changes are also observed in patients with *GMPPB* mutations. These findings are not surprising due to the ubiquitous activity of these glycosylation enzymes.

Since glycosylation is a ubiquitous post-translational modification, it is highly probable that glycosylation of proteins other than those required for the formation and maintenance of the NMJ complex are misglycosylated in GFPT1 deficient mice, which explains the myopathic phenotype and disruption of contractile properties observed. Hypoglycosylation may disrupt cytoskeletal proteins that maintain the integrity of skeletal muscle during muscle contractions (Huizing *et al.*, 2004; Reed *et al.*, 2004; Herbst *et al.*, 2009) or affect regulatory and contractile proteins that modulate Ca^{2+} homeostasis and muscle contraction, as well as structural proteins of the sarcomere (Hedou *et al.*, 2007; Cieniewski-Bernard *et al.*, 2012; Leung *et al.*, 2013; Cieniewski-Bernard *et al.*, 2014a). Many of these proteins harbour N- and O-linked GlcNAc acceptor sites, making them potential candidates subject to misglycosylation

downstream of impaired glycosylation enzymes implicated in CMS. Proteins that maintain the integrity of the sarcolemma which are modified by N-GlcNAc moieties include the sarcoglycan subunits (α, β, δ, γ), α-dystroglycan and β-dystrogylcan. Contractile proteins such as actin, myosin heavy chain and myosin light chain proteins as well as key proteins involved in the sarcomeric structure including desmin, actinin, αB-crystallin, and ZASP are known to be O-GlcNAc modified (Hedou *et al.*, 2007; Cieniewski-Bernard *et al.*, 2012; Leung *et al.*, 2013). Localisation of OGT (the enzyme that mediates O-GlcNAcylation) at the sarcomere, and in particular the Z-disk region, suggests an important role of O-GlcNAcylation of sarcomeric proteins (Cieniewski-Bernard *et al.*, 2014b). Our preliminary data shows a reduction in sarcomere length in mutant mice which may be attributed to misglycoslylated structural proteins of the sarcomere. Identification of affected proteins will require further investigation.

Analysis of muscle from 3 month old *Gfpt1*$^{tm1d/tm1d}$ mice shows the presence of tubular aggregates, which was absent in muscle tissues from younger (6 week old) mice. These findings are consistent with the idea that tubular aggregate formation is age-dependent (Boncompagni *et al.*, 2012). Not only are they present in muscle biopsies from patients with mutations in proteins involved in the glycosylation pathway (Belaya *et al.*, 2012; Huh *et al.*, 2012; Cossins *et al.*, 2013; Selcen *et al.*, 2013; Selcen *et al.*, 2014), but they are also implicated in other myopathies as a result of *STIM1* and *ORAI1* mutations (Chevessier *et al.*, 2005; Bohm *et al.*, 2014; Endo *et al.*, 2015). Tubular aggregates have also been identified in *Caveolin1*-/- and *Caveolin2*-/- mouse models (Schubert *et al.*, 2007), and wild type inbred male or ageing mice (Chevessier *et al.*, 2004). Subsarcolemmal tubular aggregates are classified as densely packed vesicular or tubular membranes derived from the terminal cisternae or longitudinal components of the SR, and are located between myofibrils beneath the sarcolemma (Chevessier *et al.*, 2004; Schubert *et al.*, 2007; Schiaffino, 2012). Other studies have demonstrated that mitochondria may be implicated in the formation of tubular aggregates (Novotova *et al.*, 2002; Schubert *et al.*, 2007). Whether tubular aggregates are direct pathological components contributing to the observed phenotype, or whether they represent a compensatory mechanism to pathological events, is poorly understood.
The main function of the SR is to regulate muscle contraction through calcium uptake, storage and release (Brady *et al.*, 2016). A common hypothesis is that tubular aggregates are products of a disruption of Ca^{2+} homeostasis. Immunohistochemistry

studies on inbred mouse muscle have shown that tubular aggregates are immunoreactive to SR markers SERCA1, sarcalumenin, calsequestrin, Ryanodine receptor 1 (RyR1), and triadin (Chevessier *et al.*, 2004). Furthermore, SERCA-1, SERCA-2, GRP78 and calsequestrin were identified in tubular aggregates found in caveolin-2 deficient mice (Schubert *et al.*, 2007). Analysis of cytoskeleton markers, spectrin, dystrophin, and desmin remain undetected (Chevessier *et al.*, 2004). Immunoblot studies further demonstrate that the expression levels of these SR proteins remained unchanged when compared to control mice, suggesting the formation of tubular aggregates is not because of an increase in SR proteins, but rather translocation of existing proteins (Schubert *et al.*, 2007).

In the context of defective glycosylation induced-CMS, one hypothesis is that the tubular aggregates occur due to an accumulation of hypoglycosylated proteins. Immunohistochemistry studies on *GFPT1*-CMS and *DPAGT1*-CMS patient muscle biopsies have confirmed the presence of proteins that regulate Ca^{2+} homeostasis, RyR1, SERCA1, SERCA2 and DHPR (dihydropyridine receptors) in tubular aggregates. Some tubular aggregates also contain dysferlin in some, but not all patient biopsies. Since these proteins do not harbour N- and O- glycosylation (GlcNAc) sites, we hypothesise that these findings occur secondary to misglycosylated muscle proteins. SR markers calsequestrin, triadin and sarcalumenin are known to harbour N-GlcNAc sites. Further investigation is required to see whether these proteins are observed in tubular aggregates of *Gfpt1*$^{tm1d/tm1d}$ muscle.

Interactions between stromal interaction molecule 1 (STIM1) and calcium release-activated calcium channel protein 1 (ORAI1), are also involved in Ca^{2+} regulation and are responsible for store-operated Ca^{2+} entry (Wang *et al.*, 2015). Stromal interaction molecule 1 (STIM1) contains an extracellular SAM domain which is modified by N-linked glycosylation (Williams *et al.*, 2002). One hypothesis that deficiency in GFPT1 may impair glycosylation of STIM1, destabilising the Ca^{2}+ channel ORAI1 (Kilch *et al.*, 2013) resulting in the formation of tubular aggregates (Endo *et al.*, 2015). Notably, STIM1 mutations identified outside of the SAM domain also induce the formation of tubular aggregates (Böhm *et al.*, 2014). Therefore, the presence of tubular aggregates is not solely attributed to hypoglycosylation of STIM1, but may occur because of a combination of pathomechanisms.

Analysis of tubular aggregates in biopsies from patients with tubular aggregate myopathies are immunoreactive to some but not all proteins mentioned here (Brady *et al.*, 2016). This further demonstrates that tubular aggregates are not defined by a conserved group of proteins but differ between patients and disease causing mechanisms. Moreover, tubular aggregates vary in size and morphology suggesting there are different subtypes of tubular aggregates with different compositions (Brady *et al.*, 2016).

We also observe abnormal subsarcolemmal vesicular structures in *Gfpt1*$^{tm1d/tm1d}$ mouse muscle that may correspond to caveolae. Caveolae are plasma membrane invaginations found in numerous cell types found under normal conditions (Cohen *et al.*, 2004; Lo *et al.*, 2016). They are characterised by their size, morphology and are accompanied by presence of caveolin proteins. Caveolins are known to have multiple functions, and are required for the formation of caveolae (Williams and Lisanti, 2004). One proposition for the functional role of caveolae in skeletal muscle is protection of muscle sarcolemma against damage. Caveolae provide an increased surface area of the sarcolemma which serves as a reservoir during excess membrane activity during muscle contraction. The number of caveolae might be upregulated as a protective mechanism in muscle disease (Lo *et al.*, 2016). There are currently no reports of distinct caveolae structures in *GFPT1*-CMS or *DPAGT1*-CMS patient muscle biopsies, nor were they immunoreactive for caveolin proteins (Brady *et al.*, 2016). Identification of caveolins in *Gfpt1*$^{tm1d/tm1d}$ mouse muscle will confirm whether these structures are indeed caveolae. These studies can be facilitated by immunoelectron microscopy.

Muscle weakness and fatigue are common characteristics of numerous muscle disorders, with several possible causes. Fatigable muscle weakness can be induced by a disruption in neuromuscular transmission, defective propagation of an action potential, or aberrant excitation-contraction coupling and contractile mechanisms (Boyas and Guevel, 2011). Whilst morphological differences are often observed in human CMS and other mouse models of CMS, suggesting impairment of the NMJ, they are not necessarily indicators of impaired neurotransmission. This is evident in recent investigations that reveal no decline in neurotransmission in age-related fragmentation of AChRs (Willadt *et al.*, 2016). It is therefore important to use direct methods to evaluate the efficacy of neurotransmission by testing muscle strength and fatigue. Here

we use functional tests including the inverted screen test and isometric force measurements of the TA muscle by direct stimulation of the sciatic nerve which demonstrates that *Gfpt1*$^{tm1d/tm1d}$ mice show a greater susceptibility to fatigue. This a common feature seen in other mouse models of congenital myasthenia (Chevessier *et al.*, 2008; Bogdanik and Burgess, 2011; Messéant *et al.*, 2015) and characteristic of human CMS (Guergueltcheva *et al.*, 2012; Huh *et al.*, 2012; Belaya *et al.*, 2015).

Interestingly, we also see a pronounced deficit in muscle strength and fatigue following direct stimulation of the diaphragm muscle from GFPT1 deficient mice. These findings are indicative of a myopathic phenotype consistent with our histopathological findings and EMG recordings in patients with mutations in *GFPT1* as well as other genes in the glycosylation pathway such as *ALG2, ALG14, DPAGT1*, and *GMPPB* (Guergueltcheva *et al.*, 2012; Huh *et al.*, 2012; Basiri *et al.*, 2013; Cossins *et al.*, 2013; Selcen *et al.*, 2013; Maselli *et al.*, 2014; Selcen *et al.*, 2014; Belaya *et al.*, 2015). Since *Gfpt1*$^{tm1d/tm1d}$ mice demonstrate fatigue following direct stimulation of the muscle, the force deficit we observe resulting from direct stimulation of the sciatic nerve is likely to be due to a combination of impaired neurotransmission and myopathic changes. Further investigation would involve isolated nerve-muscle preparations of the diaphragm which would allow us to compare differences between contractile response upon electrical stimulation of the nerve and direct stimulation of the muscle membrane. Any changes between the two contractile responses can be attributed to a defect in NMJ function. Alternatively, *ex vivo* electrophysiological recordings can be used to measure miniature EPPs and nerve-evoked EPPs which can also be used to estimate quantal release (Plomp *et al.*, 2015).

Under normal conditions, AChRs cluster and stabilise at the postsynaptic membrane. Thereafter they are endocytosed, recycled back to the membrane or are degraded. The AChR turnover rate is rapid (half-life ~ 1 day) in newly formed synapses. In adult synapses the turnover rate is slower (half-life ~10days) (Fumagalli *et al.*, 1982; Yampolsky *et al.*, 2010; Rudell and Ferns, 2013; Rudolf *et al.*, 2013; Khan *et al.*, 2014). Recycling of the AChR may serve as a quality control mechanism whereby defective AChRs are degraded, and new ones are generated and reinserted into the muscle membrane (Yampolsky *et al.*, 2010). One hypothesis is that the pathological findings seen in CMS maybe be due to instability of AChRs. In the context of GFPT1

deficiency, we hypothesise that the turnover rate of AChRs may be increased due to defective glycosylation of the AChR subunits. Alternatively, hypoglycosylation of proteins that stabilise AChRs on the muscle membrane may also increase the AChR turnover rate. Here we found that not only is the relative expression of AChRs in the *Gfpt1*$^{tm1d/tm1d}$ model maintained, but there is also no change in the turnover rate of AChRs, suggesting that the stability of AChRs are not compromised. It may be the case that (i) impaired glycosylation of individual AChR subunits is not pathogenic with regards to AChR stability, or perhaps (ii) GFPT1 is not primarily responsible for the glycosylation of NMJ proteins involved in the formation and stability of AChRs.

Our proteomic data has highlighted many differentially regulated proteins in GFPT1 deficient intercostal muscle. We observe regulation of proteins involved in organisation of the cytoskeleton (Rho GDP-dissociation inhibitor 2, Annexin A1, Ras GTPase-activating-like protein IQGAP1, KN motif and ankyrin repeat domain-containing protein 2), transport and sorting of glycoproteins (Vesicular integral-membrane protein VIP36), and extracellular matrix proteins important for skeletal muscle fibre integrity (Vitronectin). Proteins of interest discussed here include those involved in the glycosylation pathway, proteins that harbour N- and O- GlcNAc acceptor sites, and proteins that have a functional role at the NMJ.

We identify an upregulation of UDP-N-acetylglucosamine-peptide N acetylglucosaminyltransferase, also referred to as O-GlcNAc transferase (OGT), encoded by the *Ogt* gene. OGT is responsible for catalysing the addition of a single GlcNAc to a serine or threonine residue in the O-GlcNAcylation pathway (Hanover *et al.*, 2010). There are several possible reasons why we observe an increase in OGT expression resulting from GFPT1 deficiency. Notably, the most important factor that regulates OGT activity is the cellular levels of UDP and UDP-GlcNAc. Under normal conditions, upon transfer of the GlcNAc moiety, the UDP released acts as a feedback inhibitor of OGT. When UDP is removed from cells, OGT is dependent on the levels of UDP-GlcNAc. It is likely that the abnormally abundant expression of OGT we observe in GFPT1 deficient muscle occurs due to a lack of the precursor donor UDP-GlcNAc, and reduced suppression of OGT (Hart and Akimoto, 2009). Interestingly, a global increase in O-GlcNAcylation of proteins is known to occur in all mammalian cell types in response to cellular stress. An increase in OGT activity results in cells that are more tolerant to cellular stress, by upregulating heat shock proteins that protect cells from

stress, amongst numerous other mechanisms (Groves *et al.*, 2013). Therefore, it is possible that the upregulation of OGT we observe in *Gfpt1*$^{tm1d/tm1d}$ mouse muscle may occur because of the pathological changes taking place in the muscle.

Finally, OGT itself is O-GlcNAcylated. One possible explanation for the upregulation of OGT is to compensate for defective OGT activity.

Our proteomic profiling data also highlights an increase in the expression levels of the farnesyltransferase/geranylgeranyltransferase type-1 subunit alpha (FNTA) protein, an essential subunit of the geranylgeranyltransferase (GGT) complex which is implicated in synapse formation by playing an active role in the agrin/MuSK pathway (Luo *et al.*, 2003). The α subunit of GGT interacts with the kinase domain of MuSK. Thereafter, agrin increases tyrosine phosphorylation of GGT which facilitates Rho GTPase activation required for the regulation of actin dynamics responsible for AChR trafficking (Wu *et al.*, 2010). Inhibition of GGT activity prevents agrin-induced AChR clustering (Luo *et al.*, 2003; Strochlic *et al.*, 2005). Since we observe aberrant AChR clusters in GFPT1 deficient mouse muscle, we speculate that GGT is upregulated in attempt to recruit and cluster more AChRs to the muscle membrane. Notably, we also see an increase in the expression of MuSK proteins, also essential for AChR clustering (Chevessier *et al.*, 2008; Maselli *et al.*, 2010; Messéant *et al.*, 2015), which we hypothesise may serve a similar purpose. This idea stems from experimental evidence from denervation studies which show that under normal conditions MuSK is restricted to the motor endplate, but upon denervation there is a marked upregulation of MuSK in the extrasynaptic membrane (Bowen *et al.*, 1998). Moreover, increasing MuSK activity was shown to delay denervation and improve motor function mice (Perez-Garcia and Burden, 2012). Despite an upregulation of MuSK in *Gfpt1*$^{tm1d/tm1d}$ mice, AChR clusters appear smaller than those in control mice. This finding suggests that increased levels of MuSK is unable to promote AChR clustering. Further studies would involve investigating proteins downstream of MuSK in attempt to identify proteins with possible pathogenic mechanisms.

We see a robust increase in the expression levels of glypican-1, a cell surface, lipid- raft associated heparan sulphate proteoglycan (HSPG) that participates in axon guidance, Schwann cell myelination (Chernousov *et al.*, 2006), and is important for modulating growth factors and influencing skeletal muscle differentiation (Litwack *et al.*, 1998).

Since suppression of glypican-1 significantly inhibits myelination (Chernousov *et al.*, 2006), it is possible that hypomyelination of the presynaptic nerve that we observe in *Gfpt1*$^{tm1d/tm1d}$ mice may induce upregulation of glypican-1 as a compensatory mechanism. Interestingly, glypican-1 also harbours N-GlcNAc glycans, but was shown to maintain its folded conformation in the absence of N-linked glycans (Svensson *et al.*, 2012). Glypican-1 is mainly expressed in neural tissues and skeletal muscle, with some expression in other tissues. Expression of glypican-1 in skeletal muscle typically occurs during late embryonic development and in the early postnatal stages in rodents (Litwack *et al.*, 1998; Yamaguchi, 2002; Casar *et al.*, 2004; Gutierrez and Brandan, 2010; Sigoillot *et al.*, 2010). Although there is no obvious evidence of a muscle phenotype in glypican-1 knockout mice, myoblasts display defective differentiation in the absence of glypican-1 expression. Studies have also shown that glypican-1, as well as other heparan sulphate proteoglycans perlecan, syndecan-3, and syndecan-4 are upregulated during skeletal muscle regeneration (Casar *et al.*, 2004; Gutierrez and Brandan, 2010; Brandan and Gutierrez, 2013). This may account for the robust increase in glypican-1 expression we observe in GFPT1 deficient mice.

The experiments performed in this chapter establishes a muscle-specific GFPT1 deficient mouse model representative of the human *GFPT1*-CMS phenotype. This is the first report of a CMS mouse model depicting defective glycosylation. Since GFPT1 lies upstream of other glycosylation enzymes also implicated in CMS, it is possible that some of findings from this model may also be true for *DPAGT1*, *ALG2*, and *ALG14* CMS. Our model provides new insights into differentially regulated proteins that demonstrates possible pathological and compensatory mechanisms, and highlights the importance of protein glycosylation in maintaining the integrity of the NMJ and muscle.

Chapter 6: General discussion and future directions

6.1 Pre-clinical studies for CMS

An increase in the number of individuals diagnosed with CMS, together with the discovery of novel CMS-causing genes, has driven the expansion of research within this field. Genotype-phenotype correlations in CMS are greatly impeded by the rarity of the disease with few patients harbouring the same mutation, giving rise to heterogenous phenotypes. Successful treatment of CMS requires an understanding of the pathogenic mechanisms underlying the disease, making it increasingly important for conducting pre-clinical research.

So far, mouse models of CMS have been developed to facilitate the investigation of defective NMJ proteins that have a direct effect on neurotransmission, depolarisation of the endplate or the development and maintenance of the synapse. These studies have provided insights into affected pathways that give rise to the observed CMS phenotype, and demonstrate the benefits of treatment with therapeutic compounds (Webster *et al.*, 2013; Barik *et al.*, 2014; Messéant *et al.*, 2015).

Whilst CDGs have been widely studied over the years, only recently were mutations in genes encoding enzymes in the glycosylation pathway identified as CMS-causing. Correct diagnoses of disorders of glycosylation are often hindered, as patients often present with multisystem disorders that display highly variable phenotypes. Even if a patient were to present exclusively with a CMS phenotype, discovery of the exact pathological mechanisms remains challenging due to the multitude of proteins that are potentially misglycosylated. This emphasises the need for *in vivo* models designed to facilitate functional studies. A mouse model displaying aberrant glycosylation is particularly useful for testing the effects of drug therapies, as the precise molecular targets underlying this subtype of CMS remains largely unknown.

Until now, a mouse model representative of defective glycosylation in CMS had not been generated. The work presented in this thesis establishes a mouse model to investigate the pathological molecular mechanisms underlying GFPT1 deficiency. We report the generation of a novel muscle-specific GFPT1 knockout mouse model which recapitulates many aspects of the phenotype observed in patients with *GFPT1*-CMS. We further identify potential molecular pathways which are altered in response to a

deficit in GFPT1. We speculate that some of the changes in comparison to wild type animals serve as compensatory mechanisms, whilst others may contribute directly to the CMS phenotype.

6.2 Evaluation of mouse models for studying CMS

6.2.1 *The use of mouse models for investigating CMS*

Although cell culture techniques and zebrafish studies have proven useful for the initial characterisation of CMS phenotypes, they are limited to short-term studies and are not representative of the complex systems of the human body. *In vivo* mouse models are particularly useful for studying neuromuscular disorders as they permit examination of NMJ morphology, muscle pathology and allow testing of motor abilities. Mouse models can further be used to study disease progression and the benefits of therapeutic treatments.

There are however some discrepancies between humans and mice which can sometimes affect the ability to reproduce mouse models representative of human disease. An example specific to neuromuscular disorders is difference in the safety margin of the NMJ. The safety margin in humans is quite small whereby neurotransmission is impaired due to subtle pathological changes. By contrast, the safety margin in the mouse has a higher threshold (Wood and Slater, 2001; Trontelj *et al.*, 2002). This may explain why transgenic mouse models of neuromuscular diseases do not always show a phenotype, or display abnormalities that are less severe than the patient phenotype. Differences in the severity of phenotype between humans and mice are usually anticipated by the investigator and can be overcome by critical evaluation of the experimental design. Once a valid transgenic mouse line has been established, the model becomes a valuable tool for understanding the pathogenesis of the disorder and for testing therapeutic compounds (Vainzof *et al.*, 2008).

6.2.2 *The Gfpt1$^{tm1d/tm1d}$ mouse model for CMS*

The ubiquitous GFPT1 isoform in humans and the house mouse (*Mus musculus*) share approximately 99% of their amino acid sequence (Dehaven *et al.*, 2001), making GFPT1 transgenic mice good models for studying human CMS. In human *GFPT1*-CMS, mutations reside predominantly in the ubiquitous GFPT1 isoform which often results in a reduction in either one of both GFPT1 isoforms. Interestingly, even though the muscle-specific knockout mouse model results in complete loss of both isoforms, these mice are viable and do not display the debilitating symptoms seen in some patients with *GFPT1* mutations. One possible explanation for these findings is the disparity of the safety margin between humans and mice.

The *Gfpt1$^{tm1d/tm1d}$* model is muscle-specific and does not address functions of the presynaptic apparatus that are potentially disrupted. Although this can be regarded as a limitation to the model, we demonstrate that GFPT1 deficiency in the postsynaptic apparatus alone is enough to cause a CMS phenotype in mice. Moreover, we discovered morphological alterations of presynaptic components which is secondary to GFPT1 deficiency in muscle. Whether the CMS phenotype we observe in patients is exclusively attributed to postsynaptic GFPT1 deficiency, requires further investigation. It would be interesting to compare data from the muscle-specific knockout model with data from a motor neuron-specific *Gfpt1* knockout mouse model, to establish the extent to which neural and muscle GFPT1 deficiency contributes to the CMS phenotype we observe in patients with a global reduction of GFPT1.

Although GFPT1 is also expressed in cardiac tissues in humans (Dehaven *et al.*, 2001), very few patients present with a developing cardiomyopathy. This phenotype occurs because of aberrant glycosylation of cardiac proteins (Lewis *et al.*, 2014). GFPT1 is also depleted in cardiac tissues in the *Gfpt1$^{tm1d/tm1d}$* mouse model. Although we do not investigate the possibility of cardiac phenotype in this study, which has the potential to influence our muscle fatigue data, we validate our data using unbiased *ex vivo* and *in situ* techniques to measure force from mouse muscle. Studies to deduce whether these mice develop a cardiac phenotype can be facilitated by histopathological staining and MRI studies (Stuckey *et al.*, 2012).

6.2.3 *Alternative gene targeting approaches*

Developments in gene targeting strategies have revolutionised manipulation of the genome making it easier and faster to generate transgenic models of human disease. Prior to selecting the best approach for generating our transgenic mouse line, we critically evaluated the different Cre strains available at The Jackson Laboratory Cre Repository. Alternative muscle-specific Cre lines that were considered did not offer any advantage over the *Ckm-Cre* strain. Rather, some strains expressed Cre earlier in the developing embryo, whilst others illustrated ectopic expression and mosaicism making embryonic lethality more likely (Miniou *et al.*, 1999; Guo *et al*., 2002).

CRISPR/Cas9 gene editing technology has proven highly successful for studying human diseases (Ablain *et al.*, 2015; Logan *et al.*, 2015; Qin *et al.*, 2016; Torres-Ruiz and Rodriguez-Perales, 2017). The advantages of CRISPR/Cas9 over conventional gene targeting approaches include improved efficiency, simplicity of the target design and allowing mutations to be introduced in multiple genes at the same time. Global knockouts and tissue-specific knockout mice are achievable using CRISPR/Cas9, but is currently limited to small insertions into the genome which may not be suitable for some studies. Due to the novelty of CRISPR/Cas9 and the uncertainty of some of its off-site effects, the EUCOMM knockout-first approach is often the preferred choice as it is well characterised and most embryonic stem cells are readily available in the EUCOMM repository. Another advantage of using the EUCOMM knockout-first strategy is its flexibility to generate different alleles. If the global or tissue-specific knockout model happens to be embryonic lethal, an inducible Cre strain can be incorporated into the strategy to overcome this problem. For now, it is recommended that the CRISPR/Cas9 approach is used in parallel to EUCOMM strategies if possible (Coleman *et al.*, 2015).

6.3 Congenital disorders of glycosylation

Since glycosylation is a ubiquitous process, it is not surprising that patients with mutations in glycosylation genes exhibit multisystem disorders. An attempt to understand why some patients present with certain disease states and not others, as well as the selective vulnerability of certain tissues and organ systems remains challenging.

The diversity of processes required for glycosylation gives rise to thousands of potentially pathogenic mechanisms. CDG may occur because of defects in one or more of the following processes: (i) activation or transport of sugar residues, (ii) dolichol and dolichol-linked glycan synthesis, (iii) translocation of glycans to different compartments (eg. cytoplasmic to lumen of the ER), (iv) transfer of oligosaccharides to the protein (v) trafficking or processing of the glycoprotein through the Golgi apparatus, (vi) secretion at the end of the multistep pathway (Scott *et al.*, 2014).

DPAGT1 (Wu *et al*., 2003; Carrera *et al*., 2012; Imtiaz *et al*., 2012; Wurde *et al*., 2012; Jaeken *et al*., 2015), *ALG2* (Thiel *et al*., 2003) and *GMPPB* (Carss *et al*., 2013) have previously been associated with CDG. It is yet to be determined why the clinical outcome is variable amongst patients with mutations in the same gene. Some patients present with multisystem disorders such as CDG, whilst others exhibit a CMS phenotype which predominantly results in myasthenia due to impaired neuromuscular transmission (Cossins *et al*., 2003). Analysis of serum transferrin glycoform, commonly used to detect defective glycosylation (Sparks and Krasnewich, 2005; Jeppsson *et al*., 2007), suggests mild impairment of N-glycosylation in CMS patients in comparison with that from CDG patients (Cossins *et al*., 2003). Thus, it is possible that we observe a wide spectrum of clinical outcomes based on the pathogenicity of different mutations (Marklova and Albahri *et al*., 2007).

Defects in the O-linked glycosylation pathway have also been found to be responsible for multiple forms of muscular dystrophy (Martin, 2005; Muntoni *et al.*, 2007; Muntoni *et al.*, 2008). So far, mutations in 6 glycotransferases have been discovered which result in hypoglycosylation of α-dystroglycan through aberrant events in the O-mannosylation pathway. These mutations give rise to dystroglycanopathies with variable phenotypes (Muntoni *et al.*, 2007). More recently, reports of overlapping phenotypes of myasthenic disorders and dystroglycanopathies as a result of *GMPPB* mutations have been described (Belaya *et al*., 2015; Montagenese *et al*., 2016)**.** *GMMPB*-associated muscular dystrophy is marked by hypoglycosylation of α-dystrogylcan (Carrs *et al*., 2013; Raphael *et al*., 2014). These patients exhibit dystrophic features with variable severities. Some patients present with a more severe congenital muscular dystrophy phenotype with brain and eye abnormalities, whilst others display a milder limb-girdle muscular dystrophy in the proximal limb muscles. Furthermore, a neurotransmission defect is only evident in a subset of patients with *GMPPB*-muscular dystrophy

dystroglycanopathy and not others (Belaya *et al*., 2015). Further reports demonstrate an expansion in the phenotypic spectrum of *GMPPB* mutations including limb-girdle muscular dystrophies, with some cases involving intellectual impairment and rhabdomyolysis (Cabrera-Serrano *et al*., 2015). These expanding phenotypes are likely due to the ubiquitous nature of GMPPB and its involvement in the glycosylation of numerous proteins. The widespread and variable clinical outcomes due to mutations within the same gene is yet to be determined.

It is likely that patients with glycosylation deficient CMS remain undiagnosed due to presentation of a complex clinical phenotype which hinders correct diagnosis. Some patients also present with a myopathic phenotype which can often be misleading. It is possible that with time, more and more genes implicated in CDG will also be identified as pathogenic for CMS. Similarly, patients with CMS are also likely to present with multisystem disorders, and the characteristic CMS phenotype is likely to expand with time (Wurde *et al*., 2012).

Common glycotherapies that have been proposed or implemented include the delivery of synthetic glycans or glycoproteins downstream of the defective biosynthetic steps, upregulating glycosyltransferase expression or activity, and the delivery of glycosyltransferase genes via cell or gene therapy techniques (Martin, 2003; Hudak and Bertozzi, 2014). One example which demonstrates the successful use of glycotherapies in mice, is an overexpression of LARGE in *Large* ^{myd} mice that exhibit impaired glycosylation of α-dystroglycan. The outcome of this study demonstrates that hyperglycosylation of α-dystroglycan ameliorates muscle pathology and contractile performance, and restores neuromuscular junction architecture and transmission deficits (Gumerson *et al.*, 2013). Although the NMJ alterations observed in *Large* ^{myd} mice are likely to be secondary to the dystrophic phenotype, and thus an improvement in neurotransmission occurs through stabilizing the endplate, the idea of restoring glycosylation as a therapy, looks promising and can potentially be implemented in CMS-CDGs.

6.4 Future directions

Prospective studies will include characterisation of tubular aggregates in *Gfpt1*$^{tm1d/tm1d}$ mice. Tubular aggregates in mouse muscle can be tested for proteins that have previously been described in biopsies from *GFPT1*-CMS and *DPAGT1*-CMS patients and other myopathies. They can also be tested for proteins that harbour GlcNAc acceptor sites which have known functions in neurotransmission, muscle stability and muscle contraction. Identification of these aggregates will help deduce whether tubular aggregates are pathogenic or merely secondary to the CMS phenotype.

An understanding of the molecular pathology is vital for developing more targeted therapies. It is therefore important to perform studies to determine the functional significance of regulated proteins that we identified using proteomic profiling studies. Investigation of ubiquitous enzymes can be extremely challenging, and it is not feasible to address hundreds of potentially modified proteins. An alternative to proteomic profiling experiments, which will be particularly useful in this study is the use of glycomic studies to address changes in the glycosylation status of proteins. Additional experiments will involve investigating the implication of GFPT1 deficiency in cardiac tissues and further characterisation of nerve pathology.

Ultimately, the long-term goal is the discovery of therapeutic strategies that will reverse the myasthenic phenotype observed in patients with CMS. To date there are no cures for CMS but symptomatic off-label treatments are available. Clinical trial studies are currently recruiting CMS patients for the evaluation of 3,4 DAP and amifampridine phosphate (phosphate form of 3,4 DAP). These trials involve studies that will enhance our understanding of the effects of therapies on the natural course of the disease. Other trials involve dose optimisation and drug combination studies to improve muscle strength. Some trials aim to provide substantial evidence for the therapeutic benefits of these compounds in attempt to make them commercially available.

Therapies used for CMS are limited as the underlying mechanisms of action are not well understood. Some drugs display variable efficacies and side effects amongst patients and in different subtypes of CMS. The *Gfpt1*$^{tm1d/tm1d}$ mouse model will prove useful for testing current treatments in attempt to deduce the mode of action which will help maximise their clinical use. Further studies will involve the development of new compounds. *Gfpt1*$^{tm1d/tm1d}$ mice can be used to test the efficacy of compounds, determine their optimal doses, and examine potential adverse effects.

As the number of patients diagnosed with glycosylation associated CMS increases, together with the discovery of novel glycosylation enzymes, it is likely that future studies will involve the development of glycotherapies aiming to restore NMJ function. Although proven successful in muscular dystrophies, such studies will be the first of its kind for CMS. Whilst restoring glycosylation may reverse the myasthenic phenotype observed in CMS, and perhaps even reverse primary myopathic changes, it is less likely that myopathic alterations secondary to NMJ dysfunction can be reversed. Pre-clinical studies in mice that prove efficacious in ameliorating myasthenic symptoms, or perhaps even stabilising and restoring NMJ function will provide crucial evidence needed to drive forward patient therapies.

Appendix A

Differentially regulated proteins in *Gfpt1*$^{tm1d/tm1d}$ intercostal muscles, their subcellular localisation, and proposed functions. Proteins 1-29 are upregulated with 2 or more unique peptides, 30-39 are upregulated with 1 unique peptide, 40-43 are downregulated with 1 unique peptide, $p \leq 0.05$.

	Protein	Subcellular Localisation	Proposed Functions
1	**Galectin-3**	Cytoplasm, extracellular space, nucleus	Involved in acute inflammatory responses including neutrophil activation and adhesion, chemoattraction of monocytes macrophages, opsonisation of apoptotic neutrophils, and activation of mast cells.
2	**UDP-N-acetylglucosamine-peptide N-acetylglucosaminyltransferase**	Cytoplasm, nucleus, plasma membrane	Catalyses the transfer of a single *N*-acetylglucosamine from UDP-GlcNAc to a serine or threonine residue in cytoplasmic and nuclear proteins.
3	**Plastin-2**	Cytoplasm	Actin-binding protein. Plays a role in the activation of T-cells.
4	**Actin-related protein 2/3 complex subunit 1B**	Cytoplasm	Functions as component of the Arp2/3 complex which is involved in regulation of actin polymerization and together with an activating nucleation-promoting factor mediates the formation of branched actin networks.
5	**Vitronectin**	Extracellular space	Cell adhesion and spreading factor found in serum and tissues. Vitronectin interacts with glycosaminoglycans and proteoglycans. It is recognized by certain members of the integrin family and serves as a cell-to-substrate adhesion molecule. Inhibitor of the membrane-damaging effect of the terminal cytolytic complement pathway.
6	**Perilipin-1**	ER-Golgi network	Modulator of adipocyte lipid metabolism. Coats lipid storage droplets to protect them from breakdown by hormone-sensitive lipase (HSL). Its absence may result in leanness. Plays a role in unilocular lipid droplet formation by activating CIDEC.
7	**Membrane primary amine oxidase**	Plasma membrane	Has monoamine oxidase activity. May play a role in adipogenesis.

	Protein	Subcellular Localisation	Proposed Functions
8	**Histone H1.5**	Nucleus	Histone H1 protein binds to linker DNA between nucleosomes forming the macromolecular structure known as the chromatin fibre.
9	**BTB/POZ domain-containing protein KCTD12**	Extracellular space, plasma membrane	Auxiliary subunit of GABA-B receptors that determines the pharmacology and kinetics of the receptor response. Increases agonist potency and markedly alters the G-protein signalling of the receptors by accelerating onset and promoting desensitization.
10	**Rho GDP-dissociation inhibitor 2**	Cytoplasm	Regulates the GDP/GTP exchange reaction of the Rho proteins by inhibiting the dissociation of GDP from them, and the subsequent binding of GTP to them. Regulates reorganization of the actin cytoskeleton mediated by Rho family members.
11	**Sec1 family domain-containing protein 1**	Cytoplasm, ER-Golgi network	Plays a role in SNARE-pin assembly and Golgi-to-ER retrograde transport via its interaction with COG4. Involved in vesicular transport between the endoplasmic reticulum and the Golgi.
12	**Annexin A1**	Cytoplasm, nucleus, plasma membrane	Plays a role in glucocorticoid-mediated down-regulation of the early phase of the inflammatory response. Promotes rearrangement of the actin cytoskeleton, cell polarization and cell migration. Negatively regulates hormone exocytosis via activation of the formyl peptide receptors and reorganization of the actin cytoskeleton. Has high affinity for Ca^{2+} and can bind up to eight Ca^{2+} ions.
13	**Protein farnesyltransferase/geranylgeranyl transferase type-1 subunit alpha**	Cytoplasm, plasma membrane	Essential subunit of both the farnesyltransferase and the geranylgeranyltransferase complex. May positively regulate neuromuscular junction development downstream of MuSK.
14	**Macrophage-capping protein**	Cytoplasm, nucleus	Calcium-sensitive protein which reversibly blocks the barbed ends of actin filaments but does not sever preformed actin filaments. May play an important role in macrophage function.

	Protein	Subcellular Localisation	Proposed Functions
15	**Glypican-1**	Plasma membrane	Required for proper skeletal muscle differentiation by sequestering FGF2 in lipid rafts preventing its binding to receptors (FGFRs) and inhibiting the FGF-mediated signalling.
16	**Cysteine-rich protein 1**	Cytoplasm	Participates in zinc absorption and may function as an intracellular zinc transport protein.
17	**Ras GTPase-activating-like protein IQGAP1**	Plasma membrane	Binds to activated CDC42 but does not stimulate its GTPase activity. It associates with calmodulin. May serve as an assembly scaffold for the organization of a multimolecular complex that would interface incoming signals to the reorganization of the actin cytoskeleton at the plasma membrane. May promote neurite outgrowth.
18	**Vesicular integral-membrane protein VIP36**	ER-Golgi network	Plays a role as an intracellular lectin in the early secretory pathway. Interacts with N-acetyl-D-galactosamine and high-mannose type glycans and may also bind to O-linked glycans. Involved in the transport and sorting of glycoproteins carrying high mannose-type glycans
19	**Complement C4-B**	Extracellular space	Non-enzymatic component of C3 and C5 convertases and thus essential for the propagation of the classical complement pathway.
20	**Tubulin-specific chaperone A**	Cytoplasm	Tubulin-folding protein.
21	**Aminopeptidase N**	Plasma membrane	Plays a role in the final digestion of peptides generated from hydrolysis of proteins by gastric and pancreatic proteases. May be involved in the metabolism of regulatory peptides of diverse cell types, responsible for the processing of peptide hormones, such as angiotensin III and IV, neuropeptides, and chemokines. May have a role in angiogenesis.
22	**SH3 domain-binding glutamic acid-rich-like protein 3**	Cytoplasm, nucleus	May act as a modulator of glutaredoxin biological activity.

	Protein	Subcellular Localisation	Proposed Functions
23	**Syntaxin-7**	Plasma membrane	May be involved in protein trafficking from the plasma membrane to the early endosome as well as in homotypic fusion of endocytic organelles. Mediates the endocytic trafficking from early endosomes to late endosomes and lysosomes.
24	**Coatomer subunit gamma-1**	Cytoplasm, ER-Golgi network	Reversibly associates with Golgi non-clathrin-coated vesicles which further mediates biosynthetic protein transport from the ER, via the Golgi up to the trans Golgi network.
25	**Ras-related protein Rab-7a**	Cytoplasm	Key regulator in endo-lysosomal trafficking. Governs early-to-late endosomal maturation, microtubule minus-end as well as plus-end directed endosomal migration and positioning, and endosome-lysosome transport through different protein-protein interaction cascades.
26	**Myristoylated alanine-rich C-kinase substrate**	Cytoplasm, plasma membrane	The most prominent cellular substrate for protein kinase C. This protein binds calmodulin, actin, and synapsin. It is a filamentous actin cross-linking protein.
27	**Transcription intermediary factor 1-beta**	Nucleus	Nuclear corepressor for KRAB domain-containing zinc finger proteins. Mediates gene silencing. Ubiquitinates p53/TP53 leading to its proteosomal degradation;
28	**Coatomer subunit beta**	Cytoplasm, ER-Golgi network, plasma membrane	A cytosolic protein complex that binds to dilysine motifs and reversibly associates with Golgi non-clathrin-coated vesicles, which further mediate biosynthetic protein transport from the ER, via the Golgi up to the trans Golgi network.
29	**Protein disulfide-isomerase A3**	ER-Golgi network	Catalyzes the rearrangement of -S-S- bonds in proteins.
30	**60S ribosomal protein L3**	Cytoplasm, nucleus	The L3 protein is a component of the large subunit of cytoplasmic ribosomes.
31	**Periostin**	ER-Golgi network	Induces cell attachment and spreading and plays a role in cell adhesion. Enhances incorporation of BMP1 in the fibronectin matrix of connective tissues, and subsequent proteolytic activation of lysyl oxidase.
32	**Complement C1q subcomponent subunit B**	Extracellular space	C1q associates with the proenzymes C1r and C1s to yield C1, the first component of the serum complement system.

	Protein	Subcellular Localisation	Proposed Functions
33	**Coiled-coil domain-containing protein 127**	ER-Golgi network, extracellular space	Function is unknown.
34	**Bone marrow proteoglycan**	Cytoplasm	Induces non-cytolytic histamine release from basophils. It is involved in antiparasitic defense mechanisms and immune hypersensitivity reactions.
35	**Minor histocompatibility antigen H13**	ER-Golgi network, plasma membrane	Catalyzes intramembrane proteolysis of some signal peptides after they have been cleaved from a preprotein, resulting in the release of the fragment from the ER membrane into the cytoplasm. May play a role in graft rejection.
36	**KN motif and ankyrin repeat domain-containing protein 2**	Cytoplasm, mitochondria	Involved in transcription regulation. Involved in the negative control of vitamin D receptor signalling pathway. May be involved in the control of cytoskeleton formation by regulating actin polymerization. Involved in regulation of caspase-independent apoptosis. May be involved in promotion of cell proliferation
37	**Heme oxygenase 2**	ER-Golgi network	Heme oxygenase cleaves the heme ring at the alpha methene bridge to form biliverdin. Biliverdin is subsequently converted to bilirubin by biliverdin reductase. Heme oxygenase 2 could be implicated in the production of carbon monoxide in brain where it could act as a neurotransmitter.
38	**Histone H1.3**	Nucleus	Histone H1 protein binds to linker DNA between nucleosomes forming the macromolecular structure known as the chromatin fibre.
39	**Cytochrome P450 20A1**	Plasma membrane	Catalyses oxidation of flavoproteins.
40	**Selenoprotein T**	ER-Golgi network	Involved in glucose homeostasis, insulin secretion, cellular response to glucose stimulus and response to glucose.
41	**Fructosamine-3-kinase**	Cytoplasm	May initiate a process leading to the deglycation of fructoselysine and of glycated proteins. May play a role in the phosphorylation of 1-deoxy-1-morpholinofructose (DMF), fructoselysine, fructoseglycine, fructose and glycated lysozymes.
42	**Uncharacterized family 31 glucosidase KIAA1161**	Plasma membrane	Putative glucosidase.

	Protein	Subcellular Localisation	Proposed Functions
43	**Nitric oxide synthase, brain**	Plasma membrane	Produces nitric oxide (NO) which is a messenger molecule with diverse functions throughout the body. In the brain and peripheral nervous system, NO displays many properties of a neurotransmitter.

References

Abicht, A., Dusl, M., Gallenmuller, C., Guergueltcheva, V., Schara, U., Della Marina, A., Wibbeler, E., Almaras, S., Mihaylova, V., von der Hagen, M., Huebner, A., Chaouch, A., Muller, J. S. and Lochmuller, H. (2012) 'Congenital myasthenic syndromes: achievements and limitations of phenotype-guided gene-after-gene sequencing in diagnostic practice: a study of 680 patients', *Hum Mutat,* 33(10), pp. 1474-84.

Abicht, A., Juliane Müller, S. and Lochmüller, H. (2016). *Congenital Myasthenic Syndromes*. [online] Available at: https://www.ncbi.nlm.nih.gov/books/NBK1168/ [Accessed 29 Apr. 2017].

Ablain, J., Durand, E. M., Yang, S., Zhou, Y. and Zon, L. I. (2015) 'A CRISPR/Cas9 vector system for tissue-specific gene disruption in zebrafish', *Dev Cell,* 32(6), pp. 756-64.

Aebi, M. (2013) 'N-linked protein glycosylation in the ER', *Biochimica et Biophysica Acta (BBA) - Molecular Cell Research,* 1833(11), pp. 2430-2437.

Aran, A., Segel, R., Kaneshige, K., Gulsuner, S., Renbaum, P., Oliphant, S., Meirson, T., Weinberg-Shukron, A., Hershkovitz, Y., Zeligson, S., Lee, M. K., Samson, A. O., Parsons, S. M., King, M. C., Levy-Lahad, E. and Walsh, T. (2017) 'Vesicular acetylcholine transporter defect underlies devastating congenital myasthenia syndrome', *Neurology*.

Ball, R. W., Warren-Paquin, M., Tsurudome, K., Liao, E. H., Elazzouzi, F., Cavanagh, C., An, B. S., Wang, T. T., White, J. H. and Haghighi, A. P. (2010) 'Retrograde BMP signaling controls synaptic growth at the NMJ by regulating trio expression in motor neurons', *Neuron,* 66(4), pp. 536-49.

Barik, A., Lu, Y., Sathyamurthy, A., Bowman, A., Shen, C., Li, L., Xiong, W. C. and Mei, L. (2014) 'LRP4 is critical for neuromuscular junction maintenance', *J Neurosci,* 34(42), pp. 13892-905.

Barisic, N., Chaouch, A., Muller, J. S. and Lochmuller, H. (2011) 'Genetic heterogeneity and pathophysiological mechanisms in congenital myasthenic syndromes', *Eur J Paediatr Neurol*, 15(3), pp. 189-96.

Barton, E. (2008). *Measuring isometric force of isolated mouse muscles in vitro*. [online] Available at: http://www.treat-nmd.eu/downloads/file/sops/dmd/MDX/dmd_m.1.2.002.pdf [Accessed 29 Apr. 2017].

Basiri, K., Belaya, K., Liu, W. W., Maxwell, S., Sedghi, M. and Beeson, D. (2013) 'Clinical features in a large Iranian family with a limb-girdle congenital myasthenic syndrome due to a mutation in DPAGT1', *Neuromuscul Disord*, 23(6), pp. 469-72.

Bauche, S., O'Regan, S., Azuma, Y., Laffargue, F., McMacken, G., Sternberg, D., Brochier, G., Buon, C., Bouzidi, N., Topf, A., Lacene, E., Remerand, G., Beaufrere, A. M., Pebrel-Richard, C., Thevenon, J., El Chehadeh-Djebbar, S., Faivre, L., Duffourd, Y., Ricci, F., Mongini, T., Fiorillo, C., Astrea, G., Burloiu, C. M., Butoianu, N., Sandu, C., Servais, L., Bonne, G., Nelson, I., Desguerre, I., Nougues, M. C., Boeuf, B., Romero, N., Laporte, J., Boland, A., Lechner, D., Deleuze, J. F., Fontaine, B., Strochlic, L., Lochmuller, H., Eymard, B., Mayer, M. and Nicole, S. (2016) 'Impaired Presynaptic High-Affinity Choline Transporter Causes a Congenital Myasthenic Syndrome with Episodic Apnea', *Am J Hum Genet*, 99(3), pp. 753-61.

Belaya, K., Finlayson, S., Cossins, J., Liu, W. W., Maxwell, S., Palace, J. and Beeson, D. (2012) 'Identification of DPAGT1 as a new gene in which mutations cause a congenital myasthenic syndrome', *Ann N Y Acad Sci*, 1275, pp. 29-35.

Belaya, K., Rodríguez Cruz, P. M., Liu, W. W., Maxwell, S., McGowan, S., Farrugia, M. E., Petty, R., Walls, T. J., Sedghi, M., Basiri, K., Yue, W. W., Sarkozy, A., Bertoli, M., Pitt, M., Kennett, R., Schaefer, A., Bushby, K., Parton, M., Lochmüller, H., Palace, J., Muntoni, F. and Beeson, D. (2015) 'Mutations in GMPPB cause congenital myasthenic syndrome and bridge myasthenic disorders with dystroglycanopathies', *Brain*, 138(9), pp. 2493-2504.

Berke, B., Wittnam, J., McNeill, E., Van Vactor, D. L. and Keshishian, H. (2013) 'Retrograde BMP signaling at the synapse: a permissive signal for synapse maturation and activity-dependent plasticity', *J Neurosci*, 33(45), pp. 17937-50.

Bogdanik, L. P. and Burgess, R. W. (2011) 'A valid mouse model of AGRIN-associated congenital myasthenic syndrome', *Hum Mol Genet*, 20(23), pp. 4617-33.

Bohm, J., Chevessier, F., Koch, C., Peche, G. A., Mora, M., Morandi, L., Pasanisi, B., Moroni, I., Tasca, G., Fattori, F., Ricci, E., Penisson-Besnier, I., Nadaj-Pakleza, A., Fardeau, M., Joshi, P. R., Deschauer, M., Romero, N. B., Eymard, B. and Laporte, J. (2014) 'Clinical, histological and genetic characterisation of patients with tubular aggregate myopathy caused by mutations in STIM1', *J Med Genet*, 51(12), pp. 824-33.

Bohm, J., Chevessier, F., Maues De Paula, A., Koch, C., Attarian, S., Feger, C., Hantaï, D., Laforêt, P., Ghorab, K., Vallat, J. M., Fardeau, M., Figarella-Branger, D., Pouget, J., Romero, N. B., Koch, M., Ebel, C., Levy, N., Krahn, M., Eymard, B., Bartoli, M. and Laporte, J. (2013) 'Constitutive activation of the calcium sensor STIM1 causes tubular-aggregate myopathy', *Am J Hum Genet*, 92(2), pp. 271-8.

Boncompagni, S., Protasi, F. and Franzini-Armstrong, C. (2012) 'Sequential stages in the age-dependent gradual formation and accumulation of tubular aggregates in fast twitch muscle fibers: SERCA and calsequestrin involvement', *Age (Dordr)*, 34(1), pp. 27-41.

Bowen, D. C., Park, J. S., Bodine, S., Stark, J. L., Valenzuela, D. M., Stitt, T. N., Yancopoulos, G. D., Lindsay, R. M., Glass, D. J. and DiStefano, P. S. (1998) 'Localization and regulation of MuSK at the neuromuscular junction', *Dev Biol*, 199(2), pp. 309-19.

Boyas, S. and Guevel, A. (2011) 'Neuromuscular fatigue in healthy muscle: underlying factors and adaptation mechanisms', *Ann Phys Rehabil Med*, 54(2), pp. 88-108.

Brady, S., Healy, E. G., Gang, Q., Parton, M., Quinlivan, R., Jacob, S., Curtis, E., Al-Sarraj, S., Sewry, C. A., Hanna, M. G., Houlden, H., Beeson, D. and Holton, J. L. (2016) 'Tubular Aggregates and Cylindrical Spirals Have Distinct Immunohistochemical Signatures', *J Neuropathol Exp Neurol*, 75(12), pp. 1171-1178.

Brandan, E. and Gutierrez, J. (2013) 'Role of skeletal muscle proteoglycans during myogenesis', *Matrix Biol*, 32(6), pp. 289-97.

Brandon, E. P., Lin, W., D'Amour, K. A., Pizzo, D. P., Dominguez, B., Sugiura, Y., Thode, S., Ko, C. P., Thal, L. J., Gage, F. H. and Lee, K. F. (2003) 'Aberrant patterning of neuromuscular synapses in choline acetyltransferase-deficient mice', *J Neurosci*, 23(2), pp. 539-49.

Bretthauer, R. K. (2009) 'Structure, expression, and regulation of UDP-GlcNAc: dolichol phosphate GlcNAc-1-phosphate transferase (DPAGT1)', *Curr Drug Targets*, 10(6), pp. 477-82.

Brooks, S. V. and Faulkner, J. A. (1988) 'Contractile properties of skeletal muscles from young, adult and aged mice', *J Physiol*, 404, pp. 71-82.

Brown, S. D. and Moore, M. W. (2012) 'The International Mouse Phenotyping Consortium: past and future perspectives on mouse phenotyping', *Mamm Genome*, 23(9-10), pp. 632-40.

Bruning, J. C., Michael, M. D., Winnay, J. N., Hayashi, T., Horsch, D., Accili, D., Goodyear, L. J. and Kahn, C. R. (1998) 'A muscle-specific insulin receptor knockout exhibits features of the metabolic syndrome of NIDDM without altering glucose tolerance', *Mol Cell*, 2(5), pp. 559-69.

Burke, G., Hiscock, A., Klein, A., Niks, E. H., Main, M., Manzur, A. Y., Ng, J., de Vile, C., Muntoni, F., Beeson, D. and Robb, S. (2013) 'Salbutamol benefits children with congenital myasthenic syndrome due to DOK7 mutations', *Neuromuscul Disord*, 23(2), pp. 170-5.

Burkhart, J. M., Vaudel, M., Gambaryan, S., Radau, S., Walter, U., Martens, L., Geiger, J., Sickmann, A. and Zahedi, R. P. (2012) 'The first comprehensive and quantitative analysis of human platelet protein composition allows the comparative analysis of structural and functional pathways', *Blood,* 120(15), pp. e73-82.

Cabrera-Serrano, M., Ghaoui, R., Ravenscroft, G., Johnsen, R. D., Davis, M. R., Corbett, A., Reddel, S., Sue, C. M., Liang, C., Waddell, L. B., Kaur, S., Lek, M., North, K. N., MacArthur, D. G., Lamont, P. J., Clarke, N. F. and Laing, N. G. (2015) 'Expanding the phenotype of GMPPB mutations', *Brain,* 138(Pt 4), pp. 836-44.

Cao, G. and Ko, C. P. (2007) 'Schwann cell-derived factors modulate synaptic activities at developing neuromuscular synapses', *J Neurosci*, 27(25), pp. 6712-22.

Carlson, G. (2011). *The use of four limb hanging tests to monitor muscle strength and condition over time*. [online] Available at: http://www.treat-nmd.eu/downloads/file/sops/dmd/MDX/DMD_M.2.1.005.pdf [Accessed 29 Apr. 2017].

Carrera, I. A., Matthijs, G., Perez, B. and Cerda, C. P. (2012) 'DPAGT1-CDG: report of a patient with fetal hypokinesia phenotype', *Am J Med Genet A*, 158a(8), pp. 2027-30.

Carss, K. J., Stevens, E., Foley, A. R., Cirak, S., Riemersma, M., Torelli, S., Hoischen, A., Willer, T., van Scherpenzeel, M., Moore, S. A., Messina, S., Bertini, E., Bonnemann, C. G., Abdenur, J. E., Grosmann, C. M., Kesari, A., Punetha, J., Quinlivan, R., Waddell, L. B., Young, H. K., Wraige, E., Yau, S., Brodd, L., Feng, L., Sewry, C., MacArthur, D. G., North, K. N., Hoffman, E., Stemple, D. L., Hurles, M. E., van Bokhoven, H., Campbell, K. P., Lefeber, D. J., Lin, Y. Y. and Muntoni, F. (2013) 'Mutations in GDP-mannose pyrophosphorylase B cause congenital and limb-girdle muscular dystrophies associated with hypoglycosylation of alpha-dystroglycan', *Am J Hum Genet*, 93(1), pp. 29-41.

Casar, J. C., Cabello-Verrugio, C., Olguin, H., Aldunate, R., Inestrosa, N. C. and Brandan, E. (2004) 'Heparan sulfate proteoglycans are increased during skeletal muscle regeneration: requirement of syndecan-3 for successful fiber formation', *J Cell Sci*, 117(Pt 1), pp. 73-84.

Chaouch, A., Porcelli, V., Cox, D., Edvardson, S., Scarcia, P., De Grassi, A., Pierri, C. L., Cossins, J., Laval, S. H., Griffin, H., Muller, J. S., Evangelista, T., Topf, A., Abicht, A., Huebner, A., von der Hagen, M., Bushby, K., Straub, V., Horvath, R., Elpeleg, O., Palace, J., Senderek, J., Beeson, D., Palmieri, L. and Lochmuller, H. (2014) 'Mutations in the Mitochondrial Citrate Carrier SLC25A1 are Associated with Impaired Neuromuscular Transmission', *J Neuromuscul Dis*, 1(1), pp. 75-90.

Chen, S.-Y. and Cheng, H.-J. (2009) 'Functions of axon guidance molecules in synapse formation', *Current opinion in neurobiology*, 19(5), pp. 471-478.

Cheng, F., Mani, K., van den Born, J., Ding, K., Belting, M. and Fransson, L. A. (2002) 'Nitric oxide-dependent processing of heparan sulfate in recycling S-nitrosylated glypican-1 takes place in caveolin-1-containing endosomes', *J Biol Chem*, 277(46), pp. 44431-9.

Chernousov, M. A., Rothblum, K., Stahl, R. C., Evans, A., Prentiss, L. and Carey, D. J. (2006) 'Glypican-1 and alpha4(V) collagen are required for Schwann cell myelination', *J Neurosci*, 26(2), pp. 508-17.

Chevessier, F., Bauche-Godard, S., Leroy, J. P., Koenig, J., Paturneau-Jouas, M., Eymard, B., Hantai, D. and Verdiere-Sahuque, M. (2005) 'The origin of tubular aggregates in human myopathies', *J Pathol*, 207(3), pp. 313-23.

Chevessier, F., Girard, E., Molgó, J., Bartling, S., Koenig, J., Hantaï, D. and Witzemann, V. (2008) 'A mouse model for congenital myasthenic syndrome due to MuSK mutations reveals defects in structure and function of neuromuscular junctions', *Hum Mol Genet*, 17(22), pp. 3577-95.

Chevessier, F., Marty, I., Paturneau-Jouas, M., Hantai, D. and Verdiere-Sahuque, M. (2004) 'Tubular aggregates are from whole sarcoplasmic reticulum origin: alterations in calcium binding protein expression in mouse skeletal muscle during aging', *Neuromuscul Disord*, 14(3), pp. 208-16.

Chevessier, F., Peter, C., Mersdorf, U., Girard, E., Krejci, E., McArdle, J. J. and Witzemann, V. (2012) 'A new mouse model for the slow-channel congenital myasthenic syndrome induced by the AChR epsilonL221F mutation', *Neurobiol Dis*, 45(3), pp. 851-61.

Chiu, Y.-H., Hornsey, M. A., Klinge, L., Jørgensen, L. H., Laval, S. H., Charlton, R., Barresi, R., Straub, V., Lochmüller, H. and Bushby, K. (2009) 'Attenuated muscle regeneration is a key factor in dysferlin-deficient muscular dystrophy', *Human Molecular Genetics*, 18(11), pp. 1976-1989.

Choi, H. Y., Liu, Y., Tennert, C., Sugiura, Y., Karakatsani, A., Kroger, S., Johnson, E. B., Hammer, R. E., Lin, W. and Herz, J. (2013) 'APP interacts with LRP4 and agrin to coordinate the development of the neuromuscular junction in mice', *Elife*, 2, pp. e00220.

Cieniewski-Bernard, C., Dupont, E., Richard, E. and Bastide, B. (2014a) 'Phospho-GlcNAc modulation of slow MLC2 during soleus atrophy through a multienzymatic and sarcomeric complex', *Pflugers Arch*, 466(11), pp. 2139-51.

Cieniewski-Bernard, C., Lambert, M., Dupont, E., Montel, V., Stevens, L. and Bastide, B. (2014b) 'O-GlcNAcylation, contractile protein modifications and calcium affinity in skeletal muscle', *Frontiers in Physiology*, 5, pp. 421.

Cieniewski-Bernard, C., Montel, V., Berthoin, S. and Bastide, B. (2012) 'Increasing O-GlcNAcylation level on organ culture of soleus modulates the calcium activation parameters of muscle fibers', *PLoS One*, 7(10), pp. e48218.

Cohen, A. W., Hnasko, R., Schubert, W. and Lisanti, M. P. (2004) 'Role of caveolae and caveolins in health and disease', *Physiol Rev*, 84(4), pp. 1341-79.

Coleman, J. L. J., Brennan, K., Ngo, T., Balaji, P., Graham, R. M. and Smith, N. J. (2015) 'Rapid Knockout and Reporter Mouse Line Generation and Breeding Colony Establishment Using EUCOMM Conditional-Ready Embryonic Stem Cells: A Case Study', *Frontiers in Endocrinology*, 6, pp. 105.

Cooksey, R. C., Hebert, L. F., Jr., Zhu, J. H., Wofford, P., Garvey, W. T. and McClain, D. A. (1999) 'Mechanism of hexosamine-induced insulin resistance in transgenic mice overexpressing glutamine:fructose-6-phosphate amidotransferase: decreased glucose transporter GLUT4 translocation and reversal by treatment with thiazolidinedione', *Endocrinology*, 140(3), pp. 1151-7.

Cossins, J., Belaya, K., Hicks, D., Salih, M. A., Finlayson, S., Carboni, N., Liu, W. W., Maxwell, S., Zoltowska, K., Farsani, G. T., Laval, S., Seidhamed, M. Z., consortium, W. G. S., Donnelly, P., Bentley, D., McGowan, S. J., Müller, J., Palace, J., Lochmüller, H. and Beeson, D. (2013) 'Congenital myasthenic syndromes due to mutations in ALG2 and ALG14', *Brain*, 136(3), pp. 944-956.

DeChiara, T. M., Bowen, D. C., Valenzuela, D. M., Simmons, M. V., Poueymirou, W. T., Thomas, S., Kinetz, E., Compton, D. L., Rojas, E., Park, J. S., Smith, C., DiStefano, P. S., Glass, D. J., Burden, S. J. and Yancopoulos, G. D. (1996) 'The receptor tyrosine kinase MuSK is required for neuromuscular junction formation in vivo', *Cell*, 85(4), pp. 501-12.

DeHaven, J. E., Robinson, K. A., Nelson, B. A. and Buse, M. G. (2001) 'A novel variant of glutamine: fructose-6-phosphate amidotransferase-1 (GFAT1) mRNA is selectively expressed in striated muscle', *Diabetes*, 50(11), pp. 2419-24.

Dellorusso, C., Crawford, R. W., Chamberlain, J. S. and Brooks, S. V. (2001) 'Tibialis anterior muscles in mdx mice are highly susceptible to contraction-induced injury', *J Muscle Res Cell Motil*, 22(5), pp. 467-75.

Dilena, R., Abicht, A., Sergi, P., Comi, G. P., Di Fonzo, A., Chidini, G., Natacci, F., Barbieri, S. and Lochmuller, H. (2014) 'Congenital myasthenic syndrome due to choline acetyltransferase mutations in infants: clinical suspicion and comprehensive electrophysiological assessment are important for early diagnosis', *J Child Neurol,* 29(3), pp. 389-93.

Duraku, L. S., Hossaini, M., Hoendervangers, S., Falke, L. L., Kambiz, S., Mudera, V. C., Holstege, J. C., Walbeehm, E. T. and Ruigrok, T. J. (2012) 'Spatiotemporal dynamics of re-innervation and hyperinnervation patterns by uninjured CGRP fibers in the rat foot sole epidermis after nerve injury', *Mol Pain,* 8, pp. 61.

Elbein, S. C., Zheng, H., Jia, Y., Chu, W., Cooper, J. J., Hale, T. and Zhang, Z. (2004) 'Molecular screening of the human glutamine-fructose-6-phosphate amidotransferase 1 (GFPT1) gene and association studies with diabetes and diabetic nephropathy', *Mol Genet Metab,* 82(4), pp. 321-8.

Endo, Y., Noguchi, S., Hara, Y., Hayashi, Y. K., Motomura, K., Miyatake, S., Murakami, N., Tanaka, S., Yamashita, S., Kizu, R., Bamba, M., Goto, Y., Matsumoto, N., Nonaka, I. and Nishino, I. (2015) 'Dominant mutations in ORAI1 cause tubular aggregate myopathy with hypocalcemia via constitutive activation of store-operated Ca(2)(+) channels', *Hum Mol Genet,* 24(3), pp. 637-48.

Engel, A. G. (2007) 'The therapy of congenital myasthenic syndromes', *Neurotherapeutics,* 4(2), pp. 252-7.

Engel, A. G. (2012) 'Current status of the congenital myasthenic syndromes', *Neuromuscul Disord,* 22(2), pp. 99-111.

Engel, A. G., Shen, X.-M., Selcen, D. and Sine, S. M. (2015) 'Congenital myasthenic syndromes: pathogenesis, diagnosis, and treatment', *The Lancet. Neurology,* 14(4), pp. 420-434.

Engel, A. G. and Sine, S. M. (2005) 'Current understanding of congenital myasthenic syndromes', *Curr Opin Pharmacol,* 5(3), pp. 308-21.

Feng, Z., Koirala, S. and Ko, C. P. (2005) 'Synapse-glia interactions at the vertebrate neuromuscular junction', *Neuroscientist,* 11(5), pp. 503-13.

Ferraro, E., Molinari, F. and Berghella, L. (2012) 'Molecular control of neuromuscular junction development', *J Cachexia Sarcopenia Muscle,* 3(1), pp. 13-23.

Finlayson, S., Morrow, J. M., Rodriguez Cruz, P. M., Sinclair, C. D., Fischmann, A., Thornton, J. S., Knight, S., Norbury, R., White, M., Al-Hajjar, M., Carboni, N., Jayawant, S., Robb, S. A., Yousry, T. A., Beeson, D. and Palace, J. (2016) 'Muscle magnetic resonance imaging in congenital myasthenic syndromes', *Muscle Nerve,* 54(2), pp. 211-9.

Finlayson, S., Palace, J., Belaya, K., Walls, T. J., Norwood, F., Burke, G., Holton, J. L., Pascual-Pascual, S. I., Cossins, J. and Beeson, D. (2013) 'Clinical features of congenital myasthenic syndrome due to mutations in DPAGT1', *J Neurol Neurosurg Psychiatry,* 84(10), pp. 1119-25.

Forni, P. E., Scuoppo, C., Imayoshi, I., Taulli, R., Dastru, W., Sala, V., Betz, U. A., Muzzi, P., Martinuzzi, D., Vercelli, A. E., Kageyama, R. and Ponzetto, C. (2006) 'High levels of Cre expression in neuronal progenitors cause defects in brain development leading to microencephaly and hydrocephaly', *J Neurosci,* 26(37), pp. 9593-602.

Freeze, H. H., Chong, J. X., Bamshad, M. J. and Ng, B. G. (2014) 'Solving glycosylation disorders: fundamental approaches reveal complicated pathways', *Am J Hum Genet,* 94(2), pp. 161-75.

Friedel, R. H., Wurst, W., Wefers, B. and Kuhn, R. (2011) 'Generating conditional knockout mice', *Methods Mol Biol,* 693, pp. 205-31.

Fumagalli, G., Engel, A. G. and Lindstrom, J. (1982) 'Ultrastructural aspects of acetylcholine receptor turnover at the normal end-plate and in autoimmune myasthenia gravis', *J Neuropathol Exp Neurol,* 41(6), pp. 567-79.

Gallardo, T., Shirley, L., John, G. B. and Castrillon, D. H. (2007) 'Generation of a germ cell-specific mouse transgenic Cre line, Vasa-Cre', *Genesis*, 45(6), pp. 413-7.

Gautam, M., Noakes, P. G., Moscoso, L., Rupp, F., Scheller, R. H., Merlie, J. P. and Sanes, J. R. (1996) 'Defective neuromuscular synaptogenesis in agrin-deficient mutant mice', *Cell*, 85(4), pp. 525-35.

Groves, J. A., Lee, A., Yildirir, G. and Zachara, N. E. (2013) 'Dynamic O-GlcNAcylation and its roles in the cellular stress response and homeostasis', *Cell Stress & Chaperones*, 18(5), pp. 535-558.

Guergueltcheva, V., Müller, J. S., Dusl, M., Senderek, J., Oldfors, A., Lindbergh, C., Maxwell, S., Colomer, J., Mallebrera, C. J., Nascimento, A., Vilchez, J. J., Muelas, N., Kirschner, J., Nafissi, S., Kariminejad, A., Nilipour, Y., Bozorgmehr, B., Najmabadi, H., Rodolico, C., Sieb, J. P., Schlotter, B., Schoser, B., Herrmann, R., Voit, T., Steinlein, O. K., Najafi, A., Urtizberea, A., Soler, D. M., Muntoni, F., Hanna, M. G., Chaouch, A., Straub, V., Bushby, K., Palace, J., Beeson, D., Abicht, A. and Lochmüller, H. (2012) 'Congenital myasthenic syndrome with tubular aggregates caused by GFPT1 mutations', *J Neurol*, 259(5), pp. 838-50.

Gumerson, J. D., Davis, C. S., Kabaeva, Z. T., Hayes, J. M., Brooks, S. V. and Michele, D. E. (2013) 'Muscle-specific expression of LARGE restores neuromuscular transmission deficits in dystrophic LARGE(myd) mice', *Human Molecular Genetics*, 22(4), pp. 757-768.

Guo, C., Yang, W. and Lobe, C. G. (2002) 'A Cre recombinase transgene with mosaic, widespread tamoxifen-inducible action', *Genesis*, 32(1), pp. 8-18.

Gutierrez, J. and Brandan, E. (2010) 'A novel mechanism of sequestering fibroblast growth factor 2 by glypican in lipid rafts, allowing skeletal muscle differentiation', *Mol Cell Biol*, 30(7), pp. 1634-49.

Guven, A., Demirci, M. and Anlar, B. (2012) 'Recurrent COLQ mutation in congenital myasthenic syndrome', *Pediatr Neurol*, 46(4), pp. 253-6.

Hanover, J. A., Krause, M. W. and Love, D. C. (2010) 'The Hexosamine Signaling Pathway: O-GlcNAc cycling in feast or famine', *Biochimica et biophysica acta*, 1800(2), pp. 80.

Hantai, D., Nicole, S. and Eymard, B. (2013) 'Congenital myasthenic syndromes: an update', *Curr Opin Neurol*, 26(5), pp. 561-8.

Hart, G. and Akimoto, Y. (2009). *The O-GlcNAc Modification*. [online] Available at: https://www.ncbi.nlm.nih.gov/books/NBK1954/ [Accessed 29 Apr. 2017].

Hayashi, S., Tenzen, T. and McMahon, A. P. (2003) 'Maternal inheritance of Cre activity in a Sox2Cre deleter strain', *Genesis*, 37(2), pp. 51-3.

Hebert, L. F., Jr., Daniels, M. C., Zhou, J., Crook, E. D., Turner, R. L., Simmons, S. T., Neidigh, J. L., Zhu, J. S., Baron, A. D. and McClain, D. A. (1996) 'Overexpression of glutamine:fructose-6-phosphate amidotransferase in transgenic mice leads to insulin resistance', *J Clin Invest*, 98(4), pp. 930-6.

Hedou, J., Cieniewski-Bernard, C., Leroy, Y., Michalski, J. C., Mounier, Y. and Bastide, B. (2007) 'O-linked N-acetylglucosaminylation is involved in the Ca2+ activation properties of rat skeletal muscle', *J Biol Chem*, 282(14), pp. 10360-9.

Heffner, C. S., Herbert Pratt, C., Babiuk, R. P., Sharma, Y., Rockwood, S. F., Donahue, L. R., Eppig, J. T. and Murray, S. A. (2012) 'Supporting conditional mouse mutagenesis with a comprehensive cre characterization resource', *Nat Commun*, 3, pp. 1218.

Herbst, R., Iskratsch, T., Unger, E. and Bittner, R. E. (2009) 'Aberrant development of neuromuscular junctions in glycosylation-defective large(myd) mice', *Neuromuscular disorders : NMD*, 19(5), pp. 366-378.

Herrmann, D. N., Horvath, R., Sowden, J. E., Gonzalez, M., Sanchez-Mejias, A., Guan, Z., Whittaker, R. G., Almodovar, J. L., Lane, M., Bansagi, B., Pyle, A., Boczonadi, V., Lochmuller, H., Griffin, H., Chinnery, P. F., Lloyd, T. E., Littleton, J. T. and Zuchner, S. (2014) 'Synaptotagmin 2 mutations cause an autosomal-dominant form of lambert-eaton myasthenic syndrome and nonprogressive motor neuropathy', *Am J Hum Genet*, 95(3), pp. 332-9.

Hoch, W., McConville, J., Helms, S., Newsom-Davis, J., Melms, A. and Vincent, A. (2001) 'Auto-antibodies to the receptor tyrosine kinase MuSK in patients with myasthenia gravis without acetylcholine receptor antibodies', *Nat Med*, 7(3), pp. 365-8.

Hoffmann, K., Müller, J. S., Stricker, S., Megarbane, A., Rajab, A., Lindner, T. H., Cohen, M., Chouery, E., Adaimy, L., Ghanem, I., Delague, V., Boltshauser, E., Talim, B., Horvath, R., Robinson, P. N., Lochmüller, H., Hübner, C. and Mundlos, S. (2006) 'Escobar Syndrome Is a Prenatal Myasthenia Caused by Disruption of the Acetylcholine Receptor Fetal γ Subunit', *American Journal of Human Genetics*, 79(2), pp. 303-312.

Howe, K. and Clark, M. D. and Torroja, C. F. and Torrance, J. and Berthelot, C. and Muffato, M. and Collins, J. E. and Humphray, S. and McLaren, K. and Matthews, L. and McLaren, S. and Sealy, I. and Caccamo, M. and Churcher, C. and Scott, C. and Barrett, J. C. and Koch, R. and Rauch, G.-J. and White, S. and Chow, W. and Kilian, B. and Quintais, L. T. and Guerra-Assunção, J. A. and Zhou, Y. and Gu, Y. and Yen, J. and Vogel, J.-H. and Eyre, T. and Redmond, S. and Banerjee, R. and Chi, J. and Fu, B. and Langley, E. and Maguire, S. F. and Laird, G. K. and Lloyd, D. and Kenyon, E. and Donaldson, S. and Sehra, H. and Almeida-King, J. and Loveland, J. and Trevanion, S. and Jones, M. and Quail, M. and Willey, D. and Hunt, A. and Burton, J. and Sims, S. and McLay, K. and Plumb, B. and Davis, J. and Clee, C. and Oliver, K. and Clark, R. and Riddle, C. and Eliott, D. and Threadgold, G. and Harden, G. and Ware, D. and Mortimer, B. and Kerry, G. and Heath, P. and Phillimore, B. and Tracey, A. and Corby, N. and Dunn, M. and Johnson, C. and Wood, J. and Clark, S. and Pelan, S. and Griffiths, G. and Smith, M. and Glithero, R. and Howden, P. and Barker, N. and Stevens, C. and Harley, J. and Holt, K. and Panagiotidis, G. and Lovell, J. and Beasley, H. and Henderson, C. and Gordon, D. and Auger, K. and Wright, D. and Collins, J. and Raisen, C. and Dyer, L. and Leung, K. and Robertson, L. and Ambridge, K. and Leongamornlert, D. and McGuire, S. and Gilderthorp, R. and Griffiths, C. and Manthravadi, D. and Nichol, S. and Barker, G. and Whitehead, S. and Kay, M. and Brown, J. and Murnane, C. and Gray, E. and Humphries, M. and Sycamore, N. and Barker, D. and Saunders, D. and Wallis, J. and Babbage, A. and Hammond, S. and Mashreghi-Mohammadi, M. and Barr, L. and Martin,

S. and Wray, P. and Ellington, A. and Matthews, N. and Ellwood, M. and Woodmansey, R. and Clark, G. and Cooper, J. and Tromans, A. and Grafham, D. and Skuce, C. and Pandian, R. and Andrews, R. and Harrison, E. and Kimberley, A. and Garnett, J. and Fosker, N. and Hall, R. and Garner, P. and Kelly, D. and Bird, C. and Palmer, S. and Gehring, I. and Berger, A. and Dooley, C. M. and Ersan-Ürün, Z. and Eser, C. and Geiger, H. and Geisler, M. and Karotki, L. and Kirn, A. and Konantz, J. and Konantz, M. and Oberländer, M. and Rudolph-Geiger, S. and Teucke, M. and Osoegawa, K. and Zhu, B. and Rapp, A. and Widaa, S. and Langford, C. and Yang, F. and Carter, N. P. and Harrow, J. and Ning, Z. and Herrero, J. and Searle, S. M. J. and Enright, A. and Geisler, R. and Plasterk, R. H. A. and Lee, C. and Westerfield, M. and de Jong, P. J. and Zon, L. I. and Postlethwait, J. H. and Nüsslein-Volhard, C. and Hubbard, T. J. P. and Crollius, H. R. and Rogers, J. and Stemple, D. L. (2013) 'The zebrafish reference genome sequence and its relationship to the human genome', *Nature*, 496(7446), pp. 498-503.

Hudak, J. E. and Bertozzi, C. R. (2014) 'Glycotherapy: New Advances Inspire a Reemergence of Glycans in Medicine', *Chemistry & biology*, 21(1), pp. 16-37.

Huh, S. Y., Kim, H. S., Jang, H. J., Park, Y. E. and Kim, D. S. (2012) 'Limb-girdle myasthenia with tubular aggregates associated with novel GFPT1 mutations', *Muscle Nerve*, 46(4), pp. 600-4.

Huizing, M., Rakocevic, G., Sparks, S. E., Mamali, I., Shatunov, A., Goldfarb, L., Krasnewich, D., Gahl, W. A. and Dalakas, M. C. (2004) 'Hypoglycosylation of alpha-dystroglycan in patients with hereditary IBM due to GNE mutations', *Mol Genet Metab*, 81(3), pp. 196-202.

Huze, C., Bauche, S., Richard, P., Chevessier, F., Goillot, E., Gaudon, K., Ben Ammar, A., Chaboud, A., Grosjean, I., Lecuyer, H. A., Bernard, V., Rouche, A., Alexandri, N., Kuntzer, T., Fardeau, M., Fournier, E., Brancaccio, A., Ruegg, M. A., Koenig, J., Eymard, B., Schaeffer, L. and Hantai, D. (2009) 'Identification of an agrin mutation that causes congenital myasthenia and affects synapse function', *Am J Hum Genet*, 85(2), pp. 155-67.

Imtiaz, F., Al-Mostafa, A. and Al-Hassnan, Z. N. (2012) 'Further Delineation of the Phenotype of Congenital Disorder of Glycosylation DPAGT1-CDG (CDG-Ij) Identified by Homozygosity Mapping', *JIMD Rep*, 2, pp. 107-11.

Ioos, C., Barois, A., Richard, P., Eymard, B., Hantai, D. and Estournet-Mathiaud, B. (2004) 'Congenital myasthenic syndrome due to rapsyn deficiency: three cases with arthrogryposis and bulbar symptoms', *Neuropediatrics,* 35(4), pp. 246-9.

Ishikawa, T. O. and Herschman, H. R. (2011) 'Conditional bicistronic Cre reporter line expressing both firefly luciferase and beta-galactosidase', *Mol Imaging Biol,* 13(2), pp. 284-92.

Jacob, S., Viegas, S., Lashley, D. and Hilton-Jones, D. (2009) 'Myasthenia gravis and other neuromuscular junction disorders', *Pract Neurol*, 9(6), pp. 364-71.

Jaeken, J., Lefeber, D. and Matthijs, G. (2015) 'Clinical utility gene card for: DPAGT1 defective congenital disorder of glycosylation', *Eur J Hum Genet*, 23(12).

Jeppsson, J. O., Arndt, T., Schellenberg, F., Wielders, J. P., Anton, R. F., Whitfield, J. B. and Helander, A. (2007) 'Toward standardization of carbohydrate-deficient transferrin (CDT) measurements: I. Analyte definition and proposal of a candidate reference method', *Clin Chem Lab Med,* 45(4), pp. 558-62.

Khan, M. M., Strack, S., Wild, F., Hanashima, A., Gasch, A., Brohm, K., Reischl, M., Carnio, S., Labeit, D., Sandri, M., Labeit, S. and Rudolf, R. (2014) 'Role of autophagy, SQSTM1, SH3GLB1, and TRIM63 in the turnover of nicotinic acetylcholine receptors', *Autophagy,* 10(1), pp. 123-36.

Kilch, T., Alansary, D., Peglow, M., Dorr, K., Rychkov, G., Rieger, H., Peinelt, C. and Niemeyer, B. A. (2013) 'Mutations of the Ca2+-sensing stromal interaction molecule STIM1 regulate Ca2+ influx by altered oligomerization of STIM1 and by destabilization of the Ca2+ channel Orai1', *J Biol Chem,* 288(3), pp. 1653-64.

Kim, N. and Burden, S. J. (2008) 'MuSK controls where motor axons grow and form synapses', *Nat Neurosci,* 11(1), pp. 19-27.

Kollipara, L. and Zahedi, R. P. (2013) 'Protein carbamylation: in vivo modification or in vitro artefact?', *Proteomics,* 13(6), pp. 941-4.

Labisch, T., Buchkremer, S., Phan, V., Kollipara, L., Gatz, C., Lentz, C., Nolte, K., Vervoorts, J., Coraspe, J. A., Sickmann, A., Carr, S., Zahedi, R. P., Weis, J. and Roos, A. (2017) 'Tracking Effects of SIL1 Increase: Taking a Closer Look Beyond the Consequences of Elevated Expression Level', *Mol Neurobiol*.

Latvanlehto, A., Fox, M. A., Sormunen, R., Tu, H., Oikarainen, T., Koski, A., Naumenko, N., Shakirzyanova, A., Kallio, M., Ilves, M., Giniatullin, R., Sanes, J. R. and Pihlajaniemi, T. (2010) 'Muscle-derived collagen XIII regulates maturation of the skeletal neuromuscular junction', *J Neurosci,* 30(37), pp. 12230-41.

Le Panse, R. and and Berrih-Aknin, S. (2013) 'Autoimmune myasthenia gravis: autoantibody mechanisms and new developments on immune regulation', *Curr Opin Neurol,* 26(5), pp. 569-76.

Leroy, J. G. (2006) 'Congenital disorders of N-glycosylation including diseases associated with O- as well as N-glycosylation defects', *Pediatr Res,* 60(6), pp. 643-56.

Leung, M. C., Hitchen, P. G., Ward, D. G., Messer, A. E. and Marston, S. B. (2013) 'Z-band alternatively spliced PDZ motif protein (ZASP) is the major O-linked beta-N-acetylglucosamine-substituted protein in human heart myofibrils', *J Biol Chem,* 288(7), pp. 4891-8.

Lewis, A., Finlayson, S., Mahmod, M., Karamitsos, T. D., Dass, S., Ashrafian, H., Francis, J. M., Watkins, H., Beeson, D., Palace, J. and Neubauer, S. (2014) 'Characterisation of a novel cardiac phenotype in patients with GFPT1 or DPAGT1 mutations', *Journal of Cardiovascular Magnetic Resonance,* 16(Suppl 1), pp. P332-P332.

Li, X.-M., Dong, X.-P., Luo, S.-W., Zhang, B., Lee, D.-H., Ting, A. K. L., Neiswender, H., Kim, C.-H., Carpenter-Hyland, E., Gao, T.-M., Xiong, W.-C. and Mei, L. (2008) 'Retrograde regulation of motoneuron differentiation by muscle [beta]-catenin', *Nat Neurosci,* 11(3), pp. 262-268.

Lin, W., Burgess, R. W., Dominguez, B., Pfaff, S. L., Sanes, J. R. and Lee, K. F. (2001) 'Distinct roles of nerve and muscle in postsynaptic differentiation of the neuromuscular synapse', *Nature,* 410(6832), pp. 1057-64.

Litwack, E. D., Ivins, J. K., Kumbasar, A., Paine-Saunders, S., Stipp, C. S. and Lander, A. D. (1998) 'Expression of the heparan sulfate proteoglycan glypican-1 in the developing rodent', *Dev Dyn,* 211(1), pp. 72-87.

Lodish, H., Berk, A., Zipursky, S., Matsudaira, P., Baltimore, D. and Darnell, J. (2000). *Molecular Cell Biology*. [online] Available at: https://www.ncbi.nlm.nih.gov/books/NBK21475/ [Accessed 29 Apr. 2017].

Logan, Clare V., Cossins, J., Rodríguez Cruz, Pedro M., Parry, David A., Maxwell, S., Martínez-Martínez, P., Riepsaame, J., Abdelhamed, Zakia A., Lake, Alice V., Moran, M., Robb, S., Chow, G., Sewry, C., Hopkins, Philip M., Sheridan, E., Jayawant, S., Palace, J., Johnson, Colin A. and Beeson, D. (2015) 'Congenital Myasthenic Syndrome Type 19 Is Caused by Mutations in COL13A1, Encoding the Atypical Non-fibrillar Collagen Type XIII α1 Chain', *American Journal of Human Genetics,* 97(6), pp. 878-885.

Loonstra, A., Vooijs, M., Beverloo, H. B., Allak, B. A., van Drunen, E., Kanaar, R., Berns, A. and Jonkers, J. (2001) 'Growth inhibition and DNA damage induced by Cre recombinase in mammalian cells', *Proceedings of the National Academy of Sciences of the United States of America,* 98(16), pp. 9209-9214.

Lorenz, C. and Jones, K. E. (2014) 'IH activity is increased in populations of slow versus fast motor axons of the rat', *Front Hum Neurosci,* 8, pp. 766.

Lorenzoni, P. J., Scola, R. H., Kay, C. S. and Werneck, L. C. (2012) 'Congenital myasthenic syndrome: a brief review', *Pediatr Neurol,* 46(3), pp. 141-8.

Luo, Z. G., Je, H. S., Wang, Q., Yang, F., Dobbins, G. C., Yang, Z. H., Xiong, W. C., Lu, B. and Mei, L. (2003) 'Implication of geranylgeranyltransferase I in synapse formation', *Neuron,* 40(4), pp. 703-17.

Lynch, G. (2009). *Measuring isometric force of isolated mouse skeletal muscles in situ*. [online] Available at: http://www.treat-nmd.eu/downloads/ file/sops/dmd/MDX/ DMD_ M.2.2.005.pdf [Accessed 29 Apr. 2017].

Lyon, G. J. and Wang, K. (2012) 'Identifying disease mutations in genomic medicine settings: current challenges and how to accelerate progress', *Genome Med,* 4(7), pp. 58.

Lyons, G. E., Muhlebach, S., Moser, A., Masood, R., Paterson, B. M., Buckingham, M. E. and Perriard, J. C. (1991) 'Developmental regulation of creatine kinase gene expression by myogenic factors in embryonic mouse and chick skeletal muscle', *Development,* 113(3), pp. 1017-29.

Marklova, E. and Albahri, Z. (2007) 'Screening and diagnosis of congenital disorders of glycosylation', *Clin Chim Acta,* 385(1-2), pp. 6-20.

Martin, P. T. (2003) 'Glycobiology of the neuromuscular junction', *J Neurocytol,* 32(5-8), pp. 915-29.

Martin, P. T. (2005) 'The dystroglycanopathies: the new disorders of O-linked glycosylation', *Semin Pediatr Neurol,* 12(3), pp. 152-8.

Maselli, R. A., Arredondo, J., Cagney, O., Ng, J. J., Anderson, J. A., Williams, C., Gerke, B. J., Soliven, B. and Wollmann, R. L. (2010) 'Mutations in MUSK causing congenital myasthenic syndrome impair MuSK-Dok-7 interaction', *Hum Mol Genet,* 19(12), pp. 2370-9.

Maselli, R. A., Arredondo, J., Nguyen, J., Lara, M., Ng, F., Ngo, M., Pham, J. M., Yi, Q., Stajich, J. M., McDonald, K., Hauser, M. A. and Wollmann, R. L. (2014) 'Exome sequencing detection of two untranslated GFPT1 mutations in a family with limb-girdle myasthenia', *Clin Genet,* 85(2), pp. 166-71.

Maselli, R. A., Fernandez, J. M., Arredondo, J., Navarro, C., Ngo, M., Beeson, D., Cagney, Ó., Williams, D. C., Wollmann, R. L., Yarov-Yarovoy, V. and Ferns, M. J. (2012) 'LG2 Agrin Mutation Causing Severe Congenital Myasthenic Syndrome Mimics Functional Characteristics of Non-neural (z−) Agrin', *Human genetics,* 131(7), pp. 1123-1135.

Maselli, R. A., Ng, J. J., Anderson, J. A., Cagney, O., Arredondo, J., Williams, C., Wessel, H. B., Abdel-Hamid, H. and Wollmann, R. L. (2009) 'Mutations in LAMB2 causing a severe form of synaptic congenital myasthenic syndrome', *J Med Genet,* 46(3), pp. 203-8.

Merlie, J. P., Sebbane, R., Tzartos, S. and Lindstrom, J. (1982) 'Inhibition of glycosylation with tunicamycin blocks assembly of newly synthesized acetylcholine receptor subunits in muscle cells', *J Biol Chem,* 257(5), pp. 2694-701.

Messéant, J., Dobbertin, A., Girard, E., Delers, P., Manuel, M., Mangione, F., Schmitt, A., Le Denmat, D., Molgó, J., Zytnicki, D., Schaeffer, L., Legay, C. and Strochlic, L. (2015) 'MuSK frizzled-like domain is critical for mammalian neuromuscular junction formation and maintenance', *J Neurosci,* 35(12), pp. 4926-41.

Miniou, P., Tiziano, D., Frugier, T., Roblot, N., Le Meur, M. and Melki, J. (1999) 'Gene targeting restricted to mouse striated muscle lineage', *Nucleic Acids Res,* 27(19), pp. e27.

Mohrmann, R., de Wit, H., Connell, E., Pinheiro, P. S., Leese, C., Bruns, D., Davletov, B., Verhage, M. and Sorensen, J. B. (2013) 'Synaptotagmin interaction with SNAP-25 governs vesicle docking, priming, and fusion triggering', *J Neurosci,* 33(36), pp. 14417-30.

Montagnese, F., Klupp, E., Karampinos, D. C., Biskup, S., Glaser, D., Kirschke, J. S. and Schoser, B. (2016) 'Two patients with GMPPB mutation: The overlapping phenotypes of limb-girdle myasthenic syndrome and limb-girdle muscular dystrophy dystroglycanopathy', *Muscle Nerve*.

Muntoni, F., Brockington, M., Godfrey, C., Ackroyd, M., Robb, S., Manzur, A., Kinali, M., Mercuri, E., Kaluarachchi, M., Feng, L., Jimenez-Mallebrera, C., Clement, E., Torelli, S., Sewry, C. A. and Brown, S. C. (2007) 'Muscular dystrophies due to defective glycosylation of dystroglycan', *Acta Myologica*, 26(3), pp. 129-135.

Muntoni, F., Torelli, S. and Brockington, M. (2008) 'Muscular dystrophies due to glycosylation defects', *Neurotherapeutics*, 5(4), pp. 627-32.

Nagy, A. (2000) 'Cre recombinase: the universal reagent for genome tailoring', *Genesis*, 26(2), pp. 99-109.

Naiche, L. A. and Papaioannou, V. E. (2007) 'Cre activity causes widespread apoptosis and lethal anemia during embryonic development', *Genesis*, 45(12), pp. 768-75.

Nicole, S., Chaouch, A., Torbergsen, T., Bauche, S., de Bruyckere, E., Fontenille, M. J., Horn, M. A., van Ghelue, M., Loseth, S., Issop, Y., Cox, D., Muller, J. S., Evangelista, T., Stalberg, E., Ioos, C., Barois, A., Brochier, G., Sternberg, D., Fournier, E., Hantai, D., Abicht, A., Dusl, M., Laval, S. H., Griffin, H., Eymard, B. and Lochmuller, H. (2014) 'Agrin mutations lead to a congenital myasthenic syndrome with distal muscle weakness and atrophy', *Brain*, 137(Pt 9), pp. 2429-43.

Niimi, M., Ogawara, T., Yamashita, T., Yamamoto, Y., Ueyama, A., Kambe, T., Okamoto, T., Ban, T., Tamanoi, H., Ozaki, K., Fujiwara, T., Fukui, H., Takahashi, E. I., Kyushiki, H. and Tanigami, A. (2001) 'Identification of GFAT1-L, a novel splice variant of human glutamine: fructose-6-phosphate amidotransferase (GFAT1) that is expressed abundantly in skeletal muscle', *J Hum Genet*, 46(10), pp. 566-71.

Novotova, M., Zahradnik, I., Brochier, G., Pavlovicova, M., Bigard, X. and Ventura-Clapier, R. (2002) 'Joint participation of mitochondria and sarcoplasmic reticulum in the formation of tubular aggregates in gastrocnemius muscle of CK-/- mice', *Eur J Cell Biol,* 81(2), pp. 101-6.

O'Connor, E., Topf, A., Muller, J. S., Cox, D., Evangelista, T., Colomer, J., Abicht, A., Senderek, J., Hasselmann, O., Yaramis, A., Laval, S. H. and Lochmuller, H. (2016) 'Identification of mutations in the MYO9A gene in patients with congenital myasthenic syndrome', *Brain,* 139(Pt 8), pp. 2143-53.

O'Grady, G. L., Verschuuren, C., Yuen, M., Webster, R., Menezes, M., Fock, J. M., Pride, N., Best, H. A., Benavides Damm, T., Turner, C., Lek, M., Engel, A. G., North, K. N., Clarke, N. F., MacArthur, D. G., Kamsteeg, E. J. and Cooper, S. T. (2016) 'Variants in SLC18A3, vesicular acetylcholine transporter, cause congenital myasthenic syndrome', *Neurology,* 87(14), pp. 1442-1448.

Ohkawara, B., Cabrera-Serrano, M., Nakata, T., Milone, M., Asai, N., Ito, K., Ito, M., Masuda, A., Ito, Y., Engel, A. G. and Ohno, K. (2014) 'LRP4 third beta-propeller domain mutations cause novel congenital myasthenia by compromising agrin-mediated MuSK signaling in a position-specific manner', *Hum Mol Genet,* 23(7), pp. 1856-68.

Okada, K., Inoue, A., Okada, M., Murata, Y., Kakuta, S., Jigami, T., Kubo, S., Shiraishi, H., Eguchi, K., Motomura, M., Akiyama, T., Iwakura, Y., Higuchi, O. and Yamanashi, Y. (2006) 'The muscle protein Dok-7 is essential for neuromuscular synaptogenesis', *Science,* 312(5781), pp. 1802-5.

Olsen, J. V., de Godoy, L. M., Li, G., Macek, B., Mortensen, P., Pesch, R., Makarov, A., Lange, O., Horning, S. and Mann, M. (2005) 'Parts per million mass accuracy on an Orbitrap mass spectrometer via lock mass injection into a C-trap', *Mol Cell Proteomics,* 4(12), pp. 2010-21.

Parkinson, W., Dear, M. L., Rushton, E. and Broadie, K. (2013) 'N-glycosylation requirements in neuromuscular synaptogenesis', *Development,* 140(24), pp. 4970-81.

Parr, J. R., Andrew, M. J., Finnis, M., Beeson, D., Vincent, A. and Jayawant, S. (2014) 'How common is childhood myasthenia? The UK incidence and prevalence of autoimmune and congenital myasthenia', *Arch Dis Child*, 99(6), pp. 539-42.

Perez-Garcia, M. J. and Burden, S. J. (2012) 'Increasing MuSK Activity Delays Denervation and Improves Motor Function in ALS Mice', *Cell reports*, 2(3), pp. 497-502.

Perlman, R. L. (2016) 'Mouse models of human disease: An evolutionary perspective', *Evolution, Medicine, and Public Health*, 2016(1), pp. 170-176.

Petryszak, R., Keays, M., Tang, Y. A., Fonseca, N. A., Barrera, E., Burdett, T., Fullgrabe, A., Fuentes, A. M., Jupp, S., Koskinen, S., Mannion, O., Huerta, L., Megy, K., Snow, C., Williams, E., Barzine, M., Hastings, E., Weisser, H., Wright, J., Jaiswal, P., Huber, W., Choudhary, J., Parkinson, H. E. and Brazma, A. (2016) 'Expression Atlas update--an integrated database of gene and protein expression in humans, animals and plants', *Nucleic Acids Res*, 44(D1), pp. D746-52.

Plomp, J. J., Morsch, M., Phillips, W. D. and Verschuuren, J. J. (2015) 'Electrophysiological analysis of neuromuscular synaptic function in myasthenia gravis patients and animal models', *Exp Neurol*, 270, pp. 41-54.

Pundir, S., Martin, M. J. and O'Donovan, C. (2017) 'UniProt Protein Knowledgebase', *Methods Mol Biol*, 1558, pp. 41-55.

Qin, W., Kutny, P. M., Maser, R. S., Dion, S. L., Lamont, J. D., Zhang, Y., Perry, G. A. and Wang, H. (2016) 'Generating Mouse Models Using CRISPR-Cas9-Mediated Genome Editing', *Curr Protoc Mouse Biol*, 6(1), pp. 39-66.

Ramanathan, V. K. and Hall, Z. W. (1999) 'Altered glycosylation sites of the delta subunit of the acetylcholine receptor (AChR) reduce alpha delta association and receptor assembly', *J Biol Chem*, 274(29), pp. 20513-20.

Raphael, A. R., Couthouis, J., Sakamuri, S., Siskind, C., Vogel, H., Day, J. W. and Gitler, A. D. (2014) 'Congenital Muscular Dystrophy and Generalized Epilepsy Caused by GMPPB Mutations', *Brain research*, 0, pp. 66-71.

Reed, P. W., Mathews, K. D., Mills, K. A. and Bloch, R. J. (2004) 'The sarcolemma in the Large(myd) mouse', *Muscle Nerve,* 30(5), pp. 585-95.

Rodriguez Cruz, P. M., Belaya, K., Basiri, K., Sedghi, M., Farrugia, M. E., Holton, J. L., Liu, W. W., Maxwell, S., Petty, R., Walls, T. J., Kennett, R., Pitt, M., Sarkozy, A., Parton, M., Lochmuller, H., Muntoni, F., Palace, J. and Beeson, D. (2016) 'Clinical features of the myasthenic syndrome arising from mutations in GMPPB', *J Neurol Neurosurg Psychiatry*, 87(8), pp. 802-9.

Roos, A., Kollipara, L., Buchkremer, S., Labisch, T., Brauers, E., Gatz, C., Lentz, C., Gerardo-Nava, J., Weis, J. and Zahedi, R. P. (2016) 'Cellular Signature of SIL1 Depletion: Disease Pathogenesis due to Alterations in Protein Composition Beyond the ER Machinery', *Mol Neurobiol,* 53(8), pp. 5527-41.

Rudell, J. B. and Ferns, M. J. (2013) 'Regulation of muscle acetylcholine receptor turnover by beta subunit tyrosine phosphorylation', *Dev Neurobiol*, 73(5), pp. 399-410.

Rudolf, R., Bogomolovas, J., Strack, S., Choi, K.-R., Khan, M. M., Wagner, A., Brohm, K., Hanashima, A., Gasch, A., Labeit, D. and Labeit, S. (2013) 'Regulation of nicotinic acetylcholine receptor turnover by MuRF1 connects muscle activity to endo/lysosomal and atrophy pathways', *Age,* 35(5), pp. 1663-1674.

Régal, L., Shen, X.-M., Selcen, D., Verhille, C., Meulemans, S., Creemers, J. W. M. and Engel, A. G. (2014) 'PREPL deficiency with or without cystinuria causes a novel myasthenic syndrome', *Neurology*, 82(14), pp. 1254-1260.

Salpietro, V., Lin, W., Delle Vedove, A., Storbeck, M., Liu, Y., Efthymiou, S., Manole, A., Wiethoff, S., Ye, Q., Saggar, A., McElreavey, K., Krishnakumar, S., Pitt, M., Bello, O., Rothman, J. E., Basel-Vanagaite, L., Hubshman, M. W., Aharoni, S., Manzur, A. Y., Wirth, B. and Houlden, H. (2017) 'Homozygous mutations in VAMP1 cause a presynaptic congenital myasthenic syndrome', *Ann Neurol*.

Schara, U. and Lochmuller, H. (2008) 'Therapeutic strategies in congenital myasthenic syndromes', *Neurotherapeutics,* 5(4), pp. 542-7.

Schiaffino, S. (2012) 'Tubular aggregates in skeletal muscle: just a special type of protein aggregates?', *Neuromuscul Disord,* 22(3), pp. 199-207.

Schubert, W., Sotgia, F., Cohen, A. W., Capozza, F., Bonuccelli, G., Bruno, C., Minetti, C., Bonilla, E., Dimauro, S. and Lisanti, M. P. (2007) 'Caveolin-1(-/-)-and caveolin-2(-/-)-deficient mice both display numerous skeletal muscle abnormalities, with tubular aggregate formation', *Am J Pathol,* 170(1), pp. 316-33.

Scott, K., Gadomski, T., Kozicz, T. and Morava, E. (2014) 'Congenital disorders of glycosylation: new defects and still counting', *Journal of inherited metabolic disease,* 37(4), pp. 609-617.

Selcen, D., Juel, V. C., Hobson-Webb, L. D., Smith, E. C., Stickler, D. E., Bite, A. V., Ohno, K. and Engel, A. G. (2011) 'Myasthenic syndrome caused by plectinopathy', *Neurology,* 76(4), pp. 327-336.

Selcen, D., Shen, X. M., Brengman, J., Li, Y., Stans, A. A., Wieben, E. and Engel, A. G. (2014) 'DPAGT1 myasthenia and myopathy: genetic, phenotypic, and expression studies', *Neurology,* 82(20), pp. 1822-30.

Selcen, D., Shen, X. M., Milone, M., Brengman, J., Ohno, K., Deymeer, F., Finkel, R., Rowin, J. and Engel, A. G. (2013) 'GFPT1-myasthenia: clinical, structural, and electrophysiologic heterogeneity', *Neurology,* 81(4), pp. 370-8.

Senderek, J., Muller, J. S., Dusl, M., Strom, T. M., Guergueltcheva, V., Diepolder, I., Laval, S. H., Maxwell, S., Cossins, J., Krause, S., Muelas, N., Vilchez, J. J., Colomer, J., Mallebrera, C. J., Nascimento, A., Nafissi, S., Kariminejad, A., Nilipour, Y., Bozorgmehr, B., Najmabadi, H., Rodolico, C., Sieb, J. P., Steinlein, O. K., Schlotter, B., Schoser, B., Kirschner, J., Herrmann, R., Voit, T., Oldfors, A., Lindbergh, C., Urtizberea, A., von der Hagen, M., Hubner, A., Palace, J., Bushby, K., Straub, V., Beeson, D., Abicht, A. and Lochmuller, H. (2011) 'Hexosamine biosynthetic pathway mutations cause neuromuscular transmission defect', *Am J Hum Genet,* 88(2), pp. 162-72.

Sharp, P. S., Akbar, M. T., Bouri, S., Senda, A., Joshi, K., Chen, H. J., Latchman, D. S., Wells, D. J. and de Belleroche, J. (2008) 'Protective effects of heat shock protein 27 in a model of ALS occur in the early stages of disease progression', *Neurobiol Dis,* 30(1), pp. 42-55.

Sharp, P. S., Bye-a-Jee, H. and Wells, D. J. (2011) 'Physiological characterization of muscle strength with variable levels of dystrophin restoration in mdx mice following local antisense therapy', *Mol Ther,* 19(1), pp. 165-71.

Shen, X.-M., Selcen, D., Brengman, J. and Engel, A. G. (2014) 'Mutant SNAP25B causes myasthenia, cortical hyperexcitability, ataxia, and intellectual disability', *Neurology,* 83(24), pp. 2247-2255.

Shen, X. M., Scola, R. H., Lorenzoni, P. J., Kay, C. S. K., Werneck, L. C., Brengman, J., Selcen, D. and Engel, A. G. (2017) 'Novel synaptobrevin-1 mutation causes fatal congenital myasthenic syndrome', *Annals of Clinical and Translational Neurology,* 4(2), pp. 130-138.

Sigoillot, S. M., Bourgeois, F., Karmouch, J., Molgo, J., Dobbertin, A., Chevalier, C., Houlgatte, R., Leger, J. and Legay, C. (2016) 'Neuromuscular junction immaturity and muscle atrophy are hallmarks of the ColQ-deficient mouse, a model of congenital myasthenic syndrome with acetylcholinesterase deficiency', *Faseb j,* 30(6), pp. 2382-99.

Sigoillot, S. M., Bourgeois, F., Lambergeon, M., Strochlic, L. and Legay, C. (2010) 'ColQ controls postsynaptic differentiation at the neuromuscular junction', *J Neurosci*, 30(1), pp. 13-23.

Skarnes, W. C., Rosen, B., West, A. P., Koutsourakis, M., Bushell, W., Iyer, V., Mujica, A. O., Thomas, M., Harrow, J., Cox, T., Jackson, D., Severin, J., Biggs, P., Fu, J., Nefedov, M., de Jong, P. J., Stewart, A. F. and Bradley, A. (2011) 'A conditional knockout resource for the genome-wide study of mouse gene function', *Nature*, 474(7351), pp. 337-42.

Slater, C. R. (2008) 'Structural factors influencing the efficacy of neuromuscular transmission', *Ann N Y Acad Sci*, 1132, pp. 1-12.

Soriano, P. (1999) 'Generalized lacZ expression with the ROSA26 Cre reporter strain', *Nat Genet*, 21(1), pp. 70-1.

Souza, P. V., Batistella, G. N., Lino, V. C., Pinto, W. B., Annes, M. and Oliveira, A. S. (2016) 'Clinical and genetic basis of congenital myasthenic syndromes', *Arq Neuropsiquiatr*, 74(9), pp. 750-760.

Sparks, S. and Krasnewich, D. (2005). *Congenital Disorders of N-Linked Glycosylation and Multiple Pathway Overview*. [online] Available at: https://www.ncbi.nlm.nih.gov/books/NBK1332/ [Accessed 29 Apr. 2017].

Spiro, R. G. (2002) 'Protein glycosylation: nature, distribution, enzymatic formation, and disease implications of glycopeptide bonds', *Glycobiology*, 12(4), pp. 43r-56r.

Srinivas, S., Watanabe, T., Lin, C.-S., William, C. M., Tanabe, Y., Jessell, T. M. and Costantini, F. (2001) 'Cre reporter strains produced by targeted insertion of EYFP and ECFP into the ROSA26 locus', *BMC Developmental Biology*, 1, pp. 4-4.

Stanley, P., Schachter, H. and Taniguchi, N. (2009). *N-Glycans*. [online] Available at: https://www.ncbi.nlm.nih.gov/books/NBK1917/ [Accessed 29 Apr. 2017].

Strochlic, L., Cartaud, A. and Cartaud, J. (2005) 'The synaptic muscle-specific kinase (MuSK) complex: new partners, new functions', *Bioessays*, 27(11), pp. 1129-35.

Stuckey, D. J., Carr, C. A., Camelliti, P., Tyler, D. J., Davies, K. E. and Clarke, K. (2012) 'In vivo MRI characterization of progressive cardiac dysfunction in the mdx mouse model of muscular dystrophy', *PLoS One*, 7(1), pp. e28569.

Sudhof, T. C. (2013) 'A molecular machine for neurotransmitter release: synaptotagmin and beyond', *Nat Med*, 19(10), pp. 1227-31.

Svensson, G., Awad, W., Hakansson, M., Mani, K. and Logan, D. T. (2012) 'Crystal structure of N-glycosylated human glypican-1 core protein: structure of two loops evolutionarily conserved in vertebrate glypican-1', *J Biol Chem*, 287(17), pp. 14040-51.

Tamayo, T., Eno, E., Madrigal, C., Heydemann, A., Garcia, K. and Garcia, J. (2016) 'Functional in situ assessment of muscle contraction in wild-type and mdx mice', *Muscle Nerve*, 53(2), pp. 260-8.

Thiel, C., Schwarz, M., Peng, J., Grzmil, M., Hasilik, M., Braulke, T., Kohlschutter, A., von Figura, K., Lehle, L. and Korner, C. (2003) 'A new type of congenital disorders of glycosylation (CDG-Ii) provides new insights into the early steps of dolichol-linked oligosaccharide biosynthesis', *J Biol Chem*, 278(25), pp. 22498-505.

Torres-Ruiz, R. and Rodriguez-Perales, S. (2017) 'CRISPR-Cas9 technology: applications and human disease modelling', *Brief Funct Genomics*, 16(1), pp. 4-12.

Trontelj, J. V., Mihelin, M. and Khuraibet, A. (2002) 'Safety margin at single neuromuscular junctions', *Muscle Nerve Suppl*, 11, pp. S21-7.

Tsujino, A., Maertens, C., Ohno, K., Shen, X. M., Fukuda, T., Harper, C. M., Cannon, S. C. and Engel, A. G. (2003) 'Myasthenic syndrome caused by mutation of the SCN4A sodium channel', *Proc Natl Acad Sci U S A*, 100(12), pp. 7377-82.

Vainzof, M., Ayub-Guerrieri, D., Onofre, P. C., Martins, P. C., Lopes, V. F., Zilberztajn, D., Maia, L. S., Sell, K. and Yamamoto, L. U. (2008) 'Animal models for genetic neuromuscular diseases', *J Mol Neurosci,* 34(3), pp. 241-8.

Vandamme, T. F. (2014) 'Use of rodents as models of human diseases', *Journal of Pharmacy & Bioallied Sciences,* 6(1), pp. 2-9.

Verschuuren, J. J., Palace, J. and Gilhus, N. E. (2010) 'Clinical aspects of myasthenia explained', *Autoimmunity,* 43(5-6), pp. 344-52.

Wang, L., Zhang, L., Li, S., Zheng, Y., Yan, X., Chen, M., Wang, H., Putney, J. W. and Luo, D. (2015) 'Retrograde regulation of STIM1-Orai1 interaction and store-operated Ca2+ entry by calsequestrin', *Sci Rep,* 5, pp. 11349.

Wargon, I., Richard, P., Kuntzer, T., Sternberg, D., Nafissi, S., Gaudon, K., Lebail, A., Bauche, S., Hantai, D., Fournier, E., Eymard, B. and Stojkovic, T. (2012) 'Long-term follow-up of patients with congenital myasthenic syndrome caused by COLQ mutations', *Neuromuscul Disord,* 22(4), pp. 318-24.

Waterston, R. H. and Lindblad-Toh, K. and Birney, E. and Rogers, J. and Abril, J. F. and Agarwal, P. and Agarwala, R. and Ainscough, R. and Alexandersson, M. and An, P. and Antonarakis, S. E. and Attwood, J. and Baertsch, R. and Bailey, J. and Barlow, K. and Beck, S. and Berry, E. and Birren, B. and Bloom, T. and Bork, P. and Botcherby, M. and Bray, N. and Brent, M. R. and Brown, D. G. and Brown, S. D. and Bult, C. and Burton, J. and Butler, J. and Campbell, R. D. and Carninci, P. and Cawley, S. and Chiaromonte, F. and Chinwalla, A. T. and Church, D. M. and Clamp, M. and Clee, C. and Collins, F. S. and Cook, L. L. and Copley, R. R. and Coulson, A. and Couronne, O. and Cuff, J. and Curwen, V. and Cutts, T. and Daly, M. and David, R. and Davies, J. and Delehaunty, K. D. and Deri, J. and Dermitzakis, E. T. and Dewey, C. and Dickens, N. J. and Diekhans, M. and Dodge, S. and Dubchak, I. and Dunn, D. M. and Eddy, S. R. and Elnitski, L. and Emes, R. D. and Eswara, P. and Eyras, E. and Felsenfeld, A. and Fewell, G. A. and Flicek, P. and Foley, K. and Frankel, W. N. and Fulton, L. A. and Fulton, R. S. and Furey, T. S. and Gage, D. and Gibbs, R. A. and Glusman, G. and Gnerre, S. and Goldman, N. and Goodstadt, L. and Grafham, D. and Graves, T. A. and Green, E. D. and Gregory,

S. and Guigo, R. and Guyer, M. and Hardison, R. C. and Haussler, D. and Hayashizaki, Y. and Hillier, L. W. and Hinrichs, A. and Hlavina, W. and Holzer, T. and Hsu, F. and Hua, A. and Hubbard, T. and Hunt, A. and Jackson, I. and Jaffe, D. B. and Johnson, L. S. and Jones, M. and Jones, T. A. and Joy, A. and Kamal, M. and Karlsson, E. K. and Karolchik, D. and Kasprzyk, A. and Kawai, J. and Keibler, E. and Kells, C. and Kent, W. J. and Kirby, A. and Kolbe, D. L. and Korf, I. and Kucherlapati, R. S. and Kulbokas, E. J. and Kulp, D. and Landers, T. and Leger, J. P. and Leonard, S. and Letunic, I. and Levine, R. and Li, J. and Li, M. and Lloyd, C. and Lucas, S. and Ma, B. and Maglott, D. R. and Mardis, E. R. and Matthews, L. and Mauceli, E. and Mayer, J. H. and McCarthy, M. and McCombie, W. R. and McLaren, S. and McLay, K. and McPherson, J. D. and Meldrim, J. and Meredith, B. and Mesirov, J. P. and Miller, W. and Miner, T. L. and Mongin, E. and Montgomery, K. T. and Morgan, M. and Mott, R. and Mullikin, J. C. and Muzny, D. M. and Nash, W. E. and Nelson, J. O. and Nhan, M. N. and Nicol, R. and Ning, Z. and Nusbaum, C. and O'Connor, M. J. and Okazaki, Y. and Oliver, K. and Overton-Larty, E. and Pachter, L. and Parra, G. and Pepin, K. H. and Peterson, J. and Pevzner, P. and Plumb, R. and Pohl, C. S. and Poliakov, A. and Ponce, T. C. and Ponting, C. P. and Potter, S. and Quail, M. and Reymond, A. and Roe, B. A. and Roskin, K. M. and Rubin, E. M. and Rust, A. G. and Santos, R. and Sapojnikov, V. and Schultz, B. and Schultz, J. and Schwartz, M. S. and Schwartz, S. and Scott, C. and Seaman, S. and Searle, S. and Sharpe, T. and Sheridan, A. and Shownkeen, R. and Sims, S. and Singer, J. B. and Slater, G. and Smit, A. and Smith, D. R. and Spencer, B. and Stabenau, A. and Stange-Thomann, N. and Sugnet, C. and Suyama, M. and Tesler, G. and Thompson, J. and Torrents, D. and Trevaskis, E. and Tromp, J. and Ucla, C. and Ureta-Vidal, A. and Vinson, J. P. and Von Niederhausern, A. C. and Wade, C. M. and Wall, M. and Weber, R. J. and Weiss, R. B. and Wendl, M. C. and West, A. P. and Wetterstrand, K. and Wheeler, R. and Whelan, S. and Wierzbowski, J. and Willey, D. and Williams, S. and Wilson, R. K. and Winter, E. and Worley, K. C. and Wyman, D. and Yang, S. and Yang, S. P. and Zdobnov, E. M. and Zody, M. C. and Lander, E. S. (2002) 'Initial sequencing and comparative analysis of the mouse genome', *Nature*, 420(6915), pp. 520-62.

Weatherbee, S. D., Anderson, K. V. and Niswander, L. A. (2006) 'LDL-receptor-related protein 4 is crucial for formation of the neuromuscular junction', *Development,* 133(24), pp. 4993-5000.

Webster, R. G., Cossins, J., Lashley, D., Maxwell, S., Liu, W. W., Wickens, J. R., Martinez-Martinez, P., de Baets, M. and Beeson, D. (2013) 'A mouse model of the slow channel myasthenic syndrome: Neuromuscular physiology and effects of ephedrine treatment', *Exp Neurol,* 248, pp. 286-98.

Weis, J., Dimpfel, W. and Schroder, J. M. (1995) 'Nerve conduction changes and fine structural alterations of extra- and intrafusal muscle and nerve fibers in streptozotocin diabetic rats', *Muscle Nerve,* 18(2), pp. 175-84.

Whittaker, R. G., Herrmann, D. N., Bansagi, B., Hasan, B. A., Lofra, R. M., Logigian, E. L., Sowden, J. E., Almodovar, J. L., Littleton, J. T., Zuchner, S., Horvath, R. and Lochmuller, H. (2015) 'Electrophysiologic features of SYT2 mutations causing a treatable neuromuscular syndrome', *Neurology,* 85(22), pp. 1964-71.

Willadt, S., Nash, M. and Slater, C. R. (2016) 'Age-related fragmentation of the motor endplate is not associated with impaired neuromuscular transmission in the mouse diaphragm', *Scientific Reports*, 6, pp. 24849.

Williams, R. T., Senior, P. V., Van Stekelenburg, L., Layton, J. E., Smith, P. J. and Dziadek, M. A. (2002) 'Stromal interaction molecule 1 (STIM1), a transmembrane protein with growth suppressor activity, contains an extracellular SAM domain modified by N-linked glycosylation', *Biochim Biophys Acta,* 1596(1), pp. 131-7.

Williams, T. M. and Lisanti, M. P. (2004) 'The caveolin proteins', *Genome Biology,* 5(3), pp. 214-214.

Wisniewski, J. R., Zougman, A., Nagaraj, N. and Mann, M. (2009) 'Universal sample preparation method for proteome analysis', *Nat Methods,* 6(5), pp. 359-62.

Witzemann, V., Chevessier, F., Pacifici, P. G. and Yampolsky, P. (2013) 'The neuromuscular junction: selective remodeling of synaptic regulators at the nerve/muscle interface', *Mech Dev,* 130(6-8), pp. 402-11.

Wood, S. J. and Slater, C. R. (2001) 'Safety factor at the neuromuscular junction', *Prog Neurobiol,* 64(4), pp. 393-429.

Wu, H., Xiong, W. C. and Mei, L. (2010) 'To build a synapse: signaling pathways in neuromuscular junction assembly', *Development (Cambridge, England),* 137(7), pp. 1017-1033.

Wu, X., Rush, J. S., Karaoglu, D., Krasnewich, D., Lubinsky, M. S., Waechter, C. J., Gilmore, R. and Freeze, H. H. (2003) 'Deficiency of UDP-GlcNAc:Dolichol Phosphate N-Acetylglucosamine-1 Phosphate Transferase (DPAGT1) causes a novel congenital disorder of Glycosylation Type Ij', *Hum Mutat,* 22(2), pp. 144-50.

Wurde, A. E., Reunert, J., Rust, S., Hertzberg, C., Haverkamper, S., Nurnberg, G., Nurnberg, P., Lehle, L., Rossi, R. and Marquardt, T. (2012) 'Congenital disorder of glycosylation type Ij (CDG-Ij, DPAGT1-CDG): extending the clinical and molecular spectrum of a rare disease', *Mol Genet Metab,* 105(4), pp. 634-41.

Yamaguchi, Y. (2002) 'Glycobiology of the synapse: the role of glycans in the formation, maturation, and modulation of synapses', *Biochim Biophys Acta,* 1573(3), pp. 369-76.

Yampolsky, P., Pacifici, P. G., Lomb, L., Giese, G., Rudolf, R., Roder, I. V. and Witzemann, V. (2010) 'Time lapse in vivo visualization of developmental stabilization of synaptic receptors at neuromuscular junctions', *J Biol Chem,* 285(45), pp. 34589-96.

Yang, C. T., Hindes, A. E., Hultman, K. A. and Johnson, S. L. (2007) 'Mutations in gfpt1 and skiv2l2 cause distinct stage-specific defects in larval melanocyte regeneration in zebrafish', *PLoS Genet,* 3(6), pp. e88.

Yumoto, N., Kim, N. and Burden, S. J. (2012) 'Lrp4 is a retrograde signal for presynaptic differentiation at neuromuscular synapses', *Nature,* 489(7416), pp. 438-42.

Zhang, B., Xiong, W. C. and Mei, L. (2009) 'Get ready to Wnt: prepatterning in neuromuscular junction formation', *Dev Cell,* 16(3), pp. 325-7.

Zoltowska, K., Webster, R., Finlayson, S., Maxwell, S., Cossins, J., Muller, J., Lochmuller, H. and Beeson, D. (2013) 'Mutations in GFPT1 that underlie limb-girdle congenital myasthenic syndrome result in reduced cell-surface expression of muscle AChR', *Hum Mol Genet,* 22(14), pp. 2905-13.

Zong, Y. and Jin, R. (2013) 'Structural mechanisms of the agrin-LRP4-MuSK signaling pathway in neuromuscular junction differentiation', *Cell Mol Life Sci,* 70(17), pp. 3077-88.